**AGRICULTURAL
UNIVERSITY OF ATHENS**

**DEPARTMENT OF NATURAL
RESOURCES AND AGRICULTURAL
ENGINEERING**

Low-Grade Heat Conversion into Power Using Small Scale Organic Rankine Cycles

Bertrand FANKAM TCHANCHE

Doctoral Thesis
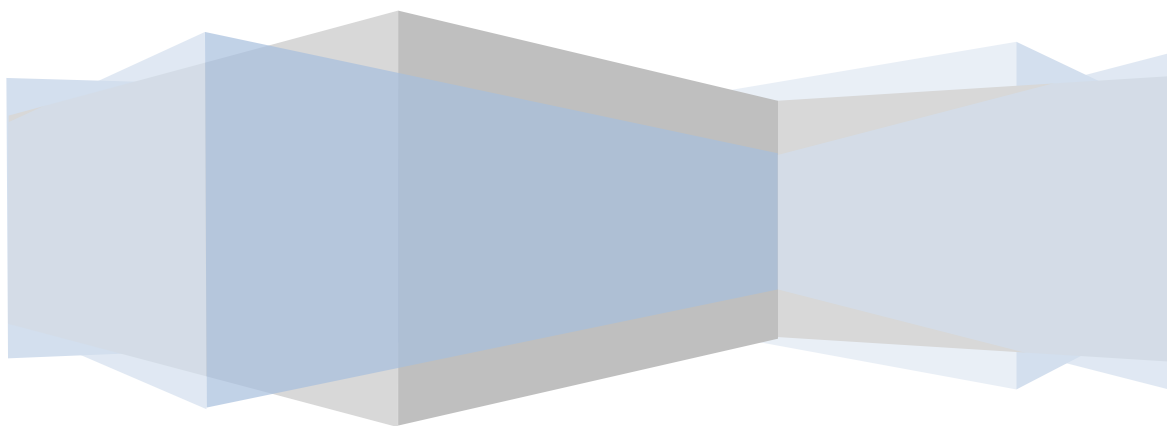
Athens, 2010

**AGRICULTURAL
UNIVERSITY OF ATHENS**

**DEPARTMENT OF NATURAL
RESOURCES AND AGRICULTURAL
ENGINEERING**

Low-Grade Heat Conversion into Power Using Small Scale Organic Rankine Cycles

A Doctoral Thesis

submitted by

Bertrand FANKAM TCHANCHE

Athens, November 2010

Low-Grade Heat Conversion into Power Using Small Scale Organic Rankine Cycles

Doctoral Thesis by Bertrand Fankam Tchanche

Department of Natural Resources and Agricultural Engineering

Agricultural University of Athens, AUA

Jury committee

George Papadakis, Professor
Agricultural University of Athens
Dept. of Natural Resources and Agricultural Engineering

Gregory Lambrinos, Professor
Agricultural University of Athens
Dept. of Natural Resources and Agricultural Engineering

Antonis Frangoudakis, Professor
Agricultural University of Athens
Dept. of Natural Resources and Agricultural Engineering

Stelios Rozakis, Assistant Professor
Agricultural University of Athens
Dept. of Agricultural Economics and Rural Development

Vincent Lemort, Assistant Professor
University of Liège
Faculty of Applied Sciences

Emmanuil Rogdakis, Professor
National Technical University
School of Mechanical Engineering

Dimitrios Papantonis, Professor
National Technical University of Athens
School of Mechanical Engineering

To my family

Abstract

The present thesis regards the study of small scale organic Rankine cycles (ORCs) considered in the two philosophies that embodies its applications. Major power cycles, including vapor and gas cycles were recalled with emphasis on advanced Rankine cycles and its derivates that are Kalina and Uehara cycles. Organic Rankine cycles as presented are well adapted for low and medium temperature heat resources below 400 ºC. The applications intensely investigated are: solar electricity, solar desalination, biomass combined heat and power plants (CHP), geothermal and energy recycling from thermal devices and processes.

Suitable Working fluids for a solar ORC driven by heat source temperature below 100 ºC are selected using predefined criteria such as higher fluid densities, maximum cycle efficiency, safety and environmental data, and moderate critical temperature. R134a, R600, R152a emerged as good fluids among 20 potential candidates. The ORC configurations for the same level of temperature are also subject to an investigation. Exergy topology analysis was applied to suitably choose the optimal configuration based on additional parameters: exergy efficiency, degree of thermodynamic perfection and coefficient of influence. The simple Rankine cycle proved to be more adequate and potentially cost effective in comparison with modified Rankine cycles with internal heat exchangers or with integrated feedliquid heaters.

Experimental investigations carried out on a small ORC designed for exhaust gas heat recovery confirmed the technical feasibility of the technology. The test bench was made up of several heat exchangers, two diaphragm pumps and an open-drive oil-free scroll expander. Cycle and expander performances were evaluated and compared for three fluids: R123, R245fa and HFE7000. The maximum power output delivered is about 2 kW, the cycle efficiency is less than 8% and the global efficiency does not exceed 5%. The oil free open-drive expander yields a maximum efficiency of about 70%.

The final section deals with the economic evaluation and optimization of small scale ORCs in heat recovery application. The heat source considered is hot air at about 180 °C with a mass flow rate of 0.21 kg/s. The optimized cycle system is based on the experimental investigations and models derived. It produces 2 kW power and yields 8% thermal efficiency. Using appropriate mathematical formula the system was scaled-up to 50 kW. The study concludes that the organic Rankine cycle is a promising technology for small-scale waste heat recovery applications. For illustration, the levelized electricity cost (LEC) is about 13.27 c€/kWh for very small systems (2 kW) and decreases down to 7 c€/kWh for a 50 kWe system. This value could be significantly lower, below 5 c€/kWh for medium and large size systems. By means of a thermo-economic model the mismatch between the optimal technical point and the minimum specific cost was demonstrated. The analysis of the mismatch allowed concluding that economic optimization instead of thermodynamic optimization or a compromise between them is recommended when seeking for profitable environmental solutions.

Extended Abstract

Solar, biomass and geothermal energy considered as renewable and clean energy sources, and industrial waste heat could potentially cover the world electricity demand. Unfortunately, conventional power generation techniques cannot efficiently convert the low temperature heat generated from these sources into electrical power. Hence, large amount of low temperature heat is simply wasted. In this context, research on low-grade heat conversion for power generation is of great significance.

Thermodynamic cycles such as the organic Rankine cycle (ORC), transcritical Rankine cycle, supercritical Rankine cycle, Kalina cycle (KC), Uehara cycle (UC), Goswami cycle (GC), and trilateral flash cycle (TFC) have been proposed, evaluated and compared for the conversion of low-grade heat sources into electricity. Among the proposed solutions, the organic Rankine cycle is the most widely investigated and implemented. This cycle involves the same components as in a conventional steam power plant, but uses refrigerants, hydrocarbons, solvents and other organic compounds as working fluid instead of water. It is worth to mention that organic fluids compared to water have lower boiling temperature, what results in a reduced evaporating temperature.

The growing concern over the future depletion of the fossil fuels reserves and the destruction of the environment have pushed governments, industries and researchers to intensify the R&D on low-grade energy recovery technologies with emphasis on the ORC technology. This explains the intense activity observed in this field during last ten years. The ORC technology presents many features:

- adaptability to various heat sources

- proven technology with great maturity

- less complex and less maintenance

- possibility of small scales

- distributed generation system

- low investment and maintenance costs

- good market availability and well known market suppliers

Nevertheless, the ORC solutions available on the market are designed to produce power from a hundred of kW up to few MW, and a very limited number of solutions can be found for small scale systems of few kW. Therefore, there is still room for research on small scale ORC systems. This justifies the will to focus on small scale Organic Rankine Cycles in the two philosophies that embody their applications in the present thesis.

In the first part of the thesis, major power cycles, including vapor and gas cycles are recalled to highlight their differences. Then, advanced Rankine cycles and its derivates that are Kalina and Uehara cycles are presented. All over the development stages of Rankine cycles, the preoccupation has always been the maximization of the energy efficiency. Several techniques could be employed to increase the cycle performance: regenerator, feedliquid heaters, superheater, reheater and evaporation above the critical point. Fluid mixtures such as ammonia/water are also used in absorption cycles such as Kalina and

Uehara cycles with as benefit better performance of heat exchangers that leads to overall improvement of the system.

The second part is a review of Organic Rankine Cycle applications. These applications include solar thermal electricity, solar thermal driven reverse osmosis desalination (Solar ORC-RO), Duplex-Rankine cooling, solar pond power systems, ocean thermal energy conversion (OTEC), biomass combined heat and power plants (CHP), binary geothermal systems and low-grade waste heat recycling (ORC-WHR) from thermal devices and processes. Rankine cooling systems are almost abandoned with preference to sorption cooling systems which require less moving parts and use more environmentally friendly substances. Solar ORC-RO is still at the research stage. Solar thermal power and solar pond power although proven, are not yet widely adopted. OTEC is intensely investigated as future major technology for isolated islands with favorable seawater thermodynamic characteristics. Biomass and binary geothermal CHP are already mature. ORC-WHR is the fastest growing business among ORC solutions, with great potential in industry and combined cycle power plants.

Part three regards the fluid selection for a small solar ORC driven by low-temperature heat below 100 °C. This is a critical issue. Various kinds of substances such as refrigerants, hydrocarbons, alcohols and solvents can be adapted, but the choice of a suitable substance depends on the operating parameters of the cycle and the application. General characteristics of a good fluid are:

- high molecular mass

- appropriate critical parameters

- vapor saturation curve with positive or large slope

- high vapor/liquid density

- high performance (efficiency, power)

- high thermal stability

- moderate evaporator pressure

- condensing pressure above atmospheric

- good compatibility with materials

- low environmental impact and high safety level

- good availability and low cost

Using the above mentioned criteria, a general methodology was established to detect the most suitable fluids. It encompasses three steps: data collection, data analysis and decision. For a simple Rankine Cycle driven by hot water and cooled by ambient air, a total of 20 fluids with critical temperature above 90 °C were screened and R134a, R152a, R600, R600a and R290 emerged as good fluids.

In the fourth part, exergy analysis as the most developed tool for thermodynamic systems evaluation was used to theoretically determine the most suitable configuration for a solar Rankine engine operating at temperature below 90 °C. The state-of-art of the concept was recalled and newly proposed approach applied. This approach called *"exergy topology"* combines the traditional exergy analysis and mathematical graph theory. It provides more performance indicators: the degree of thermodynamic perfection and the coefficient of

influence. The simple Rankine Cycle proved to be more adequate and potentially cost effective in comparison with modified Rankine cycles with internal heat exchangers or with integrated feedliquid heaters. The exergy loss distribution of a small solar ORC operating at a temperature below 90 °C shows that 91% of the exergy destroyed in the system is lost in the solar collector array. The overall exergy efficiency obtained is 3.1% and raised the issue of the solar collector selection and the opportunity to design a solar system operating at such low temperature. The new approach proved from the results it could serve not only as an evaluation tool but also as decision support tool.

Proof of concept of utilization of scroll compressor as expansion machine in a small organic Rankine cycle is demonstrated in the fifth part. The test bench is made up of several heat exchangers, two diaphragm pumps, a liquid receiver and an open-drive oil-free scroll expander. The system is driven by hot air whose maximum temperature does not exceed 200 °C and cooled by water. Sensors and other instruments are mounted at various parts of the bench to record the thermodynamic data. Components and cycle performance were evaluated and compared for several fluids: R123, R245fa and HFE7000. The maximum power output delivered is about 2 kW, the cycle efficiency is less than 8% and the global efficiency does not exceed 5%. The oil free open-drive expander yields a maximum efficiency of about 70%.

The last section deals with the economic study of small scale ORCs in heat recovery application. The optimized cycle system used for the analysis is based on the experimental investigations and cycle models derived. The heat source considered is hot air at about 180 °C with a mass flow rate of 0.21 kg/s and the system is cooled by water at 10 °C. The system is assumed to produce 2 kW power with 8% cycle energy efficiency. Using appropriate mathematic formula the system was scaled-up to 50 kW. The study concludes that the Organic Rankine Cycle is a promising technology for small-scale waste heat recovery applications. For illustration, the levelized electricity cost (LEC) is about 13.27 c€/kWh for very small systems and decreases down to 7 c€/kWh for a 50 kW system. This value could be significantly lower, below 5 c€/kWh for medium and large size systems. By modeling of components costs the mismatch between the optimal technical point and system minimum specific cost was highlighted. This mismatch leads to the conclusion that economic optimization instead of thermodynamic optimization should be recommended when seeking for profitable environmental solutions.

List of Publications

International Journals

1. Bertrand F. Tchanche, G. Papadakis, G. Lambrinos, A. Frangoudakis. "Fluid selection for a low-temperature solar organic Rankine cycle". Applied Thermal Engineering 29 (2009) 2468-2476.

2. Bertrand F. Tchanche, Gr. Lambrinos, A. Frangoudakis, G. Papadakis. "Exergy analysis of micro-organic Rankine power cycles for a small scale solar driven reverse osmosis desalination system". Applied Energy 87 (2010) 1295-1306.

3. Bertrand F. Tchanche, Gr. Lambrinos, A. Frangoudakis, G. Papadakis. "Low-grade heat conversion into power using organic Rankine cycles – A review of various applications". Renewable Energy (submitted).

Conferences

1. B.F. Tchanche, G. Papadakis, G. Lambrinos, A. Frangoudakis. Criteria for working fluids selection in low-temperature solar organic Rankine cycles, in: Proc. of International Conference on Solar Heating, Cooling and Buildings, Eurosun2008, 7-10 Oct. 2008, Lisbon-Portugal. (Poster)

2. B.F. Tchanche, G. Papadakis, G. Lambrinos, A. Frangoudakis. Effects of regeneration on low- temperature solar organic Rankine cycles, in: Proc. of International Conference on Solar Heating, Cooling and Buildings, Eurosun2008, 7-10 Oct. 2008, Lisbon-Portugal. (Poster)

3. B.F. Tchanche, G. Papadakis, G. Lambrinos, A. Frangoudakis. Exergy analysis of a low-temperature solar thermal power system based on exergy-topological models, in Proc. of International Exergy, Energy and Environmental Symposium, IEEES-4, 19-23 April 2009, Sharjah- United Arab Emirates.(Oral)

4. B.F. Tchanche, G. Papadakis, G. Lambrinos, A. Frangoudakis. Optimal evaporating temperature for working fluids in Rankine heat engines, in Proc. of International Exergy, Energy and Environmental Symposium, IEEES-4, 19-23 April 2009, Sharjah-United Arab Emirates.(Oral)

5. B.F. Tchanche, Essam Sh. Mohamed, and G. Papadakis. Solar energy: A solution for energy poverty in Africa?, in Proc. of ISES Solar World Congress, 11-14 Oct. 2009, Johannesburg, South Africa. (Oral)

6. B.F. Tchanche, S. Quoilin, S. Declaye, G. Papadakis & V. Lemort. Economic Optimization of Small Scale Organic Rankine Cycles, in Proc. of 23rd International Conference on Efficiency, Cost, Optimization, Simulation and Environmental Impact of Energy Systems (ECOS), June 14-17, 2010, Lausane-Switzerland.

7. B.F. Tchanche, S. Quoilin, S. Declaye, G. Papadakis & V. Lemort. Economic Feasibility Study of a Small Scale Organic Rankine Cycle System in Waste Heat Recovery Application, in Proc. of the ASME 2010 10th Biennial Conference on Engineering and Systems Design and Analysis (ESDA), July 12-14, 2010, Istanbul-Turkey.

Acknowledgements

People have often inquired about my decision to stay and carry out my doctoral studies in Greece. Any attempt to justify the reason why I chose to come to a country, where the climate, language, culture and the environment are so extremely different from my own native country, Cameroon, would be very difficult. Well, it could be explained by a strong desire for knowing more about the Theory of Energy and stand on the shoulders of the giants: Socrates, Aristotle, and others, a desire of adventure in ancient cities, love for cultural contacts, destiny, or a combination of all. Nevertheless, I would thank whatever forces that have brought me here, but in particular the Greek Interstate Scholarship Foundation (IKY) for providing me assistance during my doctoral studies.

I am grateful to my supervisor, Professor George Papadakis, for having accepted to act as my supervisor and proposed me this topic. During all these years, he has been extremely supportive of my ideas, and has provided necessary support to achieve my targets. Many thanks also to Professor Gregory Lambrinos for criticizing my work and supporting my ideas. Thanks also to Professor Antonios Frangoudakis.

I am also grateful to Dr. Vincent Lemort for supervising my work and providing me with the necessary support and administrative cover during my stay at the Thermodynamics Laboratory of the University of Liège. I am grateful to Sylvain Quoilin, whose openness and kindness brought me to the Thermodynamics Laboratory of the University of Liège. Sincere thanks to Sébastien Declaye for his impressive assistance.

During all these years in the Renewable Energy Group of the Agricultural University of Athens, I was not alone. Many highly motivated young researchers where with me. Sincere thanks to D. Manolakos, Essam Sh. Mohammed, L. Geronikolou, G. Kyriakarakos, M. Voulgarakis and A. Balafoutis for their support.

Table of Contents

List of Tables

List of Figures

Nomenclature

A	Surface area	(m^2)
c	Molar concentration	(-)
C	Cost	(€)
C	Heat capacity	(kJ/kg.K)
C	Torque	(N.m)
COP	Coefficient of performance	(-)
D	Diameter	(cm)
DPP	Depreciated payback period	(years)
e	Specific exergy	(kJ/kg)
E	Sum of exergy flow	(kW)
FF	Filling factor	(-)
g	Gravitational constant	(m/s^2)
h	Enthalpy	(kJ/kg)
I	Irreversibility	(kW)
k	Specific heat ratio	(-)
k	Interest rate	(%)
LEC	Levelized electricity cost	(€/kWh)
m	Mass flow rate	(kg/s)
N	Rotation speed	(rpm)
NPV	Net present value	(€)
P	Pressure	(MPa)
r_c	Cutoff ratio	(-)
r_P	Pressure ratio	(-)
q	specific heat	(kJ/kg)
Q	Heat rate	(kW)
s	Entropy	(kJ/kg.K)
SIC	Specific investment cost	(€/kW)
T	Temperature	(ºC)
TIC	Total investment cost	(€)
U	Overall heat transfer coefficient	(W/m²K)
UP	Unit price	(€/kg)
V	volume	(m^3)
V	Volume flow rate	(m^3/h)
V	Velocity	(m/s)
VFR	Volume flow ratio	(-)
w	Specific work	(kJ/kg)
W	Work	(kW)
x	Quality, Mole fraction	(-)
X	Capacity	(-)
z	Elevation	(m)

Greek letters

I-VII	Components	
α	Fraction of fluid extracted	(-)

β	Coefficient of influence	(%)
γ	Exergy factor	(-)
ΔT	Temperature difference	(ºC, K)
Δh	Enthalpy difference	(kJ/kg)
ε	Effectiveness	(-)
η	Efficiency	(%)
μ	Chemical potential	(J/kg)
ν	Specific volume	(m^3/kg)
ν	Degree of thermodynamic perfection	(%)
Π	Exergy loss	(kW)
ϱ	Density	(kg/m^3)
φ	Input enthalpy ratio	(%)

Subscript-superscript

0	reference state
0,htf	preheater exit (hot side)
1-16	states in the cycle, flows
a	air, available
amb	ambient
b	boiling point
BR	Brayton
c	condenser, critical
cd	condenser
ch	chemical
el	electrical
ev	evaporator
ex	exhaust, exergetic
exe	exergetic
exp	expander
fl	flow
fg	phase change
H	heat source
ht	heat source-turbine
hx	heat exchanger
htf	heat transfer fluid
i	Inlet, input
i, j, k	flows, components
II	second law
kn	kinetic
L	cold source
liq	liquid
lr	liquid reservoir
max	maximum
mech	mechanical
min	minimum
o	restricted dead state
out	outlet, exit
p	pump
pp	pinch point, pipe

ph	physical
pt	potential
r	refrigerant
R	recuperation
rot	rotation
s	isentropic
sc	solar collector
sf	secondary fluid
sh	shaft
ST	Stirling
su	supply
t	turbine
th	thermal
tp	two-phase
TR	trilateral
trq	torque
tot	total
uhx	upper heat exchangers
u	useful
w	water
wf	working fluid
Σ	system

Acronyms

CFH	closed feedliquid
CHP	combined heat and power
GWP	global warming potential
HT	high temperature
LHV	lower heating value
LT	low temperature
ODP	ozone depletion potential
OFH	open feedliquid
ORC	organic Rankine cycle
RHE	regenerative heat exchanger
RO	reverse osmosis
SRE	simple Rankine engine
TTD	terminal temperature difference

1 - General Introduction

1.1 Background

Modern societies depend critically on energy and continued economic growth requires further increases in energy consumption and energy demand. According to official reports on future global primary energy production and use, the high energy growth rates of the 20th century will continue unabated until 2050 and even beyond. Presently, the global primary energy use is roughly 500 EJ and shall double by 2050 (Moriarty and Honnery, 2009). The world economy heavily depends on fossil fuels (oil, coal and natural gas) which represent an 81.4% share of total primary energy use. Renewable energy and nuclear energy share the remainder, 12.7% and 5.9% respectively (IEA, 2009).

Nevertheless, the fossil fuel-based economy raises a certain number of issues. The dramatic destruction of the environment attributed to the excessive use of fossil fuels has reached a critical level with unpleasant consequences (Sims, 2004). Moreover, the fossil fuel resources are finite. Their future depletion results in a considerable increase in the energy price with undesirable shocks on the global economy. The growing concern for the supply and safe transportation of fossil fuels as well as the increase in the energy demand reinforce the scaling-up of fossil fuel prices and fuel international tensions.

Therefore, it is time to seek for alternate energy sources and to consider ways of saving the fast depleting fossil resources. Verbruggen (2008) analyzed potential contenders for the future electricity supply from economic and sustainability viewpoints and proposed the twin efficiency/renewable power.

The organic Rankine cycles (ORCs) as energy converter fall well in both sides of the twin. Their suitability in medium-scale power plants from hundreds kW to MW power output has already been demonstrated in solar, geothermal, waste heat recovery and biomass power plants (Quoilin and Lemort, 2009; Schuster et al., 2009).

The technology for medium and large scale is already mature. However, only a limited number of solutions are available for small size systems in the kW power range. The development of small organic Rankine power systems for several decades has been very slow due to the lack of adapted and efficient components. Today, HVAC components and specifically the compressors can be converted into expanders with good efficiency (Lemort, 2008; Smith and Stosic, 2001a). Several prototypes are under investigation throughout the world for solar/biomass combined heat and power (Orosz et al., 2009; Aoun, 2008), desalination (Manolakos et al., 2005 & 2007) and waste heat recovery applications (Quoilin, 2007; Declaye, 2009).

1.2 Structure and scope of the thesis

The Thesis is comprised of several dimensions: One broad, with the aim of providing a general picture of vapor and gas power cycles while insisting on organic Rankine cycle technologies. The second aim is the investigation of micro-organic Rankine cycles. The topic of investigation is not arbitrary; it is linked to the ongoing work carried out at the Agricultural University of Athens, Greece and at the University of Liège, Belgium in view

of developing low-temperature energy recovery systems. Solar driven reverse osmosis (RO) desalination is a potential solution for water scarcity in remote and sunny areas such as Greek islands where potable water is a major concern. A prototype of small scale solar ORC-RO system was built and tested to show its feasibility and is still under investigation. Small organic Rankine cycle machines appear progressively as the most suitable solution to recover the vast amount of heat lost during thermal processes in industries as well as in mobile and stationary power plants. A prototype of such machine driven by hot air (assimilated to exhaust gas) is also under investigation at the University of Liège. Thus, the present thesis is a step forward and a supplemental contribution in the development of small power generation technologies based on low-grade heat recovery.

A broad overview of thermodynamic power cycles is presented in **Chapter 2**. Two groups are targeted, the vapor and gas power cycles. Special attention is paid for different Rankine cycle designs operating with pure single fluids or binary mixtures of water/ammonia.

A technological and economical survey of organic Rankine cycle solutions is presented in **Chapter 3**. ORC is a promising technology for power generation from low and medium temperature heat sources. The market is steadily increasing and new segments are opening as the technology is progressively adopted for distributed power generation.

In **Chapter 4**, theoretical performances as well as thermodynamic and environmental properties of few fluids have been comparatively assessed for use in low-temperature solar organic Rankine cycle systems. Efficiencies, volume flow rate, mass flow rate, pressure ratio, toxicity, flammability, ODP and GWP were used for comparison.

In **Chapter 5**, exergy analysis of micro-organic Rankine heat engines is performed to identify the most suitable configuration for solar applications. Three modified engines derived from simple Rankine engine using regeneration (incorporation of regenerator or feedliquid heaters) are analyzed through a novel approach, called *exergy-topological method* based on the combination of exergy flow graphs, exergy loss graphs, and thermoeconomic graphs.

Experimental tests were performed to study the performance of an organic Rankine cycle system over a wide range of working conditions in waste heat recovery application. The results of tests carried out with HFE7000 as working fluid are reported in **Chapter 6.**

Chapter 7 deals with the economic assessment of small organic Rankine cycles in waste heat recovery application. A pre-design model of the ORC is proposed and simulations are run with different working fluids candidates. Then, the economic evaluation is carried out for a system operating with the best suited fluid. Finally, economic optimization of is done considering the specific installation cost as objective function.

Chapter 8 closes the Thesis with summary of main findings and presents future perspectives in the field of small organic Rankine cycle machines.

2 - Rankine Power Cycles

2.1 Introduction

The Rankine vapor power cycle is one of various cycles that were developed for power generation. It was named after the works of William John Macquorn Rankine who developed the scientific background of this cycle. The basic Rankine cycle made up of four components was later modified to give birth to more advanced and efficient Rankine cycle configurations. In this chapter, a brief recall of the history of the inventor is given and different cycles are presented to highlight the differences with the original Rankine cycle. Notes on advanced and innovative Rankine power cycles and combinations with other cycles are also given.

2.2 Heat engine definition

A heat engine is simply a device that converts the thermal energy into mechanical work. The energy conversion is driven by the temperature gradient between a heat reservoir at temperature T_H and a cold reservoir at temperature T_L, ($T_H > T_L$). An essential component of the heat engine is the working medium, which thanks to its thermophysical properties transfers the heat received from the heat source to the sink while part of it is turned into mechanical work (see Figure 2.1).
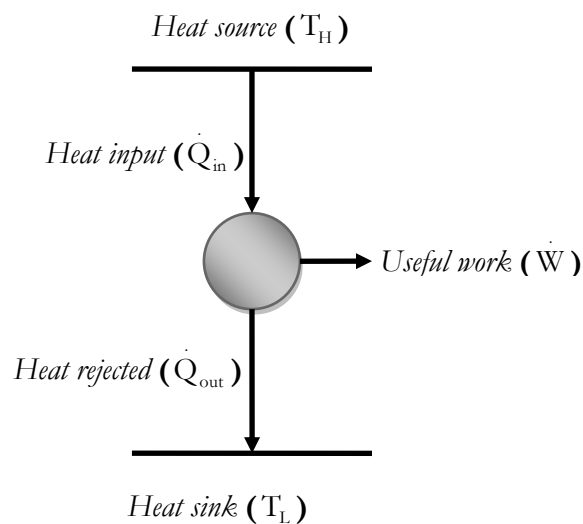
Figure 2.1 – Schematic of a heat engine

A heat engine during its operation can be open to the atmospheric air or closed to the environment. Usually, it is admitted that the higher the temperature difference between the heat source and the cold sink, the higher will be the thermal efficiency. Seeking to increase the thermal efficiency of a heat engine, a natural limit is given by the ambient temperature that cannot be lowered, thus the efforts should focus on how to increase the temperature of the heat source.

In the current literature on Thermodynamics, heat engines are modeled using engineering models termed "cycles". These models or cycles depend on the working medium and processes involved. Here are few of them:

- Vapor power cycles: e.g. Rankine, Kalina, Uehara, Maloney and Robertson.

- Gas power cycles: e.g. Ericsson, Stirling, Otto, Diesel, Joule/Brayton, Lenoir, Atkinson, Miller, etc.

In the upcoming paragraphs few of these cycles will be described with emphasis on the Clausius-Rankine cycle.

2.3 Ideal Carnot cycle

The Carnot cycle is the most efficient power cycle and provides the limit for the thermal efficiency of any heat engine operating between a heat source at temperature T_H and a sink at temperature T_L. This cycle was devised in 1824 by Sadi Carnot. It is based on the assumption that the heat reservoirs are large enough to accept or deliver heat without a change in their temperatures. Furthermore, all the processes are totally reversible. An exemplification of this cycle executed within a saturation dome of a pure working fluid can be appreciated in Figure 2.2. The processes involved are described as follows:

- Process 1-2: isentropic expansion in a turbine during which work is produced by the cycle working fluid
- Process 2-3: isothermal heat rejection in a condenser from the working fluid to a cooling medium
- Process 3-4: isentropic compression by a compressor during which work is performed on the cycle working fluid
- Process 4-1: isothermal heat addition to the working fluid from a heating medium in the boiler

On Figure 2.2, the temperatures of the heating medium and of the cooling medium are identical to that of the working fluid during processes 4-1 and 2-3, respectively. While the working fluid changes from state 4 to 1, the heating medium changes from state 1 to 4, and while the working medium changes from state 2 to 3, the cooling medium moves from state 3 to 2.

The area 12341 in Figure 2.2 represents the net useful work ($\dot{W}_{net}$) that can be generated by the cycle. The area 1ba41 represents the heat input to the cycle ($\dot{Q}_{out}$). The area b23a represents the heat rejected ($\dot{Q}_{out}$). The efficiency of the Carnot cycle defined as the proportion of the heat transformed into mechanical work can be expressed as:

$$\eta_{th}^C = \frac{\dot{W}_{net}}{\dot{Q}_{in}} = \frac{\dot{Q}_{in} - \dot{Q}_{out}}{\dot{Q}_{in}} = 1 - \frac{\dot{Q}_{out}}{\dot{Q}_{in}} \tag{2.1}$$

With $\dot{Q}_{in} = T_H(s_1 - s_4)$ and $\dot{Q}_{out} = T_L(s_2 - s_3)$, the efficiency of the Carnot cycle becomes:

$$\eta_{th}^{C} = 1 - \frac{T_L}{T_H}$$

(2.2)

T_H and T_L are the absolute temperatures of the heat and cold sources respectively. From equation 2.2, it is obvious that high temperature difference leads to high cycle efficiency. Thus, an increase in the heat source temperature or a decrease in the heat sink temperature will raise the efficiency of the cycle. However, if the increase in the heat source temperature could be technically achieved, a decrease in the heat sink temperature is naturally limited by the ambient temperature.
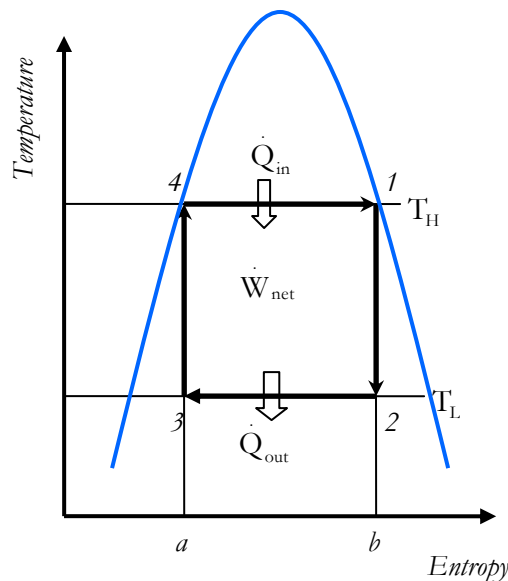
Figure 2.2 – Schematic of a Carnot cycle

Practically, the Carnot cycle is impossible for many reasons (DiPippo, 2007; Çengel and Boles, 2002). Finite temperature difference is always necessary to drive the heat transfer during heat addition and heat rejection from one system to another. In order to realize an isothermal heat transfer, the maximum temperature of the cycle should be kept far below the critical temperature of the working fluid and this lowers the efficiency of the cycle. Moreover, irreversibilities are always generated during work generation and two-phase processes are not easy to manage neither during expansion nor during the compression. Thus, real cycles will have lower efficiencies in comparison with the ideal Carnot cycle.

2.4 Real power cycles

2.4.1 Rankine cycle

2.4.1.1 Cycle description

The Carnot cycle is the basic idealized thermodynamic cycle for thermal energy conversion. Unfortunately, it is impractical and uneconomical to implement. Although less thermodynamically efficient than the Carnot cycle, the Rankine cycle is practical and adaptable. Typically, water is used as the working fluid. A difficulty that arises with the use

of water is the need of superheating in order to prevent the turbine blade erosion. Organic working fluids on the other hand can be used at moderate and lower temperatures and do not require superheating if well selected. The theoretical Rankine thermodynamic cycle consists of four processes as depicted on Figure 2.3:

- Process 1-2: isentropic expansion in a turbine or expander
- Process 2-3: isobaric heat rejection in the condenser
- Process 3-4: isentropic compression in a pump
- Process 4-1: isobaric heat addition in a boiler
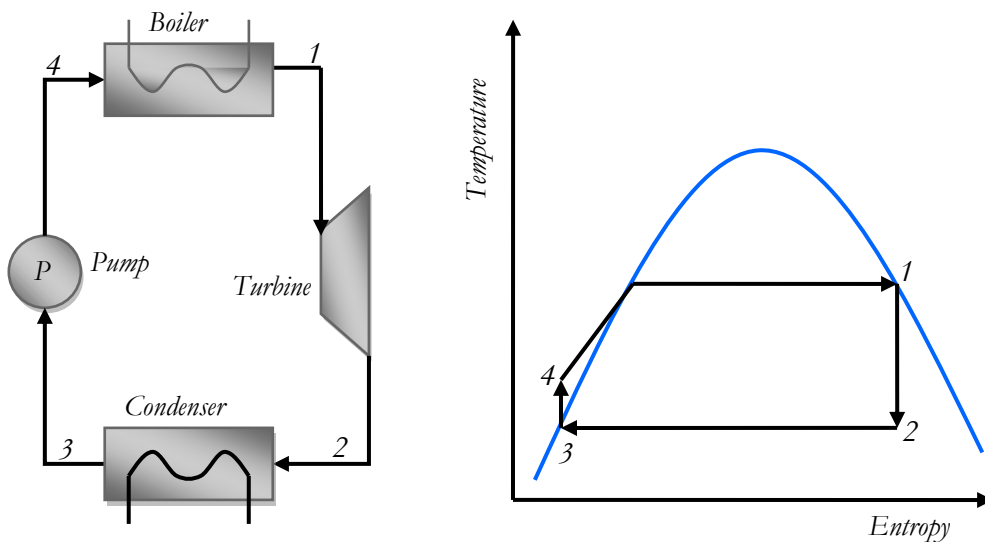
Figure 2.3 – Schematic of the Rankine cycle

Using equation 2.1 with $\dot{Q}_{in} = \dot{m}(h_1\text{-}h_4)$ and $\dot{Q}_{out} = \dot{m}(h_2\text{-}h_3)$, the thermal efficiency of the ideal Rankine cycle can be evaluated.

$$\eta_{th}^R = 1 - \frac{h_2\text{-}h_3}{h_1\text{-}h_4} \tag{2.3}$$

Where h_j (j=1-4) is the specific enthalpy at different points of the cycle.

In steam Rankine cycles, efficiency improvements can be achieved through regeneration as will be discussed later by integration of superheater or feedliquid heaters, by reheating and by increasing the boiler pressure in transcritical or supercritical cycles. The Rankine cycle devised by *Clausius and Rankine* constitutes the basic cycle for vapour based-heat engines and is widely used for power generation in thermal plants fueled by coal, gas, oil or nuclear materials. However, the environmental concerns and the future depletion of fossil fuels resources, have in recent years directed the attention of the scientific community towards more environmentally friendly fuels such as solar, biomass and geothermal resources.

2.4.1.2 Inventor's short history

Figure 2.4 - William John Macquorn Rankine (1820-1872)

William John Macquorn Rankine (Figure 2.4) was a Scottish mathematical physicist and engineer who was one of three founders along with German physicist Rudolph Clausius and English physicist William Thomson, of "Theoretical Thermodynamics". His publication record consists of several hundreds of papers and notes on science and engineering topics. He is author of several manuals which were used several decades after their publication in the 1850s and 1860s. Among his important works are (O'Connor and Robertson, 2005): A Manual of Applied Mechanics (1858), Manual of the Steam Engine and Other Prime Movers (1859), Civil Engineering (1862), Useful Rules and Tables Relating to Mensuration, Engineering, Structures and Machines (1866), Machinery and Millwork (1869), and Mechanical Textbook (1873). In 1853, he introduced the concept of "*Potential Energy*". One of the chapters of his 1859 book titled "*Principles of Thermodynamics*" is said to be the first treatise in Thermodynamics. He was honored by many scientific societies: Royal Society of Edinburgh (1849), Royal Society of London (1853), American Academy of Arts and Sciences (1856) and Royal Swedish Academy of Sciences (1868).

2.4.2 Trilateral flash cycle

It is being widely recognized in a heat engine for which the heat source temperature varies as it is cooled by the working medium as in the case of binary geothermal power plants or waste heat recovery systems, that the rectangular Carnot cycle as reference cycle for efficiency is not appropriate. Another cycle is being proposed for such cases by several authors (Wilson, 1986; Badr et al., 1986; DiPippo, 2007; Bryson, 2007) named triangular or tri-lateral cycle. Such a cycle is depicted in Figure 2.5. Four processes are observed. The working fluid in the boiler absorbs the heat at constant pressure (4-1), and then the saturated liquid is expanded in the turbine (1-2). After the expansion, the mixture of liquid and vapour is passed through the condenser in which the vapour is condensed back to liquid an then the wholly liquid working fluid is cooled at a low pressure (2-3). The cycle is completed when the sub-cooled liquid is pumped back to the boiler (3-4).
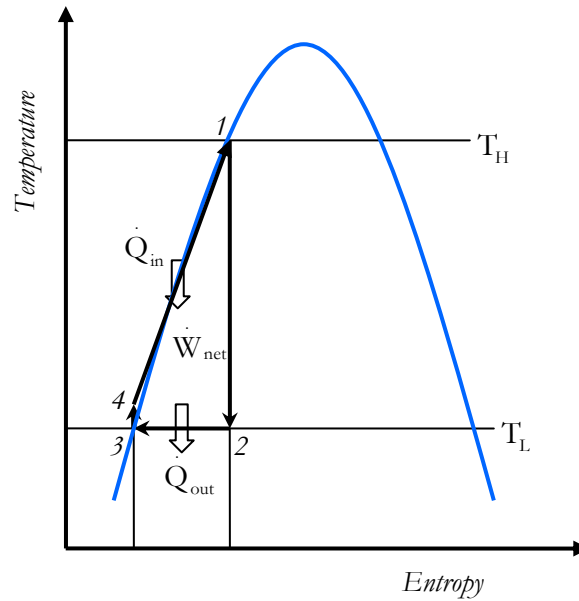
Figure 2.5 – Schematic of a trilateral flash cycle

Using Figure 2.5, the cycle efficiency can be evaluated. For the sake of simplification, the work of the pump is neglected and thus, the efficiency of the trilateral cycle derived from equation 2.1 becomes (Bryson, 2007):

$$\eta_{th}^{TR} = \frac{\dot{W}_{net}}{\dot{Q}_{in}} = 1 - \frac{\dot{Q}_{out}}{\dot{Q}_{in}} = \frac{T_H - T_L}{T_H + T_L} \tag{2.4}$$

With $\dot{Q}_{in} = \frac{1}{2}[T_H(s_2 - s_3) - T_L(s_2 - s_3)] + T_L(s_2 - s_3)$ and $\dot{Q}_{out} = T_L(s_2 - s_3)$. T_H and T_L represent the absolute temperature of the heat source and that of the cold sink, respectively. It is obvious from equations 2.2 and 2.4 that the efficiency of a trilateral cycle is lower compared to that of a Carnot cycle.

The possibility of using the trilateral cycle for power generation is being investigated. Recently, Zamfirescu and Dincer (2008), proposed an ammonia-water trilateral Rankine cycle for power generation. Their cycle uses no boiler and the saturated liquid at the pump exit is flashed by a positive displacement expander (e.g. reciprocating, centrifugal, rotating vane, and screw or scroll type expander). The proposed cycle showed good performance in comparison with Rankine and Kalina cycles. A series of research focusing the power generation using two-phase expanders in trilateral flash cycles (TFC) and the replacement of throttle valves in large vapor compression systems were carried out at City University, United Kingdom, by Smith et al., (2001a; 2001b; 2005), where they built and tested screw machines which can work in two-phase flows with satisfactory performance of 70% in expansion mode and 80% in compression mode.

2.4.3 Brayton cycle

The Brayton cycle (Joule cycle) is the thermodynamic cycle upon which all gas turbines operate. Figure 2.6 shows the simple gas turbine configuration and the cycle in a T-S diagram. The cycle consists of four processes. A compression occurs in a compressor (1-2), then, follow a heat addition at constant pressure in the combustion chamber (2-3) and an expansion process in the turbine (3-4). A constant pressure cooling process (4-1) closes the cycle.
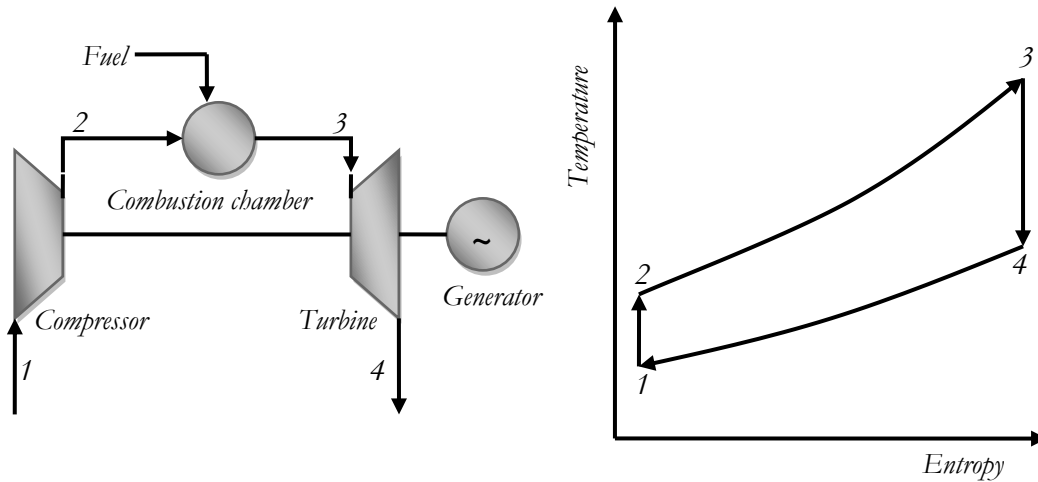
Figure 2.6 – The Joule/Brayton cycle

Assuming processes 1-2 and 3-4 are isentropic and processes 2-3 and 4-1 isobaric, the thermal efficiency of the Brayton cycle is given by

$$\eta_{th}^{BR} = \frac{\dot{W}_{net}}{\dot{Q}_{in}} = 1 - \frac{\dot{Q}_{out}}{\dot{Q}_{in}} = 1 - \frac{T_4 - T_1}{T_3 + T_2} = 1 - \frac{1}{r_p^{(k-1)/k}} \tag{2.5}$$

Where T_j (j=1-4) is the absolute temperature, $r_p = P_2/P_1$ is the pressure ratio and k the specific heat ratio. It is obvious from equation 2.5 that the efficiency of the cycle strongly depends on the pressure ratio and the firing temperature. Other factors affecting the performance of a gas turbine are fuel type, site location, air quality (humidity, temperature), steam injection, etc. Although the exhaust is released at temperature of 400-600 °C, and represents significant amount of energy lost, modern gas turbines offer higher efficiency (up to 43.8%) and power output from 0.2 up to 270 MWe. A review of major modern gas turbines can be found in Poullikkas (2005). The exhaust heat in the gas turbine engine represents a significant amount of heat wasted which can be recovered using a bottoming cycle such as Rankine or Kalina cycles, thus increasing the overall efficiency of the power plant up to 60%.

2.4.2 Stirling and Ericsson cycles

Stirling and Ericsson cycles like Carnot cycle involve two isothermal processes. They differ from the Carnot cycle in that the two isentropic processes are replaced by two constant-volume regeneration processes in the Stirling cycle and by two constant-pressure regeneration processes in the Ericsson cycle. Figure 2.7 shows the P-v and the T-s diagrams of Stirling cycle.

1-2: isothermal compression, 2-3: isochoric heat addition
3-4: isothermal expansion, 4-1: isochoric cooling
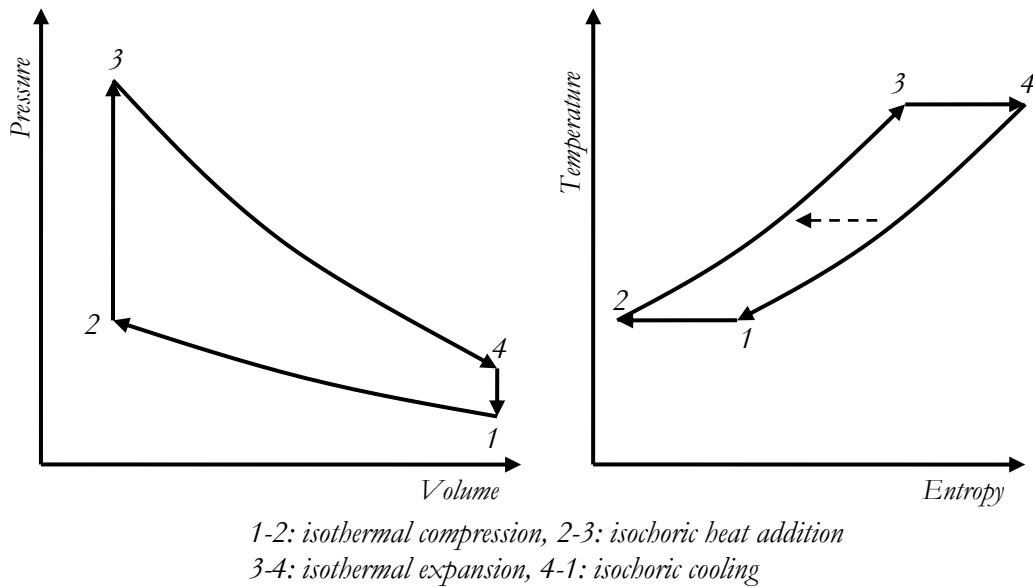
Figure 2.7 – The Stirling cycle

For an ideal Stirling–cycle engine (perfect regeneration), the thermal efficiency can be determined by (Kontragool and Wongwise, 2006):

$$\eta_{th}^{ST} = \frac{\dot{W}_{net}}{\dot{Q}_{in}} = 1 - \frac{T_1}{T_3} \tag{2.6}$$

As it can be seen from equation 2.6, the efficiency of the Stirling cycle engine strongly depends on the temperatures and equals the Carnot efficiency, and thus has the potential of reaching very high efficiencies.

The Stirling cycle can be achieved by combination of various machine components. The cycle provides a constant-volume process during the transfer of working fluid between the hot and cold space of the engine, and provides a constant-temperature heating and cooling process during compression and expansion. The compression and expansion processes of the cycle generally take place in a cylinder (power cylinder) with a piston (power piston). A displacer piston (displacer) shuttles the working fluid back and forth through the heater, regenerator, and cooler at constant volume. Three different configurations of the Stirling engine are commonly used. These configurations shown on Figure 2.8 are the alpha-, the beta- and the gamma-configurations. In all these configurations, the displacer plays the same role, which is to displace the working fluid from hot space to the cold space and vice versa.
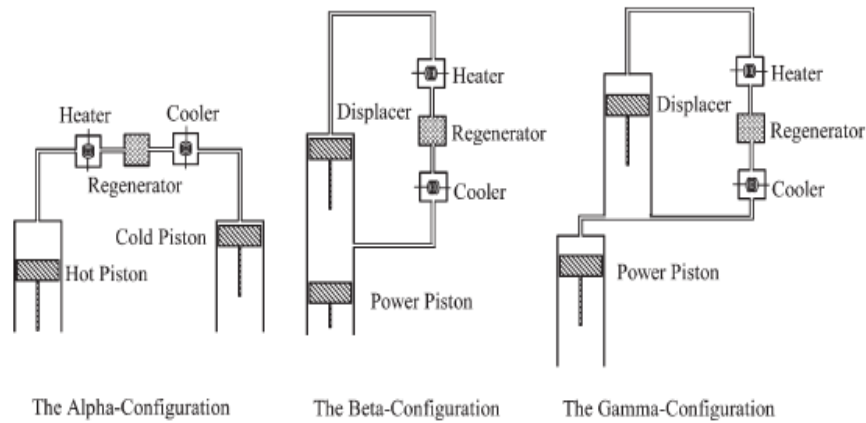
Figure 2.8 – Stirling engine configurations

Stirling and Ericsson engines are mechanical devices working theoretically on the Stirling and Ericsson cycles or their modifications. Early studies on Stirling and Ericsson engines focused only on theoretical aspects, because they were difficult to achieve in practice. However, there is a renewed interest on these engines because of their potential for higher efficiency and better emission control. As external combustion engines, the fuel for these engines is burned outside the system; allowing a more efficient combustion process and a variety of fuels such as solar energy, waste heat, or various biomass products to be used. Working fluids suitable for these engines are methane, helium, hydrogen and air.

Figure 2.9 - Micro-Biomass Stirling CHP and Solar Euro-Dish Stirling Concentrator
(Sources: Dong et al., 2009 and www.quaschning.de)

Recent reports give account of the development of small scale Stirling biomass and solar energy power systems. Typical operating temperature of these systems is about 900-1073 K resulting in an electric efficiency of about 25-40%. These power systems are well adapted for distributed electricity generation especially in remote areas. Figure 2.9 shows two prototypes of micro-stirling power generation systems. Biomass Stirling engines could use all kinds of biomass, e.g. agricultural waste, log or wood chips, sawdust, pellets, shells of fruits as fuel. Several prototypes were constructed and successfully tested in Austria with power output from 3 to 75 kWe (Podesser, 1999; Biedermann et al., 2004, Lensu and Alakangas, 2004). Solar dish engines have been under investigation for several decades now with power output from 5 up to 100 kW (Mills, 2004; Trieb et al., 1997). They offer great

modularity and possibility of hybridization with fossil fuels. Their implementation has been very slow because of the high cost of associated equipments.

2.4.3 Otto and Diesel cycles

The Diesel cycle is the ideal compression-ignition (CI) cycle and is very similar to the Otto cycle, the difference being that the heat addition occurs at constant pressure (Figure 2.10). Practically, in CI engines, the air is compressed to a temperature above the auto-ignition temperature of the fuel and the combustion starts when the fuel is injected while in SI engines, the air-fuel mixture is compressed to a temperature that is below the auto-ignition temperature of the fuel and the combustion is initiated by a firing spark plug. Using equation 2.1, the thermal efficiency of the Diesel cycle can be expressed as:

$$\eta_{th}^{Diesel} = \frac{\dot{W}_{net}}{\dot{Q}_{in}} = 1 - \frac{T_4 - T_1}{k(T_3 - T_2)} = 1 - \frac{1}{r^{k-1}} \frac{r_c^k - 1}{k(r_c - 1)} \qquad (2.7)$$

With $\dot{Q}_{in} = \dot{m} c_p (T_3 - T_2)$, $\dot{Q}_{out} = \dot{m} c_v (T_4 - T_1)$. T_j (j=1-4), r and k stand for the temperature at different states, the compression ratio (v_1/v_2) and the specific heat ratio (c_p/c_v), respectively. r_c (v_3/v_2) is the cutoff ratio defined as the ratio of the cylinder volumes after and before the combustion process. Diesel engines operate at much higher pressure than do the Otto engines with a thermal efficiency of about 35-40%.

Reciprocating Otto and Diesel engines generate waste heat with temperature of about 90-400 °C, thus allowing its recovery by bottoming cycles such as Rankine, Kalina cycle or a thermoelectric device. These engines can be integrated into Combined Heat and Power (CHP) system where the waste heat recovered drives a cooling machine and/or is transferred to heating coils for space heating (Moran et al., 2008; Thomas, 2008). Nevertheless, reciprocating engines bear several disadvantages (Korobitsyn, 1998) including slow work rate which makes the equipment bulky and heavy, higher noise levels, frequent maintenance, and higher environmentally harmful emissions.

Few other reciprocating engines similar to the above described but less popular exist in the literature such as Miller and Atkinson engines (Zhao and Chen, 2006 & 2007). The Atkinson engine was invented by James Atkinson in 1882, and the Miller engine patented by Ralph Miller in the 1940s. A recent interest was shown by automobile industries, Toyota, Mazda and Ford in Japan and USA which are looking for more efficient and less pollutant engines.
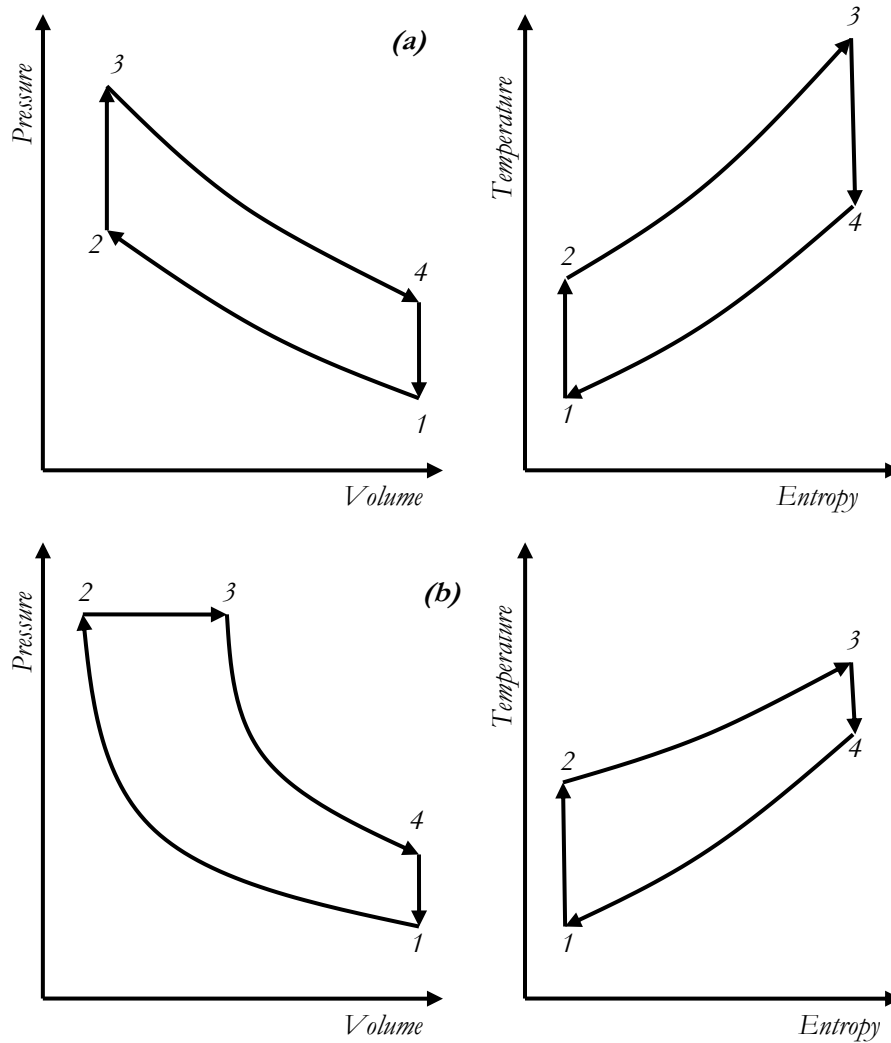
Figure 2.10 – Thermodynamic diagrams for ideal reciprocating engines: (a) Otto cycle and (b) Diesel cycle

2.5 Advanced Rankine cycles

2.5.1 Superheated Rankine cycles

In a Rankine cycle where wet fluids with high boiling points such as water, methanol or ethanol are used, the average temperature at which heat is added to the cycle can be increased during the isobaric heat addition process in the evaporator. This results in an increase in the net power output and a desirable decrease of the moisture content of the working fluid after the expansion process (Çengel and Boles, 2002). The effects of the superheating can be appreciated on the T-s diagram depicted in Figure 2.11. Superheating takes the saturated vapor (state 3) to state 3' and this results in an increase of the power output represented by the area 23'4'4 with less moisture as the expansion process ends at state 4' and not at state 4. A safe operation of the turbine is obtained when there is no droplet is the turbine during the expansion. This is obtained by superheating the saturated vapor fluid up to state 3".
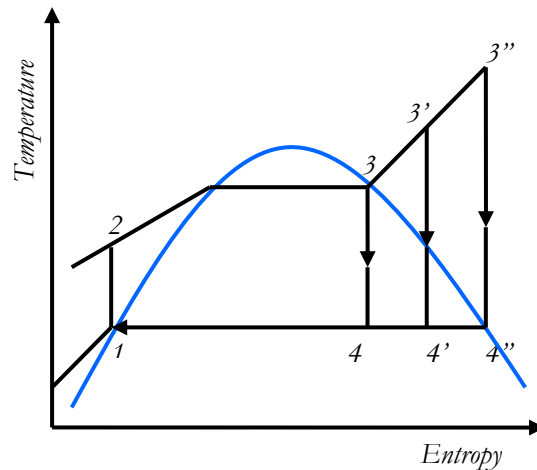
Figure 2.11 – Superheated Rankine cycles

Although the superheating has positive effects on wet fluids, this is not the case regarding dry fluids. Dry fluids possess positive saturation vapor line and the expansion process takes place in the vapor region. Thus, droplets will never appear in the turbine. Hung et al., (1997) showed that superheating increases the cycle thermal efficiency when wet fluids are used and reduces it for dry fluids. Cycle efficiency for isentropic fluids remains constant.

2.5.2 Transcritical and supercritical Rankine cycles

In a subcritical Rankine cycle, the heat addition in the boiler takes place at pressures below the critical point. Seeking for higher efficiency, the pressure in the boiler can be set above the critical pressure, giving birth to transcritical and supercritical cycles. However, the transcritical cycle for which the heat rejection takes place at a subcritical pressure, must not be confused with the entirely supercritical cycle proposed by Feher (1968) in which heat exchanges take place out of the saturation dome. Different situations can be appreciated on Figure 2.12. In practice, transcritical cycles using steam yield high efficiency (up to 45% and beyond) but require special materials and high safety precautions owing to very high pressures. In modern steam power plants the pressure could reach 375 bar and a maximum temperature of about 720 °C (Beér, 2007).

Recently, there have been attempts to use working fluids with low boiling point and low critical temperature such as organic fluids in Rankine cycles. Saleh et al. (2007), Karellas and Schuster (2008) and Schuster et al. (2009) have worked in this direction. From different studies, few conclusions can be raised: (1) efficiencies of transcritical and subcritical organic Rankine cycles are of the same order, (2) heat exchangers are more efficient when used in transcritical cycles owing to better matching with the heat source and (3) transcritical Organic Rankine Cycles in practice will require additional safety devices because of higher pressures, thus increasing the cost of such systems and slow their implementation.
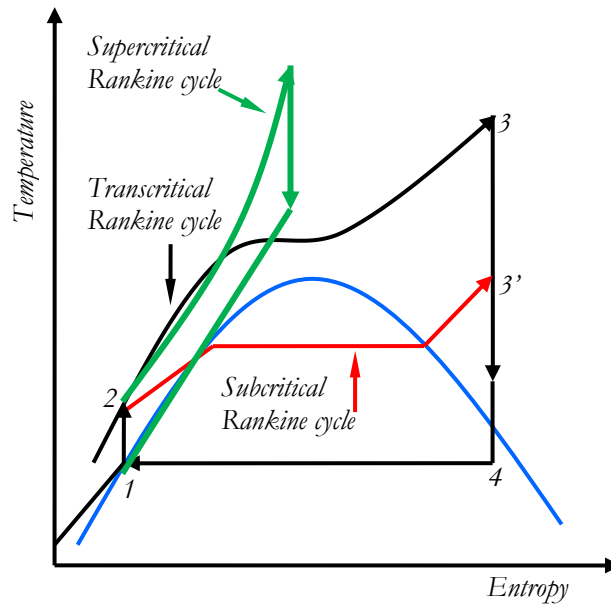
Figure 2.12 – Supercritical, transcritical and subcritical Rankine cycles

There is an increasing interest in using carbon dioxide (CO_2) as working fluid for power generation in nuclear plants, waste heat recovery systems as well as in solar thermal power installations. Carbon dioxide is chosen as working fluid for many reasons: it is abundant and environment-friendly, non-flammable, non-toxic, cheap and its thermophysical properties are well known. Chen et al., (2006), and Cayer et al., (2009), reported studies on the application of CO_2 in low-temperature transcritical Rankine cycles in waste heat recovery application. A series of theoretical and experimental investigations on solar powered Rankine cycle using transcritical carbon dioxide were carried out at Doshisha University, Japan (Zhang et al., 2006 & 2007; Yamaguchi et al., 2006).

2.5.3 Regenerative Rankine cycles

2.5.3.1 Reheat regenerative cycle

Generally, it is admitted that increasing the boiler pressure in a simple Rankine cycle using a wetting fluid such as steam increases the efficiency of the power plant. Nevertheless, it should be noted that on the other hand it could lead to excess moisture content in the turbine during the expansion process. A practical solution used in modern steam power plants is the integration of a two-stage turbine with a reheat in between. A schematic of a reheat regenerative Rankine cycle is shown on Figure 2.13. In a reheat cycle, the working fluid is expanded twice; first in the high pressure turbine (3-4) and secondly in the low pressure turbine (5-6). There is a possibility of a double reheat cycle, provided system materials can withstand very high pressures (Çengel and Boles, 2002).
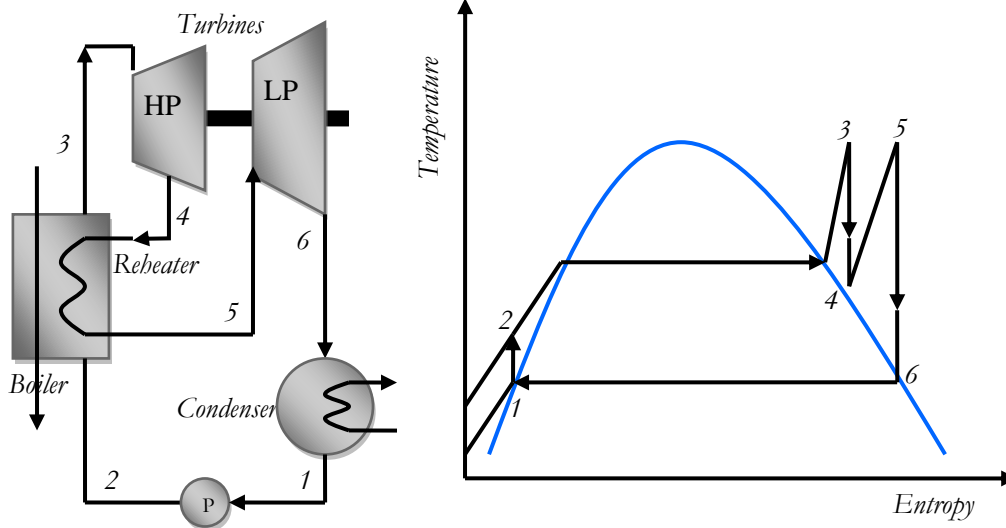
Figure 2.13 – The reheat regenerative Rankine cycle

2.5.3.2 Regenerative Rankine cycle with recuperator

Organic dry fluids with their positive slope are suitable for safe operation of the Rankine cycle system. Using such fluids, the expansion process ends in the superheated vapor zone. A regenerator/recuperator also called internal heat exchanger can be integrated into the cycle (see Figure 2.14) to increase the cycle thermal efficiency by providing additional heat to the fluid entering the evaporator: from stream 2-3 to stream 5-6. This requires that the temperature of the vapor leaving the turbine be substantially higher than the condensing temperature. Usually, as demonstrated by several studies (Dai et al., 2009; Saleh et al., 2007), dry fluids such as Pentanes, Butanes, Toluene, R141b, R245fa, R113, R123, and HFE7100 are adequate working media for Rankine cycles with integrated regenerator.
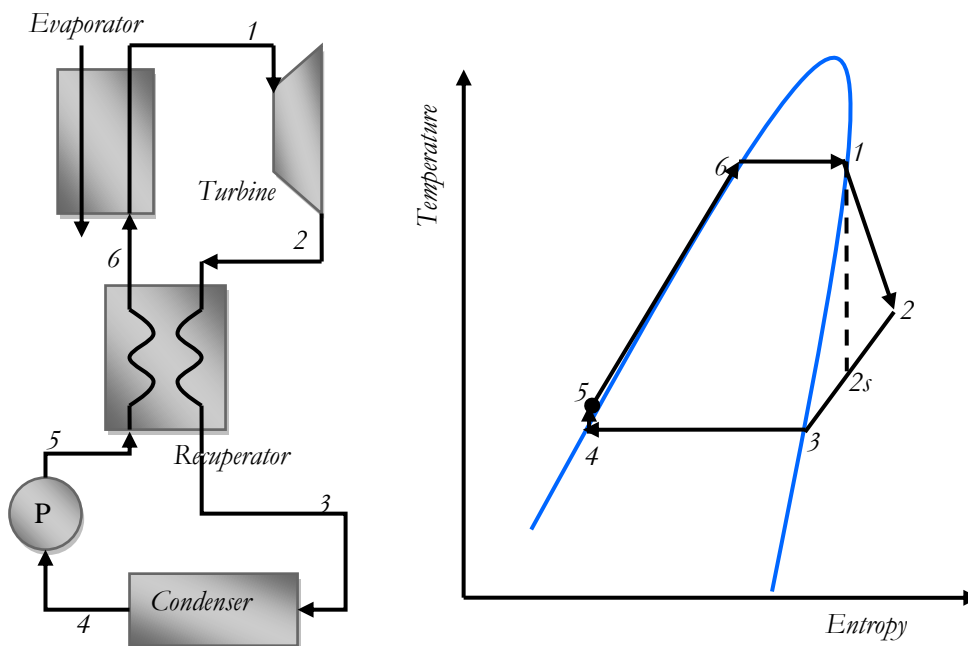
Figure 2.14 – Rankine cycle with recuperator

2.5.3.3 Regenerative Rankine cycle with feedliquid heaters
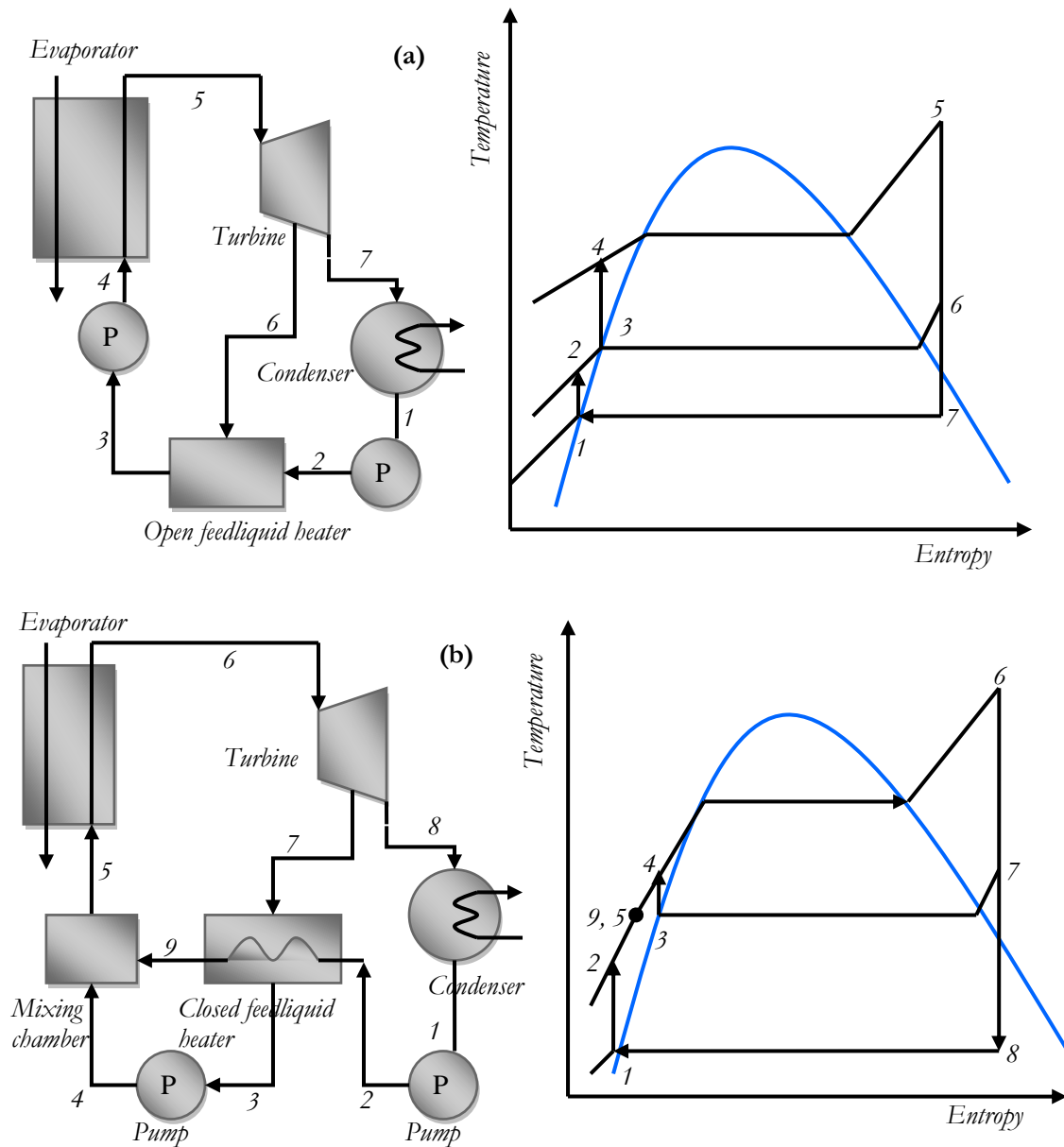
Figure 2.15 – Regenerative Rankine cycles with: (a) Open feedliquid heater and (b) Closed feedliquid heater

A constant preoccupation in fossil, biomass or solar fired Rankine based power plants is the efficiency; it should be as high as possible. The increase in efficiency is associated with the mean temperature in the evaporator. A way to increase this temperature is to incorporate into the cycle specific types of heat exchangers known as feedliquid heaters. There are two types of feedliquid heaters (Çengel and Boles, 2002). An open feedliquid heater (Figure 2.15a) is a mixing chamber where the feedliquid (2) and the extracted fluid (6) from the turbine mix. In a closed feedliquid heater (Figure 2.15b), heat from the extracted fluid (7) is transferred to the feedliquid (2) without any mixing taking place. Feedliquid heaters not only improve the thermal efficiency of the power plant, but also contribute to the de-aeration of the system and to the control of the working fluid mass flow rate. Mago et al. (2007; 2008), showed that open feedliquid heaters not only improve the energy efficiency of the organic Rankine cycle system, but also improve the exergy

efficiency and the overall thermodynamic behavior of the system as well. Srinivas et al. (2007) analyzed the effect of 'n' feedwater heaters on the performance of a steam power cycle with a generalized mathematical formulation. According to their findings, maximum efficiency is obtained with the first feedwater heater and the extent of the increment with second and next feedwater heaters is not as large as with the first.

2.5.4 Innovative absorption power cycles

Absorption power cycles use mixtures as working fluids instead of pure or single components fluids. The advantage of mixtures over pure fluids is the temperature increase during the isobaric heat exchange taking place in the evaporator that leads to a good matching of the streams and better operation of the heat exchangers. As example, taking a binary mixture of water and ammonia, the temperature glide with a mass fraction of 0.7 and a pressure of 2.5 MPa is 94 ºC (Galanis et al., 2009). First power cycle operating on this scheme was proposed by Robertson and Maloney in 1953. However, the cycle proposed didn't give satisfaction as the performance was below that of the Rankine cycle. Thus, it was abandoned for almost three decades. In the 1980s the investigations resumed and several water/ammonia power systems with performance superior to that of the pure fluid Rankine cycle system were devised. Operation and state-of-the-art of these innovative Rankine power cycles will be summarized in this section.

2.5.4.1 Maloney and Robertson cycle
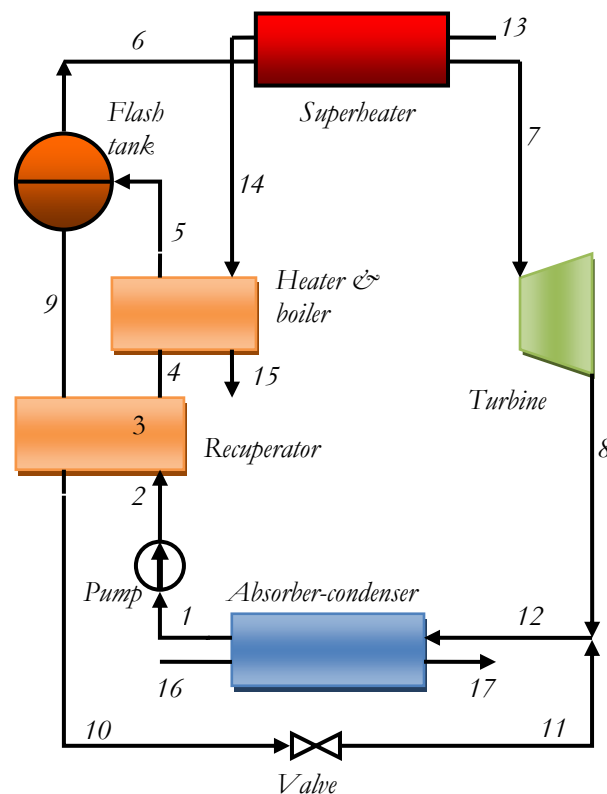
Figure 2.16 – Schematic representation of the Maloney and Robertson cycle
(Ibrahim & Klein, 1996)

The Maloney and Robertson cycle differs from the traditional Rankine cycle by the way it integrates a mixture as working fluid and a flash tank. A schematic of the cycle is depicted on Figure 2.16. The heater/boiler delivers a vapor rich in ammonia (6). The vapor is then superheated (7). Power is obtained by expanding the vapor to low pressure in a turbine. The turbine exhaust (8) is reunited with the weak solution from the distillation unit (11) and is used to absorb the rich vapor in ammonia to regenerate the basic solution (1). The basic solution is then pumped to a high pressure and then heated and partially boiled before entering the flash tank (5) to complete the cycle. Hot (13) and cold (16) fluids are used as the heat source and sink, respectively. Maloney and Robertson performed the thermodynamic analysis of their cycle based on the configuration shown in Figure 2.16, and their conclusion showed that the absorption cycle in this configuration, has no thermodynamic advantage over the Rankine Cycle and didn't continue their investigations (Ibrahim and Klein, 1996).

2.5.4.2 Kalina cycle
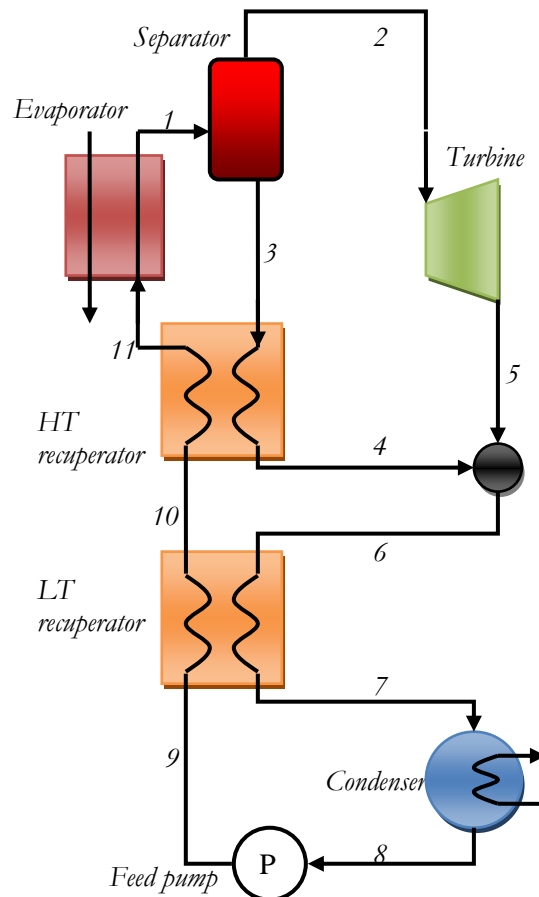
Figure 2.17 – Schematic diagram of the Kalina cycle process
(Source: Ogriseck, 2009)

Alexander I. Kalina continued the work of Maloney and Robertson on absorption power cycles and proposed several cycle designs for application in geothermal as well as in biomass power plants (Mlcak, 2002). The first of what is known as "Kalina Cycle" was

presented in 1983 (Kalina, 1984), 30 years after the Robertson and Maloney cycle was devised. Additional components namely a separator, a recuperator and an absorber were incorporated into a simple Rankine cycle to give birth to the new cycle. The cycle design used for the Husavik geothermal power plant, Iceland, is shown in Figure 2.17. The cycle in this configuration operates as follows. The ammonia-water mixture is heated in the evaporator. Before the turbine, the ammonia-rich vapor is separated from the liquid phase in a separator. Afterwards, the ammonia-rich vapor expands in the turbine. The molecular weight of the ammonia (17 kg/kmol) is close to that of the water (18 kg/kmol) and therefore it is possible to use normal back-pressure turbines. After the turbine, the vapor and liquid phases are merged together and condensed in the condenser. Because of the change in the mixing ratio, the evaporation temperature increases continuously in the two-phase region while it decreases during condensation. The recuperators included are used for residual heat management within the cycle.

At its beginning many authors including the inventor, claimed theoretical advantages of the Kalina cycle over the Rankine cycle. Thermal efficiencies 10 to 60% higher than comparable steam plants were reported (Galanis et al, 2009). However, recent studies do not confirm the "remarkable" superiority of the Kalina cycle over the Rankine cycle. DiPippo (2004) performed the comparison of existing geothermal plants using the second Law of Thermodynamics. The plants under investigation included the Husavik plant. He concluded that under identical conditions of ambient temperature and cooling systems, the calculated performance difference is about 3% in favor of a Kalina cycle. More recently, Bombarda et al. (2009) compared Kalina and Rankine cycles in waste heat recovery application. Although the Kalina design produced slightly more power, it is less cost-effective compared to organic Rankine cycle because of the high evaporator pressure and large evaporator surface required. The commercial marketing of this power generating system despite recent developments has been too slow and a very small number of plants based on Kalina principle are in operation (Table 2.1).

Table 2.1 – Kalina based power plants (Ogriseck, 2009)

Plant /location	Heat source	Power output (MW)	Start up
Canoga Park (USA)	Exhaust gas of gas turbine (515 °C), solar centaur gas turbine	3 / 6.5	1992-1996
Fukuoka City (Japan)	Waste heat from incineration plant	5	1999
Kashima steel works (Japan)	Waste hot water (98 °C)	3.1	1999
Husavik (Iceland)	Geothermal heat (124 °C)	2	2000
Unterhaching (Germany)	Geothermal	3.4	2007

2.5.4.3 Uehara cycle

At the Saga University, Japan, Uehara et al. (1994) examined various cycles for implementation in ocean thermal energy conversion (OTEC) plants. A particular attention on the Kalina cycle operating at very low temperature (~25 °C) revealed the poor performance of the heat exchangers. They proposed as solution a novel cycle called "Uehara cycle". It is an improved Kalina cycle in which a second turbine, a heater and an after-condenser are added. A schematic representation of the cycle is depicted on Figure

2.18. A prototype was later constructed and tested (Uehara et al., 1997). The Uehara cycle uses a mixture of ammonia and water as the working fluid. The processes taking place in the Uehara cycle are described as follows. First, the warm surface seawater flowing in the evaporator heats up the working fluid mixture. The working fluid then turns into a mixed vapor of ammonia and water and moves into the separator where it is separated into ammonia/water and vapor of ammonia/water. The mixed vapor turns the first turbine. Part of the mixed vapour is extracted by the heater and the rest is directed to the second turbine. In the meantime, water-ammonia separated in the separator passes through the regenerator and then into the absorber via a diffuser. The mixed vapour from the second turbine is absorbed with ammonia/water in the absorber. Some of the mixed vapour which cannot be absorbed with ammonia water is cooled and condensed by the cold seawater and turns into liquid. The working fluid pumps take this fluid into the heater, the regenerator and then to the evaporator, thus the cycle is repeated. With 28 °C warm seawater and 6 °C cold seawater, Uehara cycle yields 5.4% thermal efficiency, that is 10% higher than that of the Kalina cycle and 30% larger than that of Rankine cycle operating with ammonia (Uehara et al., 1994).
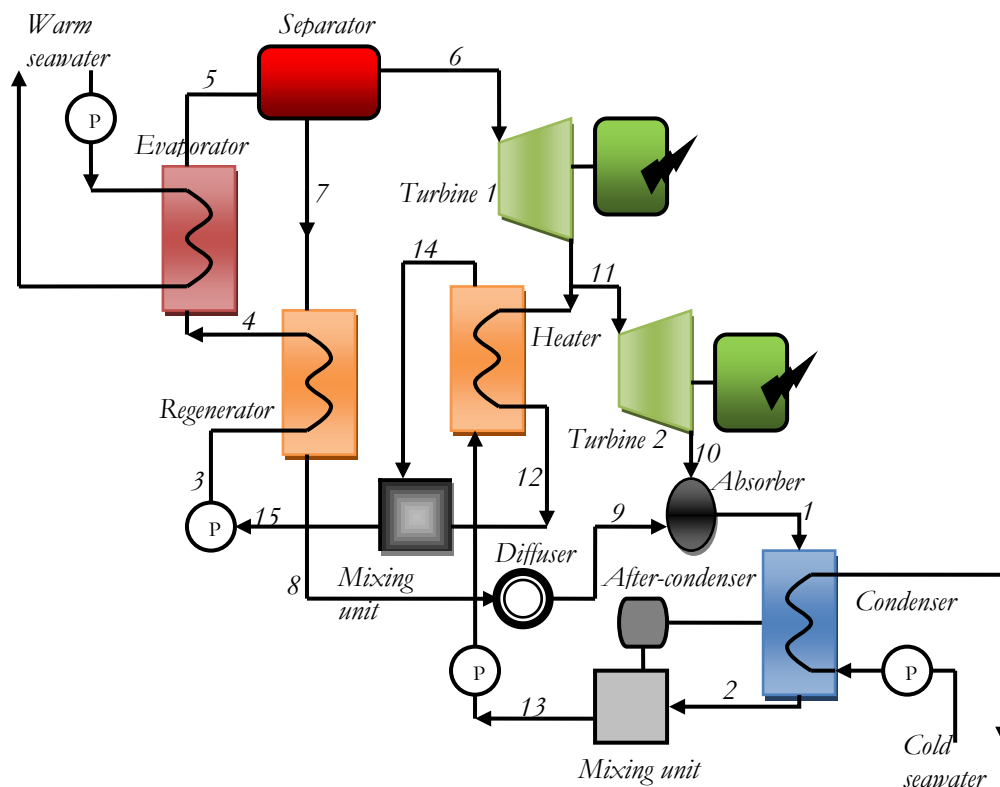
Figure 2.18 – Schematic representation of the Uehara cycle
(Source: Uehara, 1997)

2.5.4.4 Combined power/cooling cycle

The combined power/cooling cycle was invented by Goswami and his colleagues in 1995 (Xu et al., 2000). It combines two thermodynamic cycles, the Rankine cycle and the ammonia-absorption refrigeration cycle. A schematic of the Goswami cycle is shown in Figure 2.19. The ammonia/water mixture used as working fluid undergoes a certain number of processes. A strong mixture of ammonia/water leaves the absorber at saturated

liquid at low pressure (1). After the absorber the mixture is pumped to a high pressure (2) and preheated before entering the boiler by recovering heat from the weak hot solution returning to the absorber. In the next step, the mixture is partially boiled in a boiler (4). A condenser/rectifier is used to increase concentration of volatile component (ammonia) in the vapor, by partially condensing water out of the vapor from the boiler (6). The condensate is richer in water and returned to the boiler (5). Ammonia is superheated after the condenser/rectifier to raise its temperature (7). The superheated vapor, which is almost pure ammonia, can be expanded through a turbine to produce work (8). Due to the low boiling point of ammonia the expanded vapor after turbine yields the potential for refrigeration. The vapor is finally absorbed back into the liquid, giving off heat as the cycle heat output (9). Since its invention, the combined power/cooling cycle has been the focus point of intense investigation as it is being considered as promising for solar as well as for geothermal applications. Optimum operating conditions of the cycle have been investigated by Sandrameli and Goswami (2007), Vijayaraghavan (2003) and Pouraghaie et al. (2010). A prototype was built and tested at the University of Florida by Tamm (2003).
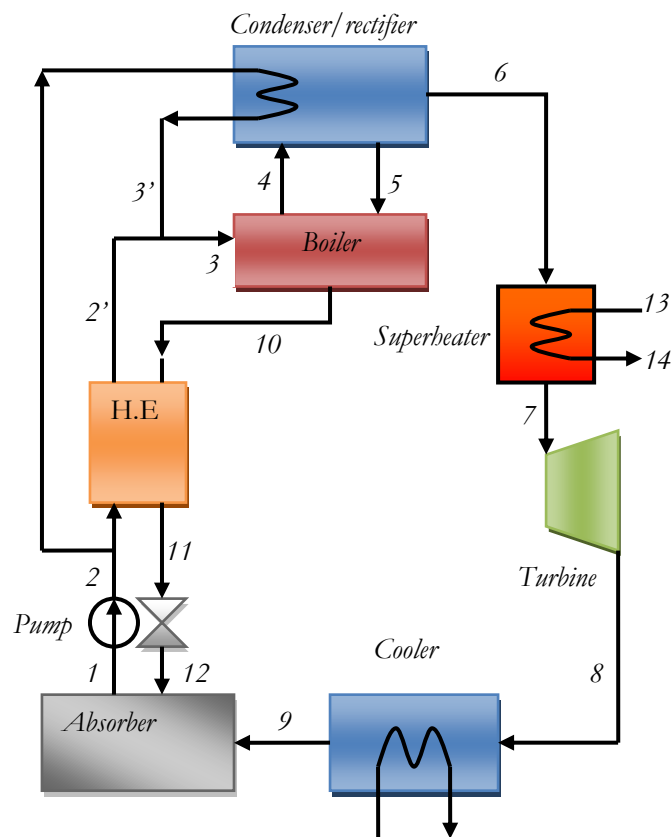
Figure 2.19 – A combined ammonia-based combined power/cooling cycle
(Source: Xu et al., 2000)

2.5.5 Rankine combined cycles

In section 2.4 a recall of major power cycles was done showing differences between various existing engineering designs. Some engines possess a high maximum temperature and reject heat at relatively high temperature. On the other hand, others have moderate maximum temperature and reject heat at a temperature close to the ambient temperature. A

classification of different cycles according to their maximum temperature was done by Korobitsyn (1998) and is duplicated in Figure 2.20. He examined theoretically and technically achievable combinations: Brayton/Brayton, Otto/Kalina, Rankine/Kalina, Fuel cell/Stirling, etc. Kalina and organic Rankine cycles operate at the lowest maximum temperature, making them potentially suitable to recover the heat exhausted from high temperature fuel cells, gas turbines and diesel engines.

At the moment the concern is growing in regard to the increasing energy demand and the inherent environmental pollution, combined power cycles have an important role to play. Combined cycles provide several advantages (Poullikas, 2005; Beér, 2007): higher thermal efficiency (up to 60%), low emissions of harmful substances (NOx, CO, CO_2, SOx, etc), low capital costs and short construction time and flexibility in plant size.
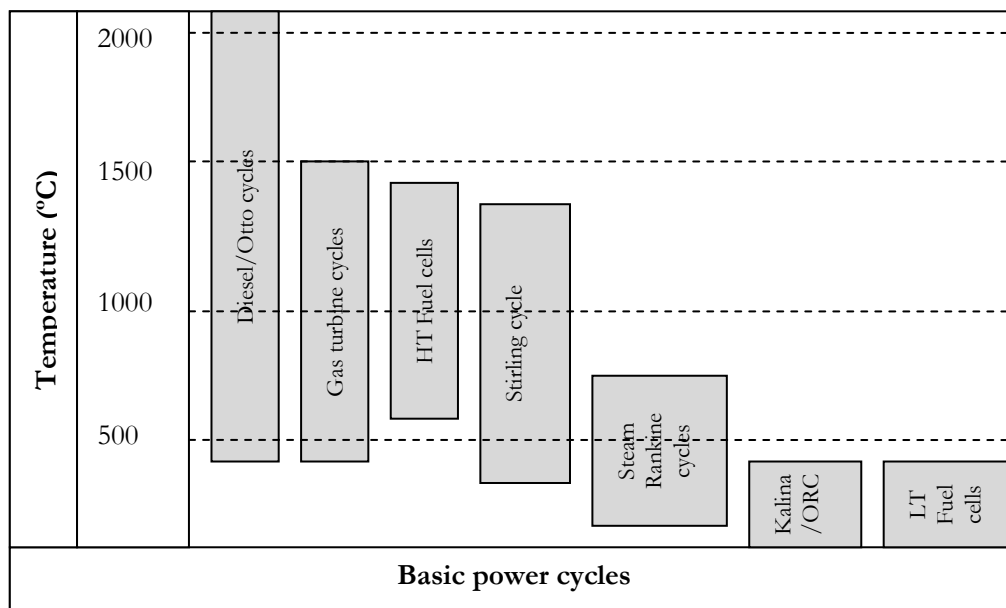
Figure 2.20 – Basic power cycles classification with respect to the operating temperature (Adapted from Korobitsyn, 1998)

2.6 Conclusion

In this chapter, major thermodynamic power cycles were presented to highlight the differences with the basic Rankine cycle as devised by William J.M. Rankine. Emphasis was given to Rankine vapor power cycles and various derivate cycles. Using single component fluids such as steam, hydrocarbons and refrigerants, the efficiency of the traditional Rankine cycle can be increased trough regeneration processes i.e. a temperature increase in the evaporator. Provided the materials are well selected to resist at high temperature and pressure, supercritical and transcritical can achieve very high thermal efficiencies. In view of reducing the exergy losses in heat exchangers, the use of ammonia-water mixtures is being proposed in Kalina, Uehara and Goswami cycles. Rankine cycles by the way they operate at lower temperature compared to gas power cycles, are suitable for waste heat recovery, which leads to higher overall efficiencies and considerable fuel savings.

3 - Organic Rankine Cycle Applications

3.1 Introduction

The Rankine cycle is one of the most important ways to transform on large scale thermal energy into mechanical or electrical power. Main components forming the cycle are: steam generator (in which the thermal energy is supplied), a turbine (in which the working fluid expands), a condenser (cools the working fluid) and a pump (feeds the steam generator). Schematic of a conventional steam power plant is depicted in Figure 3.1.
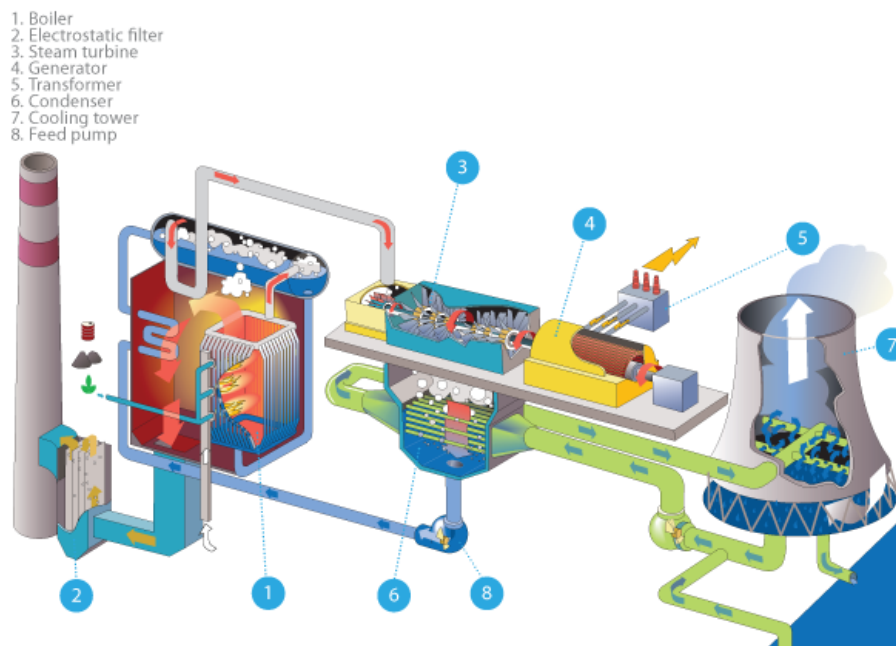
Figure 3.1 – Schematic of a steam power plant
(Source: www.orcycle.be)

The Rankine Cycle from its origin is usually implemented with water as the working fluid. Water has very small molecular weight (18 kg/kmol), a high boiling point of 100 °C, and a critical temperature of 374 °C. Its *T-s* diagram is in form of a bell that characterizes wet fluids (Figure 3.2). The main benefits to using water as working fluid are that water is chemically very stable and no special requirements are therefore needed for construction materials. Moreover, water has a very low viscosity and the power needed for its transportation is limited. The specific heat of water (4.18 kJ/kg.K) is relatively high, and this makes it a good energy carrier. Water is also cheap, abundant, non-toxic and has no negative impact on the environment.

However, many problems are encountered when using water/steam as working fluid: need of superheating (up to 600 °C) to prevent condensation during expansion, risk of erosion of turbine blades, excess pressure in the evaporator, complex and expensive turbines due to large steam volumes at the turbine exit. Because of the aforementioned reasons, water is more suitable for high temperature applications and large centralized systems.
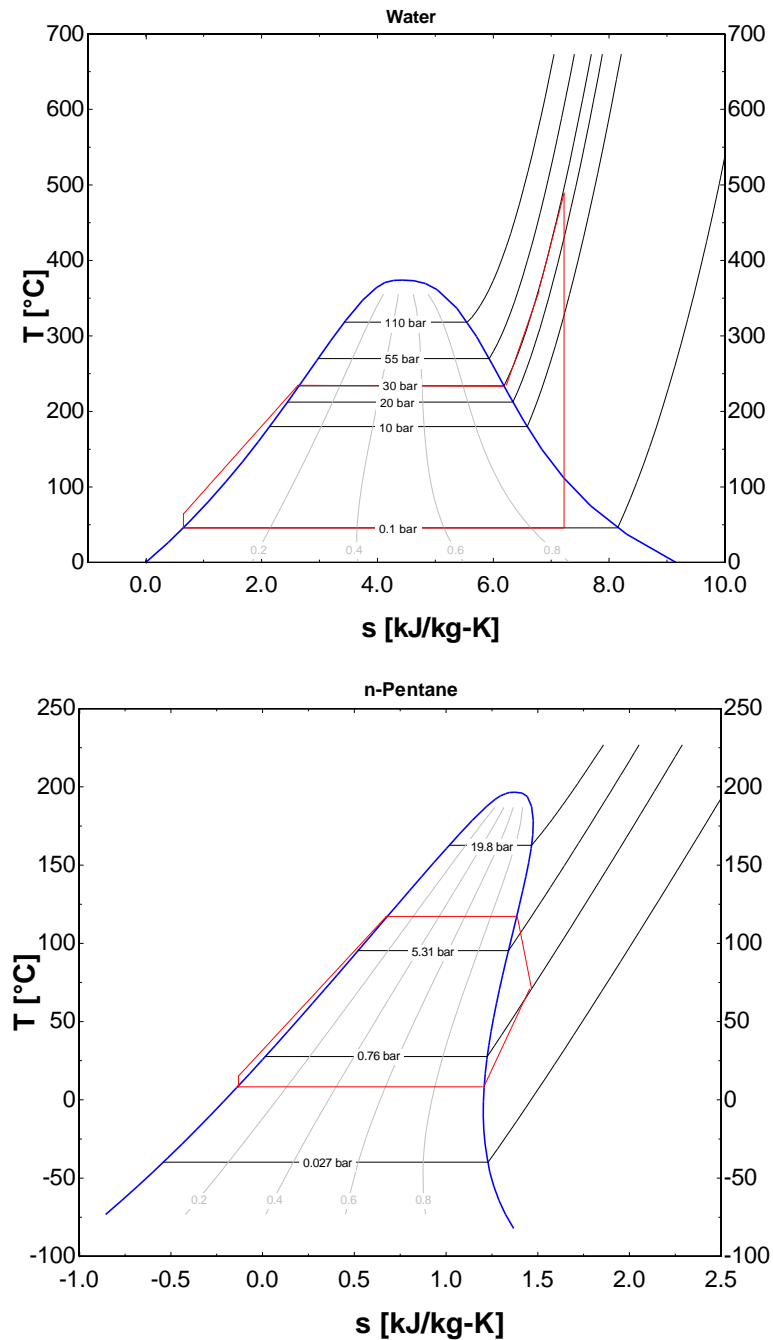
Figure 3.2 – T-s diagrams of water and that of an organic fluid

The problems encountered with water can be partially mitigated by selecting an appropriate fluid. Organic compounds characterized by higher molecular mass and lower ebullition temperature than water can be used in so called "Organic Rankine Cycles". An organic Rankine cycle presents several advantages (Tchanche et al., 2010c). In comparison with water, less heat is needed to evaporate an organic fluid. The evaporation of organic fluids takes place at lower pressure and temperature. Usually the expansion process ends in the vapor region and hence the superheating is not required and the risk of blades erosion is avoided (see Figure 3.2). The smaller temperature difference between evaporation and condensation also means that the pressure drop/ratio will be much smaller and thus simple single stage turbines can be used. This makes ORCs suitable for small and medium scale applications.

Although investigated since the 1880s, organic Rankine cycles have never been popular until today's growing concern over the future depletion of fossil fuels and the global warming is turning the interest on low-grade energy recovery systems.

Depending upon the working fluid, an ORC can suitably recover heat from various sources: solar energy, geothermal heat sources, biomass combustion, industrial waste heat, etc. In this chapter, most developed applications are reported and analyzed from technical and economical viewpoints.

3.2 ORC applications

3.2.1 Binary geothermal power plants

The Earth is increasingly warmer the deeper one goes. At some points of the Earth's surface, such as Iceland, temperature of up to 1000 °C exists just several meters from the surface. This underground energy usually called geothermal energy can be used for electricity generation or for process heat in buildings, industries and farm structures.

First use of geothermal energy for electricity generation started in Italy with experimental work by Prince Gionori Conti in 1904-1905. And first commercial plant of 250 kWe is reported to have been erected in 1913 at Larderello, Italy (Lund, 2006). These developments were followed by New Zealand (1958), Mexico (1959), USA (1960), Japan (1966) and Russia (1967). Currently, there are 504 geothermal power plants in operation in 27 countries with a combined installed capacity of about 10 GW (DiPippo, 2008). Major types of geothermal power plants are: dry steam, single-flash, double-flash and binary-cycle plants. Comparison between available options is summarized in Table 3.1. Flash systems are used for moderate and liquid-dominated resources, dry steam plants for dry-steam resources and binary cycles are well adapted for low temperature liquid-dominated resources.

Table 3.1 – Comparison of different types of geothermal plants (Source: DiPippo, 2008)

Type	Resource temperature (°C)	Utilization efficiency (%)	Plant cost and complexity
Double-flash	240-320	35-45	Moderate ►high
Dry-steam	180-300	50-65	Low-moderate
Single-flash	200-260	30-35	Moderate
Basic binary	125-165	25-45	Moderate ►high

In a binary plant (Figure 3.3), the thermal energy of the geofluid is transferred to a secondary working fluid via a heat exchanger for use in a conventional Rankine cycle. The organic working fluid (Butanes, Pentanes, etc) chosen for its appropriate thermodynamic properties receives heat from the geothermal fluid evaporates and drives the turbine before being condensed and returned back to the evaporator by the feed pump. Cooling is assured by air coolers, surface water cooling systems, wet-type cooling towers or dry-type cooling towers.
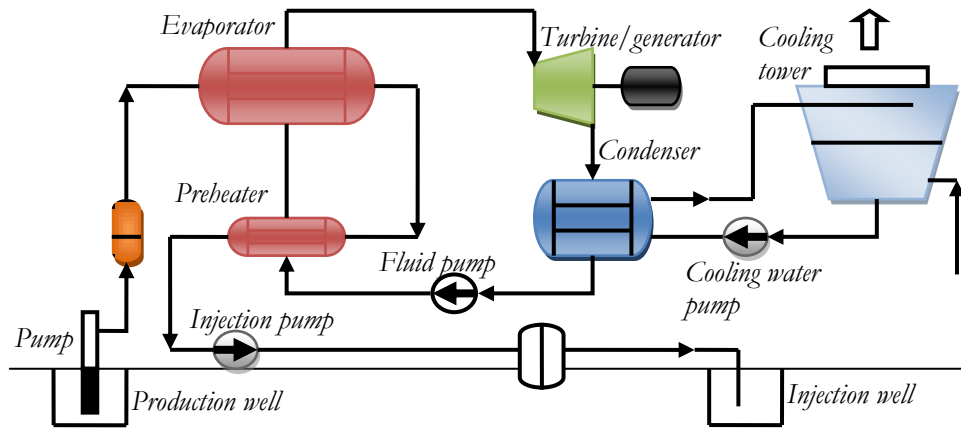
Figure 3.3 – Flow diagram for a binary geothermal power plant
(Source: DiPippo, 2008)

The first binary geothermal plant was put into operation at Paratunka, Russia in 1967. It was rated at 680 kWe using water at a temperature of 81 °C – the lowest temperature ever reported in the world for electricity generation from geothermal energy. The later proved the feasibility of binary concept. For low temperature geofluids below 150 °C, it is difficult to implement cost effective flash steam plants. Therefore, the binary option is the sole solution for low temperature heat resources. Today, binary power plants are the most widely used type of geothermal power plant with 162 units, generating 373 MW of power. They constitute 32.14% of all geothermal units in operation but generate only 4% of the total power (DiPippo, 2008). Few binary plants are given in Table 3.2.

Table 3.2 – Few binary ORC geothermal power plants

(Sources: Bloomquist, 2003; DiPippo, 2004; Kanoglu and Bolatturk, 2008)

Plants/location	Resource temp. (°C)	Resource mass flow	Working fluid	Gross/Net power (MW)	Thermal efficiency (%)
Amedee, USA	104	205 *l/s*	R-114	2.0/1.5	-
Wineagle, USA	110	63 *l/s*	isobutane	0.75/0.6	-
Altheim, Austria	106	86 *l/s*	-	-/1.0	-
Otake, Japan	130	14.661 *kg/s*	isobutane	-/1.0	12.9
Nigorikawa, Japan	140	50 *kg/s*	R-114	-/1.0	9.81
Reno, NV, USA	158	556 *kg/s*	isobutane	27/21.744	10.2

In geothermal plants, the constant preoccupation is the optimal resource utilization. This is measured in terms of energy and exergy efficiencies. However, it should be pointed out that since the brine cools down as it transfers heat to the working fluid, a more realistic ideal cycle for a geothermal binary power plant is a triangular cycle instead of the Carnot cycle (DiPippo, 2007). And a reasonable approach for plant optimization is the power output instead of the thermal efficiency as the heat source is free. According to Borsukiewicz-Gozdur & Nowak (2007a), geothermal water mass flow should be appropriately chosen for power maximization. Kanoglu and Bolatturk (2008) performed the thermodynamic analysis of the Reno binary plant. The investigated plant which receives geothermal fluid at 158 °C and uses isobutane as working fluid yields an exergy efficiency of 21% and has an energy efficiency of 10.2%. The brine reinjected at relatively high

temperature 90 °C, accounts for 35.3% of exergy losses and 55.7% of energy losses. Thus it is suggested that the water injected in the wells at temperature around 50-90 °C being used for district heating to realize the so-called combined heat and power (CHP) to increase the overall efficiency of the plant.

An important component of binary systems is the working fluid. These should be well selected so as to decrease the exergy destroyed in heat exchangers by better matching with the brine, minimize heat exchangers and turbine size and provide maximum power output. Health, safety and environmental characteristics of the fluid should not be overlooked. Saleh et al. (2007), DiPippo (2008), Madhawa et al. (2007) and Borsukiewicz-Gozdur and Nowak (2007b) investigated potential candidates for binary plants. From the aforementioned studies, ammonia, butanes, pentanes and synthetic fluids such as R-245fa and R-227ea are well suited for ORC binary plants.

New designs have been proposed for better utilization of geothermal resource. These include dual-pressure and dual-fluid binary cycles, combined and integrated flash binary plants. Dual pressure plants employ two turbines or two-level pressure turbines while dual fluid plant integrates two cycles for the same resource. Combined and integrated flash binary plants couple flash and binary plants.

At the moment many governments stressed by the negative effects of climate change, are looking for clean electricity generation technologies, geothermal binary systems with the advantages of almost zero harmful emission and a well established industry can play a certain role where conditions are favorable.

3.2.2 Solar thermal power systems
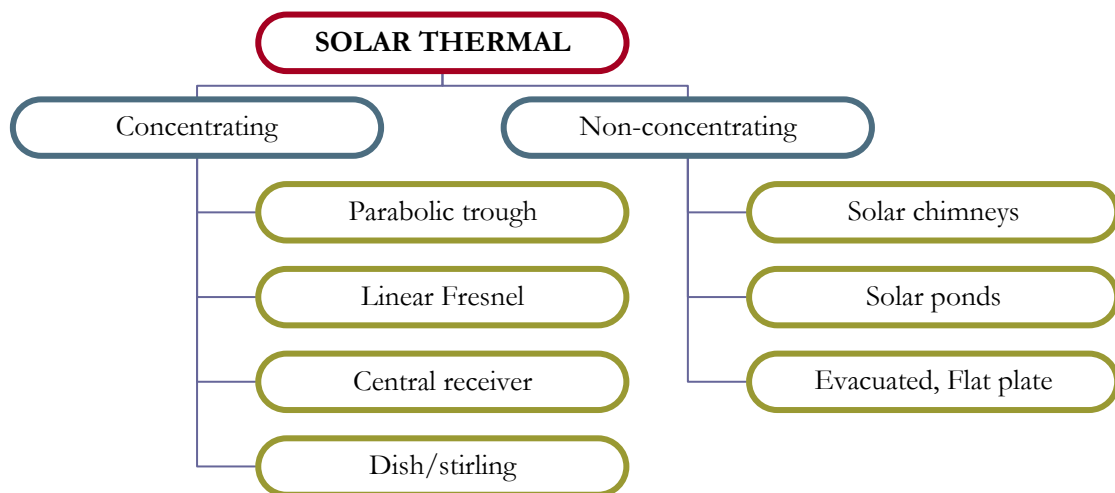
Figure 3.4 - Overview of solar thermal electricity technologies

Solar thermal electricity generation systems can be grouped into two groups (Tchanche et al., 2009c): concentrating and non-concentrating systems. Solar concentrating systems are based on the concept of concentrating solar radiation to produce steam or hot air, which can then be used for electricity generation using conventional power cycles. In concentrating systems we distinguish point focusing systems (central receiver, paraboloidal dish) and line focusing systems (parabolic trough, linear Fresnel). Non-concentrating

systems are: solar ponds, solar chimneys and low/medium-temperature collectors (flat plate, evacuated tube and compound parabolic collectors). Figure 3.4 gives an overview of different technologies.

Solar concentrating systems are best suited for locations with average annual direct incidence radiation above 1800 kWh/m^2/year (Muller-Steinhagen & Trieb, 2004). Figure 3.5 shows various locations of the world with different potentials; most suitable areas being located in the sun-belt: Southern Europe, North-Africa, Middle-East, Australia, Nevada, Sahara and Kalahari deserts. The above areas are characterized by higher proportion of direct irradiance compared with diffuse irradiance, and even considering fast cost reduction for photovoltaic systems in near future, solar thermal will remain more competitive in these locations (Quaschning and Blanco, 2001).
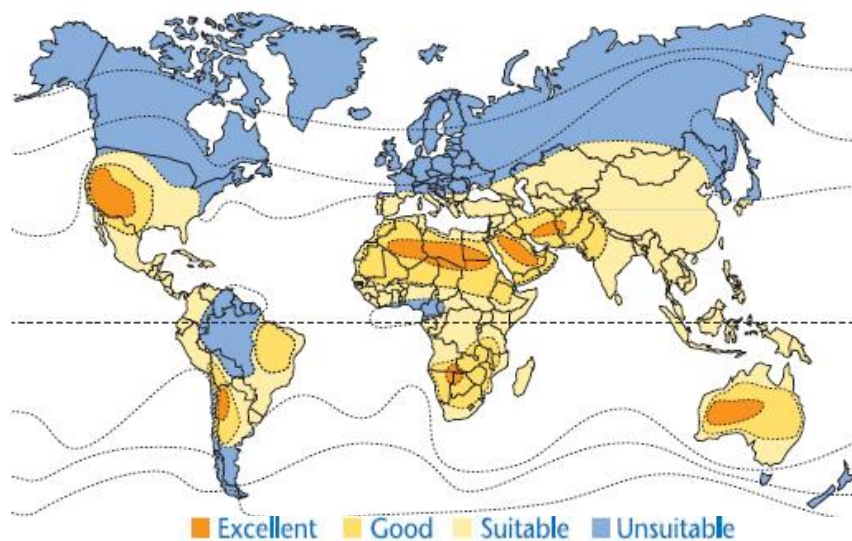
Figure 3.5 - World suitable areas for solar thermal power plants (Hamnet, 2010)

3.2.2.1 Line focusing systems

A | The technologies

Linear focusing collectors include two types of collectors: parabolic troughs and Fresnel collectors. Parabolic trough systems use reflectors curved around one axis using a linear parabolic shape, which has the property of collecting parallel rays along a single line focus and nearly parallel rays from the solar beam in a line image. A long tube receiver placed at the focal line of the trough shaped mirror reflectors receives the concentrated sunlight and heats the heat transfer fluid. The linear Fresnel reflector (LFR) technology is also a single axis tracking technology as the parabolic trough but differs from it in that the absorber is fixed in space above the mirror field and the reflector is composed of many long row segments which focus collectively on an elevated long tower receiver running parallel to the reflector rotational axis. Both technologies are illustrated in Figure 3.6.

Figure 3.6 - Parabolic Trough and Compact Linear Fresnel collectors

B| *The principle of operation*

The collector collects the solar radiation rays and direct them towards the absorber tubes in which thermal heat transfer fluids, such as synthetic oil, mineral oil, nitrate salt, ionic liquids, water/steam, and silicon oil are usually circulated. Heated up to 400 °C, the heat transfer fluid is then pumped through series of heat exchangers to produce superheated steam. Thermal energy of steam is then converted into electrical energy in a conventional steam power cycle or integrated into a combined steam and gas turbine cycle. The impact of the fluctuations of the solar radiation on the output of the system can be offset by integration of backup system (heat transfer fluid heater or boiler) or heat storage system. Figure 3.7 shows a flow diagram of a two-tank system.
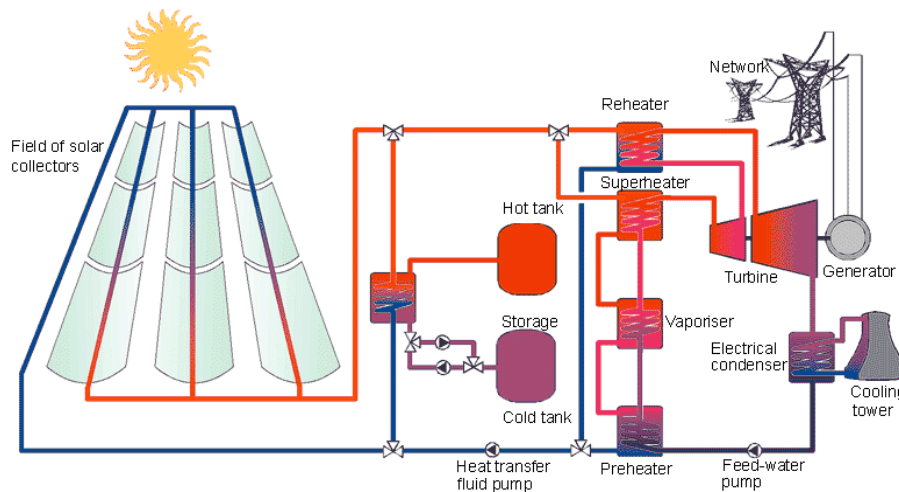
Figure 3.7 - Principle of a Parabolic Trough System
(Source: Muller-Steinhagen and Trieb, 2004)

C| *The status*

Parabolic trough technology has demonstrated its ability to operate in a commercialized environment by nine solar thermal power plants in California, USA, which developed by Luz International Ltd between 1984 and 1990 (Table 3.3). The accumulated 154 years operation experiences of these plants indicate the low technical and financial risk in developing near-term plants. Parabolic trough system is considered as the most mature

CSP technology. Linear Fresnel system is still under development and first plants integrating this relatively new technology are awaited.

Table 3.3- Performance data of the nine solar electricity generating systems built in California, USA (source: Muller-Steinhagen and Trieb, 2004)

Name	SEG I-II	SEGS II-VII	SEGS VIII-IX
Site	Dagget	Krammer Junction	Harper Lake
Capacity (MW)	14+30	5 x 30	2 x 80
Commissioning year	1985-1986	1987-1989	1990-1991
Annual solar-electric (%)	9.0-10.5	11.0-12.5	13.8
Max. temperature (°C)	307-350	370-390	390
Investment ($/kWe)	3800-4500	3200-3800	2890
Electricity cost ($/kWh)	0.27-0.18	0.18-0.12	0.14-0.11
Annual output (GWh/y)	30+80	5 x 92	2 x 250

3.2.2.2 Modular Organic Rankine Cycle Solar Systems

A number of factors are creating an increased market potential for small power plants (Tchanche et al., 2009c): the need of distributed power systems for rural settlements in remote areas, the need to generate clean electricity, the need for sustainable power for economic growth in developing countries, and the deregulation and privatization of the electrical generation sector worldwide. Mature binary geothermal and medium collector technologies can be merged to produce distributed modular power plants in the kW to MW range. Advantages of small solar trough/linear Fresnel ORC systems include (Hassani and Price, 2001): Low temperature operation (<300 °C), modularity, reduced capital and O&M costs, and good economy-of-scale. However, up to now very few CSP plants combining medium temperature collectors and ORC modules have been investigated.

Collector: Parabolic Trough, Array area: 75m2, Thermal efficiency: 0.6, ORC efficiency: 0.1, System output: 3 kW, Thermal input: 37 kW, Working fluid: R245fa
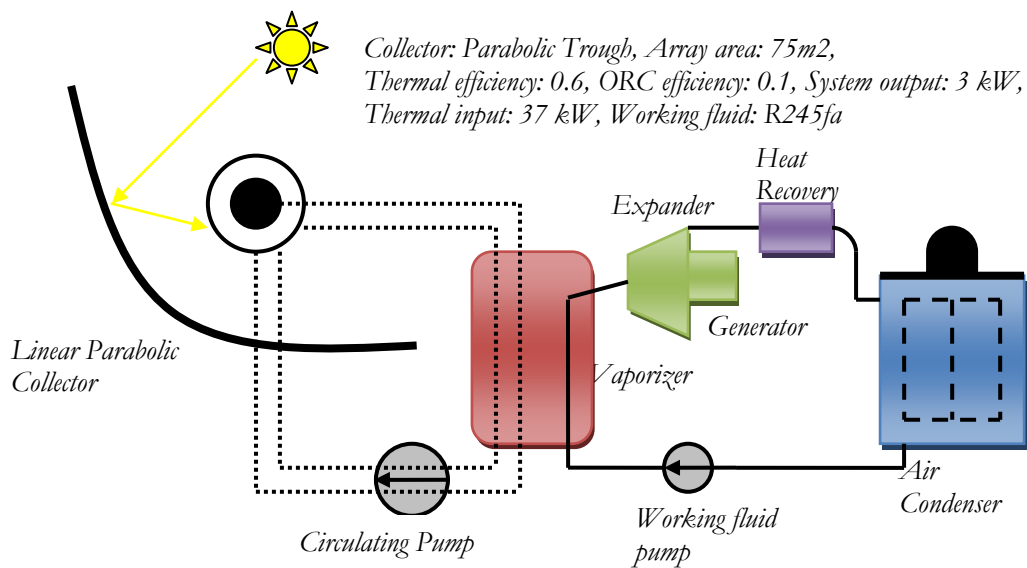
Figure 3.8 – Schematic of the solar ORC tested in Lesotho (Orosz et al., 2009)
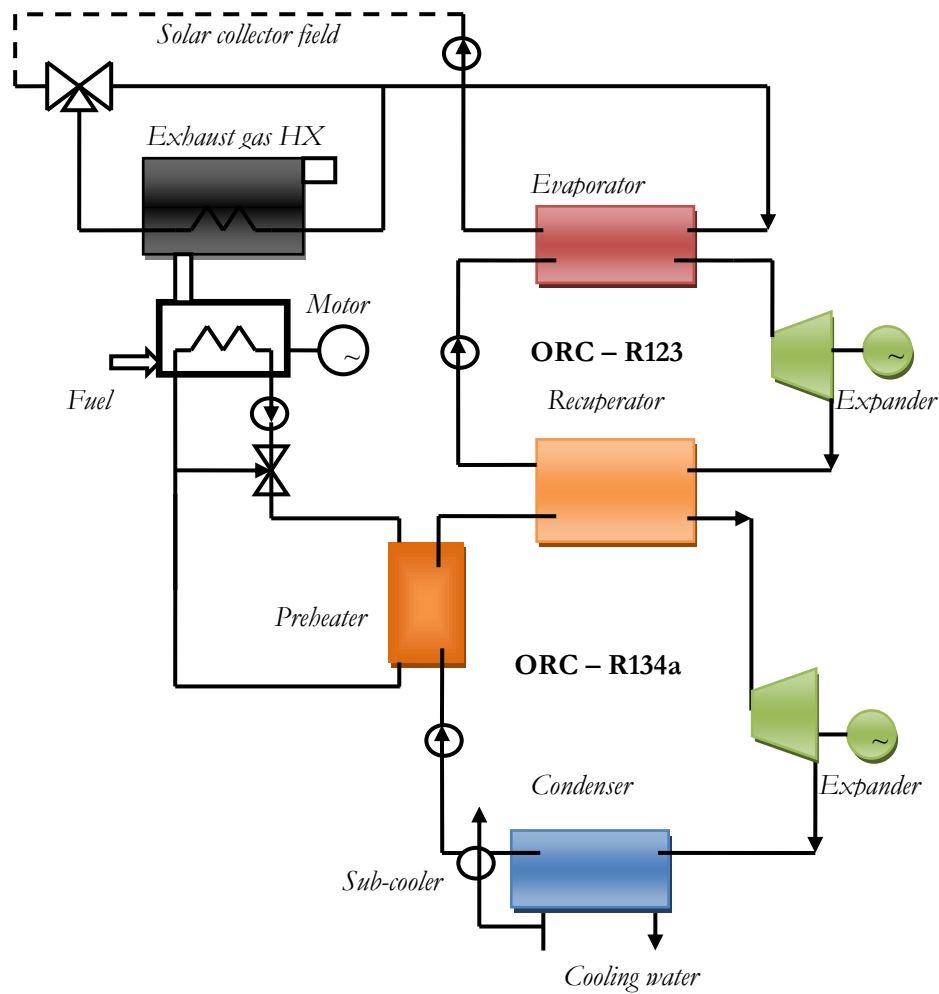
Figure 3.9 – Schematic of the SPS power unit (Kane et al., 2003)

Arizona Public Service (APS) in order to satisfy its obligation under the Arizona Environmental Portfolio Standard (EPS) issued a request for proposal for a 1 MW parabolic trough plant in 2002. The construction started in 2004 and ended in 2005. LS-2 collectors were provided by Solargenix and the ORC supplied by ORMAT with n-pentane as working fluid. The ORC and solar to electricity efficiency were 20.7% and 12.1% respectively (Canada, 2004; Fischer et al. 2004).

Small scale solar ORCs have been investigated for several decades, but could not be widely applied mostly because of lack of small and efficient expansion devices. Research has been intensified last years as a result of the successful conversion of the conventional compressors into expanders with global isentropic efficiency up to 75%. Several trials prove that small scale solar ORCs can be built with good reliability using HVAC components. Medium temperature collectors coupled with ORC modules could efficiently work as cogeneration systems producing water and clean electricity. On-site tests carried out in Lesotho by STG (Solar Turbine Group, MIT) showed that the technology is feasible and cost-effective in off-grid areas and could be applied in developing countries where billions of people live without access to electricity (Orosz, 2009; Orosz et al., 2009). Figure 3.8 shows the Solar ORC tested and the design specifications.

An advanced concept of mini-hybrid solar power plant integrating solar concentrators, two superposed organic Rankine cycles and a Diesel engine was proposed by Kane et al. (2003). Linear Fresnel collectors were used to track the sun and concentrate the solar radiation on the receiver tube in which pressurized water circulates. Superposed Rankine cycles used R123 as working fluid in the topping cycle and R134a in the bottoming cycle (Figure 3.9). Hermetic scroll expander/generators were used for electricity generation. The Diesel engine was integrated to guarantee a minimum level of both power and heat availability at night or during periods of low radiation. Both laboratory and in situ tests were carried out at Ecole Polytechnique Fédérale de Lausanne (EPFL), Switzerland. The system overall efficiency was 7.74% in "solar only" mode and 41% in "fossil fuel" mode.

3.2.2.3 Solar Pond Systems

A solar pond power plant (SPPP) is made of two subs—systems: a salt gradient solar pond and a conventional Organic Rankine Cycle. The salt gradient solar pond (SGSP) is a flat and uncovered large reservoir of water acting as a liquid solar thermal collector/heat store. It absorbs solar radiation (diffuse and direct), transforms it into heat and stores it in the form of hot water. A salt gradient solar pond is artificially divided into three zones (Trieb, 1997):

- The upper convective layer of thickness between 0.15-0.30 m with low salinity water acts as a transparent cover and thermal insulator.

- The bottom layer of thickness from 2 up to 7 m with high-concentration brine that acts as a heat absorber and heat store.

- The middle layer of thickness between 1-1.5 m acts as an additional insulator and is called the gradient salt layer. In this layer, salinity and temperature increase from the top to the bottom.

This phenomenon was discovered in 1902 by Kalecsinsky in a lake located near Szovata, Transyslvania. The maximum temperature obtained in a pond is about 90-100 °C, making it suitable for Rankine Cycles working with low boiling point organic fluids such as R134a. The configuration of the salt gradient solar pond matches the sources of an organic Rankine cycle working at low temperature (Figure 3.10). The upper layer serves as cold source to cool the condenser while the bottom layer supplies the evaporator with heat.

The principle of operation is simple; during the day, the pond is charged while the extraction of heat can be scheduled for precise period of time. During operation, the bottom layer supplies heat to the evaporator where it is used to evaporate the working fluid. The fluid at vapor state is expanded in the turbine and cooled in the condenser before being pumped to the evaporator to close the cycle. A schematic of a solar pond power system is given in Figure 3.10. The thermal performance of a solar pond is around 15-25% while the solar-to-electric efficiency is about 0.8-2%.

Research on solar ponds started in Israel in 1950-1970 and the first solar pond with a surface area of 1100 m^2 was built in 1975 at the Dead Sea Works. Since that period, several power plants based on this technology were constructed and operated at different sites

around the world: Israel, India, USA, Italy, Egypt, China, Japan, Mexico, Portugal, Kuwait and other countries. The biggest one is the 5 MW-250,000 m^2 SPPP at Beith Ha'avara, Israel. Others are: Ein Boqek, Israel (150 kW/ 6250 m^2); Yavne, Isreal (6 kW/ 1500 m^2); Alice Springs, Australia (15 kW/ 1600 m^2); El Paso, USA (70 kW/ 3350 m^2).
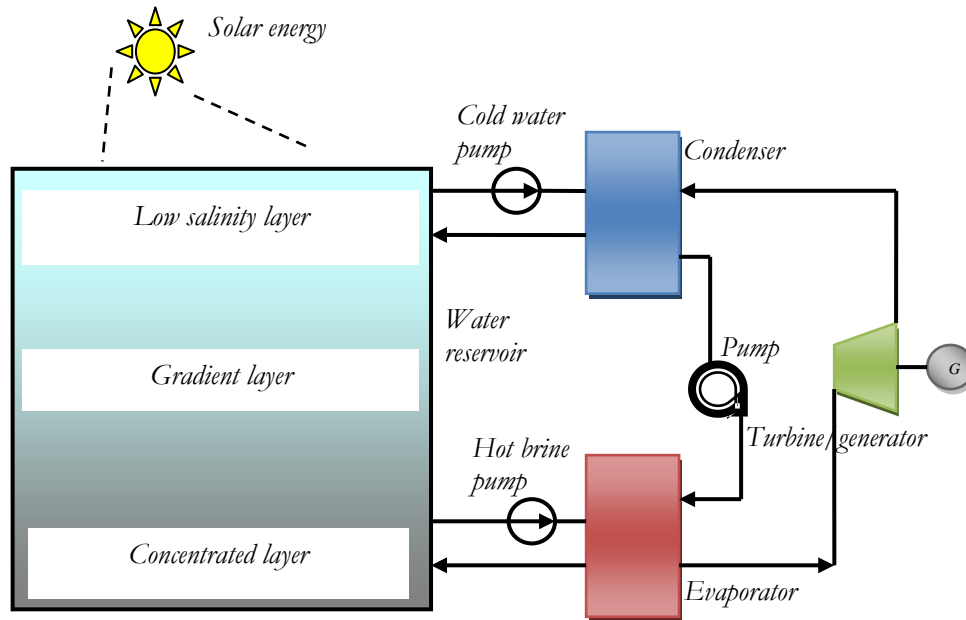
Figure 3.10 – Principle of a Solar Pond Power Plant

3.2.3 Solar ORC-RO desalination systems

Desalination can be defined as a group of techniques that consists of removing salt and other solids particles from raw water so called seawater or brackish water depending on the concentration of salts to make it suitable for human consumption. Desalination technologies can be classified in two groups according to their separation mechanism: thermal and membrane based technologies (Fritzmann et al., 2007). Thermal desalination separates salt from water by evaporation and condensation, whereas in membrane desalination water diffuses through a membrane, while the salts are almost completely retained. Major desalination techniques are given in Table 3.4. Reverse osmosis and multi-stage flash are the most widely used technologies. The cost of water produced depends upon energy source, plant size, technology, feed water salinity and required product quality (Karagiannis and Soldato., 2008).

Table 3.4 - Desalination technologies

(Fritzmann et al., 2007)

Thermal desalination technologies	Membrane desalination technologies
Multi- stage flash distillation (MSF)	Reverse osmosis (RO)
Multi-effect distillation (MED)	Nanofiltration (NF)
Vapor compression distillation (VCD)	Electrodialysis (ED)

Recently there has been a trend to couple desalination techniques with renewable in order to reduce the impact of conventional power plants on the environment (Mathioulakis et al., 2007). The aforementioned techniques can be coupled either with solar PV panels or solar thermal collectors. MSF can be heated by solar thermal collectors or can use waste heat from industrial effluents or solar power plants built as cogeneration systems. RO can be powered by electricity or mechanical power. Both of them represent about 70% of total installed systems powered by renewable energy sources in the world (Figure 3.11). At the moment, solar powered systems are expensive compared to conventional or other alternative systems such as wind and geothermal energy powered systems (Table 3.5).
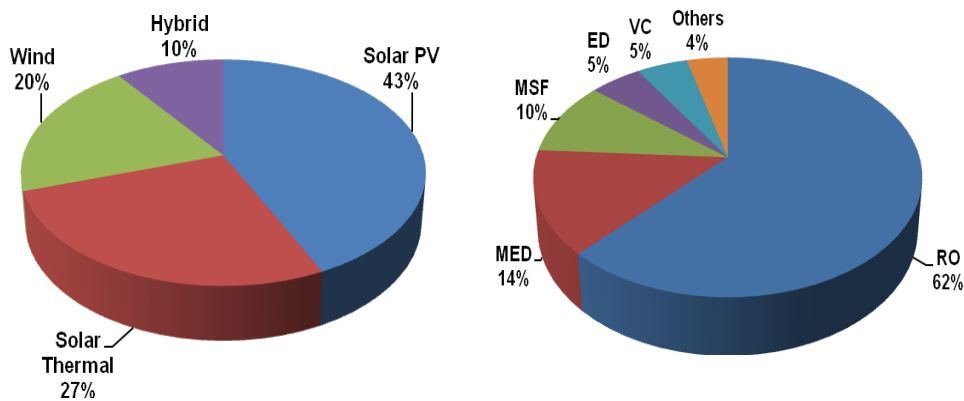
Figure 3.11 - Share of renewable energy sources and technologies in renewable energy powered desalination processes (Source: Mathioulakis et al., 2007)

Table 3.5 - Cost comparison of freshwater in relation with the energy source

(Sources: Karagianis and Soldatos, 2008; Essam et al., 2008)

Feedwater	Energy source	Cost (€/m³)
Brackish	Conventional	0.21-1.06
	Photovoltaics	0.5-5
	Geothermal	2.00
Seawater	Conventional	0.35-2.70
	Wind	1.00-5.00
	Photovoltaics	3-20
	Solar thermal collectors	3.50-8.00

Reverse osmosis (RO) is a pressure driven separation technique based on a property of certain polymers called semi-permeability. While they are very permeable for water, their permeability for dissolved substances is low. By applying a pressure difference across the membrane the water contained in the feed is forced to permeate through the membrane. In order to overcome the feed side osmotic pressure, fairly high feed pressure is required. Pressures applied in reverse osmosis applications vary from 15-25 bars for brackish water and 60-80 bars for seawater (Fritzmann et al., 2007). The process includes the following steps: pre-treatment, pumping, membrane separation, brine energy recovery and post-treatment. Pumping process can be easily achieved through electricity or shaft power thus

making RO the most suitable candidate for renewable energy powered desalination system. A solar driven ORC-RO system couples a solar thermal engine and a RO desalination sub-system (Figure 3.12). The solar thermal engine transforms the solar radiation into mechanical power. The useful power on the shaft by mechanical coupling drives the high pressure pump (HPP) of the RO unit.
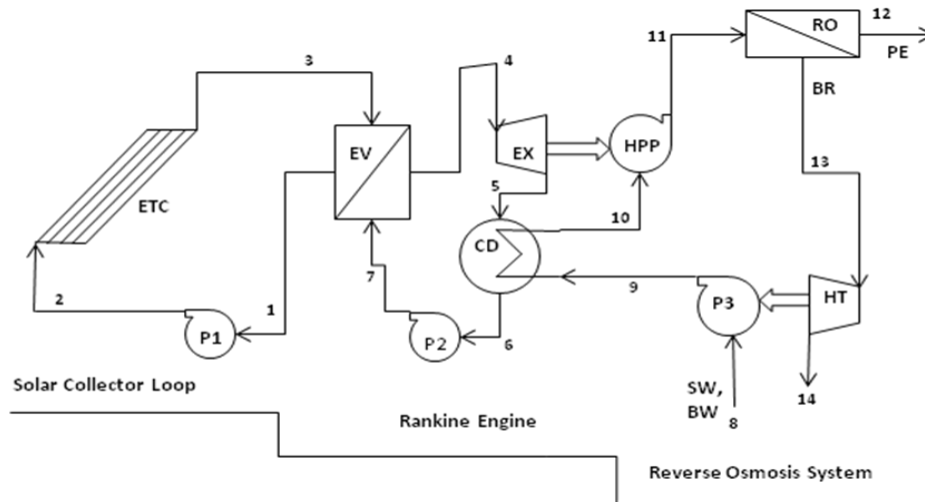
Figure 3.12 - Schematic of a Rankine driven reverse osmosis desalination system (ETC: solar thermal collectors; EV: evaporator; EX: expander; HPP: high pressure pump; P1, P2, P3: pumps, HT: hydraulic turbine; CD: condenser; RO: membrane modules; BR: brine; PE: permeate; SW: seawater; BW: brackish water) (Source: Tchanche et al., 2010)

Early research on solar thermal driven pumping systems involving the Rankine power cycle started in the second half of the 19th century with the works of Augustin Mouchot and Abel Pifre (Delgado Torres, 2009). From that time till the end of the 20th century, the main application targeted was the small scale water pumping systems for irrigation of farms. Many systems operating on this scheme were built in many countries around the world as reported by Delgado-Torres (2009) and Wong & Sumathy (1999). These systems used steam or organic compounds such as R-11, R-114 and R-113 as working fluids. Solar driven irrigation systems are of special significance in countries where the economy relies on agricultural activities undertaken by poor farmers in remote areas far from electricity grid, and in a context of water scarcity and increasing oil prices. Since the 1980s, solar PV-water pumping systems favored by the decreasing cost of PV, modularity and less moving parts are being preferred to solar thermal pumping systems.

At the moment the global warming is being considered as a major threat to our life, solar thermal engines are suggested for powering RO-desalination units. Earliest plant is reported to have been constructed in Cadarache, France (Maurel, 1979). The high pressure pump was powered by a 2.5 kW solar heat engine with R-114 as working fluid, and a fresh water production of 2.5 m^3/ h from brackish water. Steam RC-ORC systems have been studied by Voros et al. (1998) and Bouzayani et al. (2007). These aforementioned theoretical studies were carried out considering steam temperature of about 450 °C at the turbine inlet. The implementation of organic fluids with appropriate critical temperature such as Toluene, siloxanes, ammonia, pentanes, etc in medium temperature ORC-RO systems is possible. Delgado Torres and Garcia-Rodriguez (2007), Garcia-Rodriguez and Delgado Torres (2007) and Bruno et al. (2008) carried out the technical and economic

feasibility studies of solar ORC-RO desalination technologies. Bruno et al. (2008) concluded solar ORC-RO is a cost-effective option in comparison to PV-RO. Parabolic trough collectors in single or double cascade ORC with toluene, pentanes or propylbenzene as working media could form the baseline technology for large and medium size solar ORC-RO systems. Cycles operating with maximum temperature of 250-400 °C and 35 °C condensing temperature yield a cycle efficiency of about 25-35%. Under this condition, a 15 m^3/day plant could produce water at about 2.30 €/m^3 from brackish water or 5 €/m^3 from seawater.

Solar ORC-RO could be scaled down using well known HVAC components. In this perspective, Manolakos et al. (2005, 2007 & 2008) designed and tested a small stand-alone system using a scroll expander, evacuated tube solar collectors and R134a as working medium. Simulations of the latter were carried out by Schuster et al. (2007) who put in evidence the influence of the collector slope on the system productivity. Economic comparison (Manolakos et al., 2008) shows the single stage was not cost effective compared to PV-RO systems of similar size. Cost comparison study in case of seawater for Thirasia Island, Greece gave cost figures of 7.77 €/m^3 for PV-RO and 12.53 €/m^3 for ORC-RO. In sake of optimal use of solar collectors, Kosmadakis et al. (2010) suggests a dual Rankine cycle system. This new system will use evacuated tube collectors, R134a as first cycle fluid, R245fa as second cycle and scroll compressors operating in reverse mode as expanders.

3.2.4 Duplex-Rankine cooling system

Solar assisted air-conditioning systems with the advantages they have to reduce the summer electricity peak load and energy consumption in buildings as well as in industries have been a field of intensive R&D in the 1970s at the period of the oil crisis and were abandoned soon after the crisis. Recently many activities related to the development of solar cooling applications were restarted. Henning (2007), Pridasawas (2006) and Kim and Infante Ferreira (2008) have listed technical options from the solar radiation to the cooling effect: sorption (adsorption, absorption, desiccant), PV electricity (vapor compression) and thermo-mechanical option (Rankine, ejector, Stirling). In a solar thermo-mechanical refrigeration system, a heat engine converts solar heat into mechanical work, which in turn drives a mechanical vapour compression refrigeration machine. Heat engines reported in chapter 2 can be used for this purpose: Stirling engine, Brayton cycle and the Rankine engine. A schematic of such cooling system is shown in Figure 3.13.

In a Duplex-Rankine cooling system, Rankine engine serves as heat engine and solar energy captured by solar collectors is turned into heat using a heat transfer fluid which could be a thermal oil or water/steam. This thermal energy is further transferred to the working fluid of the Rankine engine through the evaporator. The Rankine engine subsequently, transforms the heat received into mechanical power to drive the compressor of the vapor compression machine. The overall Coefficient of Performance (COP$_{tot}$) of the solar combined Rankine cooling system defined as the ratio of cold energy produced to the incident solar radiation is the product of the efficiencies of the solar collector, the Rankine power cycle and the cooling machine. Thus, it can be written as:

$$COP_{tot} = \frac{\dot{Q}_o}{G_T . A_{sc}} = COP_{VC} \eta_{RC} \eta_{sc} \qquad (3.1)$$

η_{sc} and η_{RC} refer to the efficiencies of solar collector and Rankine engine, respectively. COP_{vc} is the coefficient-of-performance of the vapor compression cooling subsystem. Q_o is the cooling power, G_T, the solar irradiation and A_{sc}, the solar collector area.
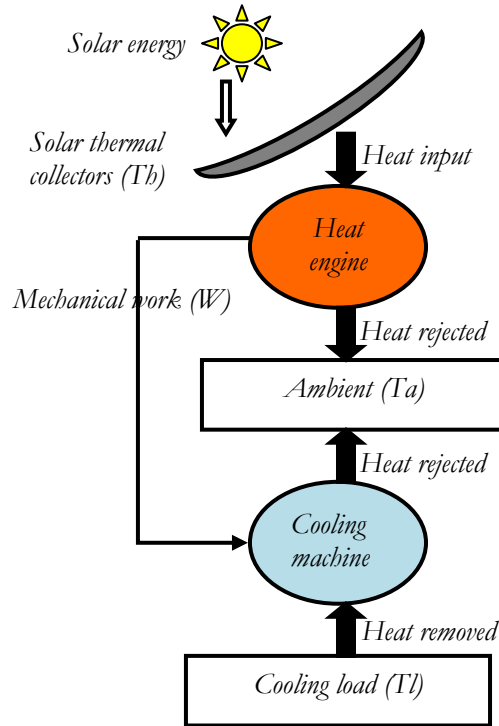
Figure 3.13 – Solar thermo-mechanical refrigeration system (Kim and Ferreira, 2008)

A literature review conducted reveals little interest on this topic. Most activities on this technology were carried in USA, Japan and Saoudi-Arabia in 1970s and 1980s and mainly theoretical investigations are reported. Lior (1977) studied a solar-powered, fuel-superheated Rankine cycle incorporating a steam turbine. A superheater is integrated into the system to avoid a two-phase operation of the turbine. This system was designed to work in cooling as well as in heating mode. The study proved the system was capable of saving substantial quantity of fuels. Because of economy-of-scale, this option would only be applicable for large refrigeration systems. For low power systems and moderate temperature heat sources, design problems arise: excessive turbine shaft speed, high degree of superheat (~560 ºC), turbine-blade erosion, etc (Wali, 1980). To overcome the design difficulties, organic fluids were suggested. Wali (1980) compared several organic compounds for application in small-scale solar applications and R-113 emerged as a potential working fluid.

A prototype of solar Rankine driven cooling system was designed and tested by Barber-Nichols Engineering Co., USA, in the framework of a project co-funded by Honeywell Inc. and the National science Foundation. The demonstration package developed for supplying residential cooling and/or electricity via a solar heated Rankine cycle as depicted in Figure 3.14, comprised a 3-ton air conditioning working with R12, 1-kW electric system, a R113 Rankine cycle, and a solar collector that provides warm water at 102 ºC (Prigmore and Barber, 1975). With a turbine efficiency of 80% and a compressor efficiency of 85%, the

coefficient of performance of the combined Rankine/air conditioning system is 0.71. The system thermal ratio or solar COP is 0.21, considering solar collector efficiency of 30%.
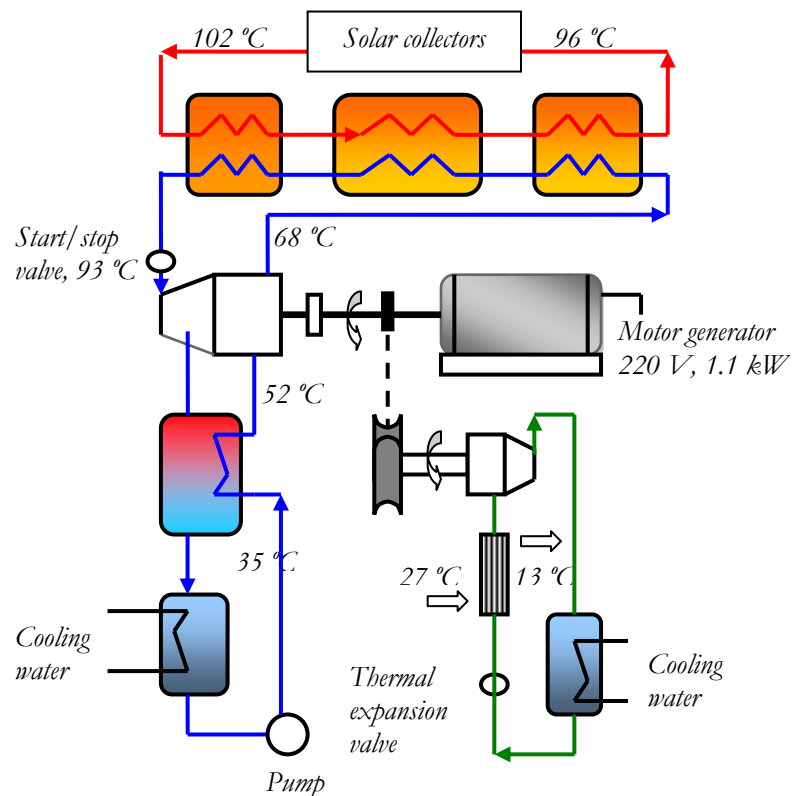
Figure 3.14 – Solar heated Rankine combined power/air conditioning system
(Prigmore and Barber, 1975)

In the 1970s, Duplex-Rankine systems were considered for further competition with absorption but it was later abandoned. In such system, the prediction of component performance at off-design conditions and the matching of components into a complete system so that the overall performance is optimized are not easy. An adequate control strategy is needed to ensure matching of the Rankine cycle and air conditioner (Mannaa et al. 1984). Moreover, substances used as working fluids are harmful for the environment. A system-cost comparison carried by Kim and Ferreira (2008) shows that duplex-Rankine with 2300 €/kWcool is cheaper compared with other thermo-mechanical systems but two to three-fold expensive in comparison to sorption options. For the abovementioned reasons, sorption systems utilizing environmentally friendly working media are preferred today.

A new path being explored is the combination of Rankine and ejector/absorption cycles for simultaneous production of cooling and power. A combined power/cooling cycle that combines Rankine and absorption refrigeration cycles and uses ammonia-water mixture as working fluid was proposed by Goswami (Xu et al., 2000). Wang et al. (2009) proposed and performed thermodynamic analysis of a new combined cooling, heating and power (CCHP) system which combines Rankine and ejector refrigeration cycles. In their system, vapor extracted from the turbine supplies the ejector and the heat users. Another combined Rankine/ejector system was designed, built and tested by Oliveira et al. (2002). As shown on Figure 3.15, the ejector is mounted in parallel with the expander. Two

prototypes were tested in Porto, Portugal and Loughborough, UK. The nominal cooling capacity was 2 kW for one and 5 kW for the other. The 1.5 kW turbo-generator used in both sites had an isentropic efficiency of 28%. The overall COP obtained was about 0.3 and the electrical efficiency between 3-4% for a boiler temperature of 95 ºC and ambient temperature around 20 ºC. The projected initial cost of such system was roughly € 8500 (cost of the collector loop not included).
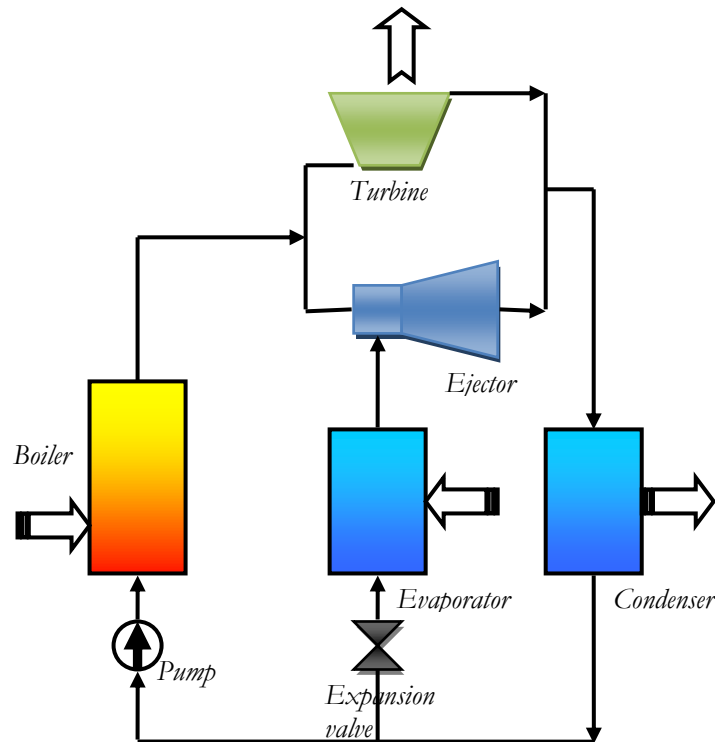
Figure 3.15 - The combined ejector/Rankine cycle (Oliveira et al., 2002)

3.2.5 Ocean Thermal Energy Conversion Systems

The Earth's oceans cover over 70% of the planet and could be utilized as a source of virtually inexhaustible renewable energy. Ocean Thermal Energy Conversion (OTEC) by the way it employs natural thermal stratification occurring in oceans is being proposed to harness this huge amount of untapped energy; it converts solar radiation stored in the upper ocean water layers into electric power. Vertical ocean seawater temperature distribution has been measured in many regions around the world; and surface seawater at less than 50 m from sea level is warm at 20-29 ºC while at a depth of about 800 m or more the temperature is about 2-7 ºC. To be effective, the minimum temperature difference between the ocean surface layers should be about 20 ºC. These temperature gradients are found in tropical regions near the Equator. Figure 3.16 shows most suitable areas.
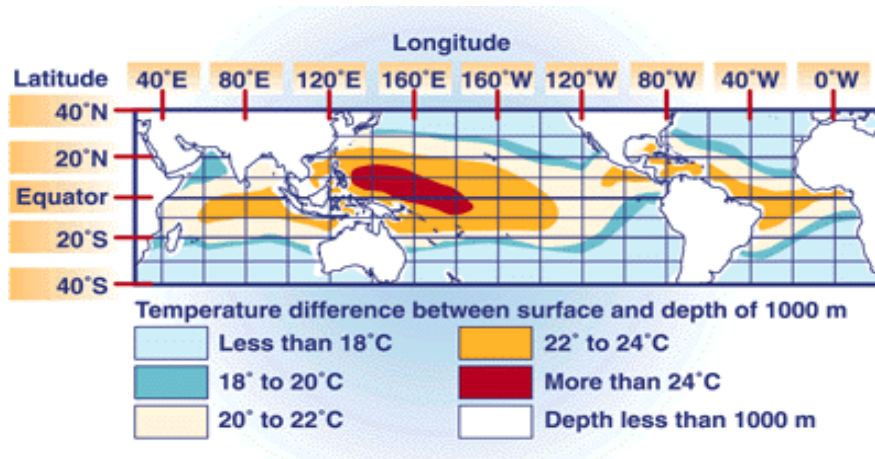
Figure 3.16 - Potential locations for OTEC plants
(Source: www.seao2.com, www.nrel.gov/otec/what.html)

The first known OTEC system was proposed by Arsene d'Arsonval, in 1881. He built a closed OTEC system with ammonia as working fluid. Ammonia was selected for its low boiling point as it could boil at low temperature. But the technology was never tested by d'Arsonval himself. George Claude overtook the challenge, by proposing and successfully testing the open-cycle concept. Nevertheless, most of his attempts to put OTEC into practical use ended in failure. In 1962, H. Anderson and his son James H. Anderson Jr., began full scale design analysis of OTEC systems and conceived a new OTEC plant which overcame the weak points of Claude's system. Later, the energy crisis of 1973 provided the motivation for Japan and USA to perform fundamental research. Today, there are five different cycles known for OTEC. These are (Uehara, 2006; Finney, 2008): open cycle, closed Rankine cycle, hybrid Rankine cycle, Kalina cycle and Uehara cycle.

A| Closed OTEC cycle
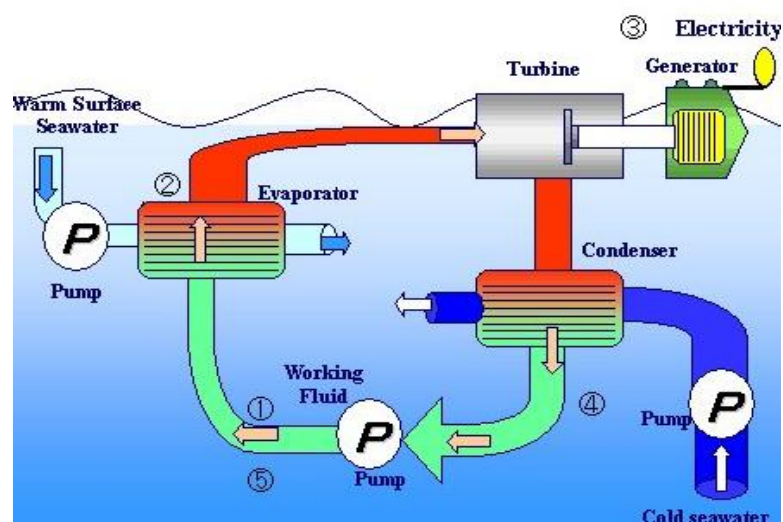
Figure 3.17 - Schematic of a closed OTEC (Source: www.seao2.com)

The closed cycle OTEC power plant concept was first proposed by D'Arsonval in 1881. It uses a working fluid with a low-boiling point, such as ammonia, propane or R134a and operates on a Rankine cycle. The working medium is heated and vaporized in the evaporator by the warm surface seawater. The steam produced drives a turbine coupled to a generator. After the expansion process, the low-pressure working fluid vapor is condensed during a heat exchange with the cold seawater from the deep ocean. The working fluid is then pumped back to the evaporator and the cycle is repeated continuously. Figure 3.17 shows a schematic of a closed OTEC cycle.

B| Open OTEC cycle

The open cycle OTEC, proposed in 1928 by George Claude uses seawater as the working fluid. Warm seawater from near the surface of the sea is pumped into a low pressure evaporator chamber where it boils at ambient temperature. The evaporator is maintained through a series of valves and careful maintenance to avoid atmospheric leakages. The vapor then drives a low pressure turbine to produce electricity. The low pressure vapor is then cooled using deep seawater. This configuration presents the advantage of producing fresh water as the warm seawater flash evaporated becomes desalinated and ready for the consumption.

C| Hybrid OTEC cycle

A hybrid OTEC is made of two stages or loops. The first loop is a closed OTEC cycle generating electricity using a low-boiling point working fluid. In a second loop, warm seawater is flashed into steam as in the open OTEC using a vacuum chamber that serves also as evaporator for the closed OTEC. A schematic of a hybrid OTEC is shown in Figure 3.18 (Takahashi and Trenka, 1992). This cycle configuration has yet to be tested.
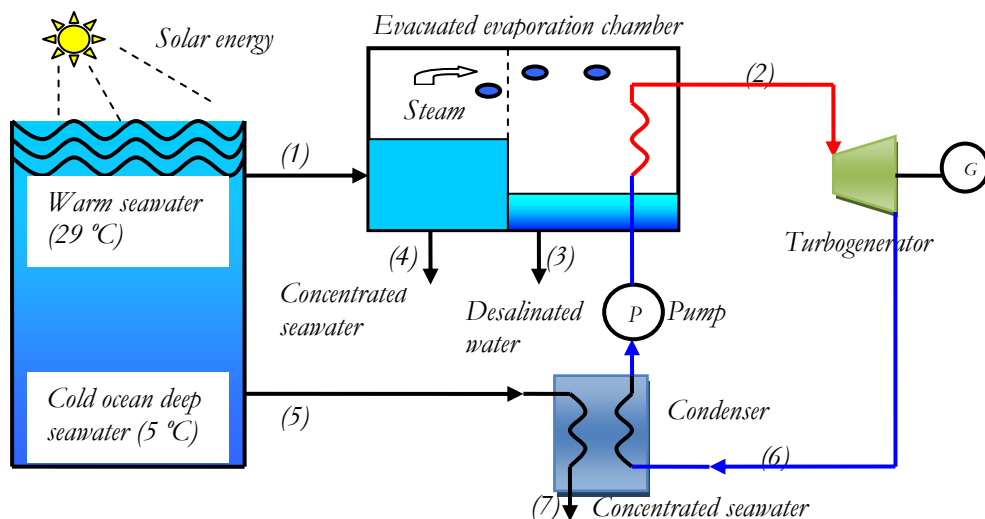
Figure 3.18 – Schematic of a hybrid OTEC system (Takahashi and Trenka, 1992)

Both cycles have been investigated for use in OTEC plants (Uehara, 1994). They operate as explained in the previous chapter and use ammonia/water mixture as working fluid.

An OTEC system utilizes very low temperature heat (20-30 °C) and yields low efficiency of about 3-5%. Therefore, generating high capacity power requires enormous quantity of seawater and pumping energy what could decrease the cost-effectiveness of this technology. It was proposed OTEC to be integrated in a multiple industrial complex. An Integrated Ocean Thermal Energy Conversion System (I-OTECS) apart from generating electricity could potentially tackle other ventures: fresh water production, air conditioning and refrigeration, cold water agriculture, aquaculture and mariculture, hydrogen production, lithium extraction, etc. Potential markets for OTEC have been identified, most of which are in Pacific Ocean and 50 countries are examining its implementation as alternative energy source and sustainable solution for water scarcity: India, Korea, Palau, Philippines, Hawaii, Papua New Guinea, etc. In 2001, as a result of cooperation between Japan and India a 1MW plant was erected and many others are planned to be constructed in the near future. A cost analysis carried out for a 10 MWe plant gives $0.089/kWh and a water cost of $0.82/m^3 while for a larger plant, 100 MWe, $0.068 and $0.51 are obtained (Uehara, 2006). At the moment, this technology is gaining worldwide attention as one of the most reliable solution to most issues facing the world and many multi-purposes OTEC plants are expected to be built in the near future.

3.2.6 Organic Rankine Cycle in waste heat recovery application

Waste heat can be defined as the heat generated in a process by way of fuel combustion or other chemical reaction and, then "dumped" to the environment. Many studies regarding the potential evaluation of the heat recovery in industries reveal its huge potential. In fact up to 70% of the input energy is released to the environment as thermal heat and contribute to the environmental pollution via the following streams (Bonilla et al., 1997, Galanis et al., 2009, Tchanche et al., 2010c): liquid streams, stack losses, steam losses, process gases and solid product streams.

Depending upon the temperature of the process, waste heat can be rejected at low temperature as in air compressors or at medium/high temperature in incinerators and furnaces. In Table 3.6, most of sources of waste heat recorded in different industries and thermal processes are classified according to the temperature level of the exhaust heat.

Thermoelectric generators, Kalina and Rankine cycles can convert heat into electricity. Steam cycles are suitable for recovering high temperature heat. In medium and low temperature ranges, organic fluids with low boiling points are preferable (Hung, 2001). Two schemes are distinguished to transfer the heat from the waste heat source to the cycle: (1) an intermediary thermal oil loop is integrated between the heat source and organic Rankine cycle system and (2) heat transfer between heat source stream and working fluid stream takes place in the same heat exchanger.

Industrial processes and particularly power plants reject vast quantities of heat carried by flue gases. Well designed ORC modules can turn this thermal energy into electricity. Process design deals with the selection of working fluids, turbines and heat exchangers.

Most of time, studies related to ORCs in heat recovery application focus the selection of working fluids (Invernizzi et al., 2007; Chacartegui et al., 2009; Angelino and Colonna di Paliano, 1998; Dai et al., 2009; Hung et al., 1997; Maizza and Maizza, 2001; Liu et al., 2004; Hung, 2001). From the abundant relevant literature, the following can be retained:

- Fluids with high critical temperature or high boiling point such as toluene, benzene and siloxanes are adapted for medium temperature.
- Pentanes, butanes, and cryogens such as R113, R123, R245fa, HFE7000, etc are best suited at low temperature.
- Fluid mixtures with the advantage of best matching with exhaust stream offer additional choice for fluids and could be well suited for systems aiming at producing hot water as additional product.

Table 3.6 – Waste heat sources and temperature range

(Source: www.energyefficiecyasia.com)

Heat recovery	Sources	Temperature (ºC)
High temperature	Solid waste and fume incinerators	650-1450
	Nickel refining furnace	1370-1650
	Glass melting furnace	1000-1550
	Aluminum, copper and zinc refining furnaces	650-110
	Cement kiln	620-730
	Hydrogen plants	650-1000
Medium Temperature	Steam boiler exhaust	230-480
	Gas turbine exhaust	370-540
	Drying and baking ovens	230-600
	Catalytic crackers	425-650
	Reciprocating engine exhausts	315-600
Low temperature	Annealing furnaces	66-230
	Internal combustion engines	66-120
	Hot processed liquids and solids	32-232
	Drying, curing and curing ovens	93-230
	Welding and injection molding machines	32-88
	Air compressors	27-50

An example of heat recovery in a biogas digestion plant using an ORC module was presented by Schuster et al. (2009). Two waste heat sources were identified: hot water from the cooling circuit of the turbocharger and the exhaust gas leaving the ICE (internal combustion engine) at around 490 ºC. In addition to 537 kWe for the ICE, 35 kWe could be produced. R245fa is the working fluid. The total efficiency of the plant was increased by 2 on point basis. Economic evaluation showed that with 7500 hours of full load operation, 5.65 c€ /kWh electricity production cost was achieved.

In automotive industry, the reduction of fuel consumption in new cars has become a preoccupation. Usually, the combustion engine onboard requires a supply of fuel three times as great as the power actually generated. This is because the combustion engine with its maximum efficiency of about 40% converts less than one third of the energy it receives into mechanical power. For illustration, the heat balance of a typical 1.4 liter spark ignition engine has a thermal efficiency ranging from 15 to 32% depending on operating

conditions. The remaining 60 to 70% of the energy input is rejected to the environment through the radiator (18-42%) and the exhaust system (22-46%) (El Chalmas and Clodic, 2005).

Solutions are being researched to recover this heat lost for use in other thermal processes for air conditioning or power/electricity generation. Rankine cycles are regarded as promising solution to serve this purpose. Several encouraging trials have been reported with steam as working fluid. For instance, Honda designed and tested a prototype (Endo et al., 2007). As result, the thermal efficiency was improved from 28.9% to 32.7% for a vehicle tested at a constant speed of 100 km/h.

The implementation organic fluids could provide substantial fuel saving by suitably recovering not only the exhaust heat but also the heat released by the cooling circuit. However, the organic fluid should be well selected so as to guarantee the safety of the passengers. An important point to be addressed is the management of transient operations as the vehicle is subject to frequent accelerations and decelerations (Quoilin and Lemort, 2009).

3.2.7 ORC biomass power plants

Biomass is the world's fourth largest energy source, contributing to nearly 10% of the world's primary energy demand (IEA, 2009). In developing countries, the contribution of biomass to the national primary energy demand is higher, up to 70-90% in some countries and usually used in unsustainable way (Karekezi, 2002). This abundant resource could be transformed into electricity and hot water when necessary in CHP plants. Various potential technologies that could serve this purpose are listed in Table 3.7.

Table 3.7 – Biomass energy conversion technologies (Dong et al., 2009)

Primary technology	Secondary technology
Combustion producing steam, hot water	Steam engine, steam turbine, stirling engine, organic Rankine cycle (ORC)
Gasification producing gaseous fuels	Internal combustion engine, micro-turbine, gas turbine, fuel cell
Pyrolysis producing gaseous, liquid fuels	Internal combustion engine
Biochemical/biological processes producing ethanol, biogas	Internal combustion engine
Chemical/mechanical processes producing biodiesel	Internal combustion engine

The combination combustion/ORC is receiving an increasing attention for application in small scale distributed electricity generation. A typical biomass-ORC cogeneration system is made up of a thermal oil boiler and an organic Rankine cycle machine coupled via a thermal oil loop (see Figure 3.19). Biomass fuel is burned in the boiler made according to well established techniques similar to those used for steam boilers. The thermal oil used as heat transfer fluid provides a number of advantages, including low pressure in the boiler, large inertia and insensitivity to load changes, simple and safe control and operation. Moreover, the adopted hot side temperature (below 350 °C) ensures a long oil life. The heat carried by the thermal oil is transferred to the organic Rankine cycle and converted

into electricity. Organic fluids such as octamethyltrisiloxanes (OMTS) and alkylbenzenes insure the optimal operation of the cycle as shown by Drescher and Bruggemann (2007). The condensation heat is used to produce the hot water at a temperature between 80 and 120 °C suitable for district heating and other thermal processes such as wood drying and sorption cooling.
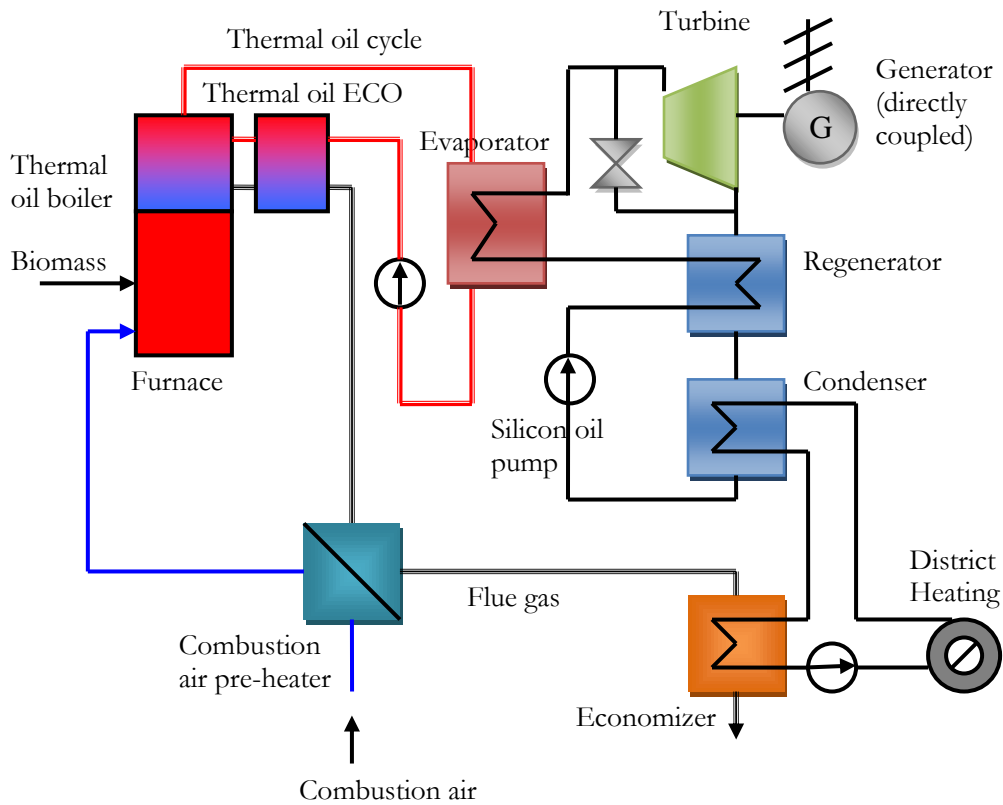
Figure 3.19 - Schematic of a biomass power plant (Obernberger et al., 2002)

Biomass ORC CHP plants at medium scale (100-1500 kW) have been successfully demonstrated and are now commercially available (Schuster et al., 2009). The number of installed plants is rapidly increasing as the technology is becoming mature and cost effective. Till now, most of installations are in Europe, and Stadtwarme Lienz Austria (1.0 MWe), Sauerlach Bavaria (0.70 MWe), Toblach South Tyrol (1.10 MWe), and Fuβach Austria (1.50 MWe) are few of them.

Although at least a hundred plants have been installed throughout the world, technical data on existing plants are very scarce. Evaluations reports were released for two plants installed for demonstration in Austria (Obernberger and Hammerschmid 2001; Obernberger et al., 2002; Dong et al., 2009): Admont CHP plant (400 kWe) and Lienz (1000 kWe). The biomass CHP plant in Lienz supplies the town of Lienz with district heat (60 GWh/year) and feeds the electricity produced (7.20 GWh/year) into the grid. The plant is fully automatic, and presents excellent part load operation with and electrical efficiency of 18%. The overall plant efficiency amounts to 82%. Specific installation cost was estimated at about 2765 €/kWe and electricity production costs in the range 9-14 c€/kWhe depending on the fuel price and capacity utilization.

3.3 Cost and applications comparison

Solar, biomass and geothermal energy considered as renewable and clean energy sources, and waste heat of any origin can serve as heat sources for organic Rankine cycles. The nature of the heat source influences technically and economically the application. However, the main aim of an organic Rankine cycle machine is power generation and as secondary purpose hot water production for district heating. Table 3.8 provides a comparison of different applications. Geothermal and biomass CHP are mature and cost-effective applications. Solar power based on low-temperature ORCs is still under development. Waste heat recovery ORCs is progressively gaining in popularity since the years 2000. They could help improving the fuel efficiency of stationary and mobile thermal power systems and reduce thermal pollution (Tchanche et al. 2010c).

Table 3.8 - Comparison of ORC applications

Applications	Maturity	Availability factor (%)	GHG emissions	Complexity, Operation & Maintenance
Geothermal	mature	100	Very low	Simple
Solar Power	Under development	25	No	Complex operation and maintenance, dispatchability
Biomass CHP	mature	100	Yes	Need of fuel, suitable for distributed generation
Waste Heat Recovery	very promising	>60	No	No fuel needed, economics depend on heat availability

Medium and large sized ORC modules are available from several manufacturers (See Table 3.9). The module can be tailored according to the customer's specifications and mounted on-site or bought ready from suppliers and delivered in a compact module as shown in Figure 3.20. Once on the site, the module is adapted to the heat source. Although medium sized systems are well developed, only few solutions are coming into market for small scale systems in the kW range.
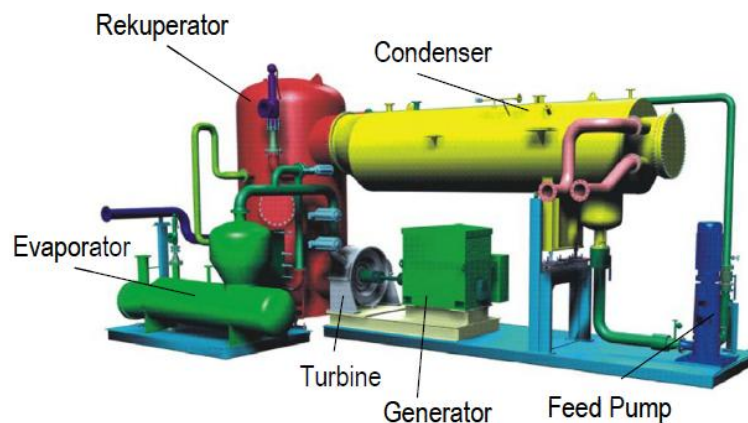
Figure 3.20 – View of a compact ORC module

The capital and operating cost of organic Rankine cycle systems vary depending on the system size and application. In general, the specific investment cost for ORC units varies in

the range 1500-3500 €/kWe for medium and large size power systems and about 3750-6000 €/kWe for small scale systems (Schuster et al., 2009; Tchanche et al., 2010b). For the ORC system installed at Lienz, Austria, the additional specific investment cost as compared to a conventional biomass heating plant amounts to 2765 €/kWe (Obernberger et al., 2002). The specific electricity production cost is 12.1 c€/kWhe. This incorporates biomass fuel costs. ORCs applied at the exhaust end of an existing gas engine, has a specific investment cost varying in the range 2500-3000 €/kWe (Invernizzi et al., 2007). The specific electricity production costs, could be below 5 c€/kWhe for medium and large scale systems and about 13.27 c€/kWhe for very small systems (Tchanche et al., 2010b).

3.4 Conclusion

Today, the organic Rankine cycle technology is a well-known and widely spread form of energy production, mostly in biomass and geothermal applications. Great rises in solar and heat recovery applications are expected in the near future. Environmental concern over climate change and rising oil prices are reasons supporting the explosive growth of this efficient, clean and reliable way of producing electricity.

Table 3.9 - Main ORC manufacturers

(Sources: Manufacturers websites; Quoilin & Lemort, 2009; Schuster et al., 2009)

Manufacturer	Applications	Heat source temperature (°C)	Power range (kW)	Electrical efficiency (%)	Fluid	Technology
ORMAT, USA (www.ormat.com)	Geo, WHR, Sol	150-300	200-7500	-	n-pentane	-
Turboden s.r.l, Italy (www.turboden.com)	Geo, CHP	100-300	200-2000	16-18	-	2-staged radial, Axial turbines
GMK GmbH, Germany (www.gmk.info)	WHR, Geo, CHP	120-350	50-2000	9-21	-	Screw motor, turbine
Kohler und Ziegler, Germany (www.kohler-ziegler.de)	CHP	>100	70-200	11	Hydrocarbons	Screw expander
Ergion GmbH, Germany (www.ergion.de)		120-300	4-300	13-16	Water-based with additives	Screw motor
ADORATEC GmbH, Germany (www.adoratec.com)	CHP	>100	300-1750	15-18		Turbine
WSK Energie und Umweltechnik GmbH, Germany (www.wsk-group.com)	WHR	490	52-65	16.3	Fluoric-hydrocarbons	Screw motor
UTC, USA, (www.utc.com)	WHR, Geo	>93	280			
Tri-o-gen, Netherlands (www.triogen.nl)	WHR	>350	60-160			Turbo-expander
FreePower, UK (www.freepower.co.uk)	WHR	180-225	6-120			
Cryostar (www.cryostar.com)	WHR, Geo	100-400			R134a, R245fa	Radial inflow turbine
Electratherm, USA, (www.electratherm.com)	WHR	>93	50			Twin screw expander

WHR: waste heat recovery; Geo: geothermal; Sol: solar; CHP: combined heat and power

4 - Fluid Selection for a Low-Temperature Solar Organic Rankine Cycle

4.1 Introduction

The performance and the economics of organic Rankine cycle systems are strictly linked to the thermodynamic properties of the working fluid (Tchanche et al., 2010b, Andersen & Bruno, 2005). This makes the working fluid selection a critical step in the design process. The present chapter provides an overview of main criteria that should fulfill a good working fluid. A methodology is presented and used in selecting appropriate fluids for a low-temperature solar driven organic Rankine cycle.

4.2 Working Fluids for Rankine Cycles

Various kinds of substances can be used as working fluids in Rankine cycles (Tchanche et al., 2009; Calm and Hourahan, 2007; Pridasawas, 2006, Chen et al., 2010). The most common ways of classifying them is by halocarbon numbering system (ASHRAE) or by chemical compounds (IUPAC). Below are summarized main families of potential fluids for organic Rankine cycles and few of them are displayed in Table 4.1.

- Alcohols: methanol, ethanol

- Inorganic fluids: Water (R718), Carbon dioxide(R744) and Ammonia (R717)

- Hydrocarbons (HCs): natural flammable substances able to react with halogens: Propane (R-290), n-Butane (R600), n-Pentane (R601), Benzene, etc.

- Chlorofluorocarbons (CFCs): all hydrogen atoms in a hydrocarbon molecule are replaced with chlorine, fluorine or bromine. e.g. R12, R13

- Hydrochlorofluorocarbons (HCFCs): partially halogenated hydrocarbons. e.g. R22

- Hydrofluorocarbons (HFCs): partially halogenated and chlorine free HCs. e.g. R134a

- Perfluorocarbons (PFCs): fully fluorinated HCs. e.g. PP50

- Ethers and Hydrofluoroethers (HFEs): eg. HFE7000, RE134, HFE7100

- Siloxanes, eg. Octamethyltrisiloxane (MDM), Hexamethyldisiloxane (MM)

- Mixtures:

  Azeotropic mixtures: mixtures of two or more compounds possess the same equilibrium vapor and liquid phase compositions at a given pressure. e.g. R500, R502.
  Zeotropic mixtures: mixtures of two or more compounds that change volumetric composition and saturation temperature as they boil. e.g. R404, R407.

Table 4.1 - Physical, safety and environmental data for few working fluids

(Source: Calm and Hourahan, 2007)

	Substances	Physical data				Safety data	Environmental data		
		Molecular Mass (kg/kmol)	T_b (°C)	T_c (°C)	P_c (bar)	ASHRAE 34 safety group	Atmospheric life time (yr)	ODP	GWP (100 yr)
1	RC318	200.03	-6.0	115.2	2.778	A1	3200	0	10250
2	R600a	58.12	-11.7	135	3.647	A3	0.019	0	~20
3	R114	170.92	3.6	145.7	3.289	A1	300	1.000	10040
4	R600	58.12	-0.5	152	3.796	A3	0.018	0	~20
5	R601	72.15	36.1	196.5	3.364	-	0.01	0	~20
6	R113	187.38	47.6	214.1	3.439	A1	85	1.000	6130
7	Cyclohexane	84.16	80.7	280.5	4.075	A3	n.a	n.a	n.a
8	R290	44.10	-42.1	96.68	4.247	A3	0.041	0	~20
9	R407C	86.20	-43.6	86.79	4.597	A1	n.a	0	1800
10	R32	52.02	-51.7	78.11	5.784	A2	4.9	0	675
11	R500	99.30	-33.6	105.5	4.455	A1	n.a	0.738	8100
12	R152a	66.05	-24.0	113.3	4.520	A2	1.4	0	124
13	R717 (Ammonia)	17.03	-33.3	132.3	11.333	B2	0.01	0	<1
14	Ethanol	46.07	78.4	240.8	6.148	n.a	n.a	n.a	n.a
15	Methanol	32.04	64.4	240.2	8.104	n.a	n.a	n.a	n.a
16	R718 (Water)	10.2	100	374	22.064	A1	n.a	0	<1
17	R134a	102.03	-26.1	101	4.059	A1	14.0	0	1430
18	R12	120.91	-29.8	112	4.114	A1	100	1.000	10890
19	R123	152.93	27.8	183.7	3.668	B1	1.3	0.020	77
20	R141b	116.95	32.0	204.2	4.249	n.a	9.3	0.120	725

4.3 Criteria and methodology for fluid selection

4.3.1 Overview of selection criteria

A selection process of an item in a precise group of similar items requires criteria and selection procedure. This applies also to the selection of working fluids for Rankine cycles. For this particular case of organic and inorganic fluids, several works have been reported in literature and a non-exhaustive list of papers dealing with the working fluids selection for organic Rankine cycle applications is given in Table 4.2. However, the study is one of the first works dealing with selection of fluids for solar applications. Majority of works available in literature focus the waste heat recovery application. Nevertheless there exist general criteria that apply to almost all applications:

- *Critical parameters*

The critical point is the point on a thermodynamic diagram for which the thermodynamic properties of liquid and vapor meet and become indistinguishable. The temperature, density and composition of the substance are the same for a liquid or gas at this point. The properties at the critical point are referred to as the critical density, critical temperature, critical volume and critical pressure. Depending on the type of the cycle (supercritical or subcritical), the critical parameters should be compared to the set operating conditions of the cycle. In case the cycle is subcritical as in most cases, the critical point should be appropriately above the system evaporating point in order to optimize the heat transfer (Badr et al., 1985; Tchanche et al., 2009b).

- *The cycle pressures*

The pressure in the evaporator should not be excessive. Moderate pressure is recommended in order to avoid mechanical stress problems. Very high pressure will cause safety problems and increase the cost of the system by requiring additional safety equipments. The condenser saturation pressure should be kept above the atmospheric pressure. A low condenser pressure could lead to problems of sealing against infiltration of the atmospheric air into the system. Therefore, for safety and economic reasons, the pressure in the heat exchange units should be kept above 1 bar for condensers and below 25 bar for evaporators (Maizza & Maizza, 1996; Badr et al., 1985).

- *The slope in a T-s diagram*

Usually, three groups of fluids are distinguished: dry (positive slope), isentropic (infinite slope) and wet (negative slope) fluids (Badr et al., 1985). For low-temperature systems and particularly with low power output levels, wet fluids like water, methanol or ethanol are not suitable (Hung et al., 2001). This category of fluids requires a superheat in order to avoid moisture after the expansion process. Fortunately, there are dry and isentropic fluids that do not exhibit excessive moisture during the expansion process. Isentropic expansion of isentropic fluids ends in saturated or superheated vapor regions and the erosion of the blades is avoided. Dry fluids with high positive slopes yield low thermal efficiencies and this can be overcome by integrating a regenerative heat exchanger in the cycle as mentioned in chapter 2.

Table 4.2 – Selected papers on working fluids selection in ORCs

Fluids	Application(s)	T_{cs} (°C)	T_{hs} (°C)	Criteria	Selected fluids	References
Water, Ethanol, R11, R123, HFE7100, n-Pentane, iso-Pentane, Benzene, Toluene, p-Xylene	Waste heat recovery	30	200-300	Performance	Benzene, Toluene, R123	Liu et al. (2004)
Benzene, Toluene, p-Xylene, R113 and R123	Waste heat recovery	5-45	225-325	Performance	p-Xylene (HT) & R113, R123 (LT)	Hung (2001)
31 pure fluids: Alkanes, fluorinated alkanes, ethers, fluorinated ethers	Geothermal	30	100	Performance	R236ea, R600, R245fa, R600a, R245ca, RE143,	Saleh et al. (2007)
Propylene, R227ea, RC318, R236fa, isobutane, R245fa, zeotropic mixtures (propane/ethane)	Geothermal	25	80-115	Performance	Propylene, R227ea, R245fa	Borsukiewicz-Gozdur & Nowak (2007)
Butylbenzene, Propylbenzene, Ethylbenzene, toluene, OMTS	Biomass CHP	90	250-350	Performance	Alkylbenzenes	Drescher and Bruggemann (2007)
Ammonia, n-Pentane, R123, PF5050	Geothermal	30	70-90	Safety, performance	Ammonia	Hettierachchi et al. (2007)
n-pentane, 2-methylbutane, 2,2-dimethylpropane, benzene, toluene	Solar ORC	-	-	Thermal stability	n-Pentane	Andersen & Bruno (2005)
Zeotropic mixtures (R245fa/R152a)	Solar ORC	25	85	Performance	90/10	Wang & Zhao (2009)
Hydrofluorocarbons: HFC-23, HFC-143a, HFC-227ea, HFC-236fa, HFC-245fa	Refrigeration, ORC	-	-	Thermal stability	HFC-227ea (400 °C)	Angelino & Ivernizzi (2003)
R-134a, R-141b, R-13I1, R-7146, R-125	Refrigeration, ORC	-	-	Thermal stability	R125 (396 °C), R134a (368 °C)	Calderazzi & Colonna di Paliano (1997)
R123, water	ORC	-	-	Performance	R123	Yamamoto et al. (2001)
Hydrocarbons, alcohols, ethers, amines, esters, ketones, inorganic fluids	Waste heat recovery	35	157	Properties, Performance	R123	Lee et al. (1993)
68 fluids: refrigerants, hydrocarbons, etc	ORC	40	120	Properties, Performance	R113, R11, R114	Badr et al. (1985)
Unconventional fluids: refrigerants and azeotrope mixtures	Waste heat recovery	35-60	80-110	Properties, performance	R123, R124	Maizza & Maizza (2001)
HCFCs, HCs, HFCs and azeotrope mixtures	Waste heat recovery	-	-	Properties, performance	R125, R134a	Maizza & Maizza (1996)
20 fluids: hydrocarbons, refrigerants, and natural fluids	solar	25	60-100	Properties, performance	R134a, R152a, R290, R600, R600a	Tchanche et al. (2009)

Fluids	Application(s)	T_{cs} (°C)	T_{hs} (°C)	Criteria	Selected fluids	References
Water, Ammonia, butane, R11, R123, R141b, R236ea, R245ca, R113	Waste heat recovery	25	145	Performance	R236ea	Dai et al. (2009)
FC-75, FC-88, R113, R114, R11	Solar Rankine Cooling	-	-	Properties	R113, FC-88	Wali (1980)
R12, R11, R134a, R113	Waste heat recovery		<370	Properties, performance	R11, R12, R134a	Hung et al. (1997)
R227ea, R236ea	Cooling of equipment	18	70-90	Performance	R227ea	Nowak et al. (2007)
n-butane, n-pentane, hexafluorobenzene, MM, toluene, benzene, p-Xylene, MM/MDM/MD$_2$M	Waste heat recovery	15	457	Performance	Siloxanes mixtures	Angelino & Colonna di Paliano (1998)
Water, R142b, R123, R245fa, R113, R114	ORC	-	98	Performance	R245fa	Gu et al. (2007)
R113, R245fa, isobutane, toluene, cyclohexane, isopentane	Waste heat recovery			performance	Toluene, cyclohexane	Chacartegui et al. (2009)
R123, HFC-43-10mee, CFC-113, siloxanes, n-hexane, c-hexane, n-pentane, n-Octane, etc.	Waste heat recovery	15	250-350	Properties, performance	Esa-methyl-disiloxane	Invernizzi et al. (2007)
Propane, R134a, R227ea, R152a, ammonia, isobutene, butane, butane, R245fa, pentane, etc.	Solar	25		Collector aperture area	Isobutene, isopentane, R245fa, R245ca	Delgado Torres & Garcia-Rodriguez (2010)
Hydrocarbons, refrigerants	Solar RO-Desalination	15	different levels	performance	R218 / R245 / isopentane/n-propylbenzene	Bruno et al. (2008)
R-114, Ammonia, Propane	OTEC	40F	80F	A/Wnet	Ammonia	Ganic and Wu (1980)
R134a, R123, R227ea, R245fa, R290 and n-Pentane	Heat recovery	10 °C	<200 °C	Maximum power	R227ea, R245fa	Lakew and Bolland (2010)
R227ea, R245fa, isobutene, isopentane	Geothermal CHP	288.15 K	<450 K	Performance	Isopentane, R227ea	Heberle and Bruggeman (2010)
44 fluids: Hydrocarbons (HC), aldehydes, alcohols, amines, fluorinated amines, ether-amines, ethers, formates, fluorinated ethers and hydrofluorocarbons (HFC)	Heat recovery	20-25 °C	90 °C	Objective function (f), properties, components cost	(f) methyl-formate, methoxy-ethane, methanol, N-methyl-ethylamine, FCH$_2$-O-O-H$_2$CF	Papadopoulos et al. (2010)

- *Fluid specific volumes*

A good fluid should have low vapor and low liquid specific volumes (Badr et al., 1985). These properties affect the rates of heat transfer in the heat exchangers. The vapor specific volumes relate directly to the size and cost of the expander (Tchanche et al., 2010b). Moreover, a high vapour specific volume leads to larger volumetric flows requiring a multiplicity of exhaust ends of the expander and resulting in significant losses. The specific volume of the liquid at the condenser pressure should be as small as possible to minimize the required feed pump work.

- *Heat transfer properties*

The heat-transfer properties of the working fluids are of great importance. Desirable properties are: low viscosity, low surface tension, low liquid specific heat, high thermal conductivity and high latent heat of vaporization (Badr et al., 1985; Wali, 1980). The evaporator enthalpy ratio i.e. the ratio of enthalpy of vaporization to the sensible enthalpy required to raise the temperature of the compressed liquid should have a high value. This has the advantage of reducing the amount of heat required for the preheating of the working fluid and allows most heat to be added at relatively higher temperature and the cycle then, can approach more closely the Carnot cycle.

- *Molecular weight*

The matter of the fluid molecular weight arises when designing the turbine. From various investigations found in literature (Lee et al., 1993; Badr et al., 1985), the following conclusion can be made: for a higher temperature or higher power output level using multi-stage turbines, working fluids with low molecular weight (<90 kg/Mol) are favorable while working fluids with high molecular weight (>90 kg/Mol) are suitable for low power output plants using single-stage turbines. The illustration is given in Table 4.3 which shows the comparison of the turbine isentropic efficiencies for different power levels.

Table 4.3 - Comparison of turbine isentropic efficiencies using steam (low molecular weight) and a high molecular weight working fluid

(Source: Stine and Geyer, 2001)

	Turbine isentropic efficiency (%)	
Power level	low Molecular Weight	High Molecular Weight
>10 MW	70-80	75-80
1-5 MW	50-70	75-80
200-500 kW	30-50	75-80
10-100 kW	25-50	60-75

- *Thermal stability and fluid compatibility with materials*

Thermal stability and fluid compatibility with materials and lubricants are critical parameters. The fluid must have a high thermal stability to provide the desired lifetime and a cost-effective plant. Care should be taken to make sure that the combination fluid/lubricant/material can assure a long lifetime period of the plant. The lubricant can be miscible or immiscible with cycle fluid, but for minimum system complexity miscible oil is

desirable. Chemical decomposition of the fluid not only reduces the plant efficiency and makes the replacement of the fluid necessary but can produce non-condensable gases which have corrosive effects on the materials of the system. In order to study the fluids decomposition, two methods are available: the dynamic loop tests and the static capsule tests. In Table 4.4 are displayed the maximum stability temperature of some fluids.

Table 4.4: Maximum stability temperature (MST) of some fluids

Fluid	MST (°C)	Material	References
R227ea	425	Stainless steel (AISI 316)	Angelino and Invernizzi (2003)
R23	400	Stainless steel (AISI 316)	#
R236fa	400	Stainless steel (AISI 316)	#
R143a	350	Stainless steel (AISI 316)	#
R245fa	300	Stainless steel (AISI 316)	#
R134a	368	Stainless steel	Calderazzi and Colonna di Paliano (1997)
R141b	90	Stainless steel	#
R13I1	102	Stainless steel	#
R7146	204	Stainless steel	#
R125	396	Stainless steel	#
Methanol	175-230	#	Stine and Geyer (2001)
Toluene	400-425	#	#
R113	175-230	#	#

- *Safety properties*

The ASHRAE 34 safety classification that applies for refrigerants can be used. This classification is based on two key parameters: the toxicity and the flammability. Toxicity can be identified by some numbers such as TLV (Threshold Limit Value). Flammability is generally identified by the LFL (Lower flammability limit) and the HOC (Heat of Combustion). The ASHRAE standard 34 is made of two classes of toxicity (**A**: refrigerants for which toxicity has not been identified at concentrations less than or equal to 400 ppm and **B**: refrigerants for which there is evidence of toxicity at concentrations below 400 ppm) and three groups of flammability characteristics (**1**: refrigerants that do not show flame propagation when tested in air at 21 °C and 101 kPa, **2**: refrigerants having a LFL> 0.10 kg/m^3 at 21 °C and 101 kPa and a HOC< 19 kJ/kg and **3**: refrigerants that are highly flammable as defined by a LFL≤ 0.10 kg/m^3 at 21 °C and 101 kPa or a HOC≥ 19 kJ/kg). The matrix shown in Table 4.5 was adopted for an easy identification of the safety level of any substance. From this classification, the most desirable class is A1. In addition to the aforementioned desirable safety properties, the working fluid should be non-explosive and non-radio-active.

Table 4.5 - ASHRAE 34 Refrigerant Safety Classification

	Lower toxicity	Higher toxicity
Higher flammability	A3	B3
Lower flammability	A2	B2
No flame propagation	A1	B1

- *Economics and availability*

The phase-out of some categories of substances by the International Protocols has stimulated the research on more environmentally friendly fluids. Before considering a fluid as a potential candidate, a market investigation should be done to know if the fluid is market available and cheap. To give an idea of the prices of some fluids, the information in Table 4.6 below was taken from a supplier in Athens, Greece.

Table 4.6 - Prices of few fluids (The prices do not include VAT)

Fluids	Price (Euro/kg)
FREON 22 DU PONT	3.33
SUVA 134A DU PONT	6.34
SUVA 401B DU PONT	10.85
SUVA 407C DU PONT	6.63
SUVA 123 DU PONT	11.76

- *Environmental criteria*

The impact of a substance on the environment is characterized by parameters like ozone depletion potential (abbr. ODP; it is an indicator that measures the ability of a substance to destroy stratospheric ozone molecules. R11 is taken as reference and its ODP is 1), global warming potential (abbr. GWP; it indicates the potency of a substance to warm the planet by acting as a greenhouse gas. This indicator is calculated taking the carbon dioxide (CO_2) as reference substance), atmospheric lifetime (abbr. ALT; it is an indication of the average persistence of a substance released into the atmosphere until it decomposes, reacts with other chemicals, or is otherwise removed). Table 4.1 lists environmental data for few fluids. For many countries, it will be difficult to meet the phase-out and the mitigation of non-environmentally friendly substances as scheduled by the International Protocols, the risk being the negative impact on the economy. For the sake of a safe environment, the designers when selecting a working fluid for a particular application should insist on substances for which the ODP, GWP and ALT are as low as possible (Calm and Hourahan, 2007).

- *System performance*

In the previous subsections, a certain number of criteria that should fulfill a good fluid were listed. However, the most important step remaining is to know how could perform the system using a particular fluid in realistic conditions. The easiest and fastest way is to perform the simulation of the system using a computer program and a database of thermodynamic properties of the fluid. Using the first and second law of thermodynamics, the performance of the system can be evaluated under diverse working conditions.

4.3.2 Methodology

Most of authors while selecting a working fluid for an organic Rankine cycle, consider the cycle thermal efficiency as the most determinant parameter. This is not for sure the most appropriate way. Many other parameters should be taken into consideration. A very efficient plant can be bulky, expansive and not safer neither for the operator nor for the environment. On the other hand, it is not easy to find an ideal fluid that fulfils all the desired criteria mentioned in the previous section (4.3.1). Since, the ideal working fluid does not exist a compromise should be found among the desired criteria. A general methodology is proposed here. It comprises three main steps:

- Step 1: Data collection,

- Step 2: Data analysis and

- Step 3: Decision.

At the first step, the operating conditions are set and various data (thermophysical, safety, environmental and calculated properties) concerning different fluid candidates collected. The data are then analyzed at the second step. At this phase, the criteria are classified starting by the most critical ones and the process is done sequentially. At each sub-step, all the fluids screened using the criterion and before going to the next criterion, the fluids are put in two groups: those which fulfill the criteria and those which do not. At the last step, the best fluid should come out followed by some alternatives. All the criteria should be taken into consideration. Usually, it is not easy to make up the decision, and some authors propose to combine several criteria into one that could be used as an "objective criterion" (Madhawa et al., 2007; Mikielewicz and Mikielewicz, 2010, Papadopoulos et al., 2010). Steps are illustrated on Figure 4.1.
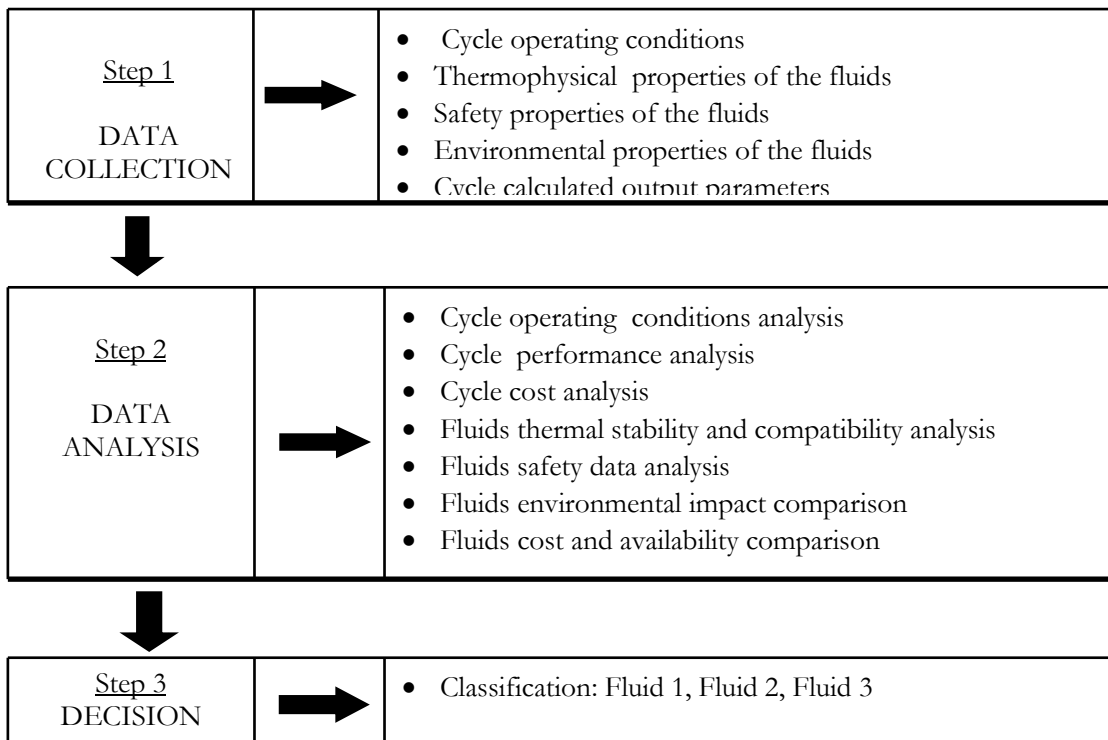
Figure 4.1 - General selection procedure

4.4 Case study: a low-temperature solar organic Rankine cycle

4.4.1 System description and modeling

4.4.1.1 System description

A schematic of the system is shown in Figure 4.2. Hot water serving as heat transfer fluid at maximum temperature of 90 °C is produced by conversion of solar radiation into heat by solar collectors. Characteristics of 20 potential working fluids are evaluated and compared for a 2 kWe micro-power system.
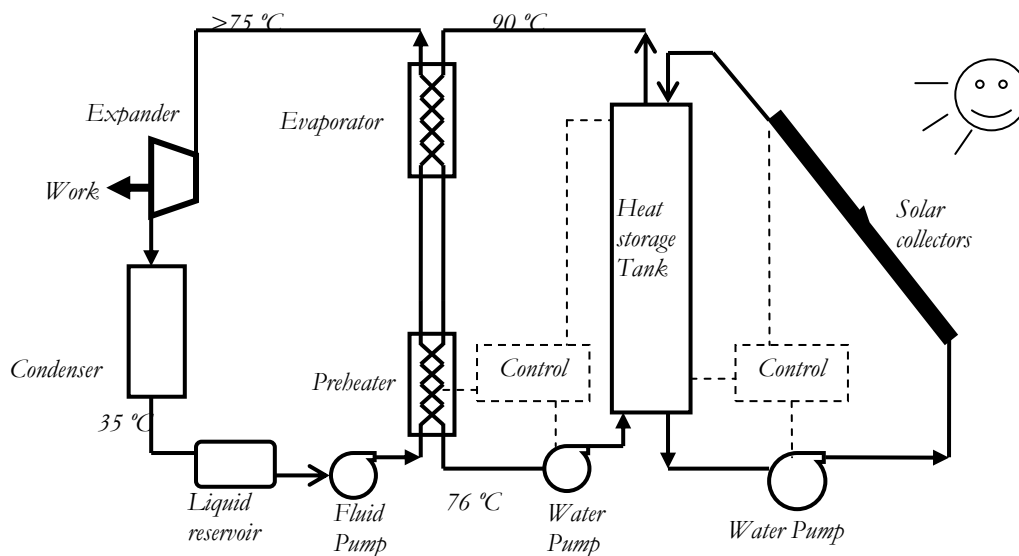
Figure 4.2 - Schematic of the low-temperature solar organic Rankine cycle with heat storage system

The present organic Rankine cycle system consists of heat exchangers (pre-heater, boiler/evaporator), a micro-turbine/expander, a condenser and a pump. The micro-turbine considered here is similar to the scroll expander investigated by Kane (2002), Manolakos et al. (2007), Quoilin et al. (2008) and Lemort (2006 & 2008). The pump supplies the working fluid to the heat exchangers (preheater, evaporator) where it is heated and vaporized by the hot water from the collector array. The generated high pressure vapor flows into the expander and its enthalpy is converted into work. The low pressure vapor exits the expander and is led to the condenser where it is liquefied by air. The liquid available at the condenser outlet is pumped back to the upper heat exchangers and a new cycle begins. All the above described processes are shown in a T-s diagram in Figure 4.3.
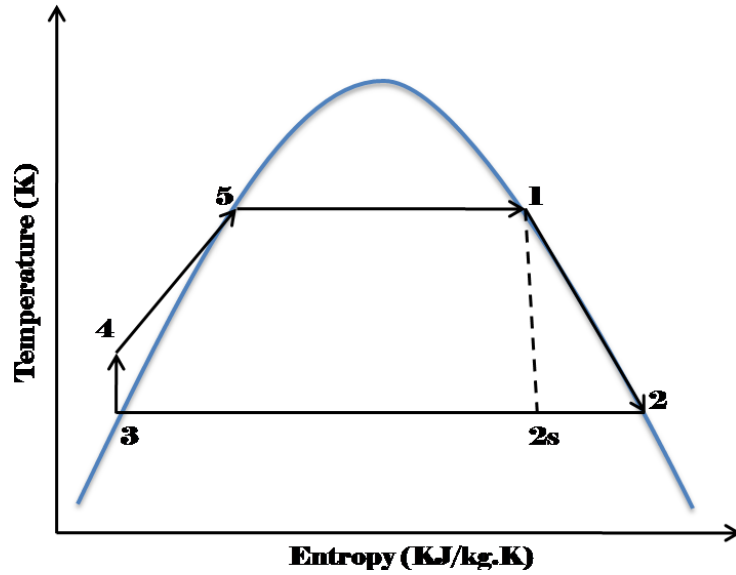
Figure 4.3 - T-s process diagram of the ORC
(1-2: Expansion, 2-3: Condensation, 3-4: Pumping, 4-5: Preheating, 5-1: Vaporization)

4.4.1.2 Modelling

Using First and Second Laws of Thermodynamics (Çengel & Boles, 2002), the performance of the system is evaluated under diverse working conditions for different organic working fluids. For simplicity, the internal irreversibility and, accordingly the pressure drops in the components other than the turbine, such as the preheater, evaporator, condenser and pipes, are ignored. For each individual component, the first and second laws of thermodynamics are applied to find the work output or input, the heat added or rejected, and the system irreversibility. The equations obtained are summarized below.

Expander

$$\dot{W}_t = \dot{m}_{wf}(h_1 - h_{2s})\eta_{st}\eta_{mech} = \dot{m}_{wf}(h_1 - h_2)\eta_{mech} \tag{4.1}$$

$$\dot{I}_t = T_0\, \dot{m}_{wf}(s_2 - s_1) \tag{4.2}$$

Condenser

$$\dot{Q}_{cd} = \dot{m}_{wf}(h_2 - h_3) \tag{4.3}$$

$$\dot{I}_{cd} = T_0\, \dot{m}_{wf}[(s_3 - s_2) - \frac{h_3 - h_2}{T_L}] \tag{4.4}$$

Upper Heat Exchangers

$$\dot{Q}_{uhx} = \dot{m}_{wf}(h_1 - h_4) \tag{4.5}$$

$$\dot{I}_{uhx} = T_0\, \dot{m}_{wf}[(s_1 - s_4) - \frac{h_1 - h_4}{T_H}] \tag{4.6}$$

Pump

$$\dot{W}_p = \dot{m}_{wf}\, \nu_3(P_4 - P_3)/\eta_p \tag{4.7}$$

$$\dot{I}_p = T_0\, \dot{m}_{wf}(s_4 - s_3) \tag{4.8}$$

First Law Efficiency

$$\eta_{th} = (\dot{W}_t - \dot{W}_p)/\dot{Q}_{uhx} \tag{4.9}$$

| Second Law Efficiency | $\eta_{II} = \eta_{th}/(1-T_L/T_H)$ | (4.10) |

$$\dot{I}_{tot} = \sum_j \dot{I}_j = T_0 \, \dot{m}_{wf} \left[-\frac{h_1 - h_4}{T_H} - \frac{h_3 - h_2}{T_L} \right]$$

System Total Irreversibility (4.11)

$$\varphi = \frac{h_1 - h_5}{h_1 - h_4} = \frac{\Delta h_{fg}}{\Delta h_{tot}}$$

Input Enthalpy Ratio (4.12)

4.4.1.3 Assumptions and calculations method

The operating conditions are given in Tale 4.7 along with the characteristics of the expander and the pump. Hot water at 90 ºC is provided by solar collectors. The condenser is cooled by ambient air. The system is assumed to be located in a hot area where the average monthly ambient temperature is around 28 ºC. Figure 4.4 shows the yearly variations of the ambient temperature for such locations (Meteonorm, 2005).

Table 4.7 - Input data for the analysis of the ORC

Evaporating temperature	T_{ev} (ºC)	75
Condensing temperature	T_{cd} (ºC)	35
Mechanical efficiency of the turbine	η_{mt} (-)	0.63
Isentropic efficiency of the turbine	η_{st} (-)	0.70
Pump efficiency	η_p (-)	0.80

As result of a first screening, 20 first fluids presented in Table 4.1 emerged as potential candidates. Only one criterion was considered at this first step: $T_{ev} \ll T_c$ and preferably should satisfy $T_{ev} < 0.96 T_c$ (Tchanche et al., 2009b) because of subcritical operations. The vapor at the turbine inlet is saturated. The superheat was not found of interest as the incorporation of a superheater could bring additional cost. The thermodynamic properties of fluids and system performance were evaluated with a simulation tool EES (Engineering Equation Solver) (Klein, 2008).
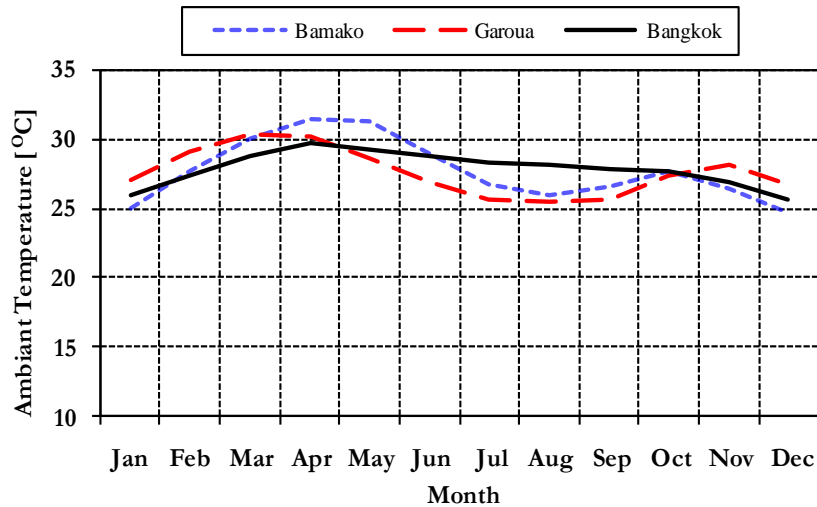
Figure 4.4 - Average Monthly Ambient Temperature for three locations: Bamako (Mali), Garoua (Cameroon) and Bangkok (Thailand).

Table 4.8 - Comparison of the performances of different working fluids for a 2 kW power output

	Substance	Type*	P_{min} [MPa]	P_{max} [MPa]	PR	$\dot{V}_2$ [m³/h]	VFR ($\dot{V}_2/\dot{V}_1$)	ν_2 (m³/kg)	$\dot{m}_{wf}$ [kg/s]	η_{th} [%]	η_{II} [%]	φ [%]	$\dot{I}_{tot}$ [kW]	$\dot{Q}_{uhx}$ [kW]	Δh_{fg} [kJ/kg]	x_2
1	RC318	d	0.425	1.201	2.825	39.48	3.294	0.028	0.381	3.715	21.76	61.48	5.104	47.01	75.83	1
2	R600a	d	0.463	1.191	2.57	39.02	2.802	0.088	0.122	4.055	23.75	71.07	4.579	44.20	255.7	1
3	R114	d	0.290	0.826	2.84	55.57	3.025	0.050	0.305	4.122	24.14	70.96	4.659	45.04	104.6	1
4	R600	d	0.329	0.907	2.758	50.36	2.893	0.128	0.108	4.236	24.81	74.21	4.462	43.91	300.2	1
5	R601	d	0.098	0.323	3.285	141	3.307	0.369	0.106	4.367	25.58	76.65	4.501	44.67	323	1
6	R113	d	0.065	0.232	3.558	197.7	3.52	0.215	0.254	4.456	26.1	77.85	4.391	44.11	134.8	1
7	Cyclohexane	d	0.020	0.084	4.232	557.7	4.038	1.58	0.098	4.609	27	81.8	4.206	43.17	360	1
8	R290	w	1.218	2.85	2.34	16.99	2.717	0.037	0.127	3.428	20.08	63.1	4.614	42.43	210.4	0.987
9	R407C	w	1.535	3.735	2.433	13.34	2.611	0.014	0.250	3.087	18.08	59.3	5.155	45.26	102.9	0.913
10	R32	w	2.19	5.417	2.474	9.019	3.015	0.011	0.212	2.611	15.3	46.51	4.724	40.79	89.28	0.728
11	R500	w	1.001	2.475	2.473	18.98	2.72	0.020	0.256	3.712	21.74	68.13	4.508	42.53	113.1	0.987
12	R152a	w	0.794	2.108	2.652	21.95	2.839	0.039	0.154	3.985	23.34	71.81	4.443	42.92	200.2	0.977
13	R717(Ammonia)	w	1.351	3.709	2.746	11.87	2.627	0.087	0.037	4.352	25.49	81.85	4.121	41.63	907.5	0.917
14	Ethanol	w	0.013	0.088	6.468	610.6	5.841	3.951	0.042	4.796	28.09	88.2	3.932	41.59	854.6	0.982
15	Methanol	w	0.027	0.148	5.416	336.1	4.725	2.704	0.034	4.845	28.38	90.77	3.856	41.14	1082	0.952
16	R718(Water)	w	0.005	0.038	6.854	1413	5.784	23.93	0.016	4.899	28.7	93.28	3.793	40.81	2321	0.949
17	R134a	i	0.887	2.366	2.666	20.1	3.056	0.022	0.244	3.703	21.69	64.94	4.651	43.57	115.8	0.992
18	R12	i	0.847	2.086	2.463	22.43	2.679	0.020	0.301	3.835	22.46	70.06	4.465	42.60	99.15	1
19	R123	i	0.130	0.431	3.298	104.9	3.304	0.128	0.227	4.457	26.11	77.48	4.318	43.54	148.2	1
20	R141b	i	0.112	0.371	3.309	121.7	3.234	0.195	0.173	4.526	26.51	80.21	4.242	43.17	199.7	1

(i: isentropic; w: wet; d: dry)

4.4.2 Results and discussion

The results displayed in Table 4.8 were obtained for a 2 kW organic Rankine cycle system.

4.4.2.1 Cycle pressure

According to Badr et al. (1985) and Maizza and Maizza (1996), good pressure values are in the range 0.1-2.5 MPa and a pressure ratio of about 3.5 is reasonable. From Table 4.8, the following observations can be made concerning the pressure in the condenser and the upper heat exchangers. R113, cyclohexane, methanol, water and ethanol present low condenser pressures. R407C, R32 and R717 have higher pressures above 3 MPa in the evaporator. Methanol, water, ethanol, cyclohexane and R113 have higher pressure ratio. Ethanol and water have low evaporating pressure. Isentropic fluids present pressure values that fall in the range prescribed by the above cited authors, and therefore are good fluids from a pressure point of view. Other fluids with good condensing and evaporating pressures are RC318, R600a, R600, R114, R601, R500 and R152a.

4.4.2.2 Turbine outlet volume flow rate

The turbine outlet volume flow rate determines its size and the system cost. Results of calculations in Table 4.8 let see that n-Pentane, R113, cyclohexane, water, ethanol, methanol, R123 and R141b exhibit high volume flow rates. Fluids with low volume flow rate are preferable for economic reasons. Among these are: R32, Ammonia, R407C, R290, R500, R134a and R152a. From Figure 4.5, it is seen that in general, the volume flow rate decreases with an increment of temperature. A prediction for fluids not suitable in the range of temperature considered here to be at higher temperature can be raised.
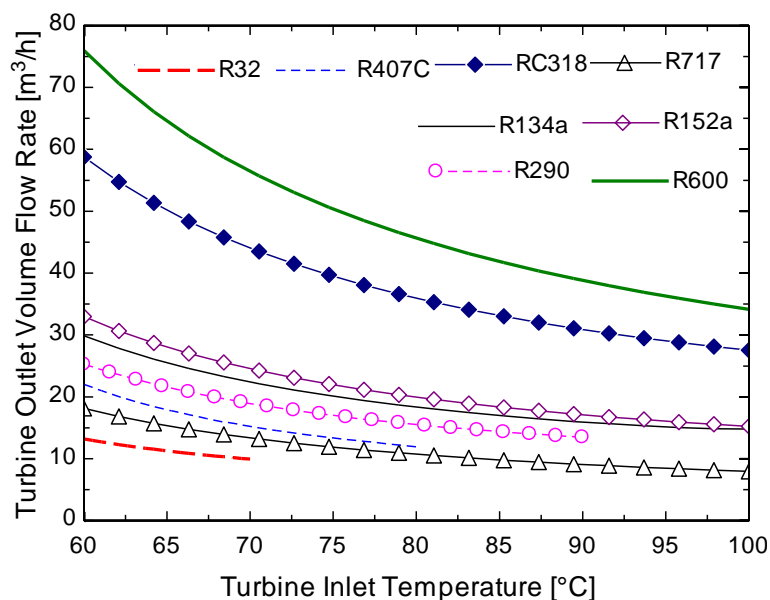
Figure 4.5 - Turbine outlet volume flow rate versus turbine inlet temperature for various working fluids at T_c=35 °C.

4.4.2.3 Cycle efficiency

The system thermal efficiency ranges from 2.61% for R32 to 4.89% for water. Figure 4.6 shows the effects of the variation of the turbine inlet pressure. The temperature difference ΔT_{ht} is maintained constant and the vapor at the expander inlet saturated. The system thermal efficiency increases with a raise of the turbine inlet pressure. For high boiling point fluids water and ethanol are more efficient compared to n-Pentane and R123.
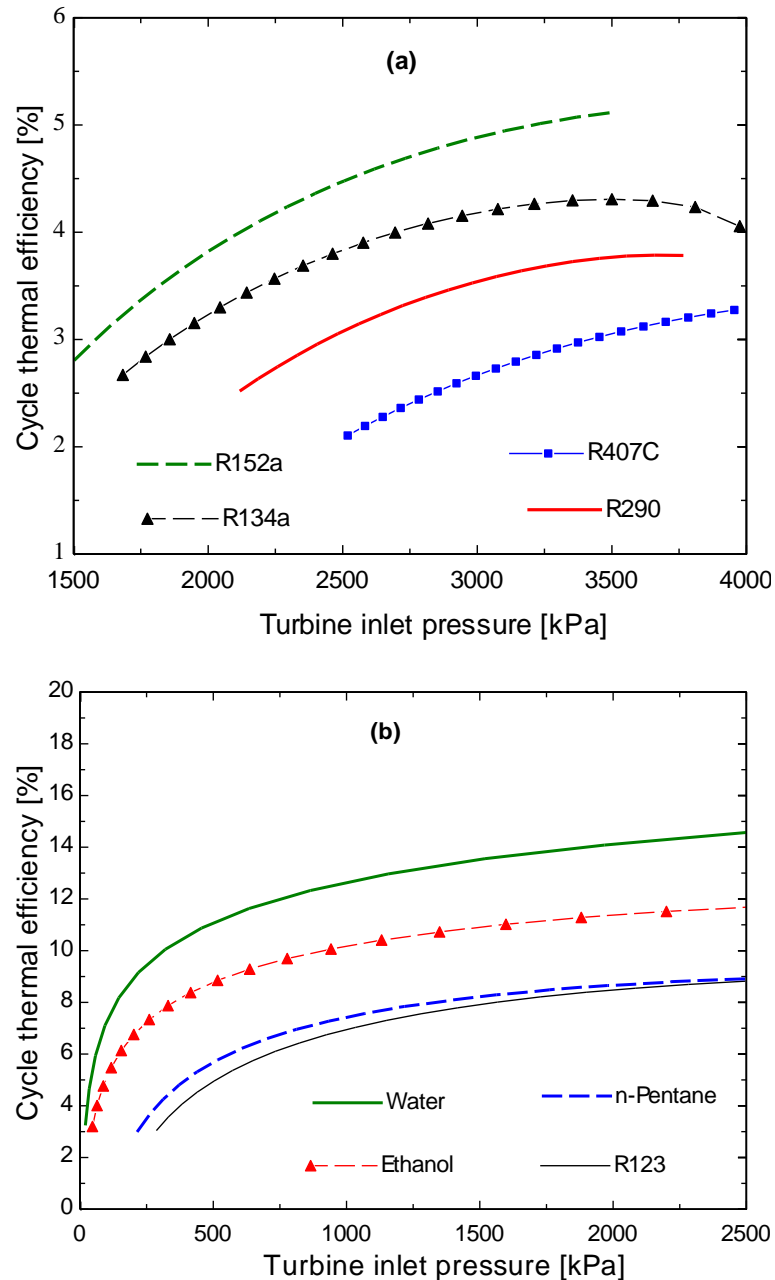
Figure 4.6 - System thermal efficiency versus turbine inlet pressure for (a) fluids with low normal boiling points and (b) fluids with high normal boiling points at $T_c=35$ °C and $\Delta T_{ht}=15$ °C

In Table 4.8, the second law efficiency varies from 15.3% (R32) to 28.7% (water). Effects of the turbine inlet pressure on the system second law efficiency can be seen on Figure 4.7. For low boiling point fluids, second law efficiency shows a maximum which suggests the existence of an optimal operating condition. System second law efficiency for the second group increases in a short range 0-1.0 MPa and decreases slightly for higher pressures.
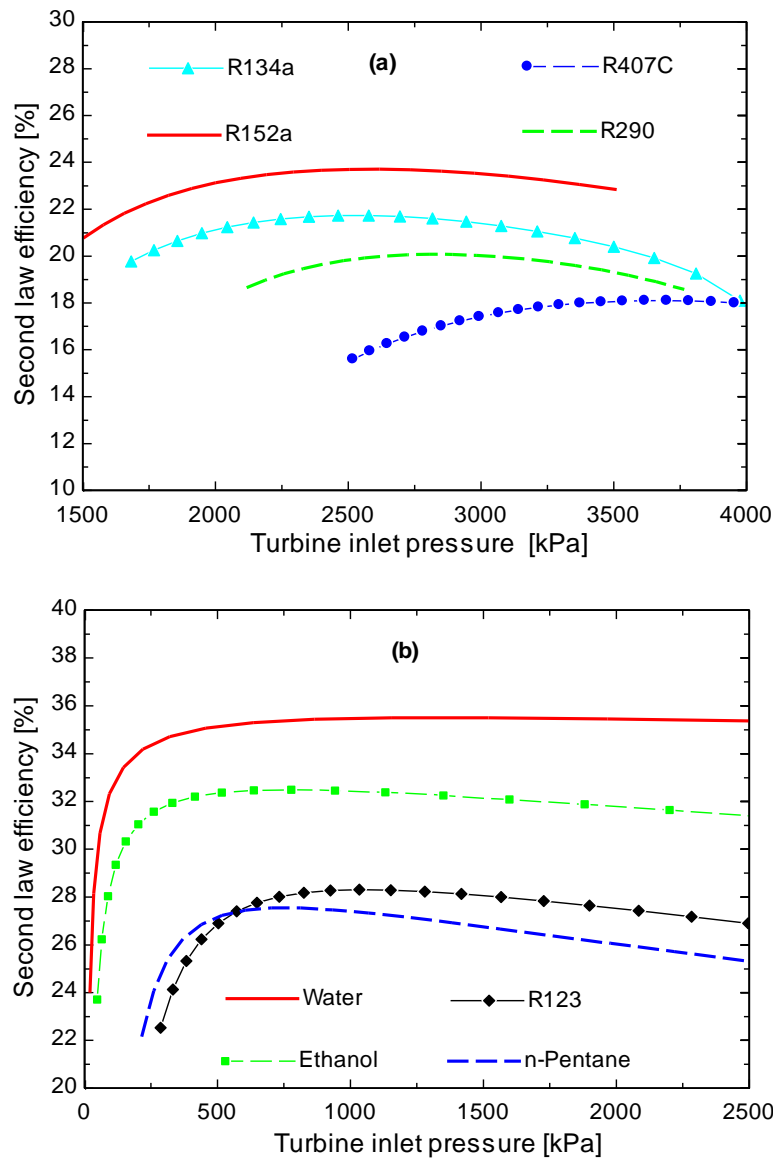
Figure 4.7 - System second law efficiency versus turbine inlet pressure for (a) fluids with low normal boiling points and (b) fluids with high normal boiling points at T_c=35 °C and ΔT_{ht}=15 °C

4.4.2.4 Irreversibility

From Table 4.8, system total irreversibility varies in the range 3.79-5.15 kW. Water and R407C yield the lowest and highest irreversibility rates, respectively. Figure 4.8 shows the irreversibility distribution for different components and for different fluids. It can be seen that the upper heat exchangers (preheater, evaporator) are the components that

have the biggest contribution to the overall irreversibility followed by the turbine. Both components represent 78% of the system total irreversibility.
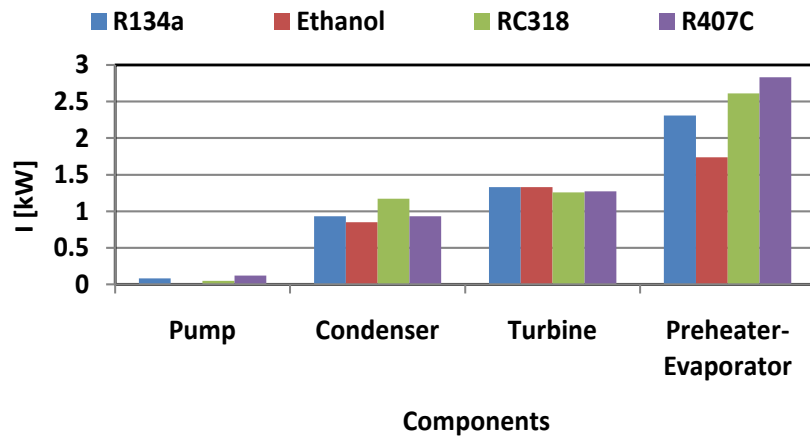
Figure 4.8 - The distribution of irreversibility in different components for several fluids: R134a, R407C, RC318 and Ethanol.

The analysis of the system irreversibility was carried out based on the changes operated on some parameters. In order to study the effects of the heat source temperature on the system irreversibility, the temperature difference between the heat source and the turbine inlet was maintained constant ($\Delta T_{ht}=15$ °C). While varying the turbine inlet temperature and keeping the working fluid state along the vapor saturation curve, Figures 4.9 show that the effects of the heat source temperature on the system irreversibility. In Figure 4.9a, the system total irreversibility decreases faster for low boiling points fluids as the operation pressure at the turbine inlet increases and reaches a limit of 4 kW. The lowest irreversibility rate is obtained for RC318. In Figure 4.9b, the system total irreversibility increases as the pressure at the turbine inlet increases. For this category, the system irreversibility is lower compared to fluids with low boiling points temperature. Water yields the lowest irreversibility rate followed by methanol and ethanol.
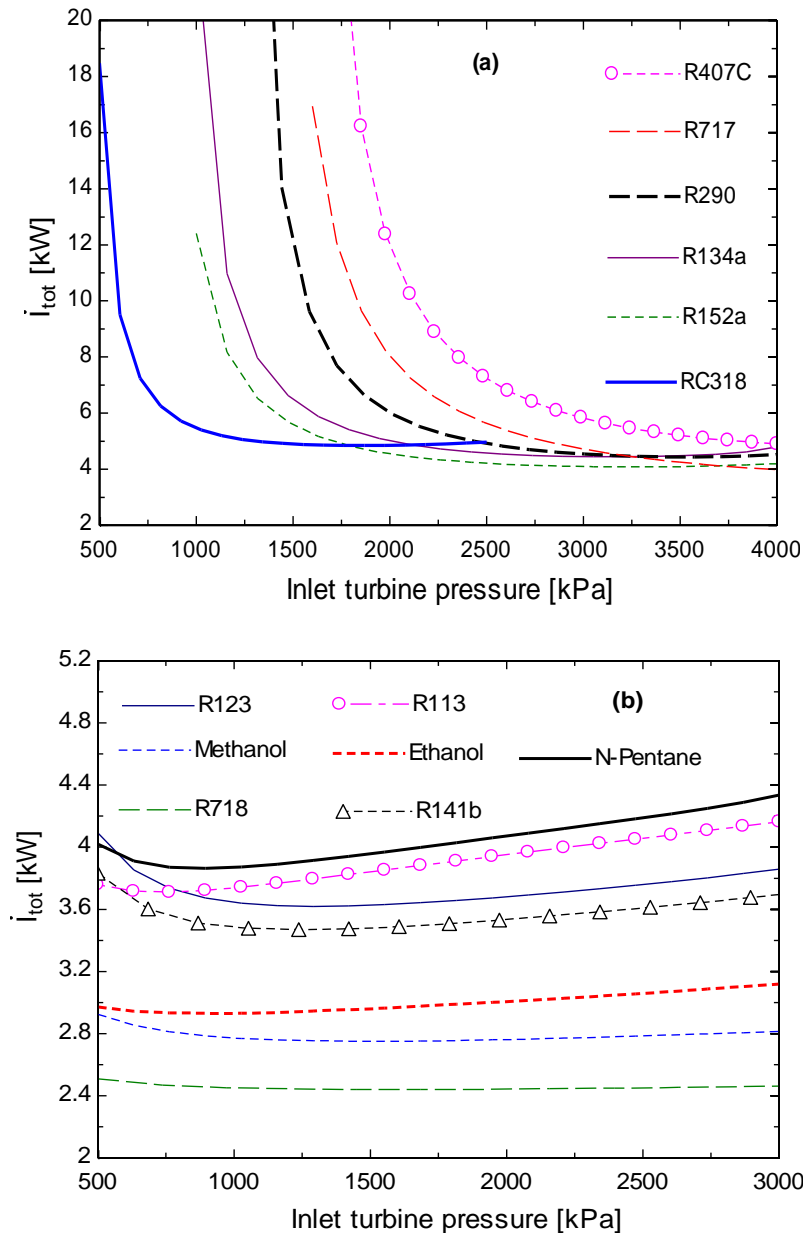
Figure 4.9 - System total irreversibility rate versus turbine inlet pressure for working fluids with (a) low normal boiling points and (b) high normal boiling points at T$_c$=35 °C.

In the second part of the analysis, the temperature of the heat source was kept constant. As shown in Figures 4.10, the system total irreversibility decreases as the turbine inlet pressure increases. As conclusion, small temperature difference between the fluid streams improves the system's performance.
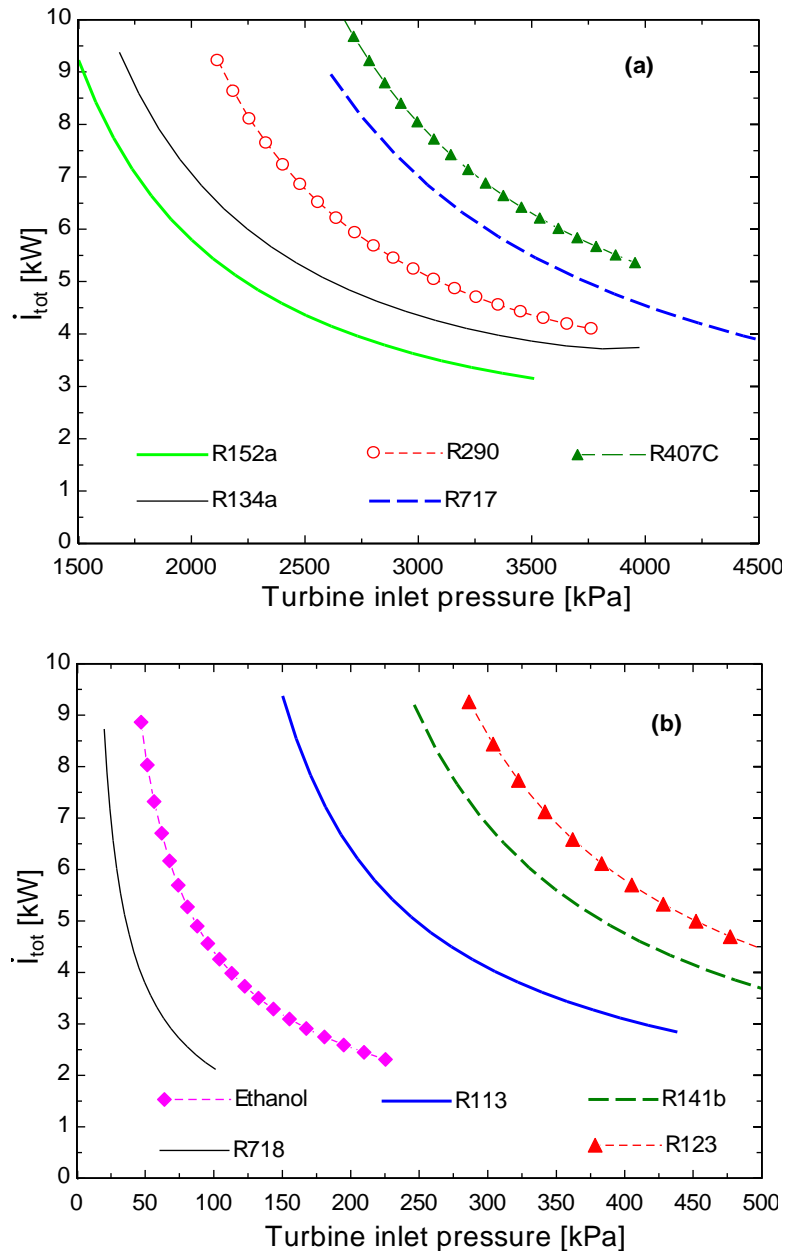
Figure 4.10 - System total irreversibility rate versus turbine inlet pressure for working fluids with (a) low normal boiling points and (b) high normal boiling points at T_c=35 °C and a heat source temperature of 90 ºC.

4.4.2.5 Mass flow rate

As can be seen on Table 4.8, water, ethanol and methanol yield lowest maximum pressures and highest enthalpy heat of evaporation (Δh_{fg}). This is an advantage for these fluids which will require lower mass flow rates, and hence lower heat input. Ammonia, has a higher evaporating pressure, but yields a low mass flow rate and high heat of vaporization. From Figure 4.11, it can be seen that the system mass flow rate decreases when the turbine inlet temperature increases. For economical reasons, fluids with low mass flow rates like ammonia, ethanol and methanol are interesting especially for large capacity systems.
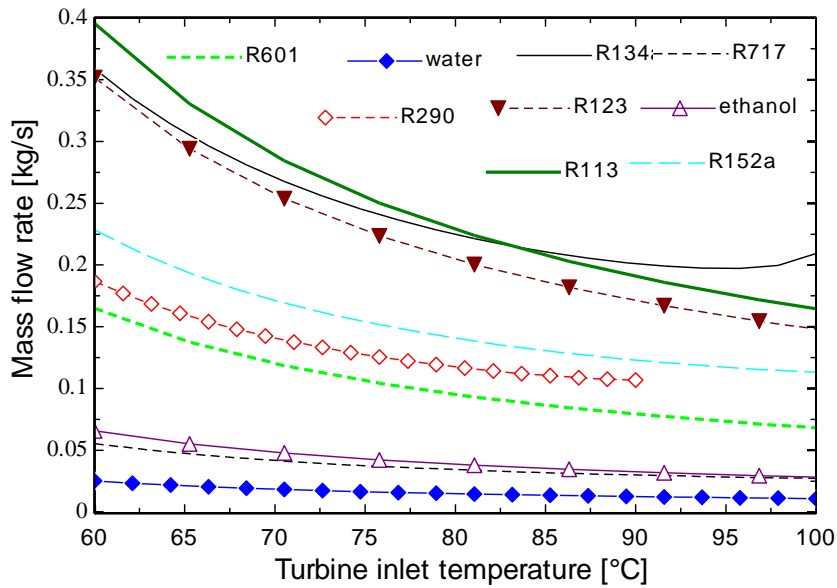
Figure 4.11 - Mass flow rate versus turbine inlet temperature for various working fluids at $T_c=35°C$.

4.4.2.6   Analysis of the heat input

System heat input is of great importance in a solar ORC. It determines the size of the collector array and constitutes major part of system cost. Therefore, solar applications will be more competitive with fluids for which the amount of heat required is small. From Table 4.8, the heat required for a 2 kW power output falls in the range 40-47 kW. Fluids with high Δh_{fg} require low heat rates; these are: water, ethanol, methanol and ammonia. From Figure 4.12, it is deduced that high temperature saturated vapors reduce the amount of heat input. This let us think that when designing a solar ORC, depending on the application, one could choose between a system with large collector area-low temperature and a system with small collector area-high operating temperature.
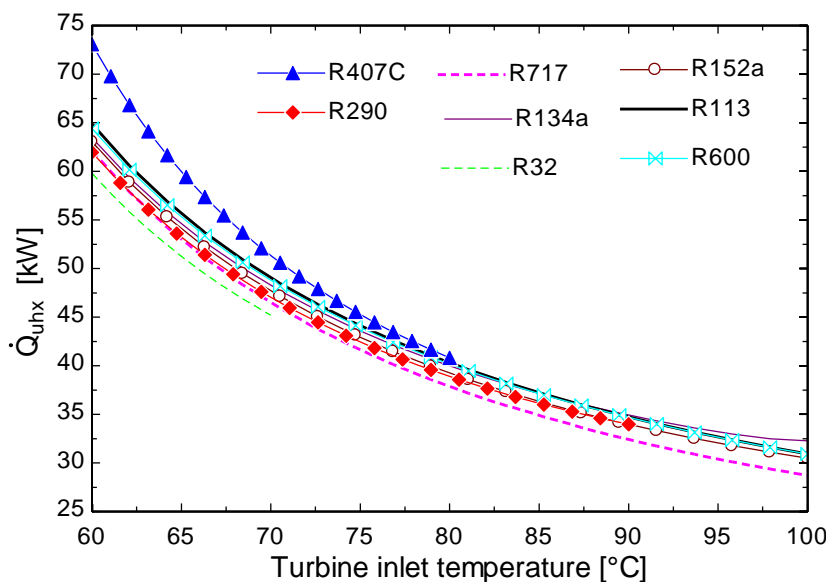
Figure 4.12 - Heat input rate versus turbine inlet temperature for various working fluids at $T_c=35°C$.

4.4.2.7 Influence of the ambient temperature

Figures 4.13 and 4.14 show the effects of the ambient temperature. The fluid used for the analysis is the R134a. From Figure 4.13, it is obvious that the ambient temperature greatly affects the condenser. As the ambient temperature gets close to the condenser temperature, the condenser irreversibility and hence the system total irreversibility is reduced. Seeking for better performance, it is suggested reasonable temperature difference between the condenser temperature and the ambient temperature be taken in the range 5-15 °C.
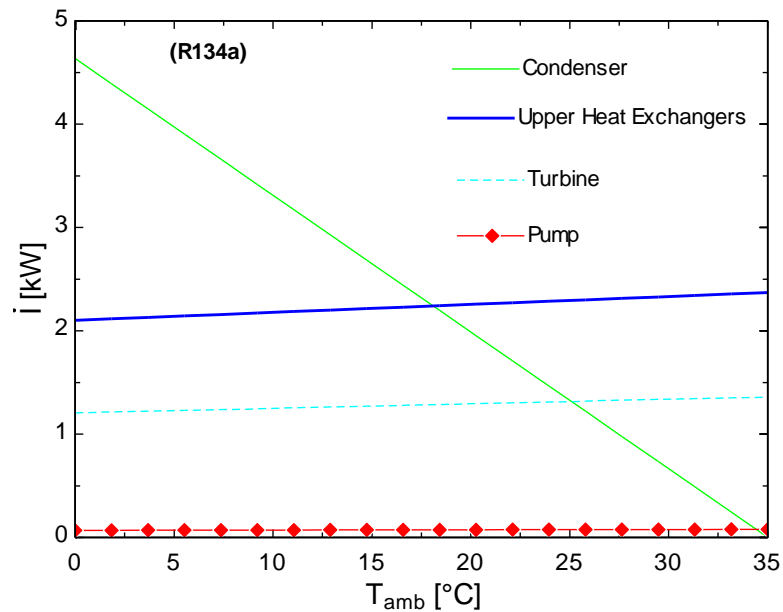
Figure 4.13 - Components irreversibility versus ambient temperature (R134a as working fluid)
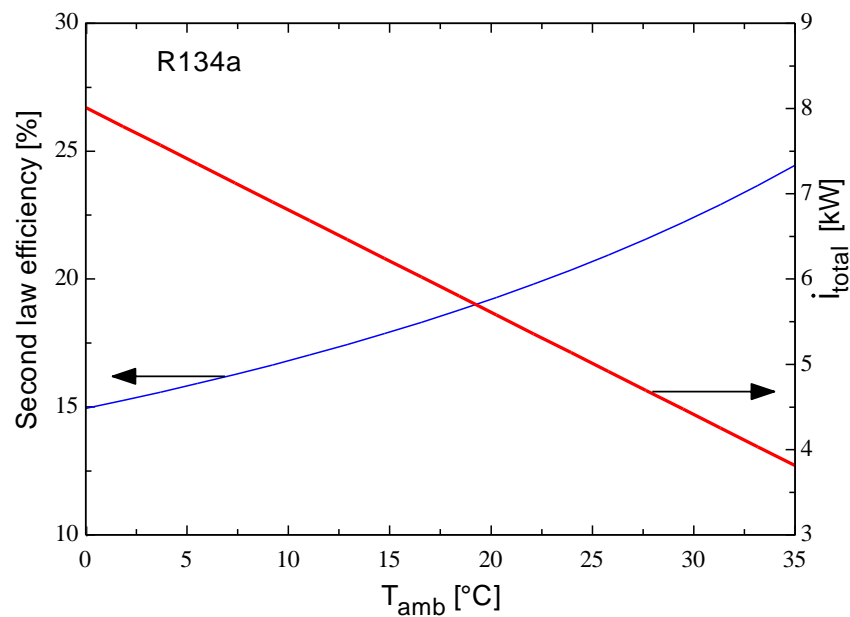
Figure 4.14 - Second law efficiency and total irreversibility versus ambient temperature (R134a as working fluid)

4.4.2.8 Study of the heat transfer in the heat exchangers

The heat exchange process between the heat transfer fluid and the working fluid is studied using the energy balance in the upper heat exchangers. It can be expressed as:

$$\dot{m}_{htf}(h_H - h_{pp,htf}) = \dot{m}_{wf}(h_1 - h_{pp,wf}) \tag{4.13}$$

$$\dot{m}_{htf}(h_{pp,htf} - h_{o,htf}) = \dot{m}_{wf}(h_{pp,wf} - h_4) \tag{4.14}$$

Where $\dot{m}_{htf}$ and $\dot{m}_{wf}$ are the mass flow rates of heat transfer fluid and working fluid, respectively. $h_{pp,htf}$ and $h_{pp,wf}$ are the enthalpies of the heat transfer fluid and the working fluid at the pinch point, respectively. $h_{o,htf}$ is the enthalpy of the heat transfer fluid after leaving the upper heat exchangers. The set pinch-point temperature difference is $\Delta T_{pp} = 6\ °C$. Figure 4.15 shows the temperature profiles in the upper heat exchangers for three working fluids: R134a, methanol and R407C. The temperature profiles depend on the properties of the fluids: latent heat of vaporization, the shape of the saturation curve, the thermal conductivity among others. From Figure 4.15, the heat amounts transferred to the cycle through the preheater and evaporator depend upon the fluid. Therefore, the pinch point analysis should be considered when designing the system for an efficient heat transfer in the preheater and evaporator. From Figure 4.15, unlike methanol which requires a small preheater and a large evaporator, R134a and R407C will require larger preheater and smaller evaporator. Using methanol most of the heat will be transferred during the phase change; this is due to the fact that at 75 ° C methanol possess high latent heat of vaporization. In case of a zoetropic fluid (R407C), the temperature varies during the phase change and leads to better efficiency of the heat exchangers.
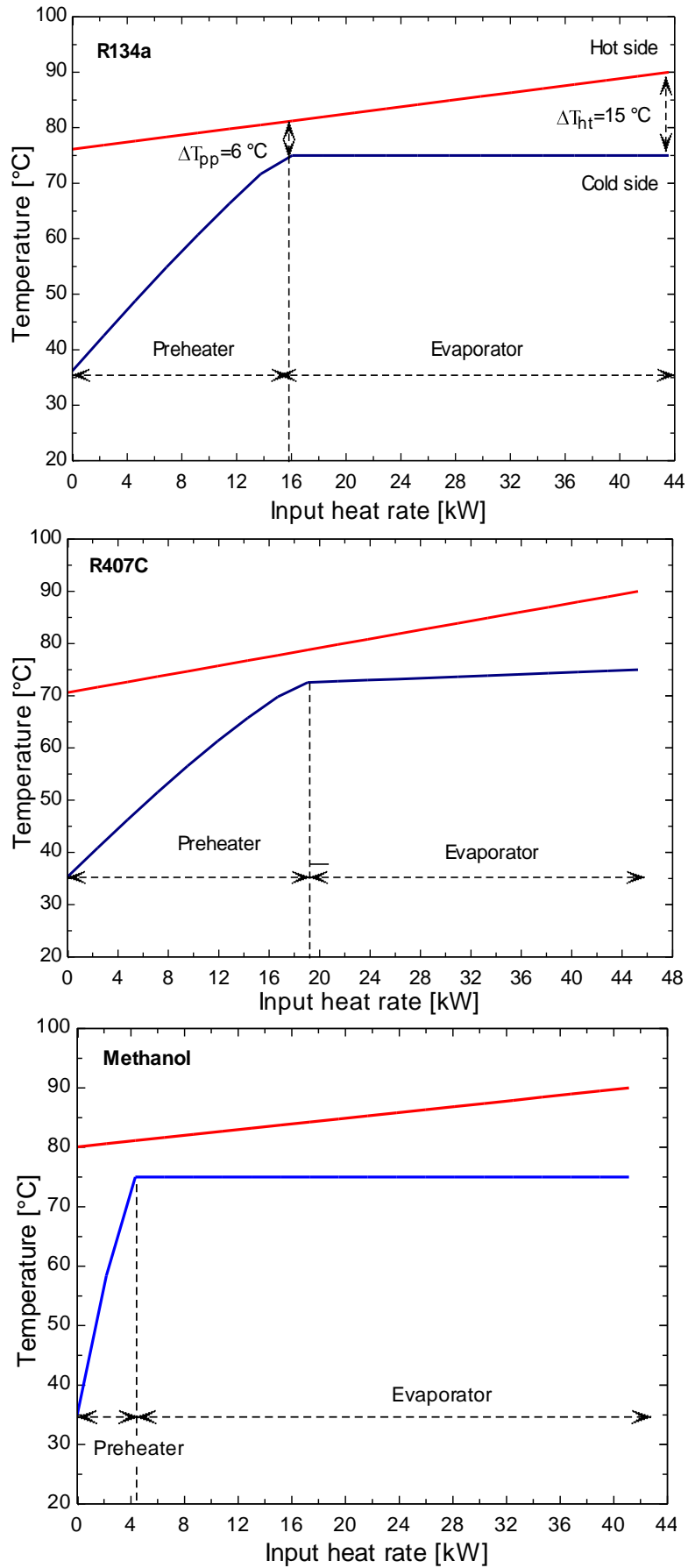
Figure 4.15 - Heat exchange process between the hot water and R134a, methanol and R407C in the upper heat exchangers.

In Table 4.9 are displayed the following parameters: the temperature of the heat transfer fluid leaving the preheater, pinch points for cold and hot fluids, the mass flow rates and the heat input for five working fluids. Ammonia and methanol have the lowest heat input rates and the lowest working fluid mass flow rates compared with other fluids. The heat input is an important parameter as it determines the size of the solar collector array and the volume of the heat store and hence, the cost of the system. Where we cannot conclude on the heat transfer fluid mass flow rate, we mention that for an efficient plant, low flow rates (10-15 l/m^2h) are preferable in the collector loop. Based on the analysis done in this section, from an economic as from a heat transfer point of view, methanol and ammonia are good fluids.

Table 4.9 - Pinch analysis for the upper heat exchangers for five different working fluids (2kW power output, heat source temperature: 90 °C)

Substance	$T_{0,htf}$ [°C]	$T_{pp,htf}$ [°C]	$T_{pp,wf}$ [°C]	$\dot{m}_{wf}$ (kg/s)	$\dot{m}_{htf}$ (kg/s)	$\dot{Q}_{uhx}$ (kW)
R134a	76.14	81	75	0.244	0.75	43.57
R407C	70.61	78.5	72.5	0.260	0.56	45.26
R152a	77.47	81	75	0.154	0.82	42.92
Ammonia	79	81	75	0.037	0.90	41.63
Methanol	80.10	81	75	0.034	0.99	41.14

4.4.2.9 Environmental considerations

Some substances, mainly refrigerants, deplete the ozone layer or/and contribute to the global warming. Because of their negative effects, there is a necessity to choose those with less harmful effects on the environment. R12, R113, R114 and R500 cannot be selected owing to their high ODP and high GWP. RC318 has a GWP of about 10250 and is excluded from the selection. Unfortunately, there is a lack of environmental data concerning some substances and this justifies the absence of some fluids in this analysis. There are few substances with low ODP or/and low GWP and these fluids used at present, will be phased-out in a near future. Among these are: R141b, R123, R407, R134a, R407C and R32. Water, ammonia, and alkanes families are environmentally friendly substances.

4.4.2. 10 Safety considerations

Safety criteria cannot be omitted. ASHRAE 34 provides a safety classification for fluids. Alkanes non toxic but flammable are class A3. They require safety devices. R152a is classified A2 (lower flammability and non-toxic). R123 is B1 (non-flammable but toxic). Ammonia classified B2 (toxic and has lower flammability limit) could be used in an open space with lesser precaution compared with alkanes. R134a is of class A1 (non-flammable and non-toxic), i.e. safer compared to other refrigerants and therefore is the preferred fluid.

4.4.2. 11 Over-all analysis

From the analyses carried out in the previous sections, none of the fluids yields all the desirable properties. All the above mentioned parameters are important for ORC design. It is difficult to find an ideal working fluid which exhibits high efficiencies, low turbine outlet volume flow rate, reasonable pressures, low ODP, low GWP and is non-flammable, non-toxic and non-corrosive. In Table 4.10, a certain number of properties were regrouped. For a value of the parameter favoring the fluid, we put the sign + (plus), – (minus) in the opposite case and +/- when the drawback can be overcome or neglected. The following fluids are not selected:

- RC318 (high GWP)

- Cyclohexane (high volume flow rate, high pressure ratio)

- R407C (high evaporator pressure, low efficiency)

- R32 (high evaporator pressure, low efficiency, high moisture after expansion)

- Ethanol, water, methanol (non convenient pressure values, high turbine outlet volume flow rates)

- R12, R113, R114 and R500 (high GWP, high ODP)

- R141b (high turbine outlet volume flow rate, high ODP)

Summing, R134a followed by R152a, R290, R600 and R600a emerge as most suitable fluids for low-temperature solar applications with heat source temperature below 90 °C.

4.5 Conclusions

In this chapter, various categories of working fluid candidates for organic Rankine cycle applications were listed. From the literature, criteria that should fulfill suitable fluids were underlined and a methodology proposed for fluids selection. Finally, thermodynamic characteristics and performances of different fluids were analyzed for selection as working fluids in a low-temperature solar organic Rankine cycle. Several criteria were used for comparison: pressures, mass and volume flow rates, efficiencies, cycle heat input, safety and environmental data. Fluids favored by the pressure values are: isentropic fluids, Butanes, n-Pentane and refrigerants R152a, RC318 and R500. Low volume flow rates are observed for R32, R134a, R290, R500 and ammonia. High latent heat of vaporization presented by water, methanol, ethanol and ammonia has as consequences low mass flow rate and small heat input, which are advantages over the rest of fluids. From an efficiency point of view, fluids with high boiling point like ammonia, methanol, ethanol and water are very efficient but the presence of droplets during the expansion process is a drawback. Following the International regulations (Kyoto and Montreal Protocols), R12, R500, RC318, R114 and R113 are harmful for the environment. Concluding, R134a, R152a, R600, R600a and R290 are most suitable fluids for low-temperature solar applications driven by heat source temperature below 90 °C.

Table 4.10 - Summary

	Substances	Calculated data									Safety data		Environmental data		Decision
	Names	P_{min}	P_{max}	PR	$\dot{V}_2$	η_{th}	η_{II}	$\dot{I}_{tot}$	ϕ_e	x_2	Toxicity	Flammability	ODP	GWP	A/R
1	RC318	+	+	+	+	+	+	-	-	+	+	+	+	-	+/-
2	R600a	+	+	+	+	+	+	+	+	+	+	-	+	+	**accepted**
3	R114	+	+	+	+	+	+	-	+	+	+	+	-	-	*rejected*
4	R600	+	+	+	+	+	+	+	+	+	+	-	+	+	**accepted**
5	R601	+	+	+	-	+	+	+	+	+	+	-	+	+	*rejected*
6	R113	-	+	+	-	+	+	+	+	+	+	+	-	-	*rejected*
7	Cyclohexane	-	-	-	-	+	+	+	+	+	+	-	n.a	n.a	*rejected*
8	R290	+	+	+	+	-	-	-	-	+	+	-	+	+	**accepted**
9	R407C	+	-	+	+	-	-	-	-	+/-	+	+	+	+	+/-
10	R32	+	-	+	+	-	-	-	-	-	+	+/-	+	+	*rejected*
11	R500	+	+	+	+	+	+	+	+	+	+	+	-	-	*rejected*
12	R152a	+	+	+	+	+	+	+	+	+	+	+/-	+	+	**accepted**
13	Ammonia	+	-	+	+	+	+	+	+	+/-	-	+/-	+	+	+/-
14	Ethanol	-	-	-	-	+	+	+	+	+	+	-	n.a	n.a	*rejected*
15	Methanol	-	+	-	-	+	+	+	+	+	-	-	n.a	n.a	*rejected*
16	Water	-	-	-	-	+	+	+	+	+	+	+	+	+	*rejected*
17	R134a	+	+	+	+	+	+	-	+	+	+	+	+	+	**accepted**
18	R12	+	+	+	+	+	+	+	+	+	+	+	-	-	*rejected*
19	R123	+	+	+	-	+	+	+	+	+	-	+	-	+	*rejected*
20	R141b	+	+	+	-	+	+	+	+	+	+	n.a	-	+	*rejected*

5 - Exergy Analysis of Micro-Organic Rankine Power Cycles

5.1 Introduction

In chapter 4, the criteria that should fulfill a good working fluid were established and a procedure proposed for the selection of most suitable ones for a low-temperature cycle driven by a heat source temperature below 90 °C. The present chapter aims at comparing several organic Rankine cycle configurations in view of seeking an improvement of the system performance. The configurations considered are obtained from regenerative processes i.e. incorporation of regenerator or feedliquid heaters. Limits in systems' efficiency are further established for different configurations and analyzed for determining if it is worth modifying the simple Rankine cycle system when designing a low-temperature solar driven system. Moreover, the effects of the heat source temperature and pinch point temperature difference are also analyzed.

5.2 Exergy analysis

Till 1970s, the most commonly-used method for analysis of energy conversion processes was the energy analysis. Since this period, the depletion of fossil fuel reserves and the will to reduce harmful emissions from energy intensive systems pushed to the development of methods of analysis of thermodynamic processes. The new methodology is exergy analysis and its optimization component known as entropy generation minimization (Sciubba and Wall, 2007; Bejan, 2002; Wall, 2009). Exergy analysis provides the tool for a clear distinction between energy losses to the environment and internal irreversibilities in the process. Exergy analysis is a methodology for the evaluation of the performance of devices and processes, and involves examining the exergy at different points in a series of energy conversion steps. Its results are often considered to provide a more meaningful and accurate representation of the efficiencies of the processes within a system. Therefore, it is an important tool in the analysis of energy conversion processes.

The exergy analysis methodology is a combination of first and second laws of thermodynamics and takes into account the environmental conditions. Exergy analysis has been under a continuous development for many decades. It is becoming the most appropriate tool for thermodynamic analysis and process optimization. As a powerful tool, it is being applied to a wide variety of processes (Koroneos and Nanakis, 2008; Wall, 1995; Cerci, 2002; Cowden et al., 2001; Hepbasli, 2007). Numerous research works related to the exergy analysis of Rankine based power systems are available at the present in the scientific literature, such as those concerning Rankine driven vapor compression system (Nilufer and Karakas, 1986), steam power plants (Acar, 1997; Aljundi, 2009), solar thermal power plants (You and Hu, 2002; Singh et al., 2000), geothermal power plants (DiPippo, 2004; Kanoglu and Bolatturk, 2008), cogeneration plants (Kanoglu and Dincer, 2009) and Rankine driven desalination plants (Bouzayani et al., 2007). However, only a few research works devoted to the comparison of different organic Rankine power cycles using simultaneous energy and exergy analyses are available. Those of Mago et al.

(2008), Tchanche et al. (2008b), Tchanche et al. (2010) and Dai et al. (2009) can be quoted.

Exergy is defined as the maximum work that may be achieved by bringing a system into thermodynamic equilibrium with its environment (Tchanche et al., 2010, Sciubba and Wall, 2007). Every substance not in equilibrium with its environment has some quantity of exergy, while an object or a system that is in equilibrium with its environment has, by definition, zero exergy since it has no ability to produce work with respect to its environment. An exergy analysis is similar to an energy analysis, but takes into account the quality of the energy as well as the quantity. Since it includes a consideration of entropy, exergy analysis allows a system to be analyzed more comprehensively by determining where in the system the exergy is destroyed by internal irreversibilities, and causes of those irreversibilities.

For an open system at steady state, the second law can be written as (Çengel and Boles, 2002; Bejan et al., 1996):

$$\Pi=\sum_{i}(1-\frac{T_o}{T_i})Q_i-W+\sum_{j}(m_je_j)_{in}-\sum_{k}(m_ke_k)_{out} \qquad (5.1)$$

Where Π represents the exergy destroyed in the system; T_o is the ambient temperature of the system's surroundings, and Q_i is the i-th heat transfer rate across the system boundary at a constant temperature T_i. W is the work transfer rate across the system boundary. The mass flow rate of each material flows crossing the system boundary is represented by m and the specific exergy associated with each flow is represented by e. The specific exergy flow, e, is made up of physical exergy (e^{ph}), kinetic exergy (e^{kn}), potential exergy (e^{pt}) and chemical exergy (e^{ch}). Summing the first three called flow exergy (e^{fl}), the expression below is obtained (Cengel and Boles, 2002; Bejan et al., 1996).

$$e^{fl}=h-h_o-T_o(s-s_o)+\frac{1}{2}(V^2-V_o^2)+g(z-z_o) \qquad (5.2)$$

The symbols h, s, V, z and g refer to the specific enthalpy, specific entropy, flow speed, the elevation above a reference position and the gravitational acceleration, respectively. o refers to the environmental conditions. Effects of kinetic and potential specific exergies represented by third and fourth terms in the right hand of the equation (5.2) are usually neglected as their contribution is very small. The chemical exergy derives from a composition imbalance between a substance and its environment, and accounts in part for a fuel's ability to react chemically with its environment. On a molar basis, the chemical exergy of a material flow can be written as follows (Wall, 2009):

$$e^{ch}=\sum_{i}x_i(\mu_i^o-\mu_{io}^o)+RT_o\sum_{i}x_i\ln(c_i/c_{io}) \qquad (5.3)$$

Where x_i is the mole fraction of the substance i in the flow; μ_i^o and c_i are the chemical potential and concentration of substance i in its present state; μ_{io}^o and c_{io} are the chemical potential and concentration of substance i in its environmental state, and R=8.31 kJ/kmol.K, the universal gas constant.

5.3 Systems analysis

5.3.1 Rankine engines

The simple Rankine engine comprises four components: a heat supplier also called evaporator or boiler, an expansion device, a condenser for heat rejection and finally a pump to feed the boiler. Such engine is presented on Figure 5.1 along with the corresponding T-s diagram. In this engine, heat in converted into work when the working fluid undergoes the following processes: 1-2: expansion of the saturated or superheated fluid, 2-3: heat rejection through a condenser, 3-4: pumping of the liquefied fluid and finally 4-1: heat addition in the evaporator. In Figure 5.2, a heat exchanger is incorporated into the cycle in parallel with the evaporator and condenser. In case the expansion process ends in the superheated vapour area, the heat exchanger will help to transfer the heat contained in the vapor to the compressed liquid entering the evaporator. Figure 5.3 represents the regenerative Rankine engine with an open feedliquid heater and the corresponding T-s diagram. An open feedliquid heater is basically a mixing chamber where fraction of fluid extracted from the turbine mixes with the feedwater exiting the pump. The last configuration shown in Figure 5.4 along with its T-s diagram is a regenerative organic Rankine engine with a closed feedliquid heater. In a closed feedliquid heater, heat is transferred from the extracted fluid to the feedliquid without any mixing taking place. Both streams can be at different pressures since they do not mix.
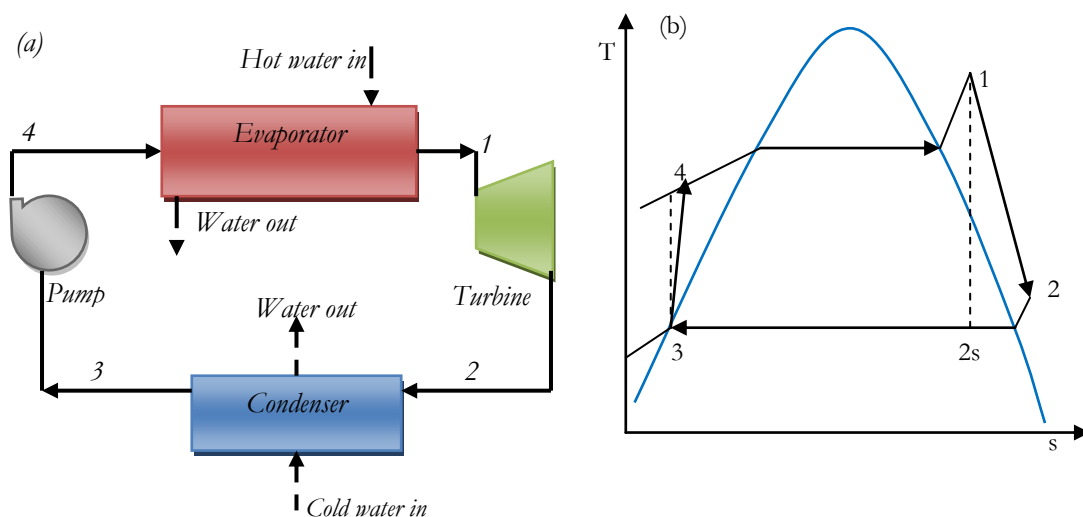
Figure 5.1 - Configuration 1 (Simple organic Rankine cycle): (a) flow sheet diagram and (b) T-s diagram
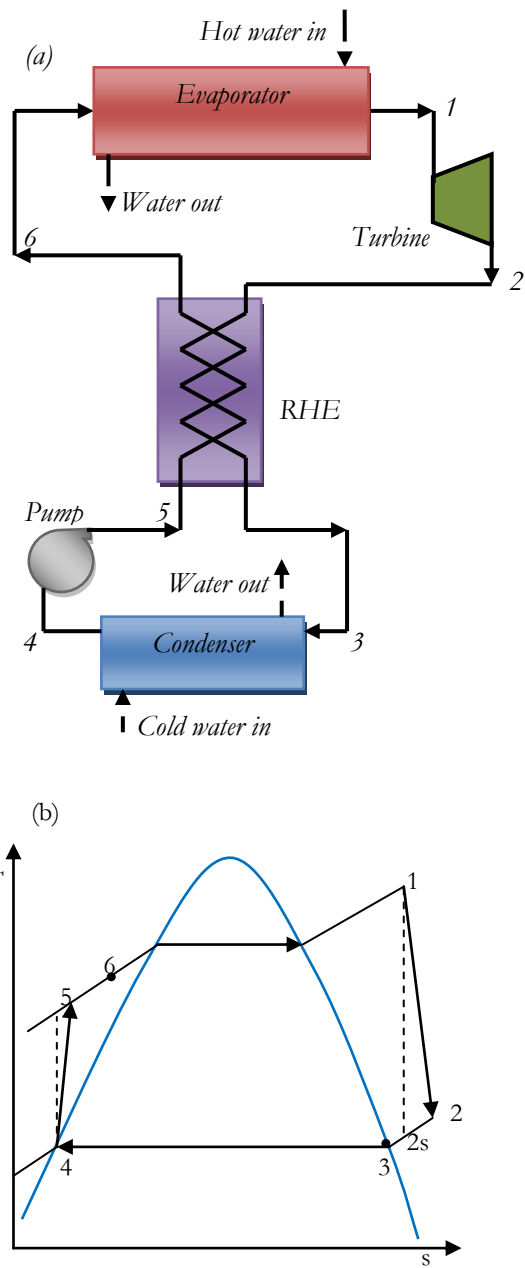
Figure 5.2 - Configuration 2 (Regenerative organic Rankine cycle with regenerative heat exchanger): (a) flow sheet diagram and (b) T-s diagram
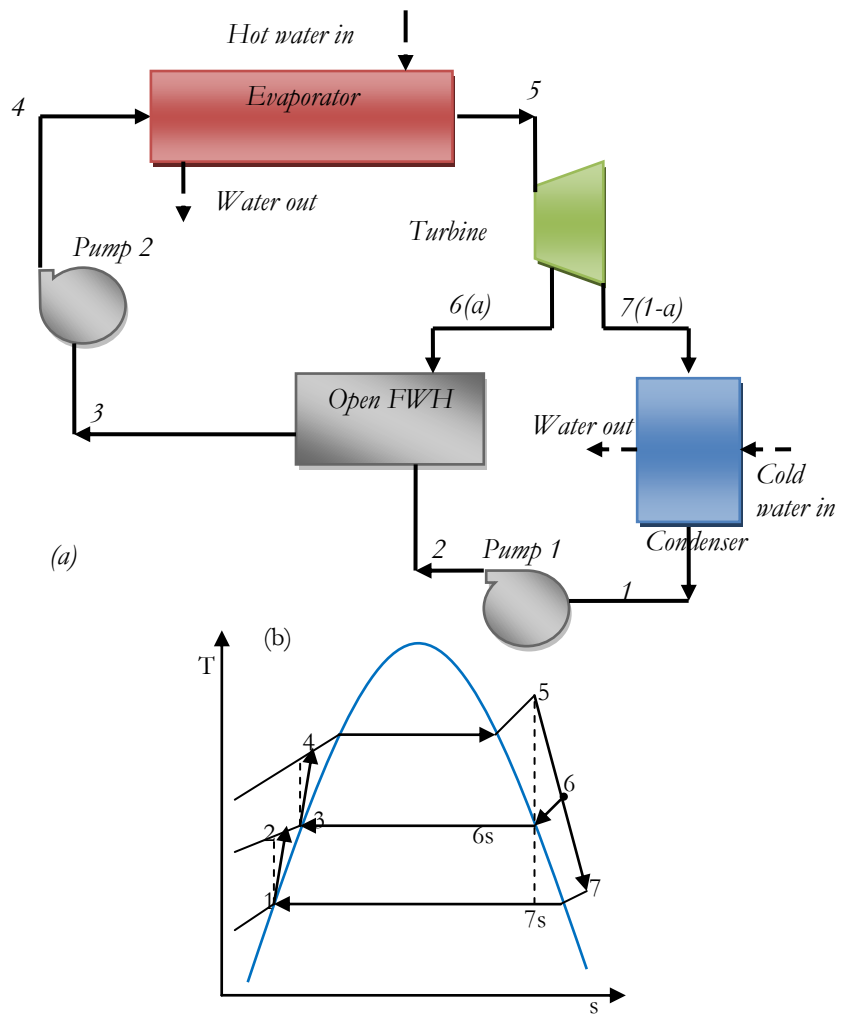
Figure 5.3 - Configuration 3 (Regenerative organic Rankine cycle with open feedliquid heater): (a) flow sheet diagram and (b) T-s diagram
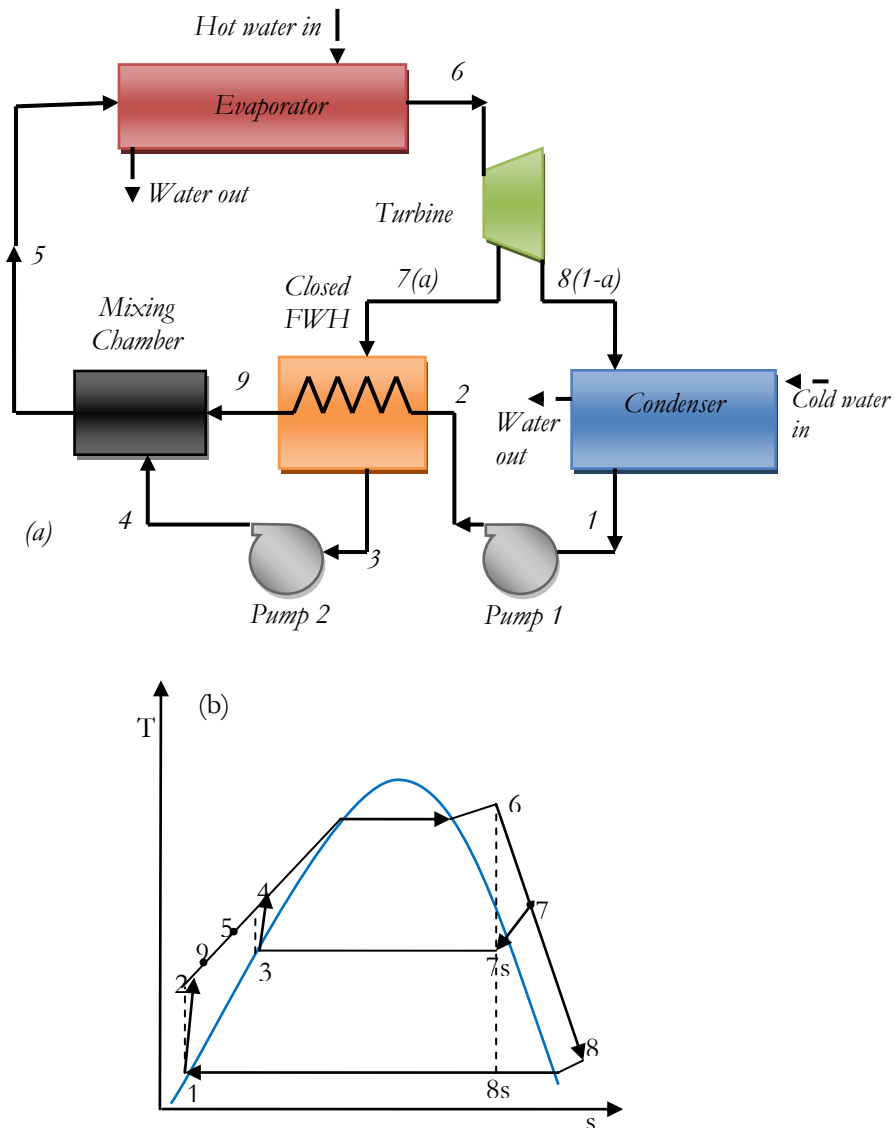
Figure 5.4 - Configuration 4 (Regenerative organic Rankine cycle with closed feedliquid heater): (a) flow sheet diagram and (b) T-s diagram

5.3.2 Modelling

The analysis of the Rankine engines will be carried out based on combination of exergy analysis and mathematical graphs theory known as exergy topological method. The components are considered as nodes or elements of a network where they are linked by pipes and valves. More details on this approach can be found in Nikulshin et al. (2002, 2002bis & 2006) and Nikulshin and Wu (2001). For components and systems performance evaluation, energy efficiency model and other models developed by Nikulshin et al (2006): exergy loss model (EXL) and exergy efficiency model (EEF) will be used. The global model is executed in three main steps or blocks:

- **First block**: Construction of the exergy flow graph and its matrix of incidence corresponding to the flow sheet diagram.

- **Second block**: Determination of exergy flows associated with each connection represented on the exergy flow graph.

For thermal power systems, there are four types of exergy flows: mass-flow, work, heat and fuel. Specific mass exergies related to these types can be calculated by the following equations:

Specific exergy associated to i-flow of mass is the sum

$$e_i = e_i^{ph} + e_i^{kn} + e_i^{pt} + e_i^{ch} \tag{5.4}$$

In absence of chemical reaction (chemical equilibrium with the surroundings), and neglecting the potential and kinetic exergies, only the physical part of exergy is considered. Equation (5.4) then becomes

$$e_i = h_i - h_o - T_o(s_i - s_o) \tag{5.5}$$

Where h_i and s_i are the specific enthalpy and specific entropy of the point considered, respectively.

Specific exergy associated to i-heat flow is expressed as

$$e_i = (1 - \frac{T_o}{T_i})q_i \tag{5.6}$$

T_i is the temperature at which the heat flow q_i is transferred (added or removed from the body).

Specific exergy of work of i-flow is equal to the specific work of the flow. Thus,

$$e_i = w_i \tag{5.7}$$

Specific exergy of fuel is approximated by the following equation,

$$e_i = \gamma.LHV \tag{5.8}$$

Where γ stands for the exergy factor and denotes LHV the lower heating value of the fuel material.

The exergy flow rate is

$$E_i = m_i e_i \tag{5.9}$$

For the full determination of the exergy flows, a reference state also called "restricted dead state" should be defined and the mass and energy balance equations applied to all components in view of determining the works output or input and the heat added or rejected. Mass and energy balances for any control volume at steady state with negligible potential and kinetic energy changes can be given, respectively, by (Çengel and Boles, 2002):

$$\sum_{j} (\dot{m}_j)_{out} = \sum_{k} (\dot{m}_k)_{in} \tag{5.10}$$

$$\dot{Q} - \dot{W} = \sum_{j} (\dot{m}_j h_j)_{out} - \sum_{k} (\dot{m}_k h_k)_{in} \tag{5.11}$$

In organic Rankine cycles, dry fluids offer several advantages over wet fluids; wet fluids are less efficient and present a risk of droplets in the turbine which could damage the blades. In case a dry fluid is chosen as working fluid, a regenerator can be used to transfer the heat contained in the vapor after expansion to the compressed stream entering the boiler. The effectiveness of this regenerative heat exchanger is defined as the ratio of the actual temperature change of the liquid stream to the maximum possible temperature change. From Figure 5.2, the regenerator effectiveness (ε) can be expressed as (Stine and Geyer, 2001):

$$\varepsilon = \frac{T_6 - T_5}{T_2 - T_5} \tag{5.12}$$

Similarly to steam power plants, the efficiency of organic power cycles could be increased by the incorporation of feedliquid heaters. In case a feedliquid heater is included to the engine as in Figure 5.4, the temperature of the feedliquid after heating can be given as

$$T_9 = T_3 - TTD \tag{5.13}$$

TTD is the terminal temperature difference i.e. the temperature difference of the outlets' streams of the feedliquid heater.

- **Third block**: Determination of exergy losses, degree of thermodynamic perfection, exergy efficiency and coefficient of influence.

Table 5.1 - Exergy rates associated with different components (Bejan et al., 1996)

Devices	Heat exchanger	Mixing unit	Pump	Turbine
Schematic				
Exergy, in (E^{in})	$E_3 + E_1$	$E_2 + E_1$	$E_3 + E_1$	E_1
Exergy, out (E^{out})	$E_2 + E_4$	E_3	E_2	$E_2 + E_3 + E_4$
Used exergy (E^u)	$E_2 - E_1$	E_3	$E_2 - E_1$	E_4
Available exergy (E^a)	$E_3 - E_4$	$E_2 + E_1$	E_3	$E_1 - E_2 - E_3$
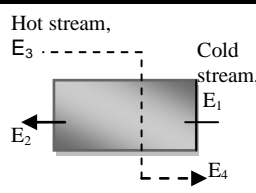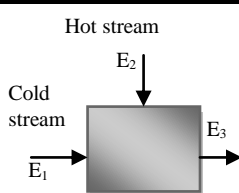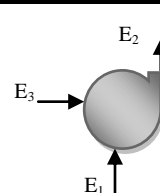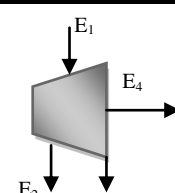
Once the exergy flows are determined, exergy input, exergy output, used exergy, available exergy, and exergy losses can be calculated using the definitions given in Table 5.1 (Bejan et al., 1996). Then, the components and systems performance can be evaluated using the parameters defined below.

Exergy losses associated with component i (Π_i), defined as the difference between the inlet and outlet exergy flow rates is expressed as:

$$\Pi_i = E_i^{in} - E_i^{out} \tag{5.14}$$

The degree of thermodynamic perfection of component i (ν_i), is the ratio of the exergy leaving to the exergy flowing into the component and is given by

$$\nu_i = E_i^{out}/E_i^{in} = 1 - \Pi_i/E_i^{in} \tag{5.15}$$

The exergy efficiency of component i (η_{ex}^i), is defined as the ratio between its used and available exergy flow rates. This is expressed by

$$\eta_{ex}^i = E_i^u/E_i^a \tag{5.16}$$

The coefficient of influence of component i (β_i), defined as the ratio of the available exergy of the component to the total available exergy of the system indicates to which extent the component influences the system performance and is expressed as

$$\beta_i = E_i^a/E_\Sigma^a \tag{5.17}$$

The engine or system total exergy loss (Π_Σ), is the sum of exergy lost in all components.

$$\Pi_\Sigma = \sum_{i=1}^{n} \Pi_i \tag{5.18}$$

The degree of thermodynamic perfection of the system (ν_Σ), is the ratio of the sum of exergy flowing out of the system to the sum of exergy flowing into the system; and is given by

$$\nu_\Sigma = E_\Sigma^{out}/E_\Sigma^{in} \tag{5.19}$$

The system exergetic efficiency (η_{ex}^Σ), is the ratio of system total exergy used to the system total available exergy and is expressed as

$$\eta_{ex}^\Sigma = E_\Sigma^u/E_\Sigma^a \tag{5.20}$$

The system thermal or energy efficiency as parameter which shows how the energy is converted in the engine is the ratio of the net power output to the heat input to the engine. It is written as

$$\eta_{th}^\Sigma = W_{net}/Q_{in} = (W_t - \Sigma W_p)/Q_{in} \tag{5.21}$$

Where W_{net} is the net power produced by the system and Q_{in} the total heat input.

5.3.3 Operating conditions

The solar system considered is designed to operate at low temperature below 90 °C. In this range of temperature, water as heat carrier is suitable and will not turn into steam and most medium temperature collectors (flat plate, evacuated tube or compound parabolic collectors) can be used. These collectors offer the advantage of low initial and low maintenance costs over parabolic trough collectors. The following operating conditions were set for the organic Rankine engine sub-system:

- Heat source: hot water is supplied at 85 °C and the pinch point is ΔT_{pp}=3 °C.

- Condenser cooling fluid: water supplied at 25 °C.

- Working fluid: R134a

- Turbine: pressure ratio, PR=3; power output, W_t=2 kW; isentropic efficiency, η_{st}=70%; mechanical efficiency, η_{lmech}= 60%.

- Pumps: isentropic efficiency, η_p= 80%.

- Feedliquid heater pressure is chosen through the following relation:

  $P_{flh}=P_{in\_exp}-\frac{1}{2}(P_{in\_exp}-P_{out\_exp})$, where P_{in_exp} and P_{out_exp} are inlet and outlet pressures of the turbine.

- Terminal temperature difference, TTD= 3 °C.

- Effectiveness of the regenerator, ε=0.80.

- Restricted dead state (ambient conditions): P_o=0.1 MPa and T_o= 25 °C.

Along with the operating conditions above set, the following assumptions are made: steady-state conditions, no heat losses and pressure drops in the heat exchangers, and the feedliquid heaters and the mixing units are well insulated. A simulation package EES (Engineering Equation Solver) that contains the thermodynamic properties of a certain number of fluids is used for calculations and evaluation of flow parameters.

5.4 Results and discussion

From the flow sheet diagrams corresponding to different configurations, the exergy flow graphs with all interconnections were built and displayed on Figures 5.5a-5.5d. Since these flow graphs sufficiently show the interactions between components and directions of flows, there is no interest for drawing the matrixes of incidence. After the execution of equations built in EES, Tables 5.2a-5.2d which show different operating points of the systems and exergy rates were produced. Using the definitions given in Table 5.1 and equations (5.14)-(5.21), performance parameters of components and systems were also calculated and stored in Table 5.3.

(a)

(b)
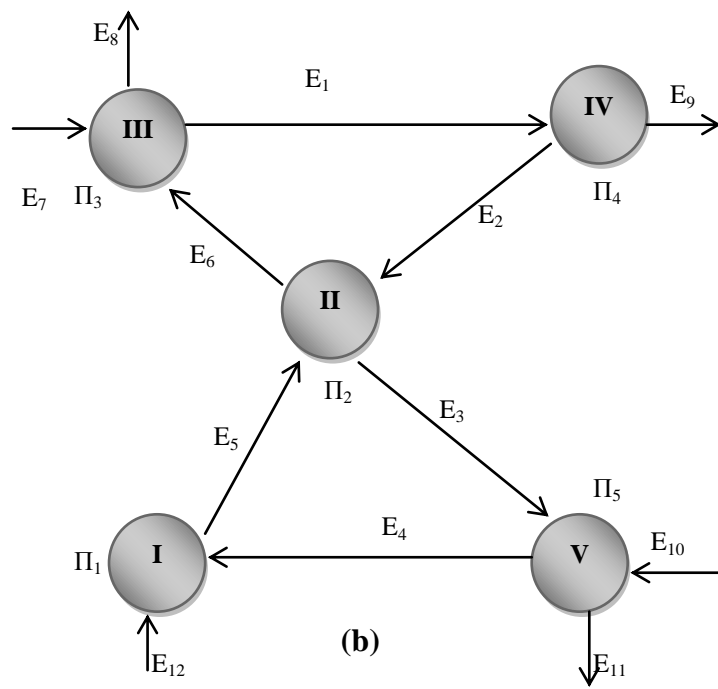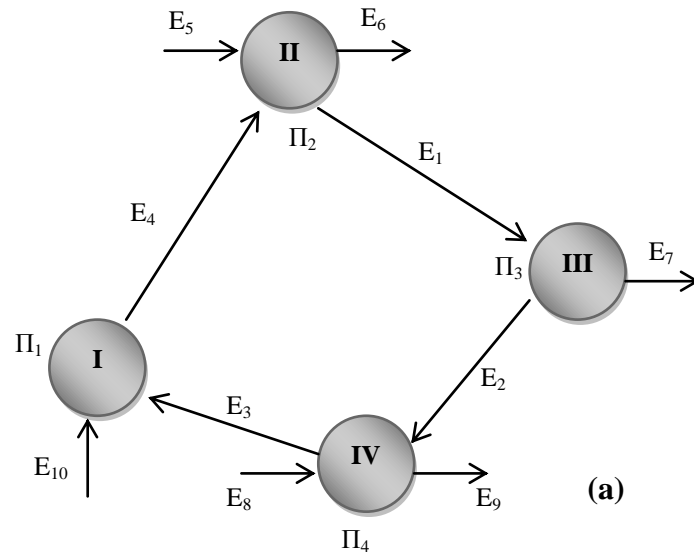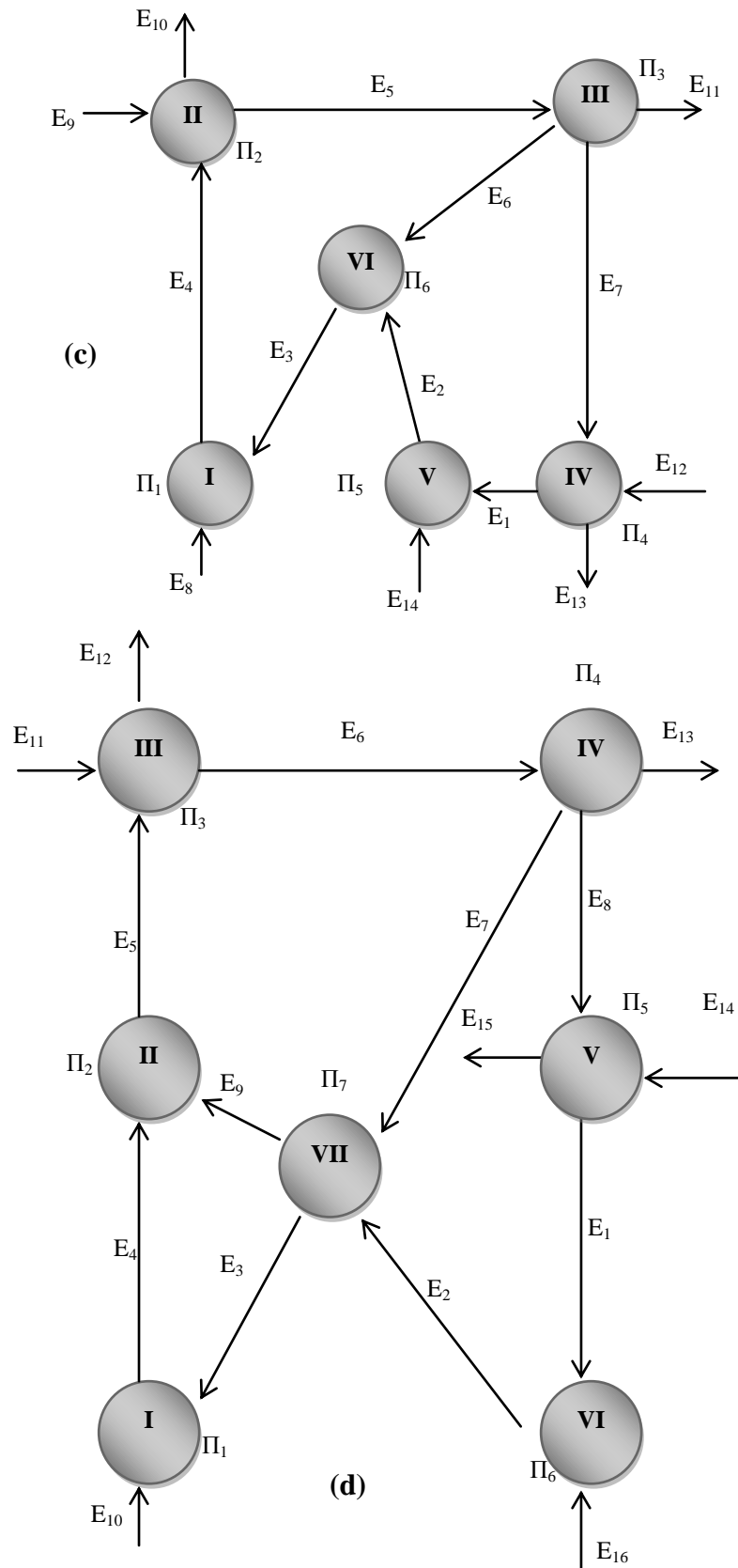
Figure 5.5 - Exergy flow graphs: (a) simple Rankine engine, (b) Rankine engine with regenerative heat exchanger, (c) Rankine engine with open feedliquid heater and (d) Rankine engine with closed feedliquid heater

Table 5.2a - Flow parameters for configuration 1 (Simple organic Rankine cycle)

State	Fluid	T (°C)	P (kPa)	h (kJ/kg)	s (kJ/kg.K)	e (kJ/kg)	E (kW)
1	R134a	75	2366	280.8	0.895	67.33	15.35
2	R134a	30.8	788.6	266.2	0.916	46.56	10.61
3	R134a	30.8	788.6	94.74	0.352	43.28	9.86
4	R134a	31.98	2366	96.41	0.353	44.61	10.17
5	Water	85	100	355.9	1.134	22.33	20.08
6	Water	73.85	100	309.2	1.002	15.11	13.59
7	-	-	-	-	-	8.773	2
8	Water	25	100	104.8	0.367	0	0
9	Water	35	100	146.7	0.505	0.686	0.64
10	-	-	-	-	-	1.665	0.38

Table 5.2b - Flow parameters for configuration 2 (Regenerative Rankine engine with internal heat exchanger)

State	Fluid	T (°C)	P (kPa)	h (kJ/kg)	s (kJ/kg.K)	e (kJ/kg)	E (kW)
1	R134a	75	2366	280.8	0.8951	67.33	15.35
2	R134a	30.8	788.6	266.2	0.9157	46.56	10.61
3	R134a	31.28	788.6	267.6	0.9202	46.59	10.62
4	R134a	30.8	788.6	94.74	0.3517	43.28	9.866
5	R134a	31.98	2366	96.41	0.3528	44.61	10.17
6	R134a	31.04	2366	95.06	0.3483	44.58	10.16
7	Water	85	100	355.9	1.134	22.33	20.08
8	Water	73.77	100	308.9	1.001	15.07	13.55
9	-	-	-	-	-	8.773	2
10	Water	25	100	104.8	0.3669	0	0
11	Water	35	100	146.7	0.5049	0.6862	0.6463
12	-	-	-	-	0.8951	1.665	0.3795

Table 5.2c - Flow parameters for configuration 3 (Rankine engine with open feedliquid heater)

State	Fluid	T (°C)	P (kPa)	h (kJ/kg)	s (kJ/kg.K)	e (kJ/kg)	E (kW)
1	R134a	30.8	788.6	94.74	0.3517	43.28	8.97
2	R134a	31.4	1577	95.57	0.3522	43.94	9.109
3	R134a	57.29	1577	135	0.4763	46.35	12.3
4	R134a	58.17	2366	135.9	0.4768	47.11	12.5
5	R134a	75	2366	280.8	0.8951	67.33	17.87
6	R134a	57.29	1577	275.6	0.9019	60.1	3.49
7	R134a	30.8	788.6	266.2	0.9157	46.56	9.651
8	-	-	-	-	-	0.924	0.2452
9	Water	85	100	355.9	1.134	22.33	23.37
10	Water	76.24	100	319.2	1.03	16.55	17.33
11	-	-	-	-	-	11.9	2
12	Water	25	100	104.8	0.3669	0	0
13	Water	35	100	146.7	0.5049	0.6862	0.583
14	-	-	-	-	-	0.8324	0.1725

Table 5.2d - Flow parameters for configuration 4 (Rankine engine with closed feedliquid heater)

State	Fluid	T (°C)	P (kPa)	h (kJ/kg)	s (kJ/kg.K)	E (kJ/kg)	E (kW)
1	R134a	30.8	788.6	94.74	0.3517	43.28	9.098
2	R134a	31.98	2366	96.41	0.3528	44.61	9.378
3	R134a	57.29	1577	135	0.4763	46.35	2.309
4	R134a	58.17	2366	135.9	0.4768	47.11	2.347
5	R134a	55.04	2366	130.9	0.4617	46.63	12.13
6	R134a	75	2366	280.8	0.8951	67.33	17.51
7	R134a	57.29	1577	275.6	0.9019	60.1	2.994
8	R134a	30.8	788.6	266.2	0.9157	46.56	9.788
9	R134a	54.29	2366	129.7	0.4581	46.53	9.781
10	-	-	-	-	-	0.924	0.04602
11	Water	85	100	355.9	1.134	22.33	22.9
12	Water	75.94	100	317.9	1.027	16.37	16.79
13	-	-	-	-	-	7.691	2
14	Water	25	100	104.8	0.3669	0	0
15	Water	35	100	146.7	0.5049	0.6862	0.5913
16	-	-	-	-	-	1.665	0.35

Table 5.3 - Thermodynamic characteristics for different configurations

Element	E_i^{in} (kW)	E_i^{out} (kW)	E_i^{a} (kW)	E_i^{u} (kW)	Π_i (kW)	η_{ex}^{i} (%)	ν_i (%)	β_i (%)
1-Simple Rankine engine								
Pump (I)	10.25	10.17	0.38	0.305	0.075	80.23	99.27	1.89
Evaporator (II)	30.25	28.94	6.487	5.179	1.308	79.83	95.68	32.31
Turbine (III)	15.35	12.61	4.735	2	2.735	42.24	82.18	23.58
Condenser (IV)	10.61	10.51	0.749	0.641	0.108	85.61	98.98	3.731
System	20.46	16.23	20.08	1.62	4.226	8.07	79.34	-
2-Regenerative Heat Exchanger								
Pump (I)	10.25	10.17	0.3795	0.305	0.075	80.23	99.27	1.89
RHE (II)	20.78	20.78	0.01	0.01	0.000	100	100	0.05
Evaporator (III)	30.24	28.9	6.531	5.186	1.345	79.41	95.55	32.53
Turbine (IV)	15.35	12.61	4.735	2	2.735	42.24	82.18	23.58
Condenser (V)	10.62	10.51	0.755	0.646	0.109	85.60	98.98	3.76
System	20.46	16.19	20.08	1.62	4.264	8.07	79.16	-
3-Open Feedliquid								
Pump 2 (I)	12.55	12.5	0.245	0.200	0.045	81.79	99.64	1.05
Evaporator (II)	35.87	35.19	6.045	5.365	0.68	88.76	98.11	25.87
Turbine (III)	17.87	15.14	4.724	2	2.724	42.33	84.75	20.22
Condenser (IV)	9.651	9.553	0.681	0.583	0.098	85.61	98.98	2.91
Pump 1 (V)	9.143	9.109	0.173	0.139	0.034	80.3	99.63	0.74
Feedliquid (VI)	12.6	12.3	12.6	12.3	0.299	97.63	97.63	53.91
System	23.79	19.91	23.37	1.538	3.88	6.77	83.69	-
4-Closed Feedliquid								
Pump 2 (I)	2.355	2.347	0.046	0.038	0.008	81.79	99.64	0.20
Mixing Unit (II)	12.13	12.13	12.13	12.13	0.001	100	100	52.95
Evaporator (III)	35.03	34.3	6.113	5.382	0.731	88.04	97.91	26.69
Turbine (IV)	17.51	14.78	4.726	2	2.726	42.32	84.43	20.63
Condenser (V)	9.788	9.689	0.69	0.591	0.099	85.61	98.98	3.02
Pump 1 (VI)	9.448	9.378	0.35	0.281	0.07	80.23	99.27	1.53
Feedliquid (VII)	12.37	12.09	0.685	0.402	0.283	58.75	97.72	2.99
System	23.3	19.38	22.9	1.604	3.92	7.0	83.18	-

5.4.1 Rankine engines with R134a as working fluid

5.4.1.1 Configuration 1- simple Rankine engine

In the simple Rankine engine, only four components are considered: expander, evaporator, pump and condenser. As can be seen in Table 5.3, the highest exergy loss occurs in the expander: 2.74 kW which represents 64% of the total exergy destroyed in the system as shown by the exergy loss distribution (Figure 5.6a). The direct consequence is the low exergy efficiency, 42.24% and low degree of thermodynamic perfection, 82.18%. The poor performance of the expander is due to the irreversibilities during the expansion process. The evaporator is the most critical component with a degree of influence of 32.31%, followed by the expander 23.58%. This simple engine consumes 4.23 kW exergy and, exergy efficiency and degree of thermodynamic perfection are 8% and 79.34%, respectively.
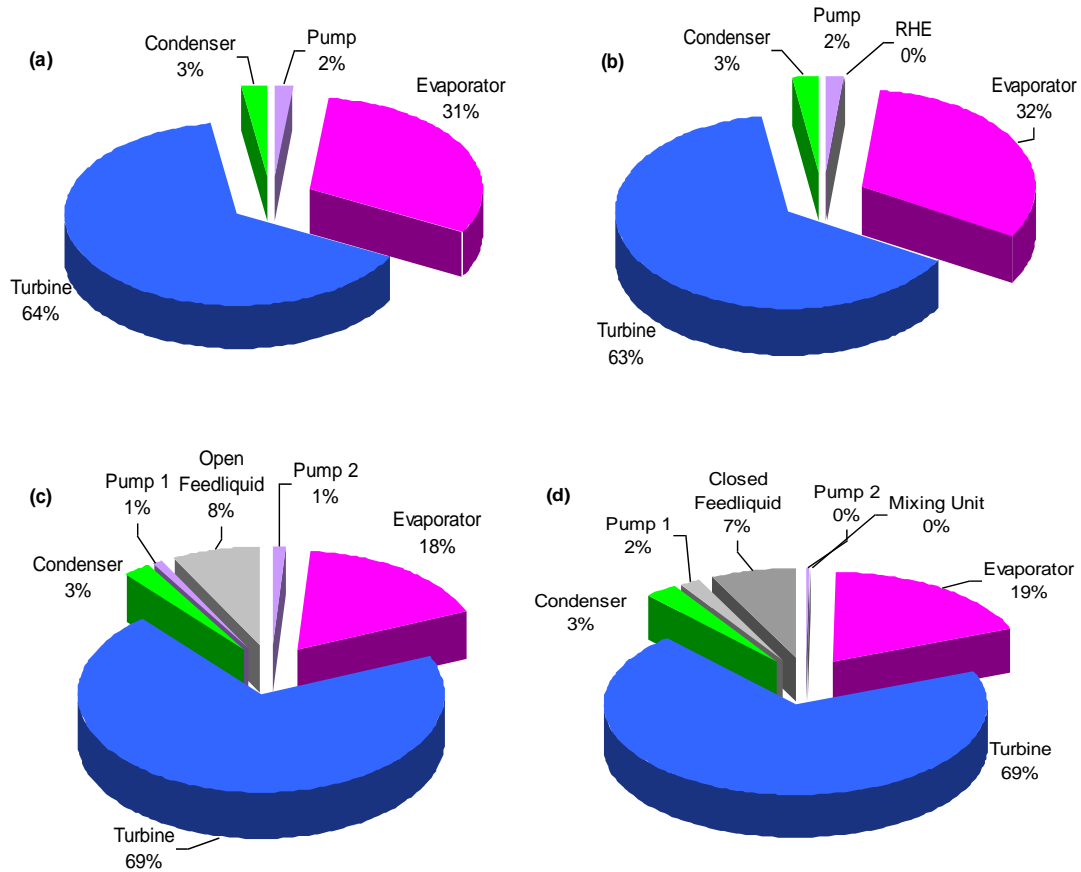
Figure 5.6 - Exergy loss distribution: (a) simple Rankine engine, (b) Rankine engine with regenerative heat exchanger, (c) Rankine engine with open feedliquid heater and (d) Rankine engine with closed feedliquid heater

5.4.1.2 Configuration 2 - Rankine engine with regenerative heat exchanger

The role assigned to the regenerator is to increase the average evaporator temperature. From Table 5.2b it can be seen that the temperature at the evaporator inlet (point 6, 31.04 °C) is lower than temperature at the pump outlet (point 5, 31.98 °C) which means that the heat exchanger cools instead of heats. From the results displayed in Table 5.3, it can be seen that the regenerator has a very small coefficient of influence (0.05%) which means very little effect on the system. And of course, the exergy efficiency of the system in comparison with the simple Rankine engine is unchanged and the degree of thermodynamic perfection is slightly decreased, by 8%. Unnecessary use of regenerator can be drawn as conclusion confirming the uselessness of this device when the working fluid is an isentropic one such as R134a. No exergy is destroyed in the regenerator and the exergy loss distribution is similar to that of the basic engine (Figure 5.6b). The evaporator is still the most important component with a coefficient of influence of 32.53% followed by the turbine.

5.4.1.3 Configuration 3 - Rankine engine with open feedliquid

In this configuration, a feedliquid or mixing unit is incorporated in the simple Rankine engine. The pump (first pump) exit exergy is mixed to exergy extracted from the expander in order to reduce the exergy destruction in the evaporator. In comparison to the basic engine, this configuration will be more expensive as it requires two more devices: an additional pump and a mixing unit. From Table 5.3, it is observed that the feedliquid plays a significant role; the total amount of exergy destroyed is reduced from 4.2 kW in first two configurations to 3.9 kW. The degree of thermodynamic perfection is also increased from 79.34% in the first configuration and 79.16% in the second configuration to 83.7%. In contrast, the exergy efficiency is reduced by 15.38% compared with first two configurations; this is due to pumps' works. The evaporator performs better in this configuration: exergy efficiency increased from 79.83% (configuration 1) and 79.41% (configuration 2) to 88.76%. The degree of thermodynamic perfection does the same as can be seen in Table 5.3. The feedliquid heater is the most critical component; it has the highest coefficient of influence (53.91%) and contributes to the reduction of exergy losses in the evaporator significantly. This reduction reaches 50% (Table 5.3) while the expander remains the site of highest exergy losses with 2.72 kW and contributes for 69% of total exergy destroyed (Figure 5.6c).

5.4.1.4 Configuration 4 - Rankine engine with closed feedliquid heater

A Rankine engine with a closed feedliquid heater is more complex than the previous configurations. Three components are added to the simple engine: an additional pump, a mixing unit and the feedliquid heater making it the most expensive engine. Compared to the Rankine engine with open feedliquid, results are similar. There is a slight increase in exergy efficiency and a slight decrease in degree of thermodynamic perfection (Table 5.3). The exergy loss distribution (Figure 5.6d) is almost the same with no exergy destroyed in the mixing unit which is also the most critical component with a coefficient of influence of 52.95%.

5.4.1.5 Conclusion

Concluding this section (5.4.1), the simplest the cycle the best it will be from an exergetic efficiency viewpoint. The regenerative heat exchanger is regarded as useless using R134a. The incorporation of feedliquid improves the thermodynamic operation of the engine by reducing the exergy losses but the cost for that is a decrease in exergetic efficiency. The mixing unit, evaporator and expander appear as the key components. However, different modifications didn't affect the expander for which the performances remained poor.

5.4.2 Rankine engines and working fluids

In this section, different Rankine engine configurations are compared using different parameters: thermal efficiency, exergetic efficiency and degree of thermodynamic perfection. The thermal efficiency indicates how the energy conversion takes place in the system. The exergetic efficiency is the ratio between the exergy gained (useful exergy) and the exergy input (contained in the hot water supplied at the evaporator inlet). The degree of thermodynamic perfection shows how the exergy input is transformed by the system i.e. exergy destruction level; thus it is a suitable indicator for entropy generation minimization.

In Figure 5.7, performances of different fluids in different configurations are displayed. From an energy point of view, the regenerative heat exchanger allows better energy conversion for dry fluids (R245fa, R600) while the closed feedliquid is suitable for the isentropic one: R134a (Figure 5.7a). The exergetic efficiency is highest for all three fluids in the simple Rankine engine as can be seen in Figure 5.7b. Figure 5.7c shows the engine with the open feedliquid heater as the configuration with the highest degree of thermodynamic perfection.

Seeking for the best fluid in the best configuration, the energy efficiency is higher for R600 in configuration 2 and the degree of thermodynamic perfection is higher for R600 in configuration 3; while the exergetic efficiency is higher for R134a in configuration 1. The incorporation of the heat exchanger for R600 leads to an increase of 7% in the energy efficiency in comparison to the simple Rankine; which is not significant. For the same fluid the incorporation of the feedliquid heater and second pump lead to an increase in the degree of thermodynamic perfection of 3.5%, comparison made with the simple Rankine engine. Although, different modifications give better energy conversion and less exergy destroyed, the improvements are not significant enough and could not probably be cost-effective. Therefore, for heat source temperature below 100 °C, the simple Rankine cycle should be adopted for easy manufacturing process and cost effectiveness.
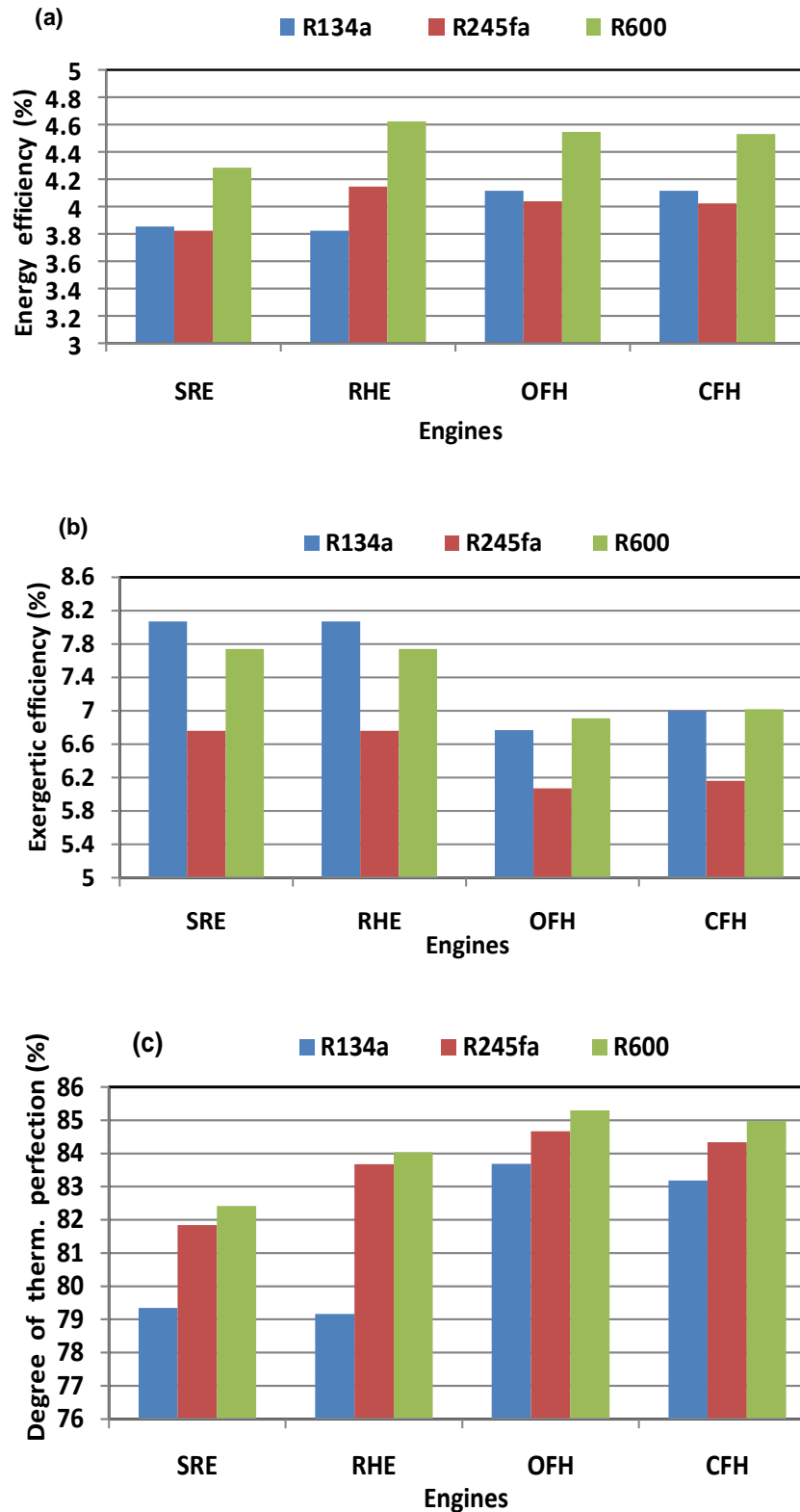
Figure 5.7 - Energy efficiency (a), Exergetic efficiency (b) and Degree of thermodynamic perfection (c)

(SRE: simple rankine engine,RHE: regenerative heat exchanger,OFH: open feedliquid heater,CFH: closed feedliquid heater)

5.4.3 Heat source temperature and pinch point temperature difference

Figure 5.8 shows the influence of the heat source temperature on the system performance. The pinch point and the temperature difference between the heat reservoir and the turbine inlet are kept at 3 °C and 10 °C, respectively, and the turbine inlet point is maintained on the saturation curve while the temperature of the water is increased. The increase in heat source temperature is followed by a decrease in exergetic efficiency while the energy efficiency remains almost constant. The degree of thermodynamic perfection decreases and passes through a minimum.
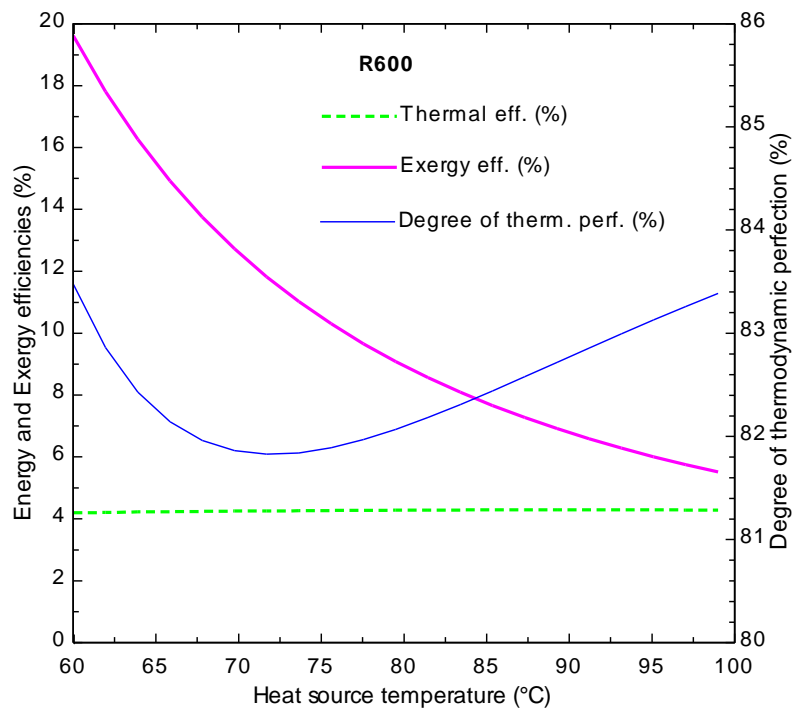
Figure 5.8 - Variation of the performance parameters with the temperature of the heat source

On Figures 5.9 and 5.10, the influence of the pinch point temperature difference can be appreciated. The increase of the pinch point reduces the exergetic efficiency but at the same time improves the thermodynamic behavior of the system. These graphs reveal an opposition between both exergetic efficiency and degree of thermodynamic efficiency; what was observed earlier on Figures 5.7b and 5.7c.
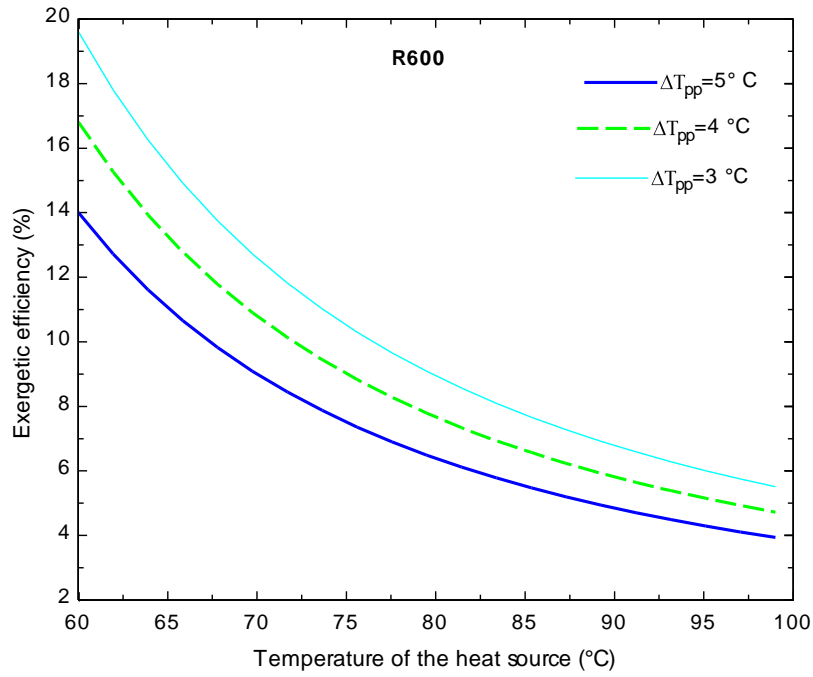
Figure 5.9 - Influence of the pinch point temperature difference on the exergetic efficiency
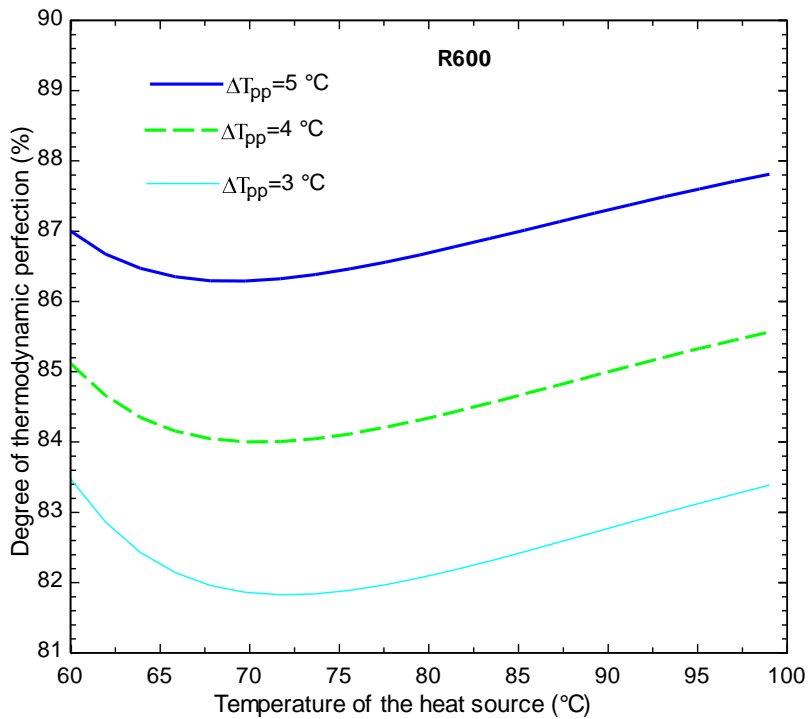
Figure 5.10 - Influence of the pinch point temperature difference on the degree of thermodynamic perfection

5.4.4 Case study of a micro-solar organic Rankine cycle

5.4.4.1 System description

In section 5.4.3, it was shown that the simple Rankine cycle operating with R134a produces the highest exergetic efficiency. Here it is coupled to a solar collector loop to form the micro-solar thermal power system. The schematic of the system is shown on Figure 5.11. Solar collectors convert solar radiation into heat. The heat captured through the absorber is later transferred to a heat transfer fluid. This can be water or thermal oil (caloria, therminol VP-1). Usually, the heat transfer fluid after the collector enters a storage device. The storage acts as a buffer and reduces the effects of the fluctuations of the radiations on the system operation. In the present case it is not taken into consideration as the exergy destruction in such device is negligible (Wei et al., 2007). Heat transfer fluid exiting the collector array enters the evaporator. The cold collector fluid exits the evaporator and is pumped by the circulator back to the collector array where it is reheated.
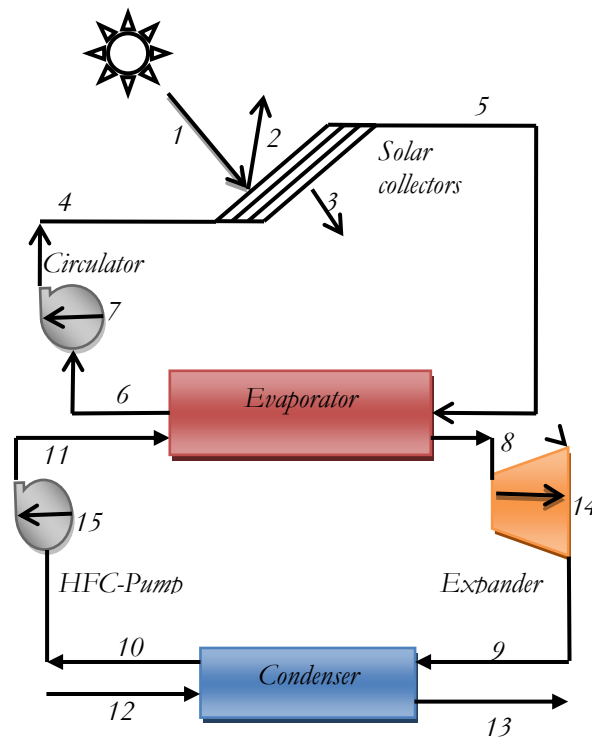
Figure 5.11 – Schematic diagram of the exergy flows in the system

5.4.4.2 Modeling of the system

The exergy flow rate at any point of the system (see Figure 5.11) should be calculated. For the analysis, the system was considered at steady state and the pressure drops in components such as evaporator and condenser ignored. The circulator is used to overcome the pressure loss in the collector array so as to obtain a pressure value equal to atmospheric pressure at the collector outlet.

The collector efficiency is given by the following relation (Delgado-Torres and Garcia-Rodriguez, 2010):

$$\eta_{sc} = \eta_0 - a_1(T_{fm} - T_{amb})/G_T - a_2(T_{fm} - T_{amb})^2/G_T \qquad (5.22)$$

Where:
η_0 = optical efficiency (-)
a_1 = linear heat loss coefficient (W/m²C)
a_2 = quadratic heat loss coefficient (W/m²C²)
G_T = solar irradiance on the aperture plane of the solar collector (W/m²)
T_{fm} = mean temperature of the heat transfer fluid (K)

Neglecting the heat losses from the insulated pipes of the collector loop, the useful heat (Q_u) collected by the collector array can be derived from the following relation:

$$\eta_{sc} = \frac{\dot{Q}_u}{G_T A_{sc}} = \frac{\dot{Q}_{evap}}{G_T A_{sc}} \qquad (5.23)$$

The determination of exergy flows in solar thermal systems can be found in Suzuki (1988), Farahat et al. (2009), Pridasawas and Lundqvist (2004) and Hepbasli (2007). The exergy equations derived from the execution of First and Second Laws of Thermodynamics for the collector loop are listed below (Tchanche et al., 2009a):

$$E_1 = G_T A_{sc}(1 - T_{amb}/T_{sun}) \qquad (5.24)$$

$$E_2 = G_T A_c(1 - \eta_0)(1 - T_{amb}/T_{sun}) \qquad (5.25)$$

$$E_3 = UA_{sc}(T_{fm} - T_{amb})(1 - T_{amb}/T_{fm}) \qquad (5.26)$$

$$E_4 = \dot{m}_{htf} C(T_{ci} - T_{amb} - T_{amb}\ln(T_{ci}/T_{amb})) + \frac{\dot{m}_{htf} \Delta P_{ci}}{\varrho_{htf}} \qquad (5.27)$$

$$E_5 = \dot{m}_{htf} C(T_{co} - T_{amb} - T_{amb}\ln(T_{co}/T_{amb})) - \frac{\dot{m}_{htf} \Delta P_{co}}{\varrho_{htf}} \qquad (5.28)$$

$$E_6 = \dot{m}_{htf} e_6 \qquad (5.29)$$

$$E_7 = W_{circ} = \dot{V}_c \Delta P_c/(\eta_{s,circ}\eta_{elec,circ}) \qquad (5.30)$$

Where:
T_{sun} = apparent sun temperature: 4350 K
U = overall heat transfer coefficient (W/m²/K)
T_{fm} = temperature of the absorber (K) : $(T_{co} + T_{ci})/2$
T_{ci} = collector inlet temperature (K)

T_{co} = collector outlet temperature (K)

$\dot{V}_c$ = volume flow rate of the heat transfer fluid (m³/s)

C = heat capacity of the heat transfer fluid (kJ/kg.K)

ϱ_{htf} = density of the hat transfer fluid (kg/m³)

m_{htf} = mass flow rate of the heat transfer fluid (kg/s)

ΔP_{ci} = pressure drop at the collector inlet (kPa)

ΔP_{co} = pressure drop at the collector outlet (kPa)

ΔPc = pressure drop across the collector array (kPa)

$\eta_{s,circ}$ = isentropic efficiency of the circulator (-)

$\eta_{elec,circ}$ = electrical efficiency of the circulator (-)

5.4.4.3 Operating conditions and assumptions

The present solar system is assimilated to the one investigated by Schuster et al. (2007) and Manolakos et al. (2007). Nevertheless, the desalination part is not taken into consideration in this investigation. Components characteristics and system operating conditions are given in Table 5.4. Hot water from solar collectors is supplied to the evaporator at 85 ºC and the pinch point temperature difference is set at ΔT_{pp}=3 ºC.

Table 5.4 - Components characteristics and operating conditions

Ambient conditions	Ambient Temperature: 25 ºC, Solar irradiation: 600 W/m²
Solar collector array	Evacuated tube collector (ETC)
	η_0=0.769, a_1=1.61 W/m²C, a_2=0.0032 W/m²C², U=1.786 W/m²K
	Slope: 40º
	Pressure loss: 200 kPa
	Collector array area: 84 m²
Circulator	Isentropic efficiency: 75%
	Electrical efficiency: 90%
Expander:	Pressure ratio: 3
	isentropic efficiency: 70%
	mechanical efficiency: 60%
HFC-Pump	Isentropic efficiency: 90%
	Electrical efficiency: 90%
Cooling medium	Water
Heat transfer fluid	Water
Working fluid	R134a
Condensing temperature	35 °C
Evaporating temperature	75 °C

5.4.4.4 Results and discussion

The flow sheet diagram is presented in Figure 5.11 from which is developed the exergy flow graph shown in Figure 5.12. Circles correspond to components and arrows to exergy flows. In Table 5.5 are displayed the flow parameters of the system including temperature, pressure, enthalpy, entropy, specific exergy and exergy rate. The values of flow parameters were obtained using EES.
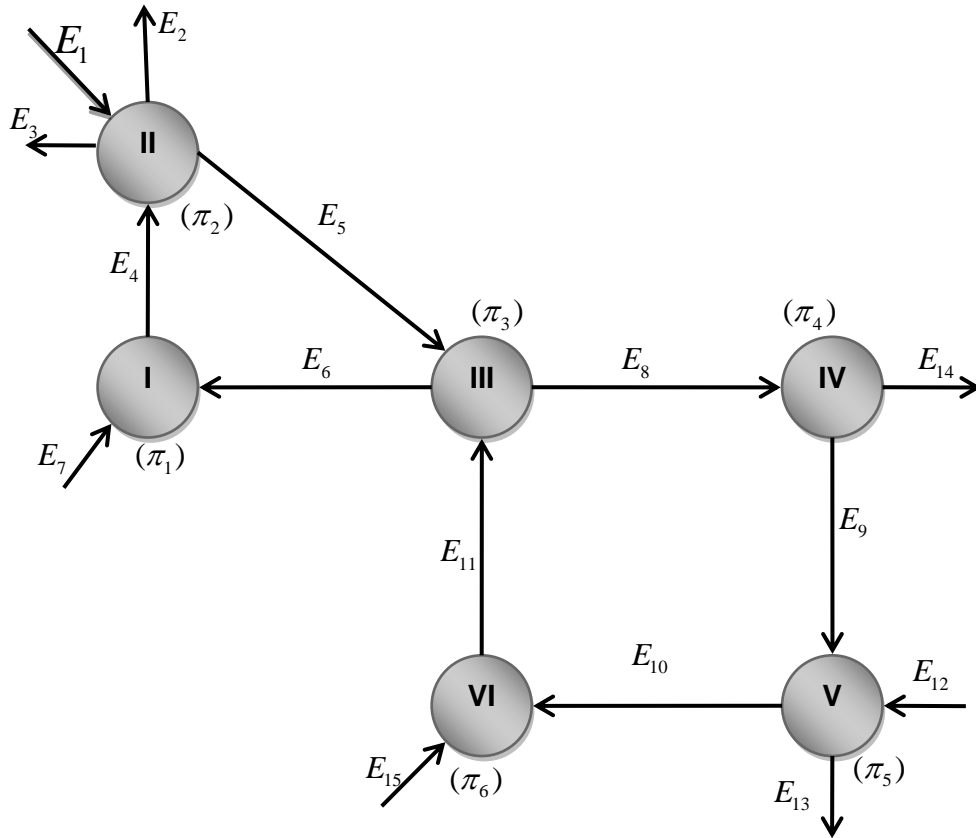
Figure 5.12 – Exergy flow graph of the system

Table 5.5 - Flow parameters of the system

State	Fluid	T (ºC)	P (kPa)	h (kJ/kg)	s (kJ/kgK)	e (kJ/kg)	E (kW)
1	-	-	-	-	-	-	46.95
2	-	-	-	-	-	-	10.84
3	-	-	-	-	-	-	1.285
4	Water	75	300	314.3	1.016	15.99	11.66
5	Water	85	100	355.9	1.134	22.4	16.27
6	Water	75	100	314	1.015	15.8	11.47
7	-	-	-	-	-	0.296	0.215
8	R134a	75	2366	280.8	0.895	67.33	11.14
9	R134a	30.8	788.6	266.2	0.916	46.56	7.701
10	R134a	30.8	788.6	94.74	0.352	43.28	7.158
11	R134a	31.97	2366	96.39	0.353	44.61	7.379
12	R134a	25	100	104.8	0.367	0	0
13	R134a	35	100	146.7	0.505	0.686	0.465
14	-	-	-	-	-	8.773	1.451
15	-	-	-	-	-	1.644	0.272

Table 5.6 presents the exergy characteristics of the evaluated system. In accordance with these results, the solar collector array appears as the most critical element of the system. It has the:

- highest coefficient of influence (100%),
- highest exergy losses (30.21 kW),
- lowest exergy efficiency (9.81%),
- lowest degree of thermodynamic perfection(48.45%).

The poor performance of the collector array is due to various losses occurring during the radiation conversion, mainly optical and thermal losses.

Table 5.6 - Exergy characteristics of different components

Element	E_i^{in} (kW)	E_i^{out} (kW)	E_i^{a} (kW)	E_i^{u} (kW)	π_i (kW)	η_{ex}^{i} (%)	ν_i (%)	β_i (%)
Circulator (I)	11.69	11.66	0.215	0.189	0.026	87.96	99.78	0.46
Solar collector (II)	58.61	28.4	46.95	4.604	30.21	9.81	48.45	100
Evaporator (III)	23.65	22.61	4.793	3.758	1.036	78.39	95.62	10.21
Expander (IV)	11.14	9.152	3.435	1.451	1.984	42.24	82.18	7.32
Condenser (V)	7.701	7.623	0.543	0.465	0.078	85.61	98.98	1.16
HFC-Pump (VI)	7.43	7.379	0.272	0.221	0.051	81.2	99.31	0.58
System	47.43	14.05	46.95	1.451	33.39	3.1	29.61	-

The evaporator is the second most important element with a coefficient of influence of 10.21% followed by the expander, 7.32%. The amount of exergy losses in the evaporator is 1kW which is half the expander's (2 kW). The irreversibility in the evaporator is associated with the heat transfer while in the expander it is associated with leakages, thermal losses and pressure drops (Lemort, 2006). The remaining components: pumps and condenser perform quite well with small exergy losses, exergetic efficiencies and degree of thermodynamic performance above 80%. The system total exergy losses is 33.39 kW of which 91% occur in the solar collectors (Figure 5.13). The system exergetic efficiency is 3.1% and the degree of the thermodynamic perfection 29.61%.
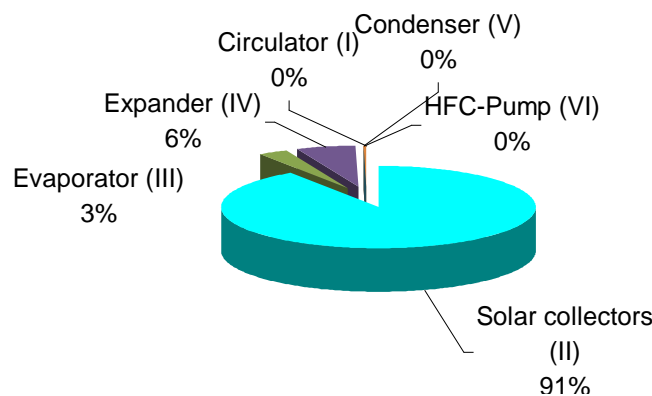
Figure 5.13 - Exergy loss distribution of the system

5.5 Conclusion

Performances of organic Rankine heat engines operating with several fluids were evaluated using an innovative exergy study approach called *exergy topological method* based on combination of exergy analysis and mathematical graph theory. Using parameters such as exergy loss, exergy efficiency, degree of thermodynamic perfection and coefficient of influence, components and systems performance were compared. Various devices incorporated in the simple Rankine cycle, gave different results: the regenerative heat exchanger has positive effects only on dry fluids; the incorporation of feedliquid heaters improve the degree of thermodynamic perfection of the system but leads to loss in exergetic efficiency. Mixing units, open feedliquid heater, evaporator and turbine are the most important elements in regard to the coefficients of influence in different configurations. For different engines and fluids considered, the energy conversion is poor, less than 5% and exergy efficiency does not exceed 10%. The integration of different devices is not significantly rewarded in terms of gain; therefore, it is preferable to keep the simple Rankine engine when designing a system such as the small scale RO desalination system with an integrated Rankine engine driven by low temperature heat below 100 °C. It was also shown how the pinch point temperature difference should be lowered so as to produce high exergy efficiency.

The exergy analysis of a micro-solar organic Rankine power cycle system was additionally carried out. Results obtained clearly point out that the solar collector array is the most critical element of the system followed by evaporator and expander. Most of exergy lost in the system occur during radiation conversion and this has as consequence a poor performance of the whole system. For a good design of a small solar thermal power system, special attention should be paid for the collector selection in view of improving the overall system performance.

Finally, it is concluded that the *exergy-topology methodology* used here is a powerful tool for systems evaluation and it could also serve as a decision support tool.

6 - Experimental Investigation of a Small Organic Rankine Cycle in Heat Recovery Application

6.1 Introduction

The present chapter reports the experimental investigation of a small scale organic Rankine cycle (ORC) carried out at the Thermodynamics Laboratory of the University of Liège, Belgium, where research on small ORCs has been a topic since many years. First prototype was built by Lemort (2006). The latter was improved by Quoilin (2007) and used R123 as working fluid. In 2009, some changes were proposed and successfully implemented by Declaye (2009) and a new refrigerant (R245fa) was tested. This study aims at testing another fluid and comparing the results with those obtained during previous works.

6.2 Potential fluids

Several fluids in regard to their characteristics were identified as potentially suitable for low-temperature heat recovery application. Some of them are displayed in Table 6.1. From the list HFE7000, SES36 and Novec649 present attractive properties: they possess appropriate critical parameters, are non-toxic, non-flammable and do not represent significant threat to the environment. However, their market availability is not guaranteed. The hydrocarbons until a radical and simple solution is found against their flammability will not be widely implemented despite their large availability and low cost. Based on the above analysis, the HFE7000 was chosen to be tested at this step.

Table 6.1 - Thermophysical, safety and environmental data of candidate fluids

Thermodynamic Properties	R-123	R-245fa	HFE 7000	SES36	Novec 649	n-Butane	n-Pentane
MW (kg/kmol)	152.93	134.05	250	184.53	316	58.12	72.15
ϱ (kg/m3)	1476.6	1352	1415	1377.21	1616.32	625.7	578.6
T_b (ºC)	27.8	15.3	61	35.64	49.26	-0.5	36.1
T_c (ºC)	183.7	154.1	195.3	177.55	168.66	152	196.5
P_c (bar)	36.68	36.4	22.3	28.49	18.646	37.96	33.64
ASHRAE 34	B1	B1	A1	A1	A1	A3	A3
ODP	0.02	0	0	Na	0	0	0
GWP	77	820	320	Na	1	0	0
Slope	positive	positive	positive	positive	positive	positive	positive
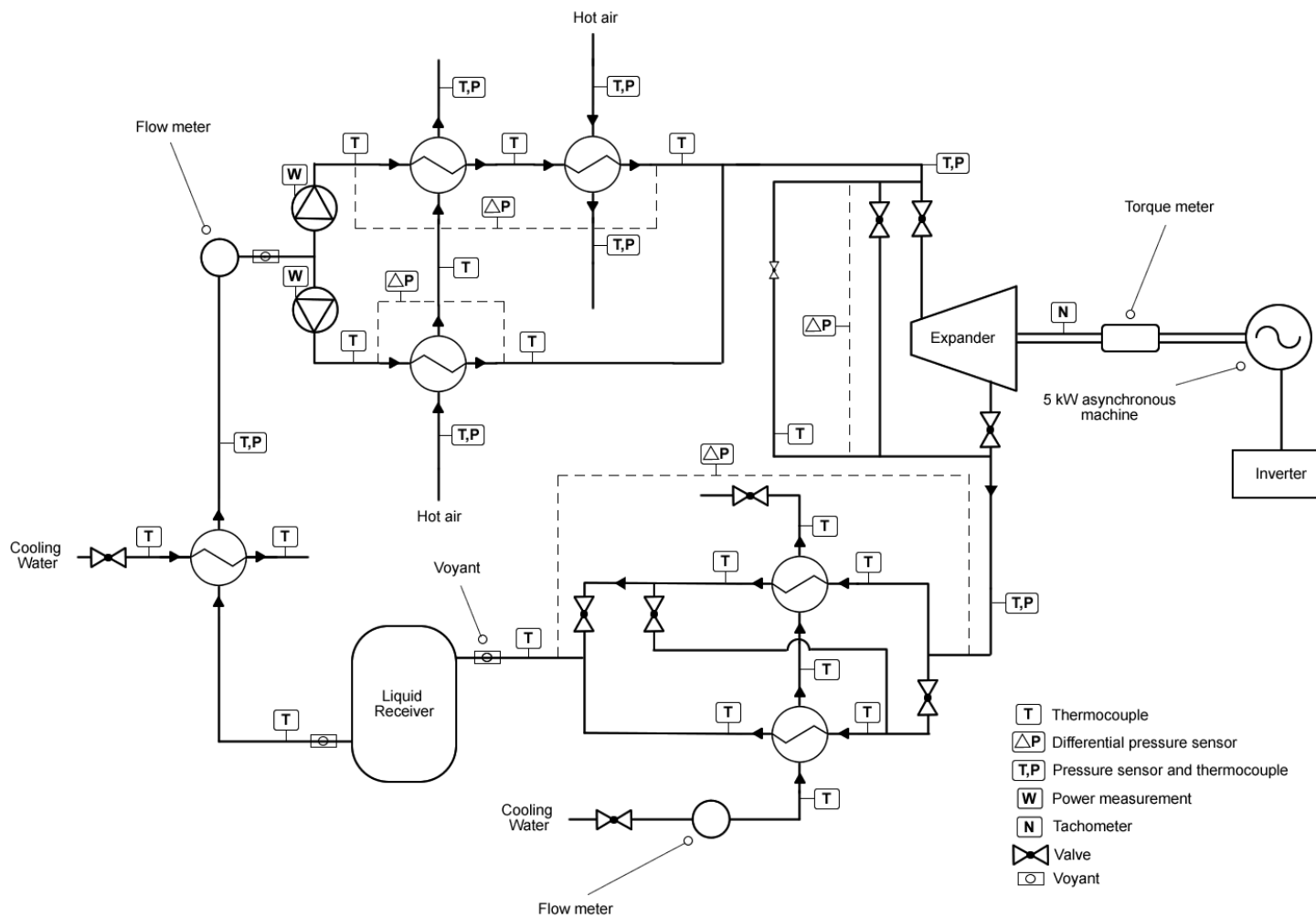
Figure 6.1 - Schematic diagram of the test bench

6.3 Description of the test bench

6.3.1 The bench diagram

The schematic diagram of the test bench is shown on Figure 6.1. The evaporator is made up of a set of three plate heat exchangers fed by hot air. The expander, a scroll compressor running in reverse mode is connected to a 5.4 kW asynchronous machine through a torque-meter mounted on the same axis. An inverter is electrically coupled to the asynchronous machine in order to control its rotational speed. The condenser consists of two plate heat exchangers fed with cold water. A liquid receiver and a small plate heat exchanger cooled by cold water are located downstream of the condenser to control the subcooling. Two membrane pumps mounted in parallel circulate the working fluid and allow the control of the flow rate. Various sensors are located at different points for measurements as can be seen on figure 6.1.

6.3.2 Components

The expander implemented on the test bench is a compressor adapted to run in reverse mode. From various types of existing compressors (Figure 6.2), the scroll type can be easily transformed into expander.
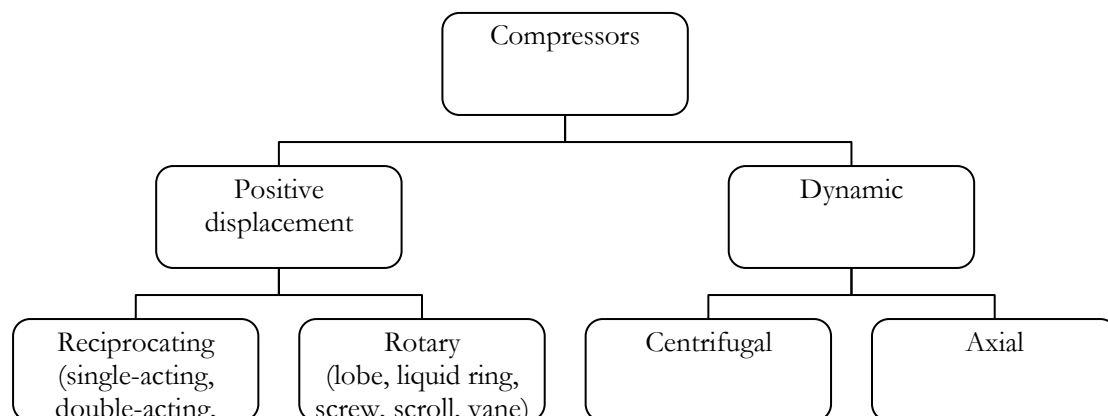
Figure 6.2 - Various types of compressors

The working principle of a scroll compressor

Scroll compressors are orbital motion, positive displacement compressors, in which suction and compression are obtained by using two mating, spiral shaped, scroll members, one fixed and the other orbiting. The working principle of a scroll compressor is shown on Figure 6.3. The compression process in a scroll compressor involves three orbits of the orbiting scroll. In the first orbit, the scrolls ingest and trap two pockets of suction gas. During the second orbit, the two pockets of gas are compressed to an intermediate pressure. In the final orbit, the two pockets reach discharge pressure and are simultaneously opened to discharge port located at the center of the two spirals. This simultaneous process of suction, intermediate compression and discharge leads to the smooth continuous compression of the scroll compressor. In expander mode, the gas flows in reverse way, from the center to the periphery.
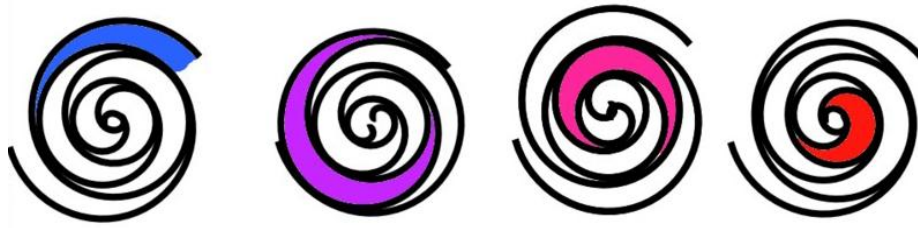
Figure 6.3 - Working principle of a scroll compressor

Types and advantages of scroll compressors

Scroll compressors are designed in agreement for the dedicated application and fluid. Depending whether the motor and the compressing part form a single body or not, two categories can be distinguished: the hermetic and the open-drive compressors. Both categories are illustrated in Figure 6.4.

1. Discharge Plenum
2. Discharge Tube
3. Fixed Scroll
4. Orbiting Scroll
5. Crankcase
6. Terminal Cover
7. Electric Terminal
8. Lower Bearing
9. Thrust Washer
10. Magnet
11. Shell
12. Eccentric Shaft
13. Stator
14. Rotor
15. Counterweight
16. Oil Drain Tube
17. Slider Block
18. O-Ring
19. Heat Shield
20. Lifting Lug
21. Internal Pressure Relief Valve (hidden)
22. Check Valve
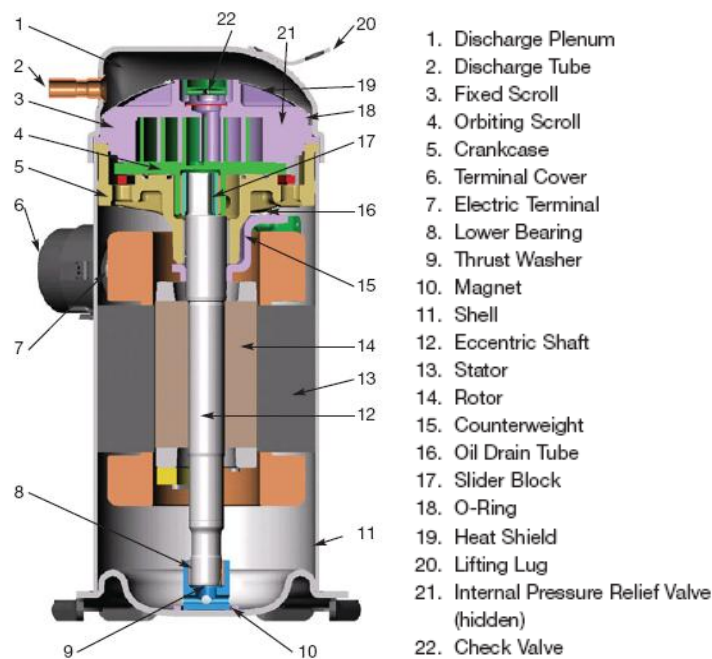
a - Hermetic type scroll compressor
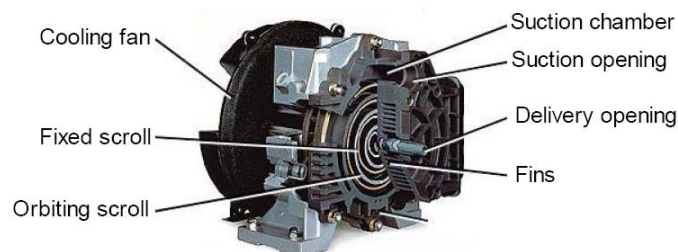
b – Open-drive oil-free air scroll compressor

Figure 6.4 - Types of scroll compressors

Scroll compressors offer several advantages such as:

- Large suction and discharge ports reduce pressure losses during suction and discharge.

- Physical separation of suction and compression reduce heat transfer to suction gas, leading to high volumetric efficiency.

- High compression efficiency, low noise and vibration compared to reciprocating compressors.

- Compact with minimum number of moving parts.

Choice of the present expander

The choice of the expansion machine was not random. The one used in this investigation is an open-drive oil-free air scroll compressor, easily converted into expander without any significant modification apart from removing the cooling fan. Moreover, an open-drive scroll compressor as expansion machine presents the following advantages:

- No need for lubrication.

- Possibility of two-phase flow operation.

- Nominal rotational speed (3500 rpm) compatible with that of an asynchronous machine.

- High maximum acceptable pressure ratio (of about 10).

A 122cc machine with a built-in volume ratio of 3.95 was selected and enclosed in a cylindrical container to avoid external leakages (Declaye, 2009). Figure 6.5 shows the expander out and inside the cylindrical container.

Figure 6.5 - The open-drive oil-free air compressor

6.3.2.2 Evaporator and condenser heat exchangers

The evaporator comprises three plate heat exchangers assembled in an asymmetric configuration and fed with hot air flow. The asymmetric configuration allows a better heat recovery and higher power generation (Declaye, 2009). Characteristics of the evaporator heat exchangers are given in Table 6.2. The condenser consists of two plate

heat exchangers fed by cold water and connected in such a way that they can be selected to operate in parallel or series configuration. For the present investigations the heat exchangers were put in parallel. The characteristics of the condenser heat exchangers are the same as those of the evaporator presented in Table 6.2. The plate heat exchangers used are illustrated in Figure 6.6.

Table 6.2 - Characteristics of the heat exchangers

Number of plates	-	75
Total volume	*l*	3.75
Dimension	mm	250x112x189
Chevron angle	°	60
Working temperature	°C	-160 up to175
Working pressure	bar	0 up to 32

Figure 6.6 - Evaporator (Left) and Condenser (right)

6.3.2.3 Pumps

Two diaphragm metering pumps suitable to suck pressurized liquids (5 to 6 bar) with low viscosity at low flow rates were selected and coupled in parallel. Thus, the working mass flow rate can be adjusted by modifying the stroke length of the pistons. The membrane pumps integrated in the cycle are depicted on Figure 6.7 and their characteristics are given in Table 6.3.

Table 6.3 - Characteristics of the pumps

		Pump 1	Pump 2
Stroke frequency	(Strokes/min)	112 (50 Hz)	96 (50Hz)
Maximum flow rate	(*l*/h)	210	180
Maximum pressure	(bar)	12	12
Motor	(W)	550 (1400 rpm)	550 (1400 rpm)
Piston diameter	(mm)	40	40
Diaphragm diameter	(mm)	120	120
Stroke length	(mm)	25	25

Figure 6.7 - The pumps

6.3.2.4 Asynchronous machine and inverter

The asynchronous machine is a 5.4 kW motor coupled to the expander through the torque-meter. The inverter electrically coupled to the motor controls its rotational speed by change of frequency. The four quadrant inverter allows the motor to operate also as a generator and in direct and reverse modes. Figure 6.8 shows the inverter (right) and the connection between the expander and the asynchronous machine.
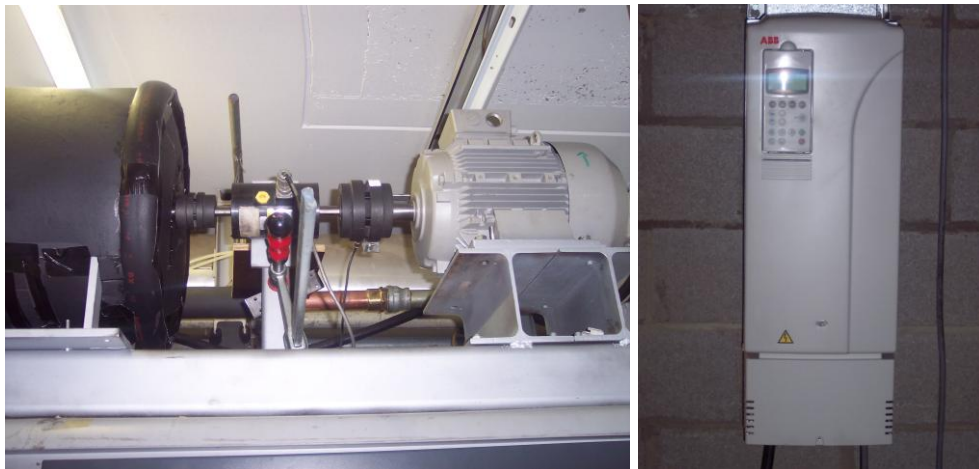
Figure 6.8 - Expander-asynchronous motor coupling and inverter

6.3.2.5 Liquid receiver and subcooler

A liquid reservoir and a subcooler (Figure 6.9) are installed on the liquid line between the condenser and the pumps to control the subcooling and ensure that the pumps suck liquid and not gas vapor to avoid cavitations' phenomena. The liquid reservoir used has a volume of 8 *l* and can stand a pressure of up to 30 bar.

Figure 6.9 - Liquid receiver and subcooler

6.3.3 The instruments

A certain number of instruments are installed on the test bench to record various parameters during the operation of the system. They are listed in Table 6.4 along with their characteristics.

Table 6.4 - Measured parameters and characteristics of the instruments used

Measured parameter	Instrument	Manufacturer	Range	Accuracy
Temperature				
(All temperatures)	Type-T Thermocouples		[-200;+350] C	±(0.3 - 1)K
Pressure				
(pumps supply)	Pressure sensor	Keller	0-5 bar	±25 mbar
(expander supply)	Pressure sensor	Keller	0-20 bar	±100 mbar
(condenser supply)	Pressure sensor	Keller	0-5 bar	±25 mbar
(air side - evaporators)	Pressure sensor	Keller	0-10 bar	±50 mbar
Differential pressure				
(Bloc evaporators 1-2)	*DP sensor	Sensotec	0-500 mbar	±2.5 mbar
(Evaporator 3)	DP sensor	Sensotec	0-500 mbar	±2.5 mbar
(Condenser)	DP sensor	Sensotec	0-1bar	±5 mbar
(Expander)	DP sensor	Sensotec	0-20 bar	±100 mbar
Flow rate				
(refrigerant)	Coriolis Type Flow meter		0-0.6 kg/s	±0.1% of rate
Electricity consumption				
(Pumps)	Energy counter			
Rotational speed				
(Expander shaft)	Inverter	ABB		
Torque				
(expander shaft)	Torque meter		20 Nm full sc.	±0.1% full sc.

*DP = differential pressure

6.4. Description of the tests

Two series of measurements were carried out with a total of 16 points. Table 6.5 indicates minimum and maximum values of imposed parameters obtained during the tests. The refrigerant mass flow rate is imposed by varying the stroke length of the pumps from 0 up to 100%. The expander supply pressure is controlled by modifying the air temperature and flow rates and shaft rotational speed. The expander rotational speed is set to different values using the inverter. The expander exhaust pressure is imposed by adjusting the cooling water mass flow rate.

Table 6.5 - Extreme values of imposed conditions

Parameters		First set (1)		Second set (2)	
		Min	Max	Min	Max
1st air source temperature	(°C)	175.8	177	192.1	195.4
2nd air source temperature	(°C)	132.6	136.5	155.9	162.9
Air mass flow rate	(g/s)	63.21	63.21	94.81	94.81
Refrigerant mass flow rate	(g/s)	46.61	50.48	68.99	77.23
water mass flow rate	(kg/s)	1.05	1.068	0.22	1.068
water supply temperature	(°C)	3.32	5.93	6.03	6.76
Expander rotation speed	(rpm)	1500	3000	1650	3000
Expander inlet temperature	(°C)	105.1	114.5	122.9	139.6
Degree of superheating	(°C)	8.34	10.57	8	14

6.5. Experimental results and discussion

6.5.1 Energy conservation

6.5.1.1 Expander supply pressure and expander rotational speed

Figure 6.10 shows the variation of the expander supply pressure with shaft rotational speed. The pressure varies linearly with the rotational speed. This is in accordance with the definition of the expander supply volume flow rate ($V_{su,exp}$) which is the swept volume ($V_{s,exp}$) multiplied by the rotational speed (N_{rot}) (Kane, 2002). The volume flow rate is also obtained from dividing the mass flow rate (m_r) by the density ($\varrho_{su,exp}$). The swept volume in expander mode is the one in compressor mode ($V_{s,cp}$) divided by the built-in volume ratio ($r_{v,in}$) of the machine. The rotational speed thus modifies the characteristics of the fluid as can be seen from equation 6.1. Therefore, an increase in the rotational speed corresponds to a reduction in the expander pressure supply and vice-versa.

$$\dot{V}_{su,exp} = N_{rot}\, V_{s,exp} = N_{rot}\, \frac{V_{s,cp}}{r_{v,in}} = \frac{\dot{m}_r}{\varrho_{su,exp}} \tag{6.1}$$
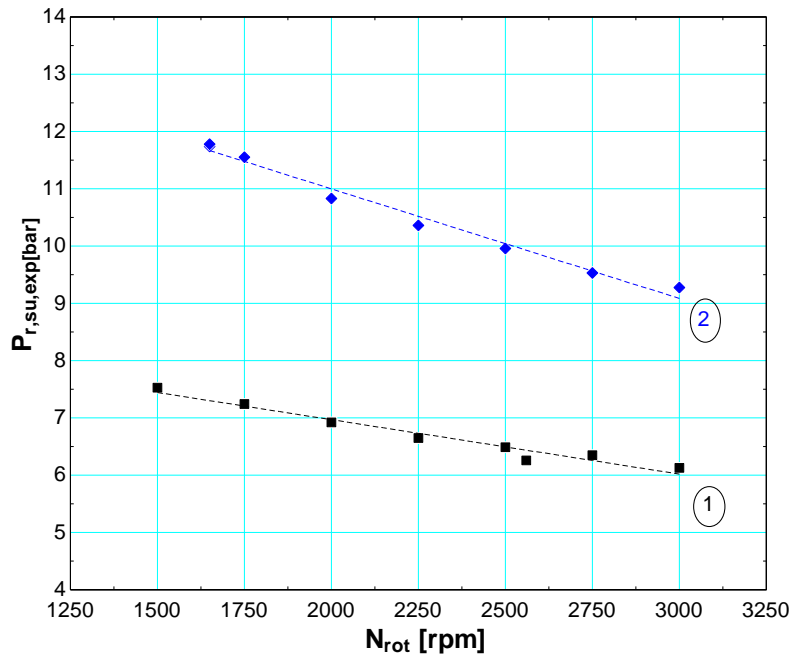
Figure 6.10 - Evolution of the expander pressure supply with the rotational speed

6.5.1.2 Pressure drops across the heat exchangers

Two differential pressure sensors are installed on the refrigerants lines to measure the pressure drops across the heat exchangers forming the evaporator. The pressure drops recorded were very small (9-17 mbar across the heat exchangers 1 and 2, and 3-27 mbar for the last heat exchanger) thus allowing considering the expander supply pressure as the evaporator pressure without significant error. The pressure drop across the condenser was about 34-56 mbar, and higher than in the evaporator. However, it should be mentioned that the instruments used are oversized in regard to the values measured (see Table 6.4). Figure 6.11 displays the values of pressure drops as measured during the tests.
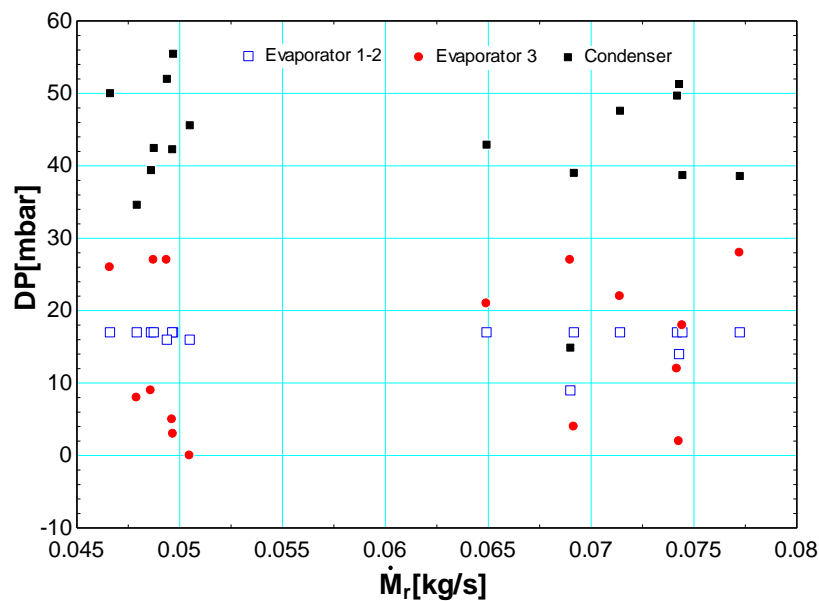
Figure 6.11 - Pressure drops recorded

6.5.1.3 Heat balances over the heat exchangers

Condenser

The heat rejection rate on both sides of the condenser is computed using equations 6.2 and 6.3, and the quantities obtained should be equal.

Water side
$$\dot{Q}_{w,cd} = \dot{m}_w \, C_{p,w} \Delta T \tag{6.2}$$

Refrigerant side
$$\dot{Q}_{r,cd} = \dot{m}_r \, \Delta h \tag{6.3}$$

As can be seen from Figure 6.12, the heat rate on the water side is higher than the heat rate on the refrigerant side. The difference is between 13 and 26%. This is explained by the high water mass flow rate (~ 1 kg/s) which decreases the accuracy of the temperature sensors located at the condenser inlet.
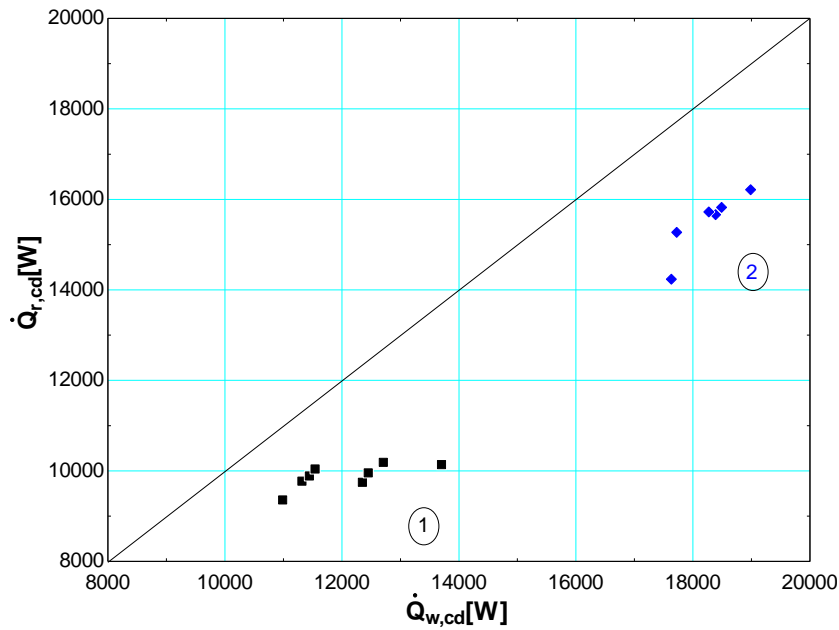
Figure 6.12 - Heat balance over the condenser

Evaporator

The heat input rate to the cycle is computed using equations 6.4 and 6.5 respectively and the quantities obtained should be equal.

Air side
$$\dot{Q}_{a,ev} = \sum_j \dot{m}_a \, C_{p,a} \Delta T_j \tag{6.4}$$

Refrigerant side
$$\dot{Q}_{r,ev} = \sum_j \dot{m}_r \, \Delta h_j \tag{6.5}$$

During the tests, the heat rate on the air side is higher than the heat rate on the refrigerant side for all points (Figure 6.13). For most of points, the difference is less than 7% except for the single point circled for which the difference is 10.6%. The difference on the air side is due to thermal losses to the ambient or measurements uncertainties.
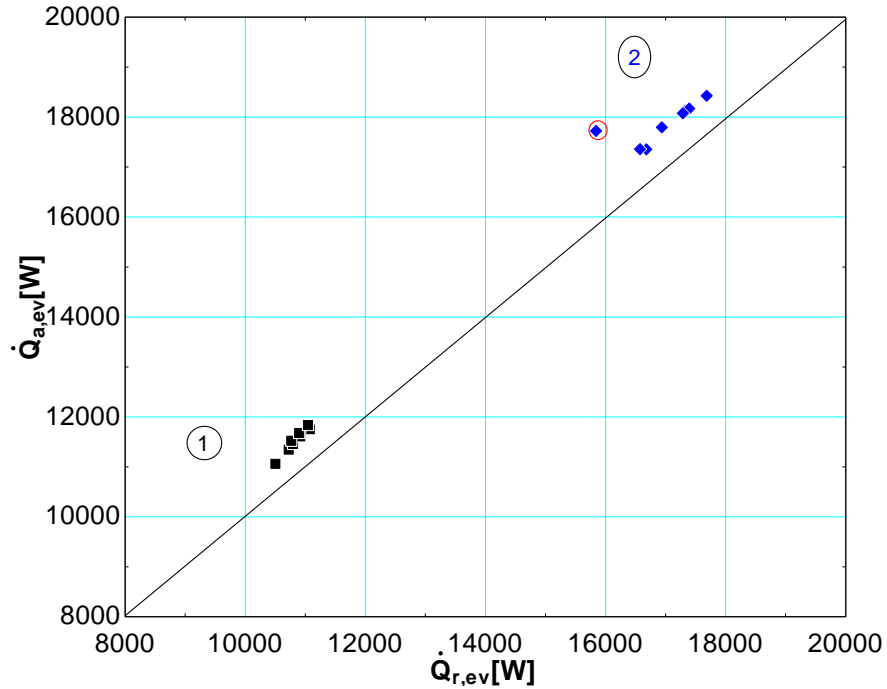
Figure 6.13 - Heat balance over the evaporator

6.5.1.4 The superheating adjustment
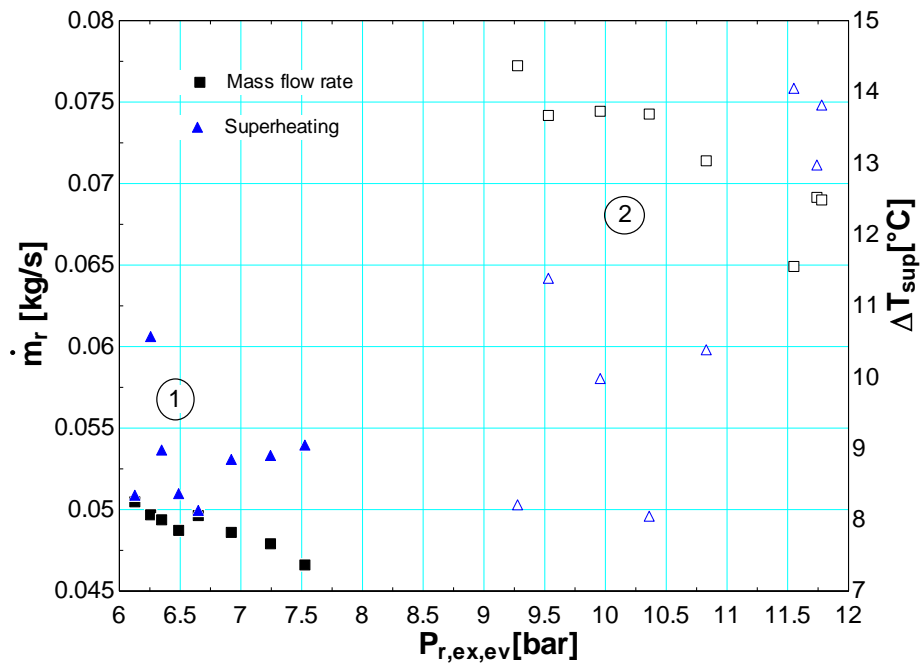
Figure 6.14 - Superheating adjustment

Figure 6.14 allows understanding how the superheating can be fixed. Two parameters can be used: the mass flow rate and the evaporator pressure (shaft rotational speed). As it is proved by both sets of tests, an increase in pressure reduces the mass flow rate but in contrast increases the fluid overheating at the expander inlet and vice versa. In the search for high efficiency, the evaporating pressure is usually increased, what could negatively affect the output of the system if the superheating is kept constant. However, a degree of superheating (ΔT_{sup}) in the range 5-15 K seems reasonable.

6.5.1.5 The torque

Expander and asynchronous machine are coupled through a torque meter. Figure 6.15 shows the linear evolution of the torque with the rotation speed. The increase of the quantity of the heat available for the cycle has as effect an increase of the torque and subsequently of the shaft power.
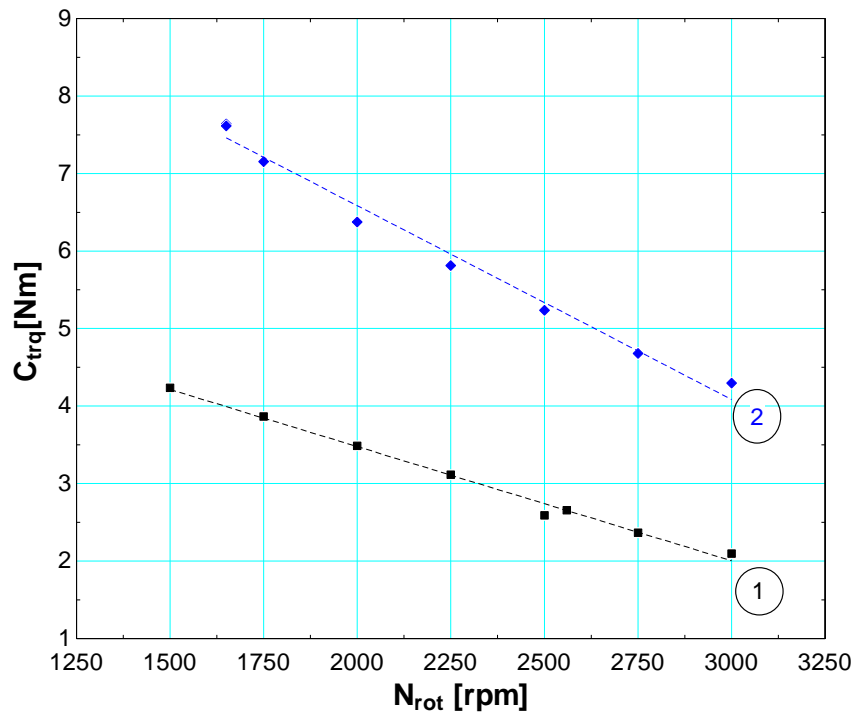
Figure 6.15 - Torque as a function of the rotation speed

6.5.1.6 Expander shaft power

The shaft power is evaluated knowing the value of the torque and the rotational speed given by the inverter screen with the following relation:

$$\dot{W}_{sh} = C_{trq}(2\pi N_{rot}/60) \tag{6.6}$$

The graph expander shaft power vs rotational speed (Figure 6.16) can be fitted as a parabola with a maximum, what could be predicted from equation 6.6 as the torque is a linear function of the rotational speed (See Figure 6.15). A maximum power of 733.5 W is obtained at 2250 rpm for the first set of points, while for the second set of tests 1369

W is obtained at the same rotational speed. The difference in output is due to the increase in heat input.
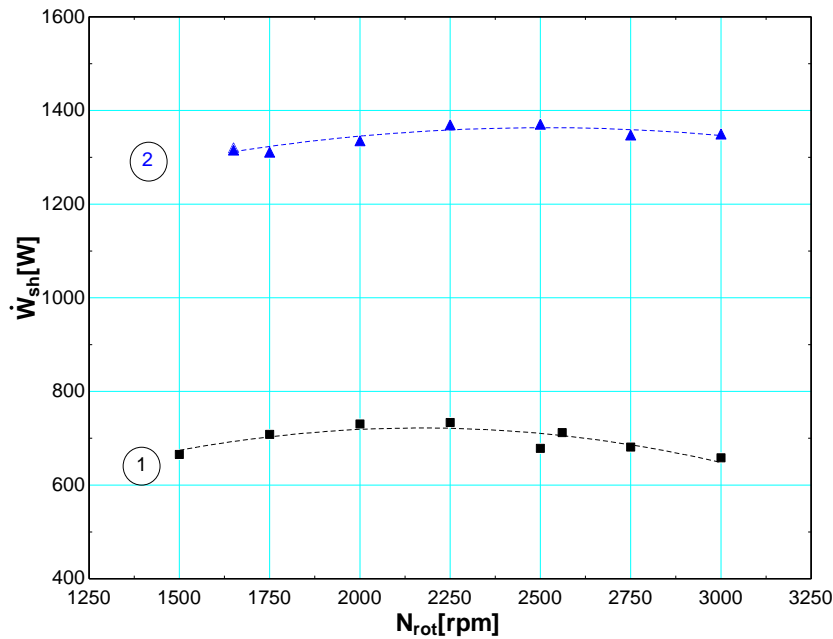
Figure 6.16 - Variation of the shaft power with the shaft rotation speed

6.5.1.7 System electrical efficiency

The shaft power is evaluated through the measurements given by the torque meter and the shaft rotational speed while the electrical output is measured by the inverter. Knowing the shaft power and the electrical output of the asynchronous machine it is therefore possible to evaluate the electrical efficiency of the coupling. The nominal power of the asynchronous machine is 5.4 kW. The inverter displays the electrical output of the asynchronous machine as the percentage of the nominal power of the asynchronous machine. From the data displayed by the inverter, the electrical power produced by the asynchronous motor is computed and the electrical efficiency of the coupling system evaluated with the following relation:

$$\eta_{el} = W_{el} / \dot{W}_{sh} = p_{inv}.W_{el,nom} / \dot{W}_{sh} \tag{6.7}$$

The electrical efficiency increases with the shaft power as it is seen on Figure 6.17. It varies between 70-79% for the first set of tests (low output power) and 79.6-90.5% for the second (high output power). Figure 6.18 shows the variation with the rotation speed. The electrical efficiency increases from low rpm passes through an optimum value and decreases afterwards. The points circled red on the graph are those for which the shaft power is maximum for each set. Concluding, the electrical efficiency and shaft power output are strongly linked.
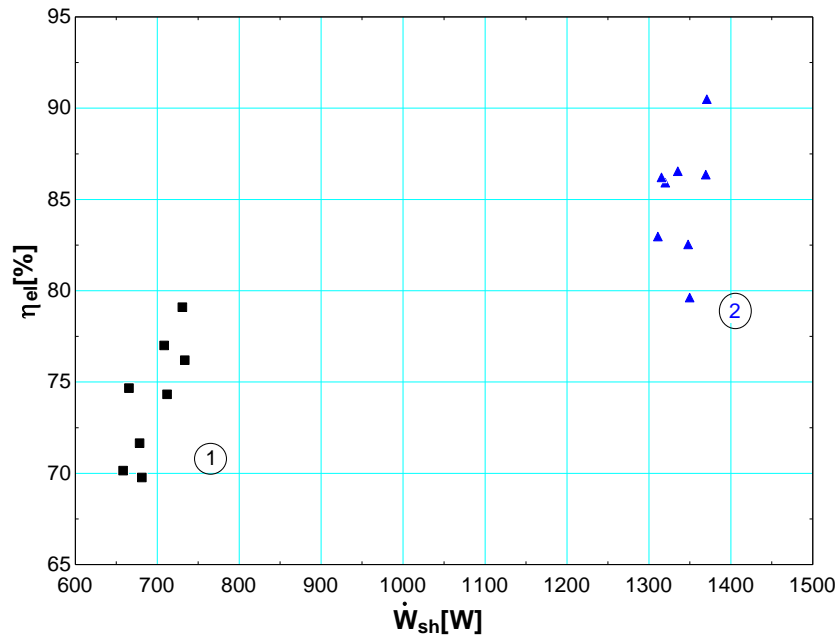
Figure 6.17 - Variation of the electrical efficiency with the shaft power
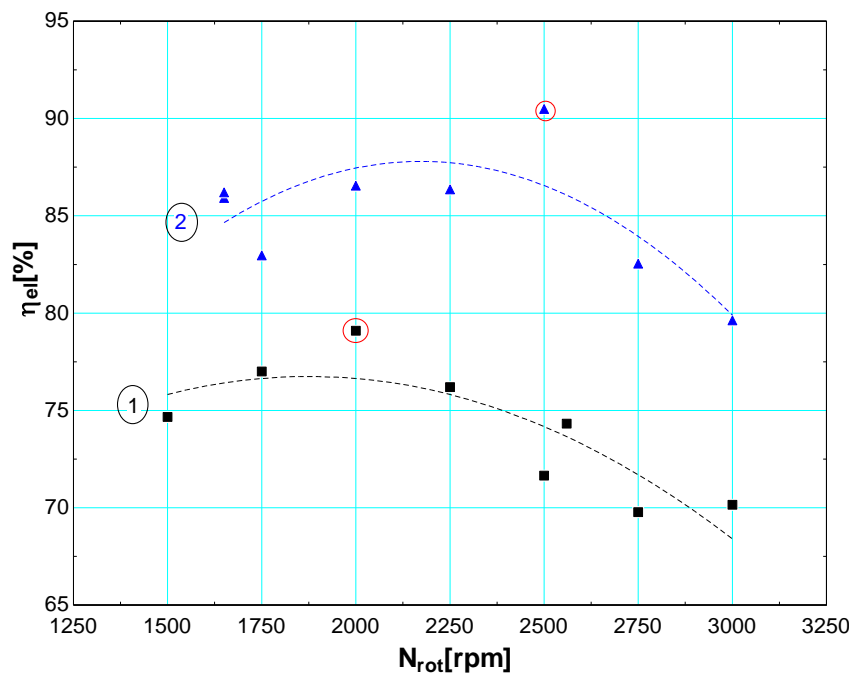
Figure 6.18 - Variation of the electrical efficiency with the rotation speed

6.5.1.8 Pumps

On the bench, only one electricity meter is used to measure the electrical consumption of the pumps and since the outlet pressure for both pumps can be considered as the evaporator pressure they are considered here as one single pump. Their consumption is between 380-400 W for the first series of tests and about 435 W during second series (Figure 6.19). This consumption is really high for a small output system. Their global efficiency is in the range 5-7% and 13-16% for first and second series respectively (Figure 6.20). The poor performance of the pumps can be explained by the fact that they are initially designed for circulating liquids and are just adapted to refrigerants. High

consumption and low efficiency conduct inadvertently to low efficiency of the cycle, thus it is important to search for other types of more efficient pumps.
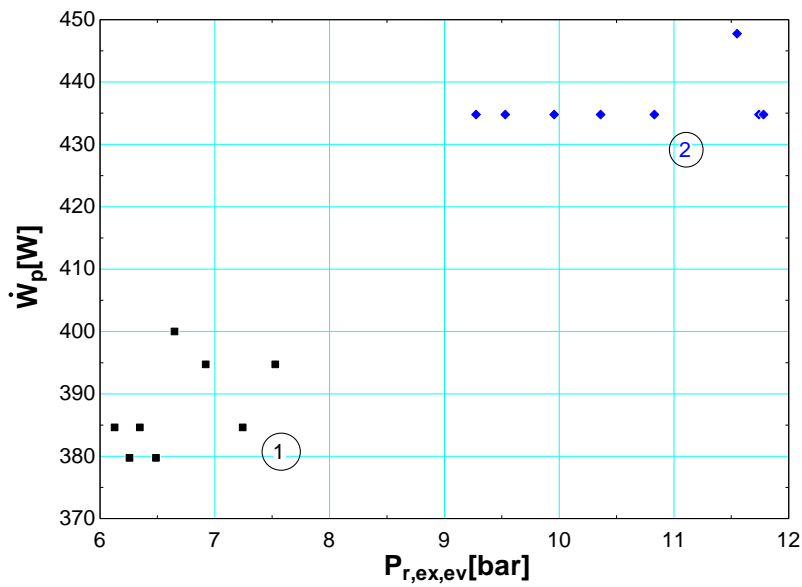
Figure 6.19 - Pumps consumption
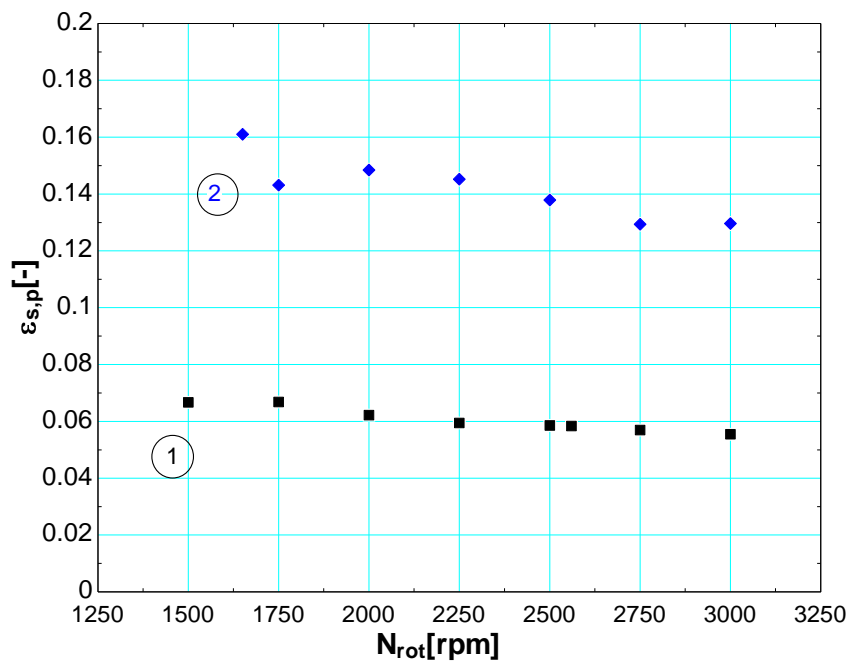
Figure 6.20 - Pumps global efficiency

6.5.1.9 The cycle and expander efficiencies

The cycle efficiency of the system is given by

$$\eta_{cycle} = \frac{\dot{W}_{net}}{\dot{Q}_{r,ev}} = \frac{\dot{W}_{sh} - \dot{W}_p}{\dot{Q}_{r,ev}}$$

(6.8)

The expander effectiveness is defined by

$$\varepsilon_{s,exp} = \frac{\dot{W}_{sh}}{\dot{W}_s} = \frac{C_{trq}(2\pi N_{rot}/60)}{\dot{M}_r (h_{r,su,exp} - h_{r,ex,exp,s})}$$ (6.9)

Where:

$\dot{W}_s$ = output work when the expansion process is isentropic
$h_{r,su,exp}$ = enthalpy of the refrigerant at the expander supply
$h_{r,ex,exp,s}$ = enthalpy of the refrigerant at the expander exit when the expansion process is considered isentropic.

The variation of expander effectiveness and cycle efficiency with the rotation speed are shown in Figure 6.21. The expander effectiveness varies is the range of 54.25- 60.92% during first set of test and in the range of 62.43-65.75 during the second set. Figure 6.21 shows that without any irregularities during the tests values that maximize the expander effectiveness exist (Quoilin et al., 2010). Indeed, it can be considered that for the first set of tests the maximum effectiveness is obtained at 2500 rpm and at 2750 rpm for the second set. The existence of the maximum values of the expander effectiveness is explained by the antagonistic effects of the rotational speed on the internal leakages and on friction losses and supply pressure drop. Optimum values are also observed with the evolution of the cycle efficiency. These are observed for a speed of about 2250 rpm (see Figure 6.21). However, maximum values of efficiencies for cycle and expander are not met for the same value of the speed.
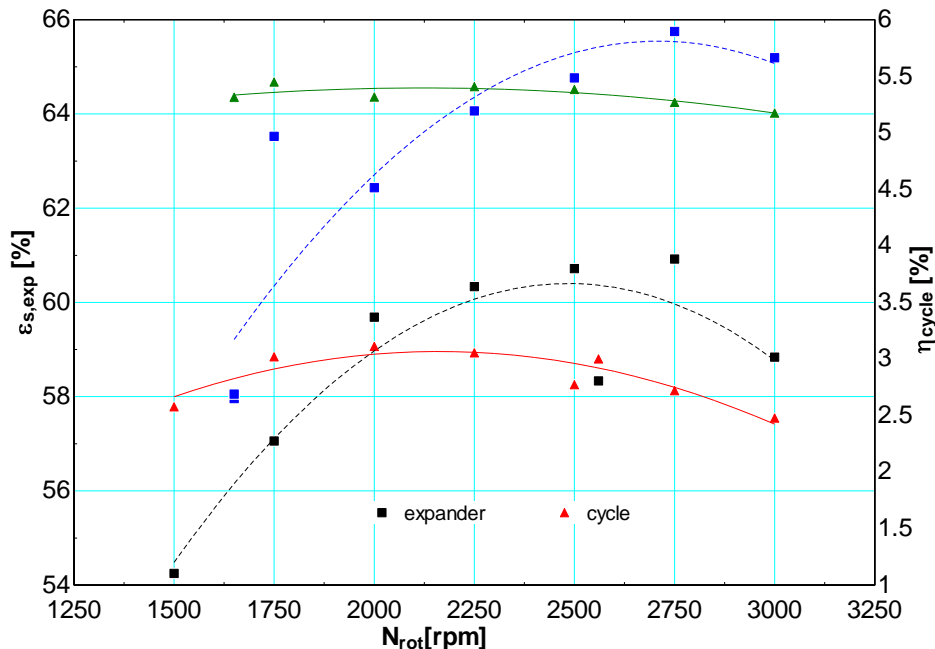
Figure 6.21 - Cycle efficiency and expander effectiveness vs rotational speed

The influence of the expander pressure ratio (r_p) is noticeable (Figure 6.22). During the experiment, the pressure ratio varied between 5 and 9.9. For fixed conditions of the heat supply to the cycle, there exists a value of the pressure ratio for which the expander

effectiveness is maximized. This is close to 5.5 during first tests and 7 during second. The pressure ratio is higher in the second set in comparison with the first set of tests; this can be explained by the increase in evaporating pressure consequence of the increase of the exergy value of the heat source.
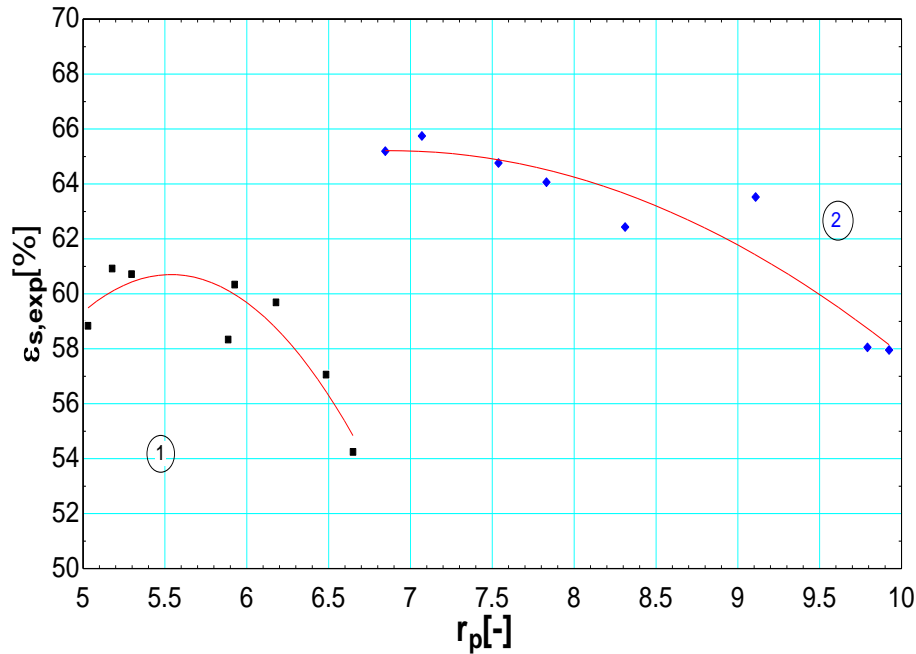
Figure 6.22 - Evolution of the expander effectiveness with the pressure ratio

6.5.1.10 Resource utilization

The recuperation efficiency is the percentage of heat recovered over the maximum amount recoverable by the cycle and is defined as:

$$\varepsilon_r = \frac{\dot{Q}_{ev}}{\dot{Q}_{ev,max}} = \frac{\sum_{j=1}^{3} \dot{Q}_{a,ev,j}}{\dot{M}_a \, C_{p,a}(T_{a,su,ev3} - T_{w,su,cd}) + \dot{M}_a \, C_{p,a}(T_{a,su,ev2} - T_{w,su,cd})} \tag{6.10}$$

The global efficiency is the product of recuperation and cycle efficiencies:

$$\eta_{global} = \varepsilon_r \cdot \eta_{cycle} \tag{6.11}$$

As can be seen from Figure 6.23, the recuperation efficiency reduces when evaporator pressure is raised. This means that increasing the evaporator pressure reduces the amount of heat recovered. For the present experiment, the recuperation efficiency is above 70%, which can be explained by the good effectiveness of the evaporator. It is also obvious, that this recuperation effectiveness increases with the quality of the heat resource available. The global efficiency as product of two efficiencies is considerably low. It is between 2 and 4% for all points. The global efficiency varies like the cycle

efficiency and has an optimum value, that is at about 7 bar for the first set of tests and about 10.5 bar for the second.
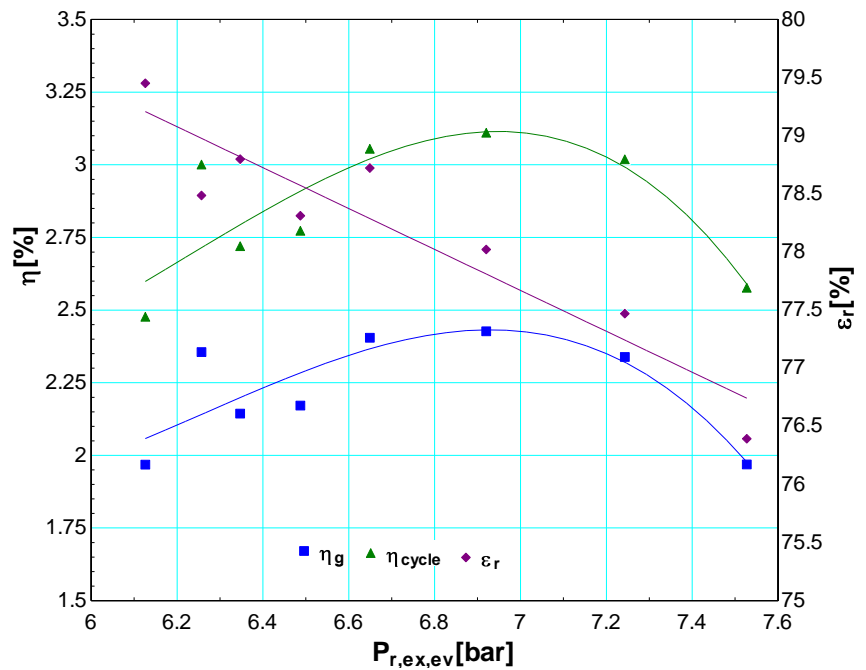
a- First tests
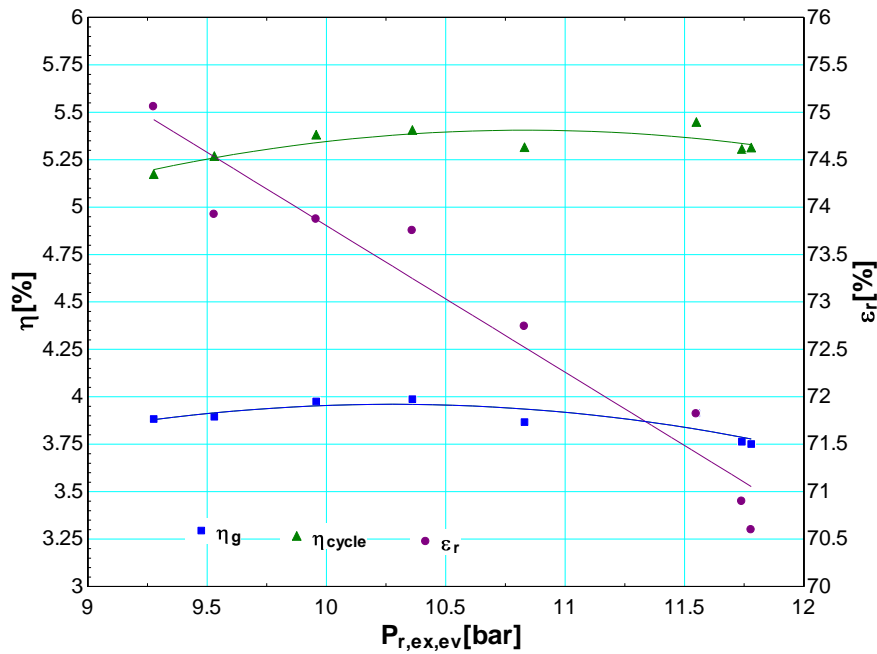
b- Second tests

Figure 6.23 - Recuperation, cycle and global efficiency with the evaporator pressure

6.5.2 Exergy analysis

The exergy flow analysis defined as the combination of First and Second Laws of Thermodynamics is applied here with the advantage of taking into account the quality of

the heat sources and heat sinks. The performances of different components as well as that of the system are evaluated in view of minimizing the exergy destroyed during the operation of the system at steady state.

If the system is considered in equilibrium with the surroundings, and neglecting the kinetic and potential exergies, the exergy associated with any flow at any step of a process taking place in the cycle can be written as:

$$E_i = \dot{M}_i [h_i - h_o - T_o(s_i - s_o)] \qquad (6.12)$$

Where M_i, h_i and s_i are the mass flow, the specific enthalpy and specific entropy of the point considered, respectively. "o" refers to the conditions of the cold water supplied to the condenser. The exergy flow graph of the system is depicted in Figure 6.24. In practice, the exergy flows are measured indirectly trough thermodynamic parameters recorded during the operation of the system. The pump consumption is measured with an electricity meter and the shaft power is deduced after the measurement of the torque and shaft rotational speed.
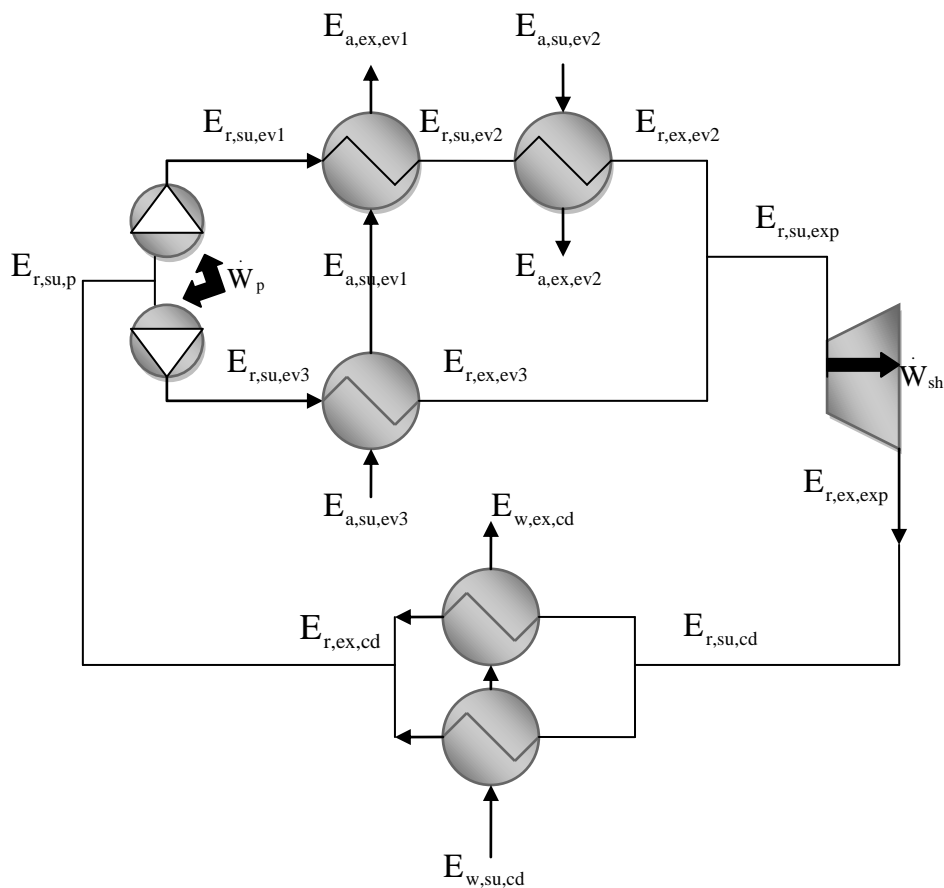
Figure 6.24 - Exergy flow graph

6.5.2.1. Irreversibilities within the system

The irreversibilities in different components can be calculated using equations displayed in Table 6.6.

Table 6.6 – Irreversibilities

Equations		
Evaporator 1	$\Pi_{ev1} = (E_{a,su,ev1} - E_{a,ex,ev1}) - (E_{r,su,ev1} - E_{r,ex,ev1})$	(6.13)
Evaporator 2	$\Pi_{ev2} = (E_{a,su,ev2} - E_{a,ex,ev2}) - (E_{r,su,ev2} - E_{r,ex,ev2})$	(6.14)
Evaporator 3	$\Pi_{ev3} = (E_{a,su,ev3} - E_{a,ex,ev3}) - (E_{r,su,ev3} - E_{r,ex,ev3})$	(6.15)
Evaporator	$\Pi_{ev} = \Pi_{ev1} + \Pi_{ev2} + \Pi_{ev3}$	(6.16)
Expander	$\Pi_{exp} = (E_{r,su,exp} - E_{r,ex,exp}) - \dot{W}_{sh}$	(6.17)
Condenser	$\Pi_{cd} = (E_{r,su,cd} - E_{r,ex,cd}) - (E_{w,ex,cd} - E_{w,su,cd})$	(6.18)
Pumps	$\Pi_{p} = \dot{W}_{p} - (E_{r,ex,p} - E_{r,su,p})$	(6.19)
System	$\Pi_{\Sigma} = \Pi_{ev} + \Pi_{cd} + \Pi_{exp} + \Pi_{p}$	(6.20)

In Figure 6.25 is depicted the amount of the exergy destroyed in different components during the tests. Larger amounts of exergy are destroyed in the heat exchangers forming the condenser and evaporator in comparison to expander and pumps. The condenser accounts for about 35-43% of total exergy destroyed followed the evaporator (30-38%), the expander (13.95-20.2%) and the pumps (8.85-13.9%). Exergy loss distribution is shown for two pressure levels on Figure 6.25b.

(a)

Pr,ex,ev=10.83 bar   *Pr,ex,ev=6.12 bar*
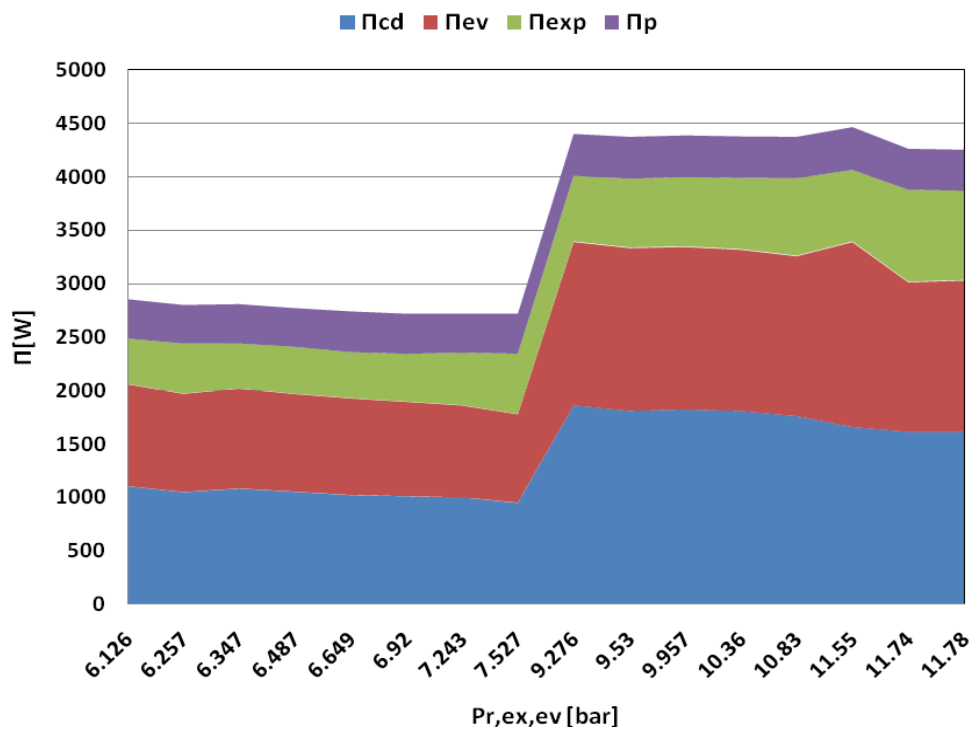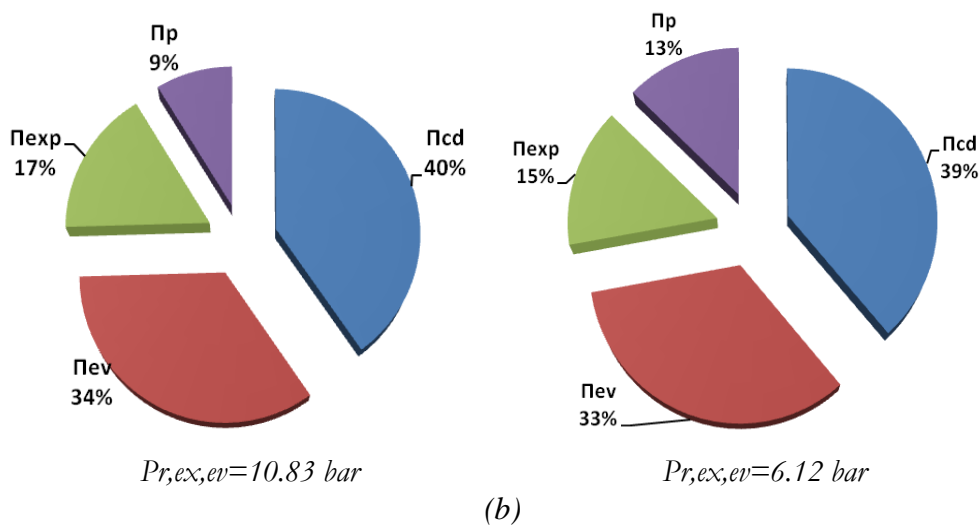
(b)

Figure 6.25 - Irreversibilities in different components

The large quantities of exergy destroyed in the evaporator and condenser are due to the heat exchange profiles as depicted in Figure 6.26 for test 14th. In fact, the superheated vapors are supplied to the condenser at about 100 ℃ while water is supplied at 6 ℃. This leads to a poor operation of the condenser. For proper operation of the condenser, the mass flow rate should be decreased, and this has as effect an increase in the condenser water outlet temperature and reduction in exergy loss. The hot water produced could be used in another process. However, there was no need to produce hot

water in so-called cogeneration system in this study. Exergy destroyed in the evaporator is explained by the mean temperature difference between air and refrigerant in third and second evaporators (See Figure 6.26).
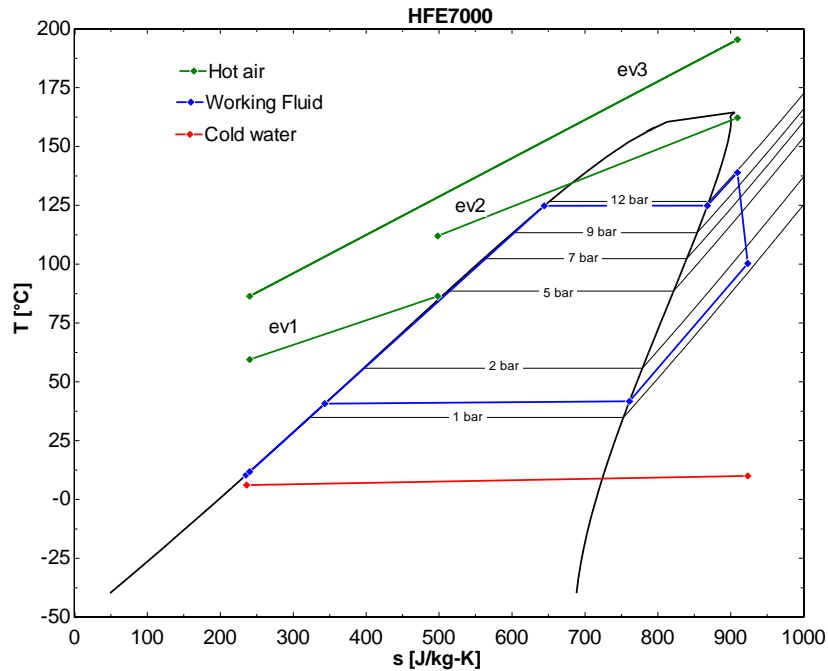
Figure 6.26 - T-s diagram and secondary fluid temperature profiles

6.5.2.2 Exergy efficiencies

The exergetic efficiencies of different components are evaluated using equations of Table 6.7.

Table 6.7 - Exergetic efficiencies

Equations		
Evaporator	$\eta_{\text{exe,ev}} = \dfrac{\Delta E_{r,ev1} + \Delta E_{r,ev2} + \Delta E_{r,ev3}}{\Delta E_{a,ev1} + \Delta E_{a,ev2} + \Delta E_{a,ev3}}$	(6.21)
Expander	$\eta_{\text{exe,exp}} = \dfrac{\dot{W}_{sh}}{E_{r,su,exp} - E_{r,ex,exp}}$	(6.22)
Condenser	$\eta_{\text{exe,cd}} = \dfrac{E_{w,ex,cd} - E_{w,su,cd}}{E_{r,su,cd} - E_{r,ex,cd}}$	(6.23)
Pumps	$\eta_{\text{exe,p}} = \dfrac{E_{r,ex,p} - E_{r,su,p}}{\dot{W}_{p}}$	(6.24)
System	$\eta_{\text{exe,cycle}} = \dfrac{\dot{W}_{sh} - \dot{W}_{p}}{E_{a,su,ev3} + E_{a,su,ev1}}$	(6.25)

A| Expander and pumps exergy effectiveness

The exergetic effectiveness of the expander depicted on Figure 6.27 reveals that it increases with the supply temperature and with the rotational speed. However there exists an optimum for a particular value of the speed. The value of the exergy efficiency of the expander varies between 54 and 69% for all tests. The pumps treated as one operate with very low efficiencies and work better at higher pressure (low rpm). For all tests, the maximum exergetic efficiency obtained was about 11.7%.
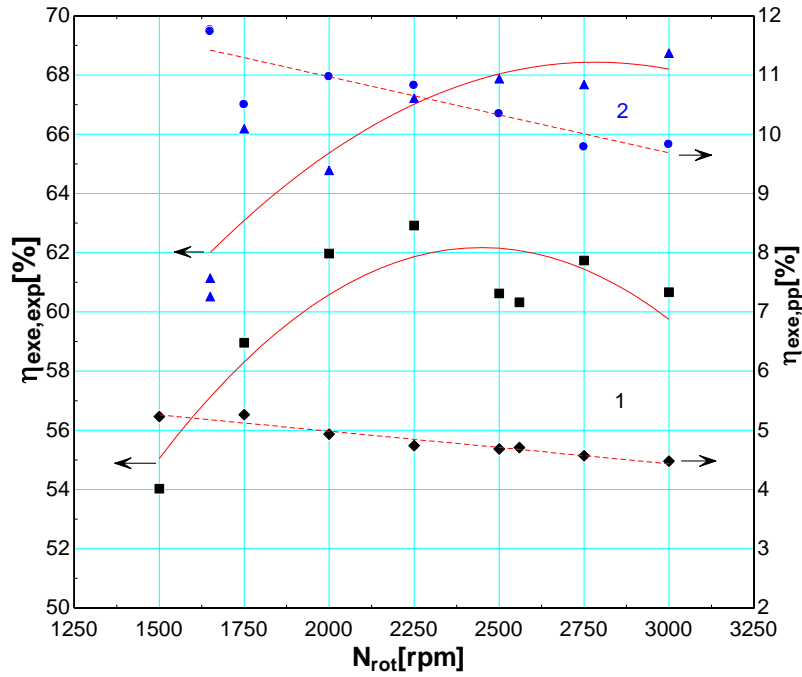
Figure 6.27 - Expander and pumps exergy efficiency vs shaft rotation speed

B| Exergetic efficiency of evaporator and condenser

The exergetic efficiency plotted in Figure 6.28 confirms the poor operation of the condenser for which values are below 12%. The poor performance is explained earlier by the cold water temperature profile which generates entropy in the condenser. Unlike the condenser, the evaporator yields better efficiency in the range 60-74%.
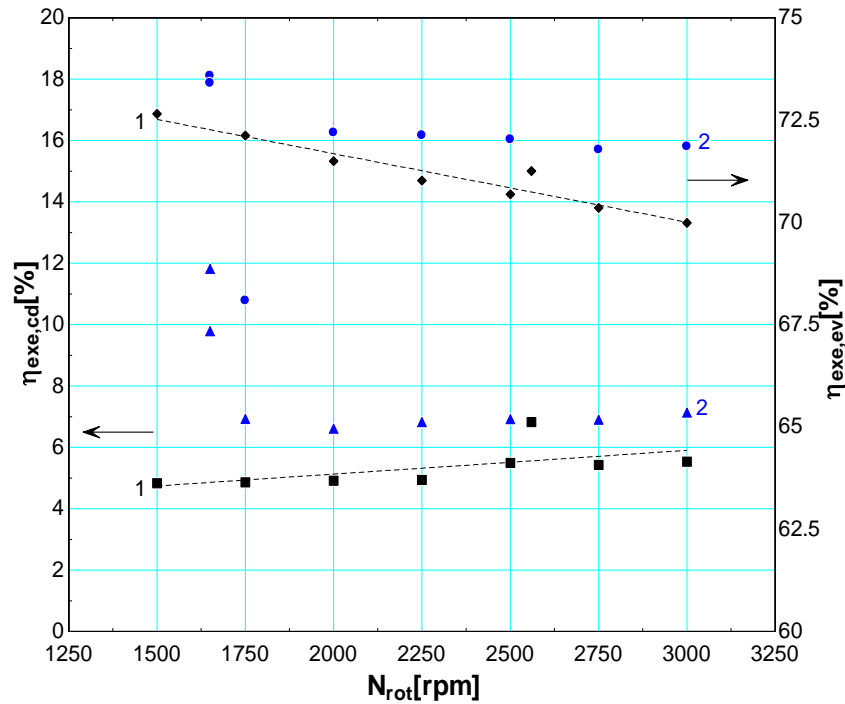
Figure 6.28 - Evaporator and condenser exergetic efficiencies

C| System exergy efficiency

The system exergetic efficiency varies between 7-8.5% for the first set of tests and 11.5-13% for the second set. This low efficiency is partly explained by the exergy destruction during heat transfer in the condenser and evaporator. Figure 6.29 shows the variation of the system exergetic efficiency with the rotation speed.
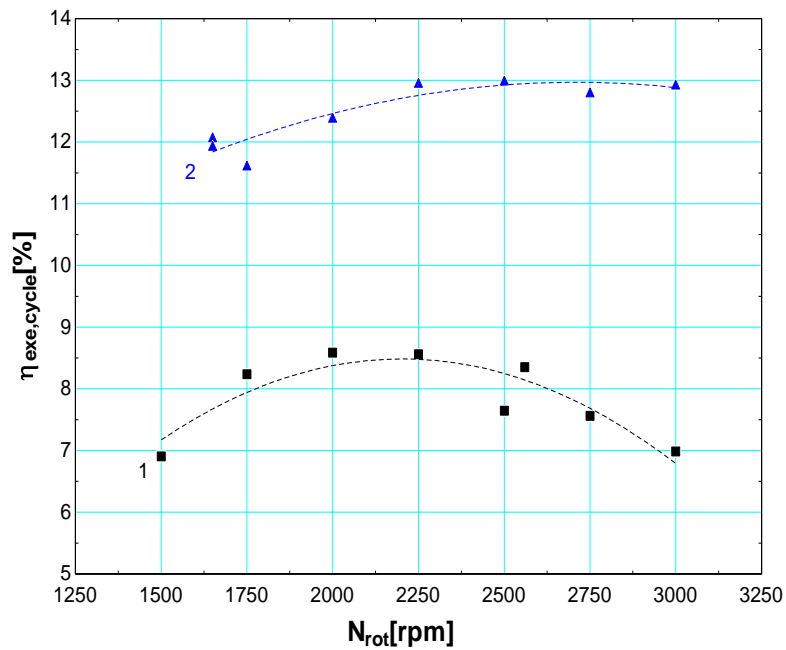
Figure 6.29 - Cycle exergy efficiency vs rotation speed

6.6. Fluids performance comparison

Main results of tests conducted on small scale ORCs in heat recovery application at the Thermodynamics Laboratory, Liege since 2007 (Quoilin, 2007; Declaye, 2009) are displayed in Table 6.8. The highest expander efficiency (70.6%) was recorded for R245fa for which the shaft power of 2164 W is the maximum recorded. The thermal and exergetic efficiency are better for R123 than for others. Of all fluids, HFE7000 is the one allowing the highest pressure ratio of about 10.

Table 6.8 - Main results obtained for different fluids

	2007	2009	2010
Fluid	R123	R245fa	HFE-7000
Expander efficiency (%)	68	70.6	65.75
Expander shaft power (W)	1820	2164	1371
ORC thermal efficiency (%)	7.4	7.1	5.45
ORC Exergetic efficiency (%)	22.8	19.8	12.96
Pressure ratio (-)	5.4	7.6	9.9
Evaporator power (W)	22.5	23.9	17.69

However, the performances of the ORC were obtained for different fluids at different conditions. Particularly the amount of heat recovered and the quality of the heat resource and heat sink were not the same. For proper comparison, the global efficiency which takes into account the heat recoverable and the power output obtained will be used. Figure 6.30 provides a meaningful picture for fluid performance comparison. First remark is the increase of the cycle global efficiency with evaporator pressure. Secondly, all fluids follow the same trendline, what means that in similar conditions all fluids could yield very close outputs. However, this is valid within certain range of values of the evaporator pressure because these fluids do not have same thermodynamic properties (see Table 6.1). Slight advantage goes to R245fa for which the highest efficiency was obtained at a pressure value of about 13 bar.
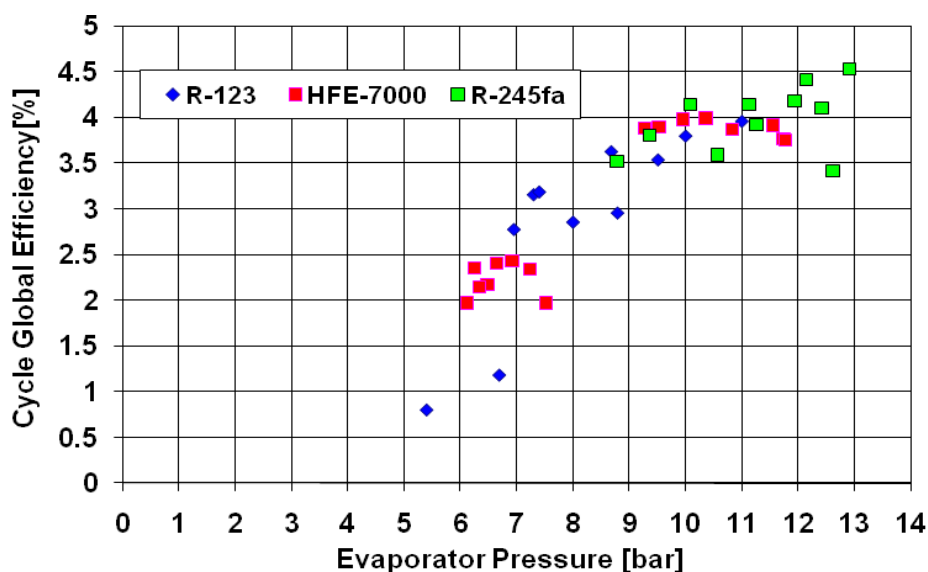
Figure 6.30 - Cycle performance comparison with different fluids

As a key component, the expander deserves a particular attention. Its performance strongly depends on the thermodynamic properties of the fluid at its supply port, and mainly the vapor density. Figure 6.31 shows that the investigated expander yields an efficiency in the range of 60-70% when operating with pressure ratio between 3.5 and 9. Maximum efficiency seems to converge towards a value of pressure ratio of about 5. Concluding, with the present expander more than 30% of enthalpy input is lost. This loss is attributed to internal leakages, pressure drop at the expander supply port and mechanical losses.
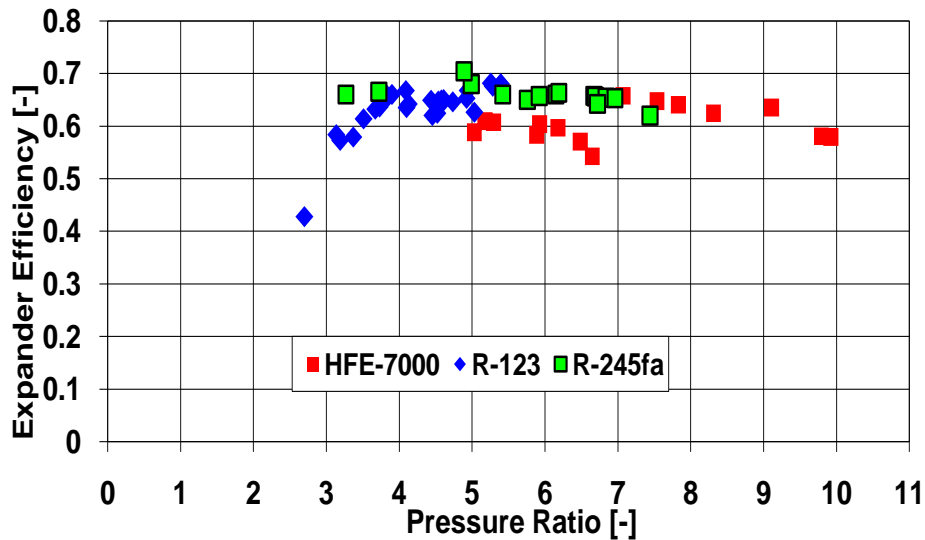
Figure 6.31 - Expander efficiency for different fluids

6.7. Conclusion

The experimental study of a small ORC in heat recovery application with integrated scroll type expander is reported. The working fluid used is a hydrofluoroether HFE7000. Two series of tests were carried out to evaluate the performances of the system as well as those of the components. Maximum cycle global efficiency achieved was about 4% meaning that more that 96% of the heat available was not converted into mechanical power. The cycle maximum exergetic efficiency was only 13% due to excessive exergy losses in the heat exchangers. Although the expander yielded satisfactory results with a global isentropic efficiency above 60%, the pumps in contrary operated with very low efficiency (less than 17%) and should be substituted by more efficient ones. Comparison with previous tests was also carried out from which it could be concluded that 70% appears as the limit for the investigated expander and following fluids: R123, R345fa and HFE7000 in similar conditions give close results with slight advantage to R245fa for better efficiency, non-corrosiveness (unlike R123) and no infiltration problem (unlike R123 and HFE7000).

7 - Economic Evaluation and Optimization of Small Scale Organic Rankine Cycles in Heat Recovery Application

7.1 Introduction

The Organic Rankine Cycle (ORC) appears progressively as a promising solution to recover waste heat from thermal processes for electricity generation. At the University of Liège, Belgium, a prototype of small-scale ORC has been built and successfully tested as reported in the previous chapter. It uses R123, R245fa and HFE7000 as working fluid, and an oil-free scroll compressor adapted to run in expander mode. The promising results obtained demonstrated the technical feasibility of the system. A further and necessary step is the economic analysis of the system in order to evaluate its economical profitability.

Thus, the present chapter aims at studying the profitability of small ORCs in waste heat recovery application (Tchanche et al., 2010a & 2010b). First, a pre-design model of the ORC is proposed and simulations are run with different working fluids candidates to select the most suitable ones. In a second step, economic evaluation is carried out for a system operating with the best suited fluid. Finally, economic optimization of small ORCs operating with different fluids is done considering the specific installation cost as objective function. The working fluids considered for the comparison are: R245fa, R113, R123, n-Pentane, and n-Butane.

7.2 ORC in heat recovery application

The simple ORC system integrates four basic components: an evaporator, a turbine/alternator group, a condenser and a working fluid pump. Although many studies conclude that the introduction of regenerating processes (recuperator, feedliquid heater) increase the efficiency of the Rankine Cycle, it was shown that this is not justified in waste heat to power application for which the power output should be maximized instead of cycle efficiency (Quoilin and Lemort, 2009). The basic configuration is therefore selected. A heat source is needed to drive an ORC. Two ways exist to capture the wasted heat: (1) waste heat source and working fluid exchange in the same heat exchanger and (2) a thermal oil loop is integrated to transfer the heat from the waste heat site to the evaporator. The configuration illustrated in Figure 7.1 corresponding to the first case is considered in the present study. Depending upon the condensing pressure, the hot water at the condenser outlet can be used for space heating or as domestic hot water. In some cases, dry cooling can be applied at the condenser to save the water resources. The electricity produced is used on-site or fed to the grid as in case of renewable energy systems (solar PV, wind turbine, biomass or geothermal power plants).
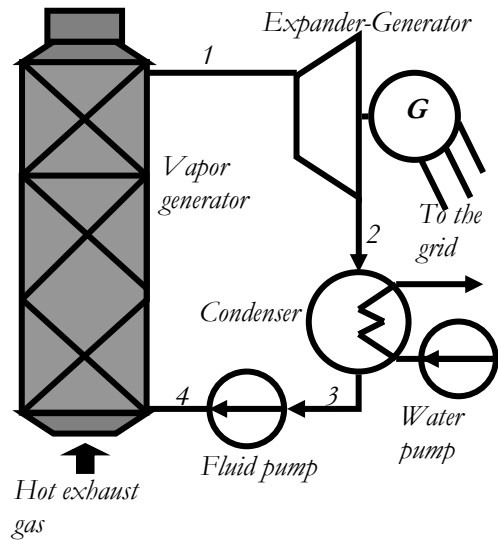
Figure 7.1 - ORC in waste heat recovery application

7.3 Fluid candidates

Selection of the most suitable working fluid is a critical step when designing an ORC. From numerous studies related to the selection of fluids for ORC-WHR, a certain number of criteria that should fulfill suitable fluids can be outlined (Badr et al. 1985; Tchanche et al., 2008a; Papadopoulos et al., 2010). Fluids with high critical temperature or high boiling point such as toluene and silicone oils are adapted for high temperature heat sources. Hydrocarbons such as Pentanes, benzene, butanes and cryogens such as R227ea, R123, R245fa, and HFE7000 are good candidates for moderate and low temperatures (Tchanche et al., 2010a, Dai et al., 2009). Zeotropic mixtures were suggested for best matching with exhaust stream which leads to better operation of the heat exchangers and resource recovery. Fluids with a high vapour density are advisable as they allow reduction of vapour turbine size and heat exchangers area. Presently, only few working fluids are available on the market and some are being progressively phased out because of their harmful effects on the environment (high ODP) reducing the range of choice. In absence of specially designed ORC fluids, any fluid used in other thermal processes as engineering fluids is welcome. Hence, there is a need to start designing specific fluids for ORCs as ORCs will become an important technology for harnessing low grade heat in the next future. Nevertheless, some of fluids present on the market are giving satisfactory results. A quick screening of several potential fluids was done and those listed in Table 7.1 emerged as suitable and will be considered in the present study.

Table 7.1 - List of considered working fluids

Fluids	$\varrho_{liq,wf}$ (kg/m³)	T_b (°C)	T_c (°C)	P_c (bar)	ASHRAE 34	GWP	ODP	UP_{wf} (€/kg)
R-245fa	1352	15.3	154.1	36.4	B1	820	0	32
R-123	1476.6	27.8	183.7	36.68	B1	77	0.02	15
R-113	1574.9	47.6	214.1	34.39	A1	6130	1	25
R-600	625.7	-0.5	152	37.96	A3	0	0	1.7
R-601	578.6	36.1	196.5	33.64	A3	0	0	1.7

7.4 Modeling of a small ORC

The ORC model is built by interconnecting several sub-models related to the components: scroll expander, heat exchanger and pump models. These sub-models will be described in the following paragraphs.

7.4.1 The scroll expander model

Volumetric expanders, such as scroll, screw or reciprocating technologies present an internal built-in volume ratio corresponding to the ratio between the inlet pocket volume and the outlet pocket volume. Under-expansion occurs when the internal pressure ratio imposed by the expander is lower than the system pressure ratio. In that case, the pressure in the expansion chambers at the end of the expansion process (P_{in}) is higher than the pressure in the discharge line (P_{ex}). Over-expansion occurs when the internal pressure ratio imposed by the expander is higher than the system pressure ratio.

Under and over expansion losses can be modeled by splitting the expansion into two consecutive steps (Zanelli and Favrat, 1994):

Isentropic expansion:

$$w_1 = h_{su} - h_{in} \tag{7.1}$$

h_{in} being the isentropic enthalpy at pressure P_{in}.

Isochoric expansion:

$$w_2 = v_{in} \left(P_{in} - P_{ex} \right) \tag{7.2}$$

w_2 is positive in case of under-expansion, and negative in case of over-expansion (Figure 7.2).
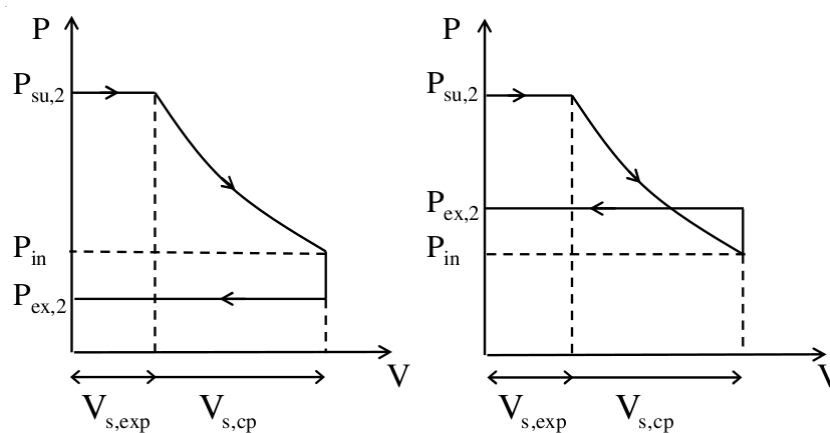
Figure 7.2 - Under and over-expansion losses

The total expansion work is then obtained by summing w_1 and w_2. Other losses such as internal leakage, supply pressure drop, heat transfers and friction are lumped into one single mechanical efficiency η_{lmech}. Thus, the actual expander work is expressed as:

$$\dot{W}_{exp} = \dot{M}_r \left(w_1 + w_2 \right) \eta_{mech} \tag{7.3}$$

For given rotational speed and fluid flow rate, the expander imposes the evaporating pressure. This is computed by:

$$\dot{M}_r = \frac{FF \cdot \rho_{su} \cdot V_s \cdot N_{rot}}{60} \tag{7.4}$$

FF is the filling factor; ρ_{su}, the density at the expander inlet; V_s, the swept volume and N_{rot} the rotational speed.

7.4.2 The heat exchanger model

The condenser and the evaporator are modeled using the ε-NTU method for counter-flow heat exchangers. The heat exchanger is divided into three zones (Figure 7.3) (Quoilin et al., 2010): a liquid zone, a two-phase zone and a vapour zone. Each zone is characterized by the heat transfer area A and a heat transfer coefficient U. The heat transfer coefficient U is given by $1/U = 1/h_r + 1/h_{sf}$.
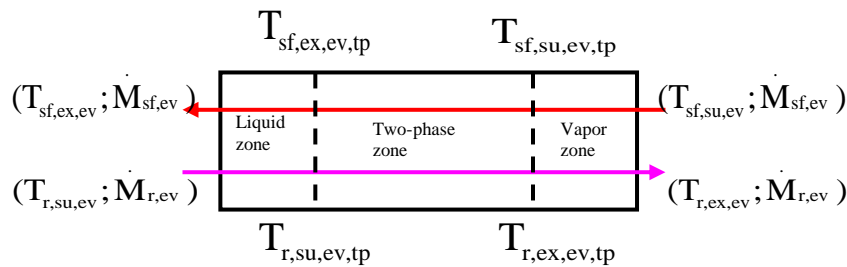
Figure 7.3 - Three-zone model of the heat exchangers

7.4.3 The pump model

The pump is characterized by its swept volume (V_s) and its global isentropic efficiency (η_p). Its electrical consumption is calculated using the relation

$$\dot{W}_{el,p} = \dot{V}_{s,p} \left(P_{r,ex,p} - P_{r,su,p} \right) / \eta_p \tag{7.5}$$

In the latter model (Figure 7.4), the mass flow rate displaced by the pump depends on the pump capacity (Xp) and swept volume. $P_{r,su,p}$ and $P_{r,ex,p}$ are the pressure at the pump's inlet and outlet respectively.
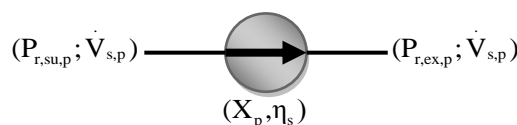
Figure 7.4 - Pump model

7.4.4 The global model

The global model of the ORC is built by interconnecting the models of different components above described to predict the system power output and cycle efficiency.

7.5 Thermodynamic optimization

7.5.1 Scope and method

The performance of a small scale ORC is predicted using the global model described in the previous section. Using that global model, the performance of the small scale ORC can be predicted. In the present case of an ORC in waste heat recovery application, the thermodynamic optimization aims at maximizing the net power output. However, other thermodynamic parameters can be used to characterize the thermodynamic behavior of the system and are described in the following lines.

The cycle thermal efficiency is an indicative parameter of the quantity of heat converted into power and is given by:

$$\eta_{ORC} = (\dot{W}_{sh} - \dot{W}_p) / \dot{Q}_{ev} \tag{7.6}$$

The recuperation efficiency is the ratio of the heat recovered to the maximum heat recoverable. It can thus be written as

$$\varepsilon_r = \frac{\dot{Q}_{ev}}{\dot{Q}_{ev,max}} = \frac{\dot{M}_a\, c_{p,a}\, (T_{su,a} - T_{ex,a})}{\dot{M}_a\, c_{p,a}\, (T_{su,a} - T_{amb})} = \frac{T_{su,a} - T_{ex,a}}{T_{su,a} - T_{amb}} \tag{7.7}$$

The global energy conversion efficiency is the product of the cycle thermal efficiency and the recuperation efficiency.

$$\eta_{global} = \varepsilon_r \eta_{ORC} \tag{7.8}$$

For the present study, many assumptions are made:
- The heat source is exhaust gas at 180 °C, assimilated to hot air with a mass flow rate of 0.21 kg/s.

- The condenser is cooled with cold water at 10 °C.

- The pinch point at the evaporator is 15 °C.

- The pinch point at the condenser is 10 °C.

- The superheating at the expander inlet, 5 °C.

- The subcooling after the condenser, 5 °C.

- The volumetric ratio of the scroll expander, 3.4.

- Hermetic scroll expander with mechanical efficiency, 70%.

- The isentropic efficiency of the pump, 60%.

The ORC global model was implemented in EES (Engineering Equation Solver) and the behavior of the system simulated under various conditions to find the optimal operation point. Figure 7.5 shows the T-s diagram of the ORC-WHR with R245fa as the working fluid.
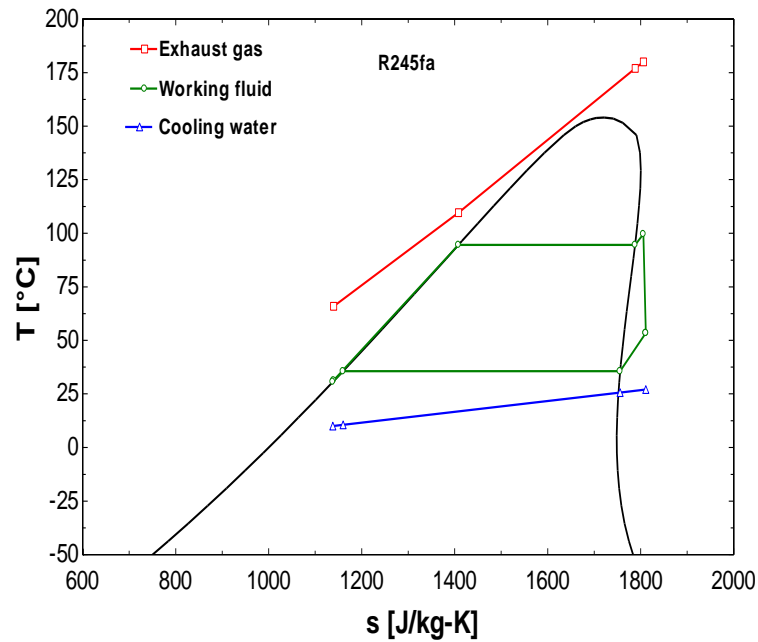
Figure 7.5 - Temperature-entropy diagram

Figures 7.6-7.8 show the evolution of different parameters related to the system under different evaporator pressure at which heat is transferred to the power cycle for R245fa. From Figure 7.6, it can be seen that an increase in evaporator pressure reduces the amount of heat transferred to the cycle and the amount of heat rejected at the condenser. The reduction of the amount of heat captured in the evaporator affects the temperature of the exhaust effluent/gas rejected to the environment; its temperature increases.
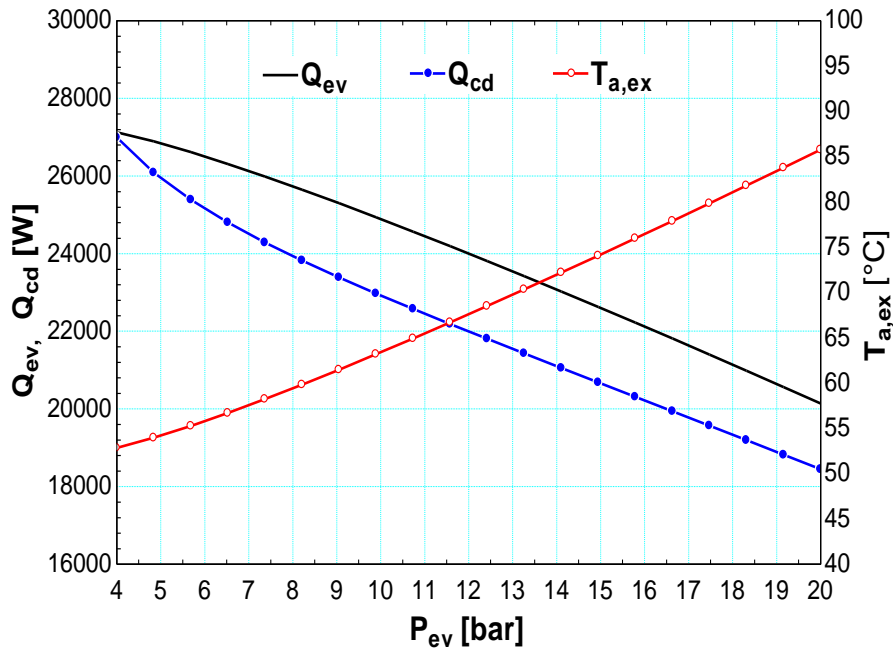
Figure 7.6 - Heat input, heat rejected and temperature of the rejected exhaust

Figure 7.7 shows the evolution of the net power output and cycle thermal efficiency. An optimum is obtained for both parameters but at different pressure values. The maximum net power of 2 kWe is obtained for 11.84 bar while the maximum cycle efficiency is observed when the pressure reaches 16 bar. The maximum cycle efficiency is explained by under-expansion losses in the expander that increase when the pressure ratio is increased. In an ORC-WHR, the heat source is free and would be otherwise discharged to the environment. And, therefore, unlike in the cases of solar or biomass ORCs for which the fuel management is of important preoccupation, the output power and not the cycle efficiency should be maximized.
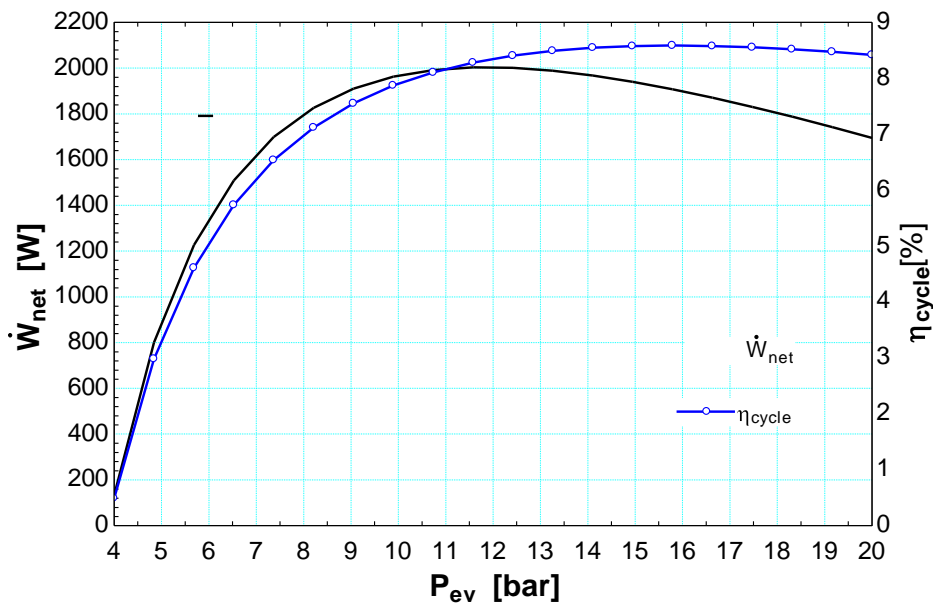
Figure 7.7 - Net power output and cycle efficiency

Figure 7.8 shows the evolution of the recuperation efficiency, cycle thermal efficiency and global efficiency. The recuperation efficiency decreases linearly as the evaporator pressure increases. The global efficiency has the same trend as the cycle efficiency. Nevertheless, they reach maximum values at different pressure values. Figure 7.8 shows that the global efficiency has a maximum value of 5.52% at 11.84 bar and has the same evolution as the net power output (Figure 7.7).
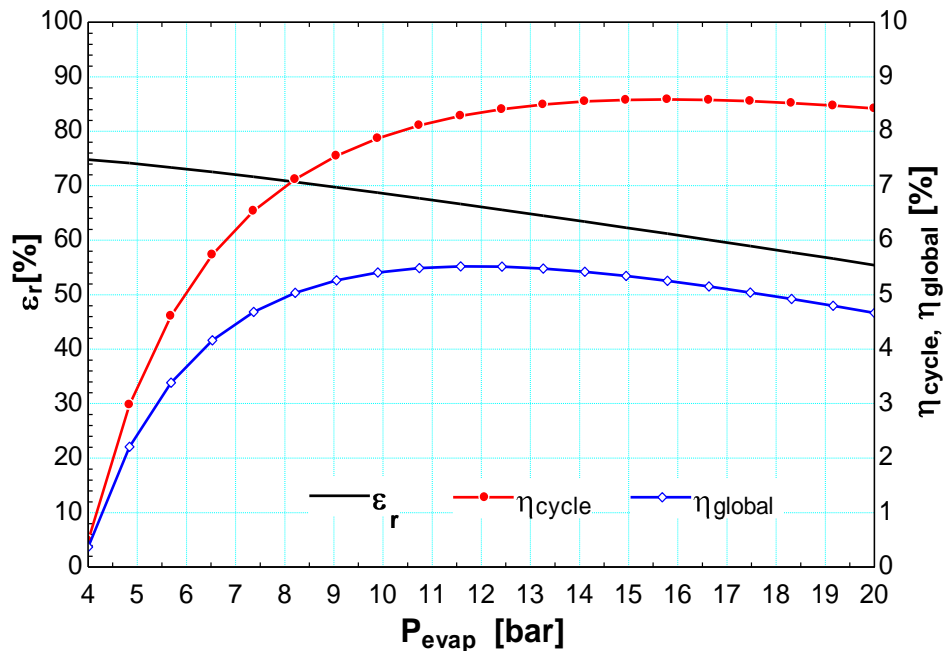
Figure 7.8 - Cycle, recuperation and global efficiency

7.5.2 Fluids comparison

Most criteria that should fulfill suitable working fluids in ORCs were established in Chapter 4. These are: adequate critical parameters, high liquid and vapour densities, good thermal stability and compatibility with materials, appreciable safety characteristics, market availability and low cost, good thermodynamic performance and low environmental impact. Fluids in Table 7.1 will be considered further.

The critical parameters for all fluids are suitable for subcritical cycles with the temperature of the heat source used. The thermal stability is not questionable for the considered fluids since the evaporating temperature does not exceed 200 °C. From compatibility point of view, only R123 is questionable as its corrosiveness has been reported. This can be solved by good selection of materials. All fluids proposed are available on the market with different prices as displayed in Table 7.1. Hydrocarbons are abundant at very cheap prices. Among the fluids proposed, R113 has a high ODP (1) and a high GWP (6130) and is phased-out in developed countries. N-Pentane and n-Butane raise the issue of flammability. Nevertheless, they can be considered as low risks substances as they are becoming familiar in domestic appliances. R245fa and R123 are toxic substances requiring special attention from the operator during manipulation. Performance parameters of ORCs associated with different fluids after power output maximization are displayed in Table 7.2. The evaporating pressures recorded are well below the maximum acceptable limit of 25 bar. Both R245fa and n-Butane yield higher

output and require high evaporating pressure. R245fa despite its toxicity has the highest vapour density at the expander inlet which would mean small expander. On the other hand, n-Butane is flammable but a very low cost fluid with the highest maximum power output. At this step, only a deep economic analysis could determine which one is to be selected.

Table 7.2 - Thermodynamic parameters at maximum net power output

Fluids	P_{ev} (bar)	W_{net} (W)	$\varrho_{p,su}$ (kg/m³)	$\varrho_{exp,su}$ (kg/m³)
R245fa	11.79	2004	1324	64.98
R123	7.31	1979	1453	42.59
R113	3.93	1942	1554	26.42
n-Butane	15.31	2078	567.3	38.04
n-Pentane	5.14	1979	616.6	13.78

7.6 Economic evaluation of a small ORC

7.6.1 System design parameters

Following the experimental results presented in Chapter 6, and the experience gained with R245fa, this fluid was selected for the economic evaluation. The simulation results derived from section 7.5 for the optimized system are displayed in Table 7.3.

Table 7.3 - Design parameters of the optimized system

Item/parameter	Units	Value
Heat source	-	Exhaust gas
Inlet temperature	°C	180
Outlet temperature	°C	67.25
Mass flow rate	kg/s	0.2104
Heat recuperated	kW	24
Working fluid	-	R-245fa
Evaporator pressure	bar	11.84
Cooling fluid	-	water
Inlet temperature	°C	10
Outlet temperature	°C	27.54
Water flow rate	kg/s	0.3
Evaporator pinch point	°C	15
Condenser pinch point	°C	10
Evaporator superheating	°C	5
Condenser subcooling	°C	5
Net electrical power	kWe	2
Thermal power	kWth	22
ORC efficiency	%	8.32
Recuperation efficiency	%	66.32
Global efficiency	%	5.52

7.6.2 Economic modelling

Several methods are used for economic evaluation of energy generating systems. The most popular ones are (Short et al., 1995; Biezma and Christobal, 2006; Nikolaidis et al., 2009):
- Depreciated payback period (DPP)
- Net present value (NPV)
- Internal rate of return (IRR)
- Savings to investment ratio (SIR)
- Levelized electricity cost (LEC)

The NPV, the DPP and the LEC will be used in the present study.

7.6.2.1 The net present value

The NPV sums the discounted cash flows; it integrates and converts at the same time amounts of money of various time periods. The formula that is used for the determination of the NPV is:

$$\text{NPV} = -C_0 + \sum_{n=1}^{N} \frac{F_n}{(1+k)^n} \tag{7.9}$$

n is the time period (year), F_n the net cash flow for year n, i.e. $F_n = B_n - C_n$, B_n the benefit (inflows) for year n, C_n the cost (outflows) for year n; C_0 is the initial investment, k the interest rate, and N is the number of years of the investment's lifetime or, the number of years for which the economic evaluation is requested. Using the NPV, an investment should be realized only if NPV>0, while in case alternative investments are considered, the best will be the one with higher NPV.

7.6.2.2 The depreciated payback period

The depreciated payback period determines the number of time periods that are required until an investor recovers the initial investment. It is given by

$$\text{DPP} = -\ln(1 - kC_0/F_n)/\ln(1+k) \tag{7.10}$$

Where it is assumed that the net cash flows F_n remain constant during the lifetime period.

7.6.2.3 The levelized cost of electricity

The levelized electricity cost (LEC) also called levelized cost of electricity (LCOE) is the cost of generating electricity from a particular system. Its calculation includes all costs necessary for the generation of electricity: initial investment, operation and maintenance, cost of fuel, insurance, etc. It represents the minimum cost at which electricity should be sold in order for the project to break even. It is written as:

$$LEC = \sum_{n=0}^{N} \frac{C_n + O\&M_n + FE_n}{(1+k)^n} \bigg/ \sum_{n=1}^{N} \frac{E_n}{(1+k)^n} \qquad (7.11)$$

$O\&M_n$ and FE_n stand for operation and maintenance costs and fuel energy costs for year n, respectively. It should be noted that in case of waste heat recovery, the energy is free and therefore there is no cost for fuel. E_n represents the energy production of year n.

7.6.3 Economic evaluation

Typical steps of an economic evaluation of a project as described below will be followed for the evaluation of the small scale ORC-WHR. These steps are (Biezma and Christobal, 2006):

1. Project/system definition.

2. Choice of the economic lifetime of the system.

3. Estimation of the cash flow profile for the project.

4. Specify the cost of capital, k, and other inflation rates, j.

5. Economic assessment through investment criteria.

6. Acceptance/rejection or study of the economic conditions for the economic viability of the project.

Table 7.4 - System cost data

Items	Cost (€)	(%)
Equipments		
Hermetic scroll expander	2,300	19.91
Evaporator	2,700	23.38
Condenser	2,700	23.38
Fluid pump	900	7.79
Working fluid	400	3.46
Piping system	200	1.73
Liquid reservoir	200	1.73
Water pump	300	2.60
Control system	500	4.33
Misc. hardware	300	2.60
Total Equipment cost (TEC)	10,500	90.91
Labor cost (10% TEC)	1,050	9.09
Total installed cost (TIC)	*11,550*	*100*
Specific installed cost	5,775	-
Annual cost		
Operation and Maint. (5% TIC)	577.50	-
Insurance (0.3% TIC)	34.65	-
Total annual cost	612.15	-

Based on the market survey, catalogues of HVAC components and offers obtained from HVAC components suppliers in the City of Liege, Belgium, cost estimation of a 2 kWe ORC-WHR was done and displayed in Table 7.4. System total installed cost (TIC) amounted to 11,550 € and the specific cost to 5,775 €/kW. Assuming 5% of TIC for operation and maintenance and 0.3% TIC for insurance, the annual cost is about 613 €/year.

The following assumptions have been considered:
- The lifetime period, 20 years.
- The load factor, 85% (7446 hours).
- The system degradation rate is estimated at 2%.
- The cost of capital or interest rate, 5%.
- The inflation rate on electricity price, 2%.
- The general inflation, 2%.
- The cost of systems of bigger size is estimated using the following relation (Bejan et al., 1996):

$$C_0 = C_{0,ref} \left(\frac{\dot{W}_{net}}{\dot{W}_{net,ref}} \right)^{0.8} \tag{7.12}$$

Where the 2 kWe ORC-WHR is the reference system.

Figure 7.9 shows the evolution of the levelized electricity cost with the lifetime period for different system size. As can be seen, the LEC decreases with the increase in the lifetime. After 10 years period the LEC decreases but not as significantly as before. A lifetime period of 20 years as proposed by Kane (2002) at LENI in Lausanne, Switzerland where similar systems were tested was chosen for this system.
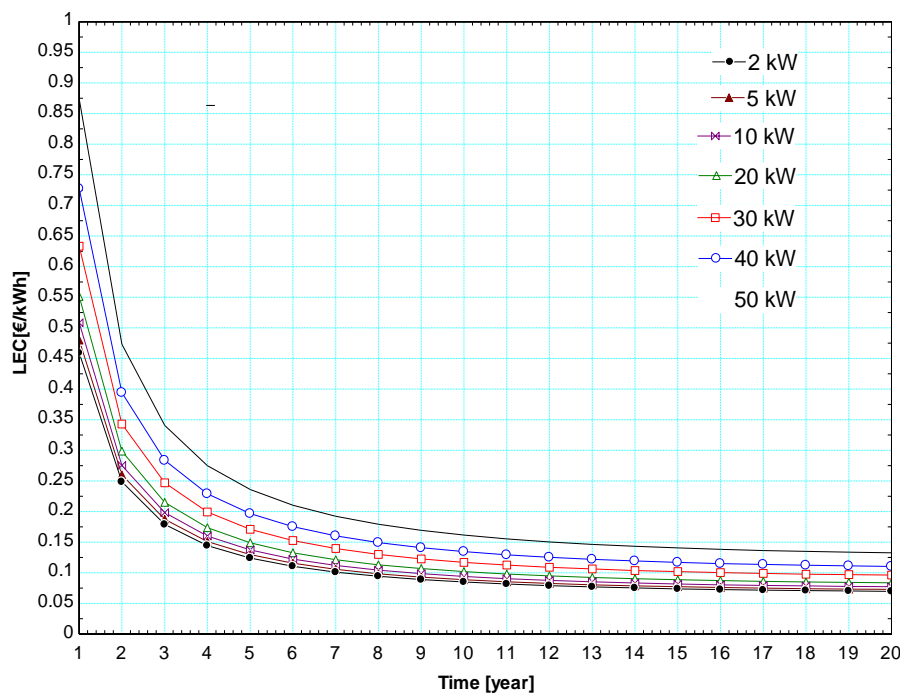
Figure 7.9 - Variation of LEC with lifetime

For 20 years lifetime period, the value of the LEC for different system sizes is given in Figure 7.10. The LEC decreases as the size of the system increases, from 13.27 c€/kWh for a 2-kWe system down to 7c€/kWh for a 50-kWe system. From the above results, it can be predicted that medium and large size system could produce electricity at cost significantly lower, below 5 c€/kWh.
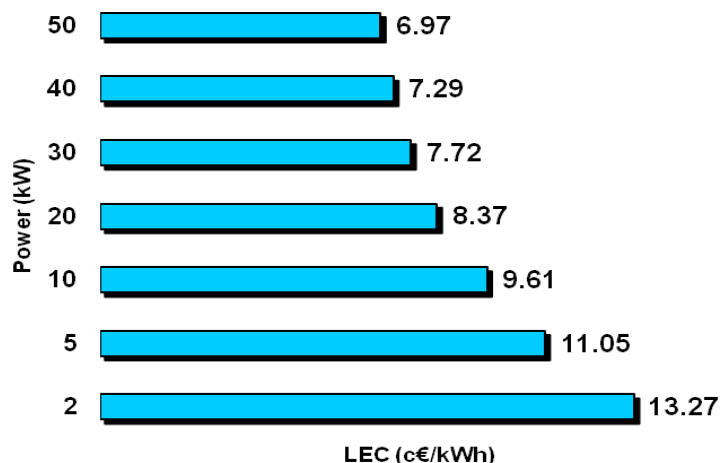
Figure 7.10 - LEC for 20 years lifetime

When the minimum price at which the electricity should be sold has been determined through the LEC calculation, the profitability can be studied through the NPV and DPP.

Figure 7.11 shows the variation of the NPV and DPP for the reference system of 2 kWe output. The DPP is about 10 years, for an electricity price of 15 c€/kWh, 6 years for 20 c€/kWh, 4.3 years for 25 c€/kWh, 3.3 years for 30 c€/kWh and 2.3 years for 40 c€/kWh. These results prove that the small scale ORC-WHR is already economically viable for countries where the electricity price is above 15 c€/kWh such as Italy, Germany and Denmark (Europe's Energy Portal, 2010). In case of countries with low electricity prices such as Greece and Finland, this system will hardly be economically viable.
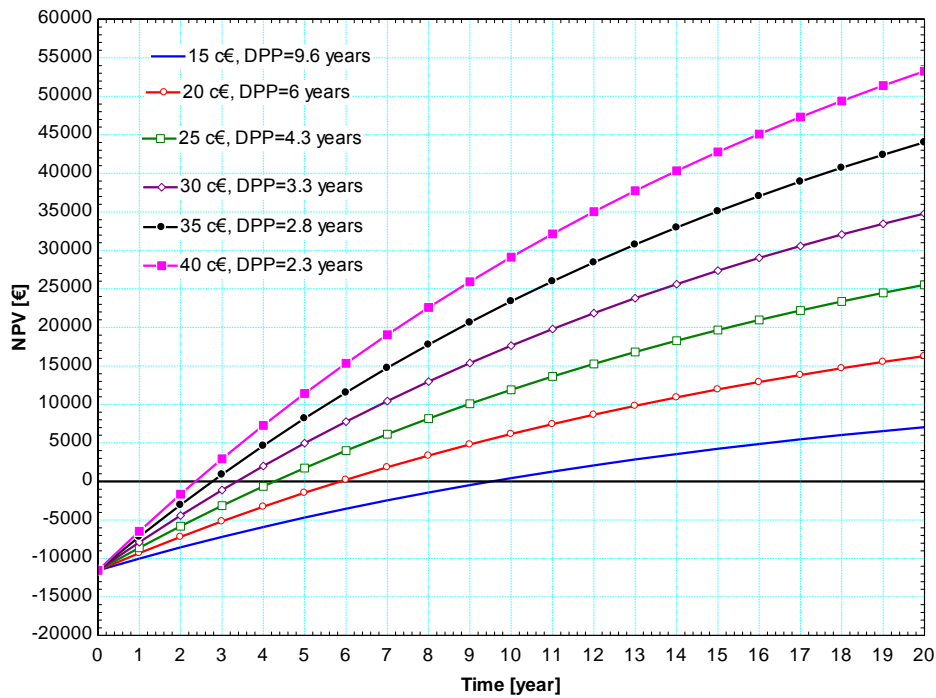
Figure 7.11 - Variation of NPV with electricity price for a 2 kWe ORC-WHR

Incentives are usually necessary for market penetration of environmental technologies. In Figure 7.12, scenarios with 20% subsidies are presented for different sizes. The electricity price is kept at 7 c€/kWh. As can be seen, systems with power output below 20 kWe are not profitable. The biggest size, 50 kWe system, has a DPP of 8 years. In order to encourage a large utilization of such systems, subsidies should be placed a reasonable level. 20% subsidies considered in the present study seem small as customers are usually attracted by low payback periods of less than 3 years.
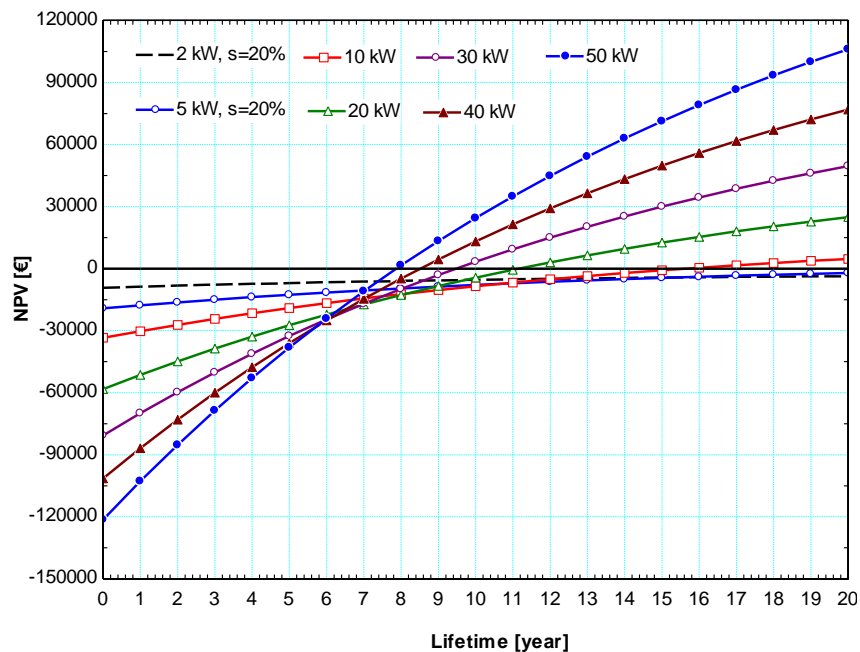
Figure 7.12 – Influence of subsidies on NPV for small ORC-WHR (Electricity Price: 7c€/kWh)

7.7 Economic Optimization of small ORCs

7.7.1 Cost modeling

7.7.1.1 Expander cost model

For recall, the present expander is a scroll compressor adapted to run in reverse mode. The size of the compressor is linked to the thermodynamic characteristics of the fluid (density, volume flow rate) at the compressor outlet which corresponds to the expander inlet. From a catalogue of scroll hermetic compressors, and taking into account the cost of transformation, the expander cost (C_{exp}) is a linear function of the expander inlet volume flow rate ($\dot{V}_s$):

$$C_{exp} = 450 + 340\,\dot{V}_s \tag{7.13}$$

7.7.1.2 Heat exchanger cost model

Heat exchangers are characterized by the heat exchange surface area which is one of parameters that determine the quantity of heat recuperated or rejected. For the present study, the cost model for heat exchangers deducted from a catalogue of flat plate heat exchangers is a linear function of the heat exchanger area (A_{hx}):

$$C_{hx} = 388 + 480 A_{hx} \tag{7.14}$$

7.7.1.3 Pump cost model

Suitable pumps for small scale ORCs are small reciprocating pumps which can suck the liquid fluid at a pressure around 2-5 bar and deliver pressurized liquid fluid at about 10-20 bar while consuming small power input. However, it should be mentioned that there is no pump designed for liquid refrigerants. The cost model used in the present study is based on the relation between the power consumption and the cost as proposed by Bejan et al. (1996):

$$C_p = C_{p,ref}(\dot{W}_p / \dot{W}_{p,ref})^m \tag{7.15}$$

m=0.25 for small reciprocating pumps (<300 W), and m=0.45 when the input power exceeds 300 W. From the offers obtained from suppliers in Liege, Belgium, the reference pump considered has a power input of 300 W and costs 900 €.

7.7.1.4 Pipes cost model

Given the same length, pipes are characterized by their diameter. In the present study, liquid and vapour pipes are distinguished and have different diameters. Depending upon the fluid, for the same thermodynamic state of the fluid the diameter may differ. From

offers of suppliers in Liege, Belgium, for cupper-type tubes which can stand pressure up to 30 bar, the cost model obtained is a linear function of the diameter (D_{pp}):

$$C_{pp} = -6.90 + 6.75 D_{pp} \qquad (7.16)$$

7.7.1.5 Fluid cost model

After examination of different prices of working fluids available on the market, it was difficult to build a correlation between the cost and thermodynamic characteristics. However, knowing the fluid charge, the cost of the working fluid for a particular system can be evaluated using the following relation:

$$C_{wf} = V_{liq,wf} \cdot UP_{wf} \cdot \varrho_{liq,wf} \qquad (7.17)$$

Where $V_{liq,wf}$ is the fluid charge; UP_{wf}, the unit price of the fluid and $\varrho_{liq,wf}$, the density of liquid fluid.

The working fluid charge can be calculated based on the assumption that only the liquid part of the circuit is considered (Quoilin, 2007); this is justified by the difference in density between vapor and liquid phases. The density of the fluid in liquid phase is much greater than the density in vapor state. Accordingly, the volume of the expander and the volume of vapor pipes as well as parts of heat exchangers are not taken into account. Thus, the liquid volume consists of ¾(1/2) of the evaporator volume, ¼(1/2) of the condenser volume, swept volume of the pump ($V_{s,p}$), liquid pipes volume ($V_{liq,pp}$) and liquid reservoir volume (V_{lr}).

$$V_{liq,wf} = (3/8) V_{ev} + (1/8) V_{cd} + V_{s,p} + V_{liq,pp} + V_{lr} \qquad (7.18)$$

7.7.2 Influence of the working conditions

The cost models in the previous section (7.7.1) show that the costs of components are linked to the geometry/size of the components which in fact depends on the thermodynamic characteristics of the working fluid used. To appreciate the influence of the thermodynamic characteristics, R123 will be used.

Figure 7.13 shows the variation of the costs of the heat exchangers and the working fluid with the evaporating pressure. The cost of the condenser decreases linearly as the evaporating pressure increases. Fluid and evaporator costs present the same trend. They increase, reach a maximum at about 7.31 bar for the evaporator and 6 bar for the fluid and decrease as the pressure increases. The decrease observed is due to the reduction of the heat exchangers area which reduces as the evaporating pressure increases.
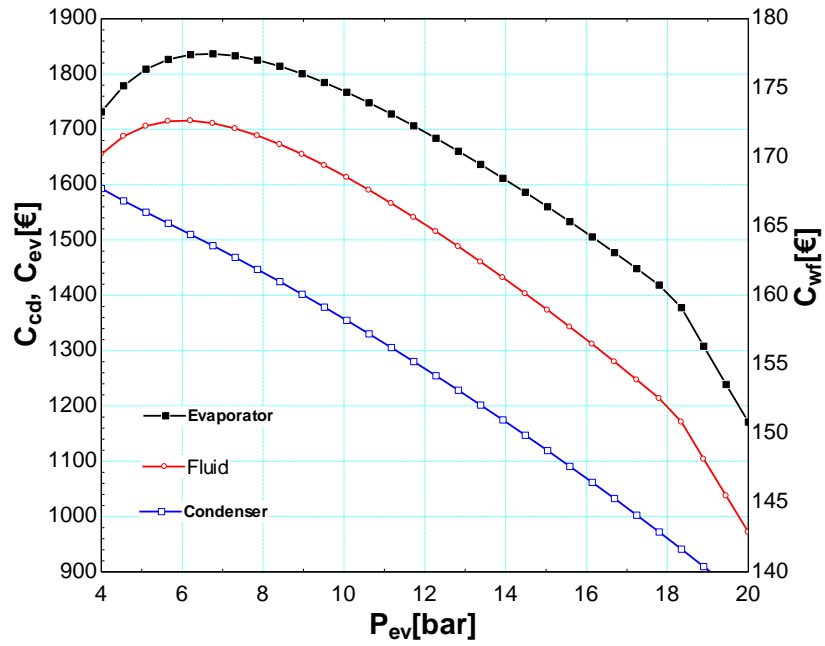
Figure 7.13 - Variation of the heat exchangers and working fluid costs

In Figure 7.14 the cost variation of active components with evaporating pressure is illustrated. If the pressure drop in the evaporator is neglected, the evaporating pressure equals the pump discharge pressure, and the expander inlet pressure. The pump cost increases progressively, reaches a maximum at about 14 bar while the expander cost decreases gradually. The variations observed for both components are due to the density of the fluid at different states. For the same pressure, the pump discharges pressurized liquid while the expander sucks superheated vapour.
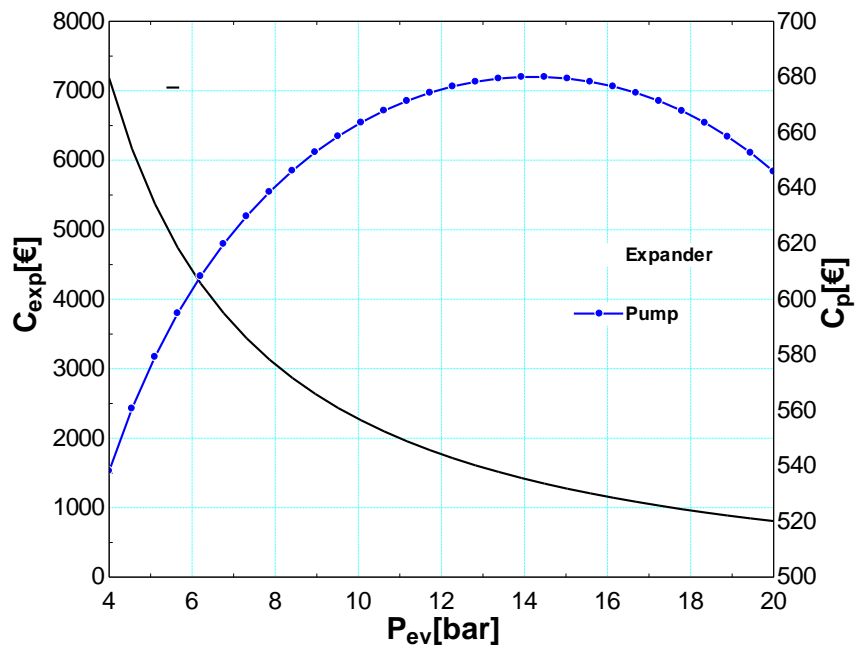
Figure 7.14 - Variation of the pump and expander costs with the evaporator pressure

7.7.3 Cycle cost model

In the previous section (7.7.2) it was seen that different components have different cost variations depending upon the working condition. This section aims at summing all components costs to build the total investment cost (TIC) and the specific investment cost (SIC).

The TIC is the sum of various costs:
- Scroll expander,

- Evaporator,

- Condenser,

- Fluid pump,

- Pipes,

- Working fluid charge,

- Other equipment: water cooling pump (300 €), liquid reservoir (200 €), control system (500 €) and miscellaneous hardware (300 €) for which the costs are neither dependant of fluids nor its thermodynamic state.

An assumption is made on the labor cost: 10% of the total equipment cost.

The total investment cost is thus given as:

$$TIC = \sum_{i=1}^{n} C_i \tag{7.19}$$

The specific system investment cost (SIC) can be deduced:

$$SIC = TIC / \dot{W}_{net} \tag{7.20}$$

On Figure 7.15, the evolution and weight of different components on the TIC are shown for R123. As can be seen, the most expensive components are the expander and the heat exchangers. The share of the expander compared to the total cost is particularly important at pressures below 11 bar, then decreases while the share of heat exchangers increases. This is due to the decrease of heat exchangers cost in narrow ranges. The influence of the working fluids and pipes are almost negligible. The system overall cost i.e. the sum of costs of different components of the Organic Rankine Cycle system decreases as the evaporating pressure increases.
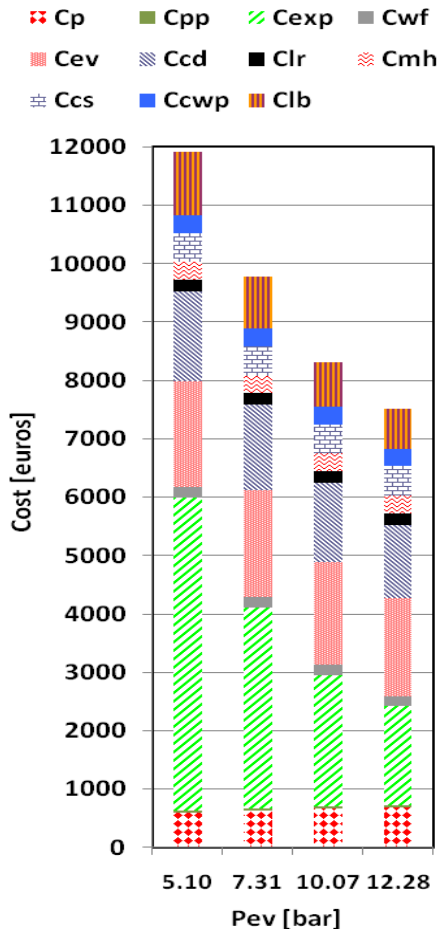
Figure 7.15 - Contribution of individual cost components on the TIC with R123 as working fluid
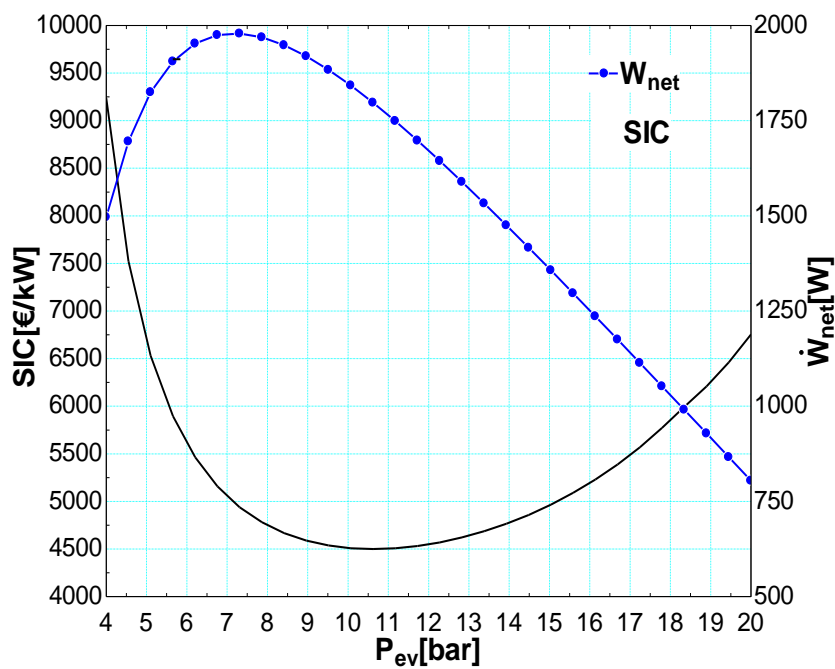
Figure 7.16 - Minimum SIC and Maximum net power

The specific investment/installed cost for any electricity generating system is a good indicator of its cost-effectiveness as it associates the investment with the capacity/performance. On Figure 7.16, the variation of the SIC with the evaporating pressure is depicted. A minimum value for the SIC is observed. For the case of R123 used here, this minimum occurs at an evaporating pressure of 10.62 bar and does not coincide with the maximum power of 1979 W obtained at 7.31 bar. This observation can be extended to any other fluid.

7.7.4 Cost optimization

The selected objective function for this optimization is the specific investment cost (SIC) expressed in €/kWe. Since waste heat sources are cost-free by definition, optimizing this parameter is equivalent to optimizing the profitability of the system if maintenance and insurance annual costs are neglected. For a given working fluid, several different working conditions can be optimized. The evaporating pressure shows an optimum in terms of overall efficiency and also in terms of profitability. The pinch point on the heat exchangers also shows an optimum value: the lower this value, the higher the cycle efficiency but the higher the heat exchanger area and the higher the cost. The choice of the pinch point value therefore results of a thermo-economic optimization of the system. Three parameters (P_{ev}, $\Delta T_{pp,cd}$, $\Delta T_{pp,ev}$) are therefore to be optimized with the objective of minimizing the SIC. This is done using the simplex algorithm (Nedler and Mead, 1965). The results of the optimization for each fluid are presented in Table 7.5. Table 7.6 shows results for power maximization with a single optimization parameter (P_{ev}).

Table 7.5 - Three-parameters optimization of the SIC

Fluids	$\Delta T_{pp,cd}$ (K)	$\Delta T_{pp,ev}$ (K)	P_{ev} (bar)	W_{net}(W)	SIC(€/kW)
R245fa	15.66	18.58	15.50	1720	4413
R123	15.46	12.54	11.31	1750	4361
R113	17.92	10.7	7.39	1586	5128
n-Pentane	15.17	12.66	8.5	1745	4440
n-Butane	14.51	17.3	19.7	1816	3869

Table 7.6 - One-parameter optimization of the net power output for $\Delta T_{pp,cd}$=10 K and $\Delta T_{pp,ev}$=15 K

Fluids	P_{ev} (bar)	W_{net}(W)	TIC(€)	SIC(€/kW)
R245fa	11.79	2004	9533	4757
R123	7.31	1979	9775	4939
R113	3.93	1942	12485	6430
n-Pentane	5.14	1979	10784	5450
n-Butane	15.31	2078	8475	4078

From Tables 7.5 and 7.6, it is seen that there is no fluid for which the minimum SIC and maximum net power coincide. For all fluids, increasing the evaporating pressure by about 3.5 bar from the point of maximum power, results in a loss in power and gain in specific cost reduction. The extent in the SIC reduction depends on the fluid.

The economic optimization offers different results for different fluids. The SIC reduction is about 5.12% for n-Butane, 7.23% for R245fa, 11.70% for R123, 18.53% for n-Pentane and 20.25% for R113. Globally, power loss of 200-400 W generates cost reduction from 1500 up to 4500 €. Translating the reduction in SIC into net power output and TIC reduction; 18.33% reduction in power leads to 34.85% of gain in TIC for R113.

Table 7.5 shows that the optimum pinch point values for both the evaporator and the condenser are comprised between 10 and 20 K, which could therefore be considered as reference values regarding the economical optimum for this kind of application.

7.8 Conclusion

In this chapter, small ORCs in waste heat recovery application already proven from technical point of view have been evaluated from an economic viewpoint. The study shows that the Organic Rankine Cycle is a promising technology for small-scale waste heat recovery applications. The minimum cost at which electricity should be sold is about 13.27 c€/kWh for very small systems. This value could be significantly low, below 5 c€/kWh for medium and large size systems. Given the advantages of recycling the waste heat energy, in comparison with renewable energy technologies, it is believed there is good prospect for ORC-WHR systems.

In the transition to the renewable energy era, efficiency through waste heat recovery has a role to play. ORC in waste heat recovery application better needs to be cost-effective than efficient. With a pre-design thermo-economic model the mismatch between the optimal technical point and the minimum specific cost was demonstrated. This mismatch is due to very different thermodynamic properties such as liquid/gas densities, which significantly influence system performance and components sizes. Seeking for profitable environmental solutions; economic optimization instead of thermodynamic optimization or a compromise is advisable.

8 - Conclusions and Perspectives

8.1 Conclusions

The interest for low grade heat recovery has been growing in recent years, due to the increasing concern over the future fossil fuels depletion and the climate change. A certain number of solutions have been proposed to transform the low temperature resource into electricity. Among the proposed solutions, the organic Rankine cycle technology appears as the most promising. An organic Rankine cycle machine is based on the same principle as a steam power plant but uses an organic compound as working fluid instead of steam and operates at lower evaporating pressure leading to an important advantage of building small size systems. Today, organic Rankine cycle modules are commercially available from various manufacturers who produce systems with power output from hundreds of kW up to MW. However, solutions are still researched for small organic Rankine cycle machines of few kW.

Selection of the most suitable working fluid is a critical step when designing an organic Rankine cycle. A certain number of criteria that should fulfill suitable fluids were established in this thesis. These are: adequate critical parameters, high liquid and vapour densities, good thermal stability and compatibility with materials, appreciable safety characteristics, market availability and low cost, good thermodynamic performance and low environmental impact. Fluids with low boiling point such as R134a, R152a, R600, R600a and R290 are suitable for low-temperature solar applications driven by heat source temperature below 100 °C. Pentanes, butanes and cryogens such as R123, R245fa, and HFE7000 are good candidates for low-temperature heat recovery applications.

A number of studies available in literature show that regenerators or feedliquid heaters improve the Rankine cycle efficiency. However, considering the extent of the influence of these devices on the organic Rankine cycles, the necessity is questionable. An advanced thermodynamic analysis method called *exergy topology analysis* was used in view of comparing different cycle configurations. Results showed that the integration of different devices is not significantly rewarded. Therefore, it is preferable to keep the simple organic Rankine cycle engine when designing a system such as the small scale ORC-RO desalination system driven by low-temperature heat below 100 °C. The analysis of a small solar ORC led to the conclusion that the solar collector array is the most critical component. It yields the lowest exergy efficiency due to poor optical performances. The *structural exergy analysis* approach proved it can serve not only as evaluation tool, but also as decision support tool.

Experimental investigation of a small organic Rankine cycle in heat recovery application with integrated scroll type expander and the hydrofluoroether HFE7000 as working fluid gave a cycle global efficiency of about 4% and cycle exergetic efficiency of 13%. The maximum shaft power obtained was 1371 W. Comparison with previous tests shows that the expander has a maximum efficiency of about 70%. R123, R245fa and HFE7000 in similar conditions give close results with slight advantage to R245fa.

The economic evaluation study showed that the organic Rankine cycle is a promising technology for small scale waste heat recovery applications. The minimum cost at which

electricity should be sold is about 13.27 c€/kWh for very small systems of about 2 kWe. This value could be reduced, below 5 c€/kWh for medium and large size systems. Using a pre-design thermo-economic model the mismatch between the optimal technical point and the minimum specific cost was demonstrated. This mismatch is due to thermodynamic properties such as liquid/gas densities, which significantly influence system performance and components sizes. Given the advantages of recycling the waste heat energy, in comparison with renewable energy technologies, it is believed there is good prospect for organic Rankine cycle machines in waste heat recovery application.

8.2 Suggested future work

Small size organic Rankine cycle machines of few kW power output before they become widely implemented require further development in many aspects.

The utilization of solar collectors as heat source is a real challenge. First, they should be well selected among various types: Flat plate (FPC), evacuated tube (ETC), compound parabolic (CPC) and parabolic through (PTC) and the operating temperature suitably set to increase the system performance. The control is important in order to offset the fluctuations of the solar radiation, insure the dispatchability of the system and keep small superheating that will avoid a two-phase expansion in the expanders.

For the specific case of a small solar ORC-RO, the working fluids selected R134a and R152a possess a drawback: a high evaporating pressure. This leads to a bulky system while a very small and compact system is desired for further competition with PV-RO. Alkanes: butane and pentane present lower evaporating pressure but are flammable. Thus, it is important to look for fluids non flammable with a condensing pressure above 1 bar and an evaporating pressure of about 10 bar.

Although, organic Rankine cycles in heat recovery application have been for quite a long time investigated, they are not yet widely implemented. As the technology for small systems is becoming progressively mastered, trials should be carried out for demonstration. On the way to its implementation, legislative conditions should be studied as it could contribute to additional power generation and fuel efficiency at the time the concern is growing over the global warming and the future energy shortage.

References

Acar H.I., 1997. Second law analysis of the reheat-regenerative Rankine cycle, Energy Conversion and Management 38:647-657

Aljundi I.H., 2009. Energy and exergy of a steam power plant in Jordan, Applied Thermal Engineering 29:324-328

Andersen W.C., Bruno T.J., 2005. Rapid screening of fluids for chemical stability in organic Rankine cycle applications, Ind. Eng. Chem. Res. 44:5560-5566.

Angelino G., Colonna di Paliano P., 1998. Multicomponent working fluids for organic rankine cycles (ORCs), Energy 23:449-463.

Angelino G., Invernizzi C., 2003. Experimental investigation on the thermal stability of some new zero ODP refrigerants, International Journal of Refrigeration 26:51-58

Aoun B, 2008. Micro-combined heat and power operating on renewable energy for residential building, PhD Thesis, Mines ParisTech.

Badr O, Probert SD, O'Callaghan PW, 1985. Selecting a working fluid for a Rankine Cycle Engine, Applied Energy 21:1-42.

Beér J.M., 2007. High efficiency electric power generation: The environmental role, Progress in Energy and Combustion Science 33:107-134.

Bejan A., Tsatsaronis G., Moran M., 1996. Thermal design and optimization, New York: Wiley.

Bejan A., 2002. Fundamentals of exergy analysis, entropy generation minimization, and the generation of flow architecture, International Journal of Energy Research 26:545-565.

Biedermann F, Carlsen H, Obernbereger I, Schoch M, 2004. Small-scale CHP plant based on a 75 kWe hermetic eight cylinder stirling engine for biomass fuels-development, technology and operating experiences, in Proc. of 2nd World Conference on Biomass for Energy, Industry and Climate Protection, 10-14 May 2004, Rome-Italy.

Biezma M.V., San Cristobal J.R., 2006. Investment criteria for the selection cogeneration plants – a state of the art review, Applied Thermal Engineering 26:583-588.

Bloomquist R.G., 2003. Integrating small power plants into agricultural projects, Geothermics 32:475-485.

Bombarda P., Ivernizzi C.M., Pietra C., 2009. Heat recovery from Diesel engines: A thermodynamic comparison between Kalina and ORC cycles, Applied Thermal Engineering 30:212-219.

Bonilla J.J., Blanco J.M., Lopez L., Sala J.M., 1997. Technological recovery potential of waste heat in the industry of the Basque Country, Applied Thermal Engineering 17:283-288.

Borsukiewicz-Gozdur A., Nowak W., 2007. Comparative analysis of natural and synthetic refrigerants in application to low temperature Clausius-Rankine cycle, Energy 32:344-352.

Borsukiewicz-Gozdur A., Nowak W., 2007. Maximizing the working fluid flow as a way of increasing power output of geothermal power plant, Applied Thermal Engineering 27:2074-2078.

Bouzayani N., Galanis N., Orfi J., 2007. Comparative study of power and water cogeneration systems, Desalination 205:243-253.

Bruno J.C., Lopez-Villada J., Letelier E., Romera S., Corona A., 2008. Modelling and optimization of solar organic Rankine cycle engines for reverse osmosis desalination, Applied Thermal Engineering 28:2212-2226.

Bryson M.J., 2007. The conversion of low grade heat into electricity using the thermosyphon Rankine engine and trilateral flash cycle, PhD Thesis, RMIT.

Calderazzi L., Colonna di Paliano P., 1997. Thermal stability of R-134a, R141b, R13I1, R7146, R125 associated with stainless steel as a containing material, International Journal of Refrigeration 20:381-389.

Calm J.M., Hourahan G.C., 2007. Refrigerant Data Update, Heating/Piping/Air Conditioning Engineering, 79:50-64.

Canada S., Cohen G., Cable R., Brosseau D., Price H., 2004. Parabolic Trough Organic Rankine Cycle Solar Power Plant, DOE Solar Energy Technologies, Program Review meeting, October 25-28, Denver – Colorado.

Cayer E., Galanis N., Desilets M., Nesreddine H., Roy P., 2009. Analysis of a carbon dioxide transcritical power cycle using a low-temperature source, Applied Energy 86:1055-1063.

Çengel Y.A., Boles M.A., 2002.Thermodynamics: An Engineering Approach, 4th edition, McGraw-Hill.

Cerci Y., 2002. Exergy analysis of a reverse osmosis desalination plant in California, Desalination 142:257-266.

Chacartegui R., Sánchez D., Munoz J.M., Sánchez T., 2009. Alternative ORC bottoming cycles for combined cycle power plants, Applied Energy 86:2162-2170.

Chen Y., Lundqvist P., Johansson A., Platell P., 2006. A comparative study of the carbon dioxide transcritical power cycle compared with an organic Rankine cycle with R123 as working fluid in waste heat recovery, Applied Thermal Engineering 26:2142-2147.

Chen H., Goswami D.Y., Stefanakos E.K., 2010. A review of thermodynamic cycles and working fluids for the conversion of low-grade heat, Renewable and Sustainable Energy Reviews, doi:10.1016/j.rser.2010.07.006

Cowden R., Nahon M., Rosen M.A., 2001. Exergy analysis of a fuel cell power system for transportation applications, Exergy an International Journal 2:112-121.

Dai Y., Wang J., Gao L., 2009. Parametric optimization and comparative study of organic Rankine cycle (ORC) for low grade waste heat recovery, Energy Conversion and Management 50:576-582.

Declaye, 2009. Design, optimization and modeling of an organic rankine cycle for waste heat recovery, MSc Thesis, University of Liege.

Delgado-Torres A.M., Garcia Rodriguez L., 2007. Double cascade organic Rankine cycle for solar-driven reverse osmosis desalination, Desalination 216:306-313.

Delgado-Torres A.M., Garcia-Rodriguez L., 2007. Preliminary assessment of solar organic Rankine cycles for driving a desalination system, Desalination 216:252-275.

Delgado-Torres A.M., 2009. Solar thermal heat engines for water pumping: An update, Renewable and Sustainable Energy Reviews 13:462-472.

Delgado-Torres A.M., Garcia-Rodriguez L., 2010. Analysis and optimization of the low-temperature solar organic Rankine cycle (ORC), Energy Conversion and Management 51:2846-2856.

DiPippo R., 2004. Second Law assessment of binary plants generating power from low-temperature geothermal plants, Geothermics 33:565-586.

DiPippo R, 2007. Ideal thermal efficiency for geothermal binary plants, Geothermics 36:276-285.

DiPippo R., 2008. Geothermal power plants: principles, applications, case studies and environmental impact, second edition, Elsevier.

Dong L., Liu H., Riffat S., 2009. Development of small-scale and micro-scale biomass-fuelled CHP systems – A literature review, Applied Thermal Engineering 29:2119-2126

Drescher U., Brűggemann D., 2007. Fluid selection for the organic Rankine cycle (ORC) in biomass power and heat plants, Applied Thermal Engineering 27:223-228.

El Chalmas R., Clodic D., 2005. Combined cycle for hybrid vehicles, in Proc. of SAE World Congress, 11-14 April, Detroit, Michigan-USA.

Endo T., Kawajiri S., Kojima Y., Takahashi K., Baba T., Ibaraki S., Takahashi T., Shinorama M., 2007. Study on maximizing exergy in automotive engines, in Proc. of SAE world Congress, April 16-19, Detroit, Michigan.

Essam Sh. Mohamed, Papadakis G., Mathioulakis E., Belessiotis V., 2008. A direct coupled photovoltaic seawater reverse osmosis desalination system toward battery based systems-a technical and economical experimental comparative study, Desalination 221:17-22.

Farahat S., Sarhaddi F., Ajam H., 2009. Exergetic optimization of flat plate solar collectors, Renewable Energy; 34:1169-1174.

Feher E.G., 1968. The supercritical thermodynamic power cycle, Energy Conversion 8:85-90.

Finney K.A., 2008. Ocean thermal energy conversion, Guelph Engineering Journal 1:17-23.

Fischer U., Ring A., Sugarmen C., 2004. Solar operated organic Rankine cycle units for 0.2 to 10 MWe systems, in Proc. of 12th Sede Boker symposium on solar energy production.

Fritzmann C., Lowenberg J., wintgers T., Melin T., 2007. State-of-the-art of reverse osmosis desalination, Desalination 216:1-76.

Galanis N., Cayer E., Roy P., Denis E.S., Desilets M., 2009. Electricity generation from low temperature sources, Journal of Applied Fluid Mechanics 2:55-67.

Ganic E.N., Wu J., 1980. On the selection of working fluids for OTEC power plants, Energy Conversion and Management, 20:9-22.

Garcia Rodriguez L. and Deldado-Torres A.M., 2007. Solar-powered Rankine cycles for fresh water production, Desalination 212:319-327.

Gu W., Weng Y., Cao G., 2007. Testing and thermodynamic analysis of low-grade heat power generation system using organic Rankine cycle, in: Proceedings of international conference on Power Engineering, October 23-27, Hangzhou, China.

International Energy Agency (IEA), 2009. Key World Energy Statistics, 2009 Report.

Hamnet K., Why have we been kept in the dark about concentrated solar power which can make coal and nuclear=history, available at [checked 9/2010] http://www.katharinehamnett.com/Campaigns/Concentrated-Solar-Power/REPORT.

Hassani V., Price H., 2001. Modular Trough Power Plants, in Proc. of Solar Forum 2001, Washington DC.

Heberle F., Bruggeman D., 2010. Exergy based fluid selection for a geothermal organic rankine cycle for combined heat and power generation, Applied Thermal Engineering 30:1326-1332.

Henning H.M., 2007. Solar assisted air conditioning of buildings – an overview, Applied Thermal Engineering 27:1734-1749.

Hepbasli A., 2007. Exergetic modeling and assessment of solar assisted domestic hot water tank integrated ground-source heat pump systems for residences, Energy and Buildings 39:1211-1217.

Hettiarachchi H.D.M., Golubovic M., Worek W.M., Ikegami Y., 2007. Optimum design criteria for an organic Rankine cycle using low-temperature geothermal heat sources, Energy 32:1698-1706.

Hung T.C., Shai T.Y., Wang S.K., (1997). A review of organic Rankine cycles (ORCs) for the recovery of low-grade waste heat, Energy 22:661-667.

Hung T.C., (2001). Waste heat recovery of organic Rankine cycle using dry fluids, Energy Conversion and Management 42:539-553.

Ibrahim O.M., Klein S.A., 1996. Absorption power cycles, Energy 21:21-27.

Invernizzi C., Lora P., Silva P., 2007. Bottoming micro-Rankine cycles for micro-gas turbines, Applied Thermal Engineering 27:100-110.

Kalina A.I., 1984. Generation of energy, US Patent No 405942.

Kane El Hadj Malick, 2002. Intégration et optimisation thermoéconomique et environomique de centrales thermiques solaires hybrides, Thèse de Doctorat, Ecole Polytechnique Fédérale de Lausanne.

Kane M., Larrain D., Favrat D., Allani Y., 2003. Small hybrid solar power system, Energy 28:1427-1443.

Kanoglu M., Bolatturk A., 2008. Performance and parametric investigation of a binary geothermal power plant by exergy, Renewable Energy 33:2366-2374.

Kanoglu M., Dincer I., 2009. Performance assessment of cogeneration plants, Energy Conversion and Management 50:76-81.

Karagiannis I.C., Soldatos P.G., 2008. Water desalination cost literature: review and assessment, Desalination 223:448-456.

Karekezi S., 2002. Poverty and energy in Africa – A brief review, Energy Policy 30: 915-919.

Karellas S., Schuster A., 2008. Supercritical fluid parameters in organic rankine cycle applications, International journal of Thermodynamics 11:101-108.

Kaushik S.C., Dubey A., Singh N., 1994. Thermal modeling and energy conservation studies on Freon Rankine cycle cooling system with regenerative heat exchanger, Heat Recovery Systems and CHP 14:67-77.

Kim D.S., Infante Fereira C.A., 2008. Solar refrigeration options – a state-of-the-art review, International Journal of Refrigeration 32:3-15.

Klein S.A., 2008. Engineering Equation Solver (EES), Academic Professional version.

Kontragool B., Wongwises S., 2006. Thermodynamic analysis of a Stirling engine including dead volumes of hot space, cold space and regenerator, Renewable Energy 31:345-359.

Korobitsyn M.A., 1998. New and advanced energy conversion technologies: Analysis of cogeneration combined and integrated cycles, PhD Thesis, University of Twente, Netherlands.

Koroneos C.J., Nanaki E.A., 2008. Energy and exergy utilization assessment of the Greek transport sector, Resources, Conservation and Recycling 52:700-706

Kosmadakis G., Manolakos D., Papadakis G., 2010. Parametric theoretical study of a two-stage solar organic Rankine cycle for RO desalination, Renewable Energy 35:989-996.

Lakew A.A., Bolland O., 2010. Working fluids for low-temperature heat source, Applied Thermal Engineering 30:1262-1268.

Lemort V., 2006. Testing and modelling scroll compressors with a view to integrate them as expanders into a Rankine cycle, DEA Thesis, University of Liege - Belgium.

Lemort V., 2008. Contribution to the characterization of scroll machines in compressor and expander modes, PhD Thesis, University of Liege-Belgium.

Lee M.J., Tien D.L., Shao C.T., 1993. Thermophysical capability of ozone-safe working fluids for an organic Rankine cycle system, Heat Recovery Systems and CHP 13:409-418.

Lensu T., Alakangas E., 2004. Small-scale electricity generation from renewable energy sources, OPET Report.

Lior N., 1977. Solar energy and the steam Rankine cycle for driving and assisting heat pumps in heating and cooling modes, Energy Conversion 6:111-123.

Liu B.T.,. Chien K.H, Wang C.C., 2004. Effect of working fluids on organic Rankine cycle for waste heat recovery, Energy 29:1207-1217.

Lund J.W., 2006. Geothermal energy focus: tapping the earth's natural heat, Refocus November/December 2006, Elsevier.

Mago P.J., Srinivasan K.K., Chamra L.M. and Somayaji C., 2008. An examination of exergy destruction in organic Rankine cycles, International Journal of Energy Research 32:926-938.

Mago P.J., Chamra L.M., Srinivasan K., Somayaji C., 2008. An examination of regenerative organic rankine cycles using dry fluids, Applied Thermal Engineering 28:998-1007.

Maizza V., Maizza A., 1996. Working fluids in non-steady flows for waste energy recovery systems, Applied Thermal Energy 16:579-590.

Maizza V., Maizza A., 2001. Unconventional working fluids in organic Rankine cycles for waste energy recovery systems, Applied Thermal Engineering 21:381-390.

Mannaa Abdul-Raouf., Ghazi M., Khalifa A., 1984. Control strategies for Rankine solar cooling systems, Solar and Wind Technology 1:259-264.

Manolakos D., Papadakis G., Essam Sh. Mohamed, Kyritsis S., Bouzianas K., 2005. Design of an autonomous low-temperature solar Rankine cycle system for reverse osmosis desalination, Desalination 183:73-80.

Manolakos D., Papadakis G., Kyritsis S., Bousianas K., 2007. Experimental investigation of an autonomous low-temperature solar rankine cycle system for reverse osmosis desalination, Desalination 203:366-374.

Manolakos D., Essam Sh. Mohamed, I. Karagianis, G. Papadakis, 2008. Technical and economical comparison between PV-RO system and RO-solar Rankine system. Case study: Thirasia island, Desalination 221:37-46.

Mathioulakis E., Belessiotis V., Dalyannis E., 2007. Desalination by using alternative energy: Review and state-of-the-art, Desalination 203:346-365.

Maurel A., 1979. Dessalement et energies renouvelables, Desalination 31:489-499.

Meteonorm, (2005). Global Meteorological Database for Engineers, Planers and Education, Version 5.1.

Mills D., 2004. Advances in solar thermal electricity technology, Solar Energy 76, 19-31

Mlcak H.A., 2002. Kalina cycle concepts for low temperature geothermal, Geothermal Resources Council Transactions 26.

Mikielewicz D. and Mikielewicz J., 2010. A thermodynamic criterion for selection of working fluid for subcritical and supercritical domestic micro CHP, Applied Thermal Engineering 30:2357-2362.

Moran A., Mago P.J., Chamra LM, 2008. Thermoeconomic modeling of micro-CHP (micro-cooling, heating, and power) for small commercial applications, International Journal of Energy Research 32:808-823.

Moriarty P., Honnery D., 2009. What energy levels can the Earth sustain?, Energy Policy (37), pp. 2469-2474.

Muller-Steinhagen H., Trieb F., 2004. Concentrating solar power: A review of the technology, Quaterly of the Royal Academy of Engineering, Ingenia 18:43-50.

Nelder J.A., Mead, R., 1965. A simplex method for function minimization, Computer Journal 7: 308–313.

Nikolaidis Y., Pilavachi P.A., Chletis A., 2009. Economic evaluation of energy saving measures in a common type of greek building, Applied Energy 86:2550-2559.

Nikulshin V., Wu C., Nikulshina V., 2002. Exergy efficiency calculation of energy intensive systems by graphs, International Journal of Thermodynamics 5:67-74.

Nikulshin V., Wu C., Nikulshina V., 2002. Exergy efficiency calculation of energy intensive systems, Exergy an International Journal 2:78-86.

Nikulshin V., Wu C., 2001. Thermodynamic analysis of energy intensive systems based on exergy-topological models, Exergy an International Journal 1:173-179.

Nikulshin V., Bailey M., Nikulshin V., 2006. Thermodynamic analysis of air refrigerator on exergy graph, Thermal Science 10:99-110.

Nilufer A. and Karakas A., 1986. Second law analysis of a solar powered Rankine cycle/vapor compression cycle, Journal of Heat Recovery Systems 6:135-141.

Nowak W., Borsukiewicz-Gozdur A., Stachel A.A., 2008. Using the low-temperature Clausius-Rankine cycle to cool technical equipment, Applied Energy 85:582-588.

Obernberger I., Hammerschmid A., 2001. Biomass fired CHP plant based on an ORC cycle – Project ORC-STIA-Admont, Final Report.

Obernberger I., Thonhofer P., Reisenhofer E., 2002. Description and evaluation of the new 1,000 kWel organic rankine cycle process integrated in the biomass CHP plant in Lienz, Austria, Euroheat and Power vol. 10.

O'Connor J.J., Robertson E.F., 2005. William John Macquorn Rankine, http://www-history.mcs.st-andrews.ac.uk/Biographies/Rankine.html [Last checked June 2010]

Ogriseck S., 2009. Integration of a Kalina cycle in a combined heat and power plant, a case study, Applied Thermal Engineering 29:2843-2848.

Oliveira A.C., Afonso C., Matos J., Riffat S., Nguyen M., Doherty P., 2002. A combined heat and power system for buildings driven by solar energy and gas, Applied Thermal Engineering 22:587-593.

Orosz M., 2009. Small scale solar ORC system for distributed power in Lesotho, in Proc. of Solar World Congress, October 11-14, Johannesburg, South Africa.

Orosz M.S., Mueller A., Quoilin S., Hemond H., 2009. Small scale solar ORC system for distributed power, in Proc. of the SolarPaces Conference, September 2009, Berlin – Germany.

Papadopoulos A.I., Stijepovic M., Linke P., 2010. On the systematic design and selection of optimal working fluids for organic rankine cycles, Applied Thermal engineering 30:760-769.

Podesser E., 1999. Electricity production in rural villages with a biomass Stirling engine, Renewable Energy 16:1049-1052.

Poullikas A., 2005. An overview of current and future sustainable gas turbine technologies, Renewable and Sustainable Energy Reviews 9:409-443.

Pouraghaie M., Atashkari K., Besarati S.M., Nariman-zadeh N., 2010. Thermodynamic performance optimization of a combined power/cooling cycle, Energy Conversion and Management 51:204-211.

Pridasawas W., Lundqvist P., 2004. An exergy analysis of a solar-driven ejector refrigeration system, Solar Energy 76:369-379.

Pridasawas W., Lundqvist P., 2006. Solar-driven refrigeration systems with focus on the ejector cycle, PhD Thesis, Royal Institute of Technology (KTH).

Prigmore D. and Barber R., 1975. Cooling with the sun's heat: Design considerations and test data for a Rankine cycle prototype, Solar Energy 17: 185-192.

Quaschning V., Muriel M.B., 2001. Solar Power-Photovoltaics or Solar Thermal power plants?: In Proc. of VGB Congress Power Plants 2001, Brussels, 10-12 October 2001.

Quoilin S., M. Orosz and V. Lemort, Modeling and Experimental investigation of an organic rankine cycle using scroll expander for small solar applications, Proc. Eurosun Conference, Lisbon-Portugal, 7-10 Oct. 2008.

Quoilin S., Lemort V., 2009. Technological and economical survey of organic Rankine cycle systems, in: Proceedings of the fifth European Conference on Economics and Management of Energy in Industry, April 14-17, Algarve-Portugal.

Quoilin S., 2007. Experimental study and modeling of a low temperature rankine cycle for small scale cogeneration, MSc Thesis, University of Liege.

Quoilin S., Lemort V., Lebrun J., 2010. Experimental study and modeling of an organic Rankine cycle using scroll expander, Applied Energy 87:1260-1268.

Saleh B., Koglbauer G., Wendland M., Fischer J., 2007. Working fluids for low-temperature organic Rankine cycles, Energy 32: 1210-1221.

Sandrameli S.M., Goswami D.Y., 2007. Optimum operating conditions for a combined power and cooling thermodynamic cycle, Applied Thermal engineering 84, 254-265

Schuster A., Karl J., Karellas S., 2007. Simulation of an innovative stand-alone solar desalination system using an organic Rankine cycle, International Journal of Thermodynamics 10:155-163.

Schuster A., Karellas S., Karakas E., Spliethoff H., 2009. Energetic and economic investigation of organic Rankine cycle applications, Applied Thermal Engineering 29:1809-1817.

Schuster A., Karellas S., Aumann R., 2009. Efficiency optimization potential in supercritical organic Rankine cycles, Energy 2:1-7.

Sciubba E., Wall G., 2007. A brief commented history of exergy from the beginnings to 2004, International Journal of Thermodynamics 10:1-26.

Short W., Packey D.J., Holt T., 1995. A manual for the Economic Evaluation of Energy Efficiency and Renewable Energy Technologies, NREL.

Sims R.E.H., 2004. Renewable energy: a response to climate change, Solar Energy 76: 9-17.

Singh N., Kaushik S.C., Misra R.D., 2000. Exergetic analysis of a solar thermal power system, Renewable Energy 19:135-143.

Smith I.K., Stosic N., 2001a. Prospects for energy conversion efficiency improvements by the use of twin screw two-phase expanders, in Proc. of the 2nd International Heat Powered Cycles Conference, Paris-France, September 2001.

Smith I.K., Stosic N., Kovacevic A., 2001b. Power recovery from low cost two-phase expanders, GRC Annual Meeting, San Diego.

Smith I.K., Stosic N., Kovacevic A., 2005. Screw expanders increase output and decrease the cost of geothermal binary power plant systems, in Proc. Of the Geothermal Resources Council Annual Meeting, Reno, Nevada-USA, September 25-28.

Srinivas T., Gupta AVSSKS, Reddy B.V., 2007. Generalized thermodynamic analysis of steam power cycles with 'n' number of feedwater heaters, International Journal of Thermodynamics 10:177-185.

Stine W.B., Geyer M., 2001. Power cycles for electricity generation: in, Power from the sun, at http//www.powerfromthesun.net/chapter12/chapter12nwe.htm, [last checked March 2009].

Suzuki A., 1988. General theory of exergy-balance analysis and applications to solar collectors, Energy; 13:153-160.

Takahashi P.K., Trenka A., 1992. Ocean thermal energy conversion: its promise as a total resource system, Energy 17:657-668.

Tamm G.O., 2003. Experimental investigation of an ammonia-based combined power and cooling cycle, PhD Thesis, University of Florida.

Tchanche B.F., Papadakis G., Lambrinos G., Frangoudakis A., 2008a. Criteria for working fluids selection in low-temperature solar organic Rankine cycles, in: Proc.

of International Conference on Solar Heating, Cooling and Buildings, Eurosun2008, 7-10 Oct. 2008, Lisbon-Portugal.

Tchanche B.F., Papadakis G., Lambrinos G., Frangoudakis A., 2008b. Effects of regeneration on low- temperature solar organic Rankine cycles, in: Proc. of International Conference on Solar Heating, Cooling and Buildings, Eurosun2008, 7-10 Oct. 2008, Lisbon-Portugal.

Tchanche B.F., Papadakis G., Lambrinos G., Frangoudakis A., 2009a. Exergy analysis of a low-temperature solar thermal power system based on exergy-topological models, in Proc. of International Exergy, Energy and Environmental Symposium, IEEES-4, 19-23 April 2009, Sharjah- United Arab Emirates.

Tchanche B.F., Papadakis G., Lambrinos G., Frangoudakis A., 2009b. Optimal evaporating temperature for working fluids in Rankine heat engines, in Proc. of International Exergy, Energy and Environmental Symposium, IEEES-4, 19-23 April 2009, Sharjah-United Arab Emirates. "Low-grade heat conversion into power using organic Rankine cycles – A review of various applications". Renewable Energy (submitted).

Tchanche B.F., Essam Sh. Mohamed, Papadakis G., 2009c. Solar energy: A solution for energy poverty in Africa?, in Proc. of ISES Solar World Congress, 11-14 Oct. 2009, Johannesburg, South Africa.

Tchanche B.F., Papadakis G., Lambrinos G., Frangoudakis A., 2009. Fluid selection for a low-temperature solar organic Rankine cycle, Applied Thermal Engineering 29:2468-2476.

Tchanche B.F., Lambrinos Gr., Frangoudakis A., Papadakis G., 2010. Exergy analysis of micro-organic Rankine power cycles for a small scale solar driven reverse osmosis desalination system, Applied Energy 87:1295-1306.

Tchanche B.F., Quoilin S., Declaye S., Papadakis G. & Lemort V., 2010a. Economic Optimization of Small Scale Organic Rankine Cycles, in Proc. of 23rd International Conference on Efficiency, Cost, Optimization, Simulation and Environmental Impact of Energy Systems (ECOS), June 14-17, 2010, Lausane-Switzerland.

Tchanche B.F., Quoilin S., Declaye S., Papadakis G. & Lemort V., 2010b. Economic Feasibility Study of a Small Scale Organic Rankine Cycle System in Waste Heat Recovery Application, in Proc. of the ASME 2010 10th Biennial Conference on Engineering and Systems Design and Analysis (ESDA), July 12-14, 2010, Istanbul-Turkey.

Tchanche B.F., Papadakis G., Lambrinos G., Frangoudakis A., 2010c. Low-grade heat conversion into power using organic Rankine cycles – A review of various applications. Renewable Energy (submitted).

Thomas B., 2008. Benchmark testing of micro-CHP units, Applied Thermal Engineering 28:2049-2054.

Trieb F., Langniβ O., Klaiβ H., 1997. Solar electricity generation - A comparative view of technologies, costs and environmental impact, Solar Energy 59:89-99.

Uehara H., Ikegami Y., Nishida T., 1994. Performance analysis of OTEC using new cycle with absorption and extraction process, in: Proc. of Oceanology International, vol. 6.

Uehara H., Ikegami Y., Nishida T., Kikuchi S., Tsuboi K., 1997. OTEC system using Uehara cycle, in: Proc. of the International OTEC/DOWA Association Conference.

Uehara H, 2006. History and the future of OTEC, in: Proceedings of Renewable Energy 2010, Japan.

Verbruggen A., 2008. Renewable and nuclear power: A common future?, Energy Policy 36:4036-4047.

Vijayaraghavan S., 2003. Thermodynamic studies on alternate binary working fluid combinations and configurations for a combined power and cooling cycle, PhD Thesis, University of Florida.

Voros N.G., Kiranoudis C.T., Maroulis Z.B., 1998. Solar energy exploitation for reverse osmosis desalination plants, Desalination 115:83-101.

Wang J., Dai Y., Gao L., Ma S., 2009. A new combined cooling, heating and power system driven by solar energy, Renewable Energy 34:2780-2788.

Wang X.D., Zhao L., 2009. Analysis of zeotropic mixtures used in low-temperature solar Rankine cycles for power generation, Solar Energy 83:605-613.

Wali E., 1980. Working fluids for solar Rankine-cycle cooling systems, Energy 5:631-639.

Wall G., Exergy- A useful concept within resource accounting, www.exergy.se [checked March 2009].

Wall G., 1995. Exergy Conversion in the Japanese Society, Energy 15:435-444.

Wei D., Lu X., Lu Z., Gu J., 2007. Performance analysis and optimization of organic Rankine cycle (ORC) for waste heat recovery, Energy Conversion and Management 4:1113-1119.

Wilson S.S., 1986. Discussion on 'selecting a working fluid for a Rankine cycle-engine', Applied Energy 24:65-68.

Wong Y.W., Sumathy K., 1999. Solar thermal water pumping systems: A review, Renewable and Sustainable Energy Reviews 3:185-217.

Xu F., Goswami D.Y., Bhagwat S.S., 2000. A combined power/cooling cycle, Energy 25:233-246.

Yamaguchi H., Zhang X.R., Fujima K., Enomoto M., Sawada N., 2006. Solar energy powered Rankine cycle using supercritical CO_2, Applied Thermal Engineering 26:2345-2354.

Yamamoto T., Furuhata T., Arai N., Mori K., 2001. Design and testing of the organic Rankine cycle, Energy 26:239-251.

You Y., Hu E.J., 2002. A medium-temperature solar thermal power system and its efficiency optimization, Applied Thermal Engineering 22:357-364.

Zaneli R., Favrat D., 1994. Experimental investigation of a hermetic scroll expander-generator, Proceedings of the 12th International Compressor Engineering Conference at Perdue, USA.

Zhang X.R., Yamaguchi H., Uneno D., Fujima K., Enomoto M., Sawada N., 2006. Analysis of a novel solar-energy powered Rankine cycle for combined power and heat generation using supercritical carbon dioxide, Renewable Energy 31:1839-1854.

Zhang X.R., Yamaguchi H., Uneno D., 2007. Experimental study on the performance of solar rankine system using supercritical CO_2, Renewable Energy 32:2617-2628.

Zhao Y., Chen J., 2007. Performance analysis of an irreversible Miller heat engine and its optimum criteria, Applied Thermal Engineering 27:2051-2058.

Zhao Y., Chen J., 2006. Performance analysis and parametric optimum criteria of an irreversible Atkinson heat-engine, Applied Energy 83:789-800.

Zamfirescu C., Dincer I., 2008. Thermodynamic analysis of a novel ammonia-water trilateral Rankine cycle, Thermochimica Acta 477:7-15.

Annexes

ANNEX 1: Results of the experimental tests – 2010 (HFE7000)

Test	Refrigerant flow rate (kg/s)	Air flow rate (kg/s)	Condenser water flow rate (kg/s)	Condenser water temperature (°C)	Pump 1 setting (X1)	Pump 2 setting (X2)	First hot air stream temperature (°C)	Second hot air stream temperature (°C)	Subcooling at the subcooler exhaust (°C)
1	0.04968	0.06321	1.05	3.324	0.25	0.39	175.8	133.3	29.1
2	0.04661	0.06321	1.068	5.889	0.21	0.38	176.9	136	29.12
3	0.04791	0.06321	1.068	5.927	0.23	0.385	177	136.5	28.94
4	0.0486	0.06321	1.068	5.936	0.235	0.39	176.8	135.8	28.79
5	0.04963	0.06321	1.068	5.96	0.245	0.395	176.7	135.3	28.73
6	0.04873	0.06321	1.068	4.297	0.23	0.395	175.6	132.6	33.08
7	0.04937	0.06321	1.068	4.36	0.24	0.395	175.9	133.1	32.74
8	0.05048	0.06321	1.068	4.411	0.25	0.4	176	132.9	32.49
9	0.07723	0.09481	1.068	6.144	0.46	0.57	192.1	155.9	31.57
10	0.07418	0.09481	1.068	6.068	0.425	0.565	192.8	156.5	31.26
11	0.07444	0.09481	1.068	6.035	0.43	0.57	193.5	157.7	30.99
12	0.07427	0.09481	1.068	6.034	0.43	0.57	193.7	157.8	30.75
13	0.0714	0.09481	1.068	6.047	0.42	0.565	194.2	158.8	30.58
14	0.06491	0.09481	1.068	6.067	0.44	0.6	195.4	162.2	30.35
15	0.06916	0.09481	0.52	6.736	0.41	0.53	194.1	162.6	25.65
16	0.06899	0.09481	0.22	6.767	0.41	0.53	195.1	162.9	24.46

Test	Overheating at the expander inlet (K)	Refrigerant temperature at the expander supply (°C)	Refrigerant pressure at the expander supply (bar)	Shaft power output (W)	Expander rotational speed (rpm)	Expander isentropic effectiveness (-)	Cycle efficiency (%)	Exergetic efficiency (%)	Expander pressure ratio (-)
1	10.57	108.2	6.257	712	2560	0.5833	3.001	8.35	5.886
2	9.048	114.5	7.527	665.4	1500	0.5425	2.577	6.905	6.649
3	8.902	112.7	7.243	708.3	1750	0.5706	3.019	8.236	6.484
4	8.846	110.7	6.92	730.5	2000	0.5969	3.111	8.587	6.179
5	8.133	108.3	6.649	733.5	2250	0.6034	3.055	8.559	5.926
6	8.367	107.5	6.487	678.3	2500	0.6072	2.773	7.645	5.296
7	8.976	107.2	6.347	681.1	2750	0.6092	2.72	7.563	5.177
8	8.345	105.1	6.126	658.2	3000	0.5884	2.477	6.987	5.03
9	8.211	122.9	9.276	1350	3000	0.6519	5.173	12.93	6.846
10	11.39	127.3	9.53	1348	2750	0.6575	5.269	12.8	7.07
11	9.981	127.9	9.957	1371	2500	0.6476	5.382	13	7.537
12	8.051	127.8	10.36	1369	2250	0.6406	5.407	12.96	7.831
13	10.38	132.2	10.83	1335	2000	0.6243	5.316	12.39	8.312
14	14.05	138.9	11.55	1311	1750	0.6352	5.449	11.62	9.109
15	12.98	138.6	11.74	1320	1650	0.5796	5.307	12.08	9.924
16	13.81	139.6	11.78	1315	1650	0.5805	5.314	11.94	9.792

Test	Evaporator pressure $P_{r,ex,ev}$ [bar]	Exergy loss in condenser Π_{cd} [W]	Exergy loss in evaporator Π_{ev} [W]	Exergy loss in expander Π_{exp} [W]	Exergy loss in pumps Π_{p} [W]	Exergy loss in ORC system Π_{tot} [W]
1	6.257	1049	921.3	468.3	361.9	2800.5
2	7.527	949.4	829.3	566.1	374.1	2718.9
3	7.243	1000	861.3	493	364.4	2718.7
4	6.92	1011	884.3	448.3	375.3	2718.9
5	6.649	1022	905.3	432.3	381	2740.6
6	6.487	1053	915.3	440.6	362	2770.9
7	6.347	1083	935.9	422.2	367	2808.1
8	6.126	1105	955.3	426.8	367.4	2854.5
9	9.276	1862	1533	613.7	392	4400.7
10	9.53	1810	1528	643.6	392.2	4373.8
11	9.957	1824	1524	648.8	389.8	4386.6
12	10.36	1809	1513	667.8	387.7	4377.5
13	10.83	1762	1499	725.8	387.1	4373.9
14	11.55	1659	1735	669.6	400.7	4464.3
15	11.74	1614	1403	861.2	383.6	4261.8
16	11.78	1614	1419	836	383.7	4252.7